UNIVERSIDADE DE BRASÍLIA
INSTITUTO DE GEOCIÊNCIAS

INTERPRETAÇÃO, INVERSÃO 3D DE DADOS MAGNÉTICOS E MODELAGEM 3D DA SUSCEPTIBILIDADE MAGNÉTICA MEDIDA, APLICADAS À PROSPECÇÃO GEOFÍSICA DE DEPÓSITOS DE ÓXIDOS DE FERRO - COBRE - OURO *(IOCG IRON OXIDE-COPPER-GOLD)* – PROVÍNCIA MINERAL DE CARAJÁS, BRASIL

MARCELO HENRIQUE LEÃO SANTOS

Tese de Doutorado N° 117

Brasília - DF
2014

UNIVERSIDADE DE BRASÍLIA
INSTITUTO DE GEOCIÊNCIAS

Área de Concentração:

Geologia Econômica e Prospecção

INTERPRETAÇÃO, INVERSÃO 3D DE DADOS MAGNÉTICOS E MODELAGEM 3D DA SUSCEPTIBILIDADE MAGNÉTICA MEDIDA, APLICADAS À PROSPECÇÃO GEOFÍSICA DE DEPÓSITOS DE ÓXIDOS DE FERRO - COBRE - OURO *(IOCG IRON OXIDE-COPPER-GOLD)* – PROVÍNCIA MINERAL DE CARAJÁS, BRASIL

MARCELO HENRIQUE LEÃO SANTOS

Tese de Doutorado N° 117

Orientador: Dr. Roberto Alexandre Vitória de Moraes – Universidade de Brasília

Co-orientadores: *Dr. Yaoguo Li – Colorado School of Mines*

Dr. Misac Nabighian – Colorado School of Mines

Banca Examinadora: Dr. Augusto César Bittencourt Pires – Universidade de Brasília

Dra. Mônica Giannoccaro Von Huelsen – Universidade de Brasília

Dr. Francisco José Fonseca Ferreira – Universidade Federal do Paraná

Dr. Marcelo de Lawrence Bassay Blum – Polícia Federal

Brasília - DF
2014

À Flávia,
Felipe, Mateus
e aos meus pais
Moisés e Telma

AGRADECIMENTOS

Agradeço a todas as pessoas, instituições e empresas que contribuíram para o desenvolvimento deste projeto de pesquisa. Caso ocorra algum esquecimento nos nomes citados perdoem o autor, pois não foi proposital.

- Primeiramente a Deus;

- A minha esposa Flávia e aos meus filhos Felipe e Mateus, pelo eterno amor, parceiros de vida e neste trabalho com a "corrida ao velho oeste" dos Estados Unidos em Golden Colorado;

- Aos meus pais Moisés e Telma, alicerce da minha vida. Aos meus irmãos Andréa e Maurício pela eterna irmandade. E a todos meus familiares;

- Ao Laboratório de Geofísica Aplicada (LGA), ao Instituto de Geociências (IG), a Universidade de Brasília (UnB), a todos os professores e funcionários do IG, as secretárias da pós Alice e Stela;

- Ao meu orientador Roberto Moraes, e aos professores Augusto Pires e Adalene Moreira, pelos ensinamentos, amizade e anos de convívio acadêmico;

- Aos membros da banca examinadora pela contribuição ao trabalho desenvolvido: Professores Dr. Augusto César Bittencourt Pires (UnB), Dra. Mônica Giannoccaro Von Huelsen (UnB), Dr. Francisco José Fonseca Ferreira (UFPR) e Dr. Marcelo de Lawrence Bassay Blum (Polícia Federal). Aos membros da banca examinadora da qualificação do doutorado.

- A todos os meus amigos da graduação e da pós-graduação. A toda comunidade geológica e geofísica. Aos amigos André Spigolon, Bruno Velasco, Edson Toledo, Fabio Mendonça, Fausto Lazarin, Helio Azevedo, Leandro Duarte, Léo Melo, Luciano Cunha, Luciano Teixeira e Lorna Crawford;

- A *Colorado School of Mines (CSM), Center for Gravity, Electrical & Magnetic Studies (CGEM)* e *Gravity and Magnetics Research Consortium (GMRC).* Aos co-orientadores Dr. Yaoguo Li e Dr. Misac Nabighian pelo aprendizado, amizade e oportunidade de viver uma experiência internacional. Aos amigos da *CSM*: Dr. Richard Krahenbuhl, Cericia Martinez, Leon Foks, Jiajia Sun, Dr. Andy Kaas, Camriel Coleman, Mohamed Abdulla, Brent Putman, Jeff Shoffner, Trevor Irons, Anya Reitz, Dr. Magnus Skold, Dr. Marios Karaoulis, Luís Martins, Yaser Kattoum, Conrad Newton, Julio Frigério, Esteban Pantin, Carla Carvajal e Miguel Nassif. Gostaria de fazer um agradecimento especial ao amigo Dr. Dionisio Uendro da Vale S.A. e a amiga professora da *China University of Geosciences* Dra. Shuling Li, parceiros de sala e muitas alegrias durante a temporada na *CSM*;

- A Professora Dra. Maria Irene Bartolomeu Raposo da Universidade da São Paulo (USP), Instituto de Geociências (IGc), Laboratório de Anisotropias Magnéticas e Magnetismo de Rocha, pelos ensinamentos, por orientar nas medidas e pelo uso do laboratório;

- A VALE S.A. – Diretoria de Exploração e Projetos Minerais e Gerência de Exploração Brasil – pela permissão em publicar este trabalho, suporte financeiro para o projeto no Brasil e no exterior, e pela cessão e permissão do uso dos dados geofísicos e geológicos neste projeto de pesquisa. Os agradecimentos são em nome dos funcionários e ex-funcionários da época do início do trabalho há cinco anos: Diretores Márcio Godoy, Fábio Masotti, Eduardo Ledsham e Tracey Keer; Gerentes Fernando Greco, Fernando Matos, Filipe Porto e Noevaldo Teixeira; e amigos Wolney Rosa, Rodrigo Mabub, Denisson Oliveira, Samuel Nunes, Gustavo Queiroz, Rigon, Carlos Medeiros Cacá, Joaquim Nascimento, Messias, Rafael Bueno, Gabriel Araújo, Juliana Araújo, Fernando Paula, Carlos Isaías Kaica, Sérgio Huhn, Edmundo Khoury, Fábio Cuoco, Douglas Zardo, Rogério Caron, Takato, Valdocir, Mariana Oliveira, Alan Freitas, Flávio Freitas, Francisco, Zenha, Saney, Rúbia, Brasileiro, Henrique, Joaniceli, Arlênia, Luiz Neto, Torquato, Robert, Cantão, Michel e Jorge. Aos geólogos Gabriel Paulo e Sálvio Ribeiro pela ajuda nos modelos de minério e gráficos. A equipe dos Recursos Humanos da empresa pelo apoio no período no exterior;

- A equipe Geofísica da VALE S.A. e todos que trabalhei junto por todo o apoio, suporte e divertido convívio. Cantidiano Freitas, Florivaldo Sena, Kiyoshi Kadekaru, Célio Barreira, Alan King, João Paulo, Daniel Brake, Rob Eso, Diogo Carvalho, Aline Silva, Chris Moura, Edvaldo Gomes, Kleiber Ferreira e Leandro Santos. Ao técnico e amigo Joaquim Feijó pelo empenho e critério nas amostragens e medidas petrofísicas, e pela sabedoria em levar a vida. Aos amigos Daniel Brake pelas revisões no inglês e Alan King pelo apoio no início do projeto de pesquisa. E especialmente ao amigo Cantidiano Freitas pelo acompanhamento e participação de toda a Tese;

- Ao Projeto Furnas da VALE S.A. pelos dados e muitas discussões geológicas usadas no estudo, Aos amigos da equipe do projeto: Otávio Rosendo, Arthur Cardoso, Rafael Bueno, Gabriel Paulo, Vicente Pinheiro, Antônio Benvindo, Cris Fianco, Junny Kyley, Maira Santos, Marco Figueiredo, Marcelo Schwarz e Silvio Lopes;

- Ao Departamento de Planejamento e Desenvolvimento de Ferrosos da VALE S.A. – pelo uso de dados magnéticos e pela oportunidade do trabalho de pesquisa no consórcio *Gravity and Magnetics Research Consortium (GMRC),* da *Colorado School of Mines*. As atuais empresas patrocinadoras são: *Anadarko, Bell Geospace, BG Group, BGP, BP, ConocoPhillips, Fugro, Gedex, Lockheed Martin, Marathon Oil, Shell, Petrobras e Vale*. Aos Gerentes Henry Galbiatti e Dr. Marco Antonio Braga, e ao Geofísico Dr. Dionísio Uendro;

- A Fundação CAPES, Coordenação de Aperfeiçoamento de Pessoal de Nível Superior, Ministério da Educação do Brasil, pela concessão da bolsa sanduíche de um ano nos Estados Unidos;

- Ao revisor da *Geophysics* Peter Lelièvre e aos revisores anônimos da *Geophysics* e *Economic Geology* pelos comentários que ajudaram a melhorar os artigos submetidos.

ABSTRACT

Leão-Santos, M.H., 2014, Interpretation, magnetic data 3D inversion and measured magnetic susceptibility 3D modeling, applied to exploration geophysics of iron oxide - copper - gold (IOCG) deposits – Carajás Mineral Province, Brazil: Doctorate thesis, Universidade de Brasília.

This thesis comprises the use of airborne magnetic data and magnetic susceptibility measurements to aid mineral prospecting of iron oxide-copper-gold (IOCG) mineralization within Furnas Southeast deposit, Carajás Mineral Province, Brazil. The susceptibility study allowed the characterization of the calcic-sodic-potassic-magnetite hydrothermal alteration magnetic signatures (biotite-garnet-grunerite-magnetite paragenesis).

The qualitative, semi-quantitative and quantitative interpretations of airborne magnetic data were used in this work aiming to obtain the best possible three-dimensional model (from 3D modeling / inversion) of the magnetic sources, responsible for the measured magnetic signature. A 3D spatial distribution model of the magnetic susceptibility measured on drill cores was also obtained. The aim of the thesis was to define a geophysical-geological prospective model of the iron oxide-copper-gold (IOCG) mineralization. Two ways were used on this purpose: by using 3D modeling / inversion of the measured local magnetic field (indirect method) and by 3D susceptibility measurements modeling (direct method). The results of the two approaches were presented and discussed throughout the thesis.

In strong magnetization environments, it is sometimes difficult to accurately interpret its sources due to the complex role played by induced field, remanent magnetizations and the demagnetization effects. Moreover, in low magnetic latitudes the remanence effect is even more pronounced and the inducing magnetic field is weaker. Carajás region IOCG type deposits are such a case.

The results of the research are described in the thesis body with an introduction of priory geological information and three papers dealing with: the magnetic interpretation (Paper 1) to achieve a 3D inverse model (Paper 2) and a 3D forward model (Paper 3). The purpose is to focus on the main prospecting stages, since the beginning of a greenfield exploration to brownfield and advanced exploration projects using magnetic data.

With respect to the prospecting stages, the approach of the first paper would be that of interpreting magnetic data in greenfield exploration. Following, the second paper describes an approach to reliably recover the distribution of effective magnetic susceptibility using inversion of magnetic data. It can be applied in either greenfield and brownfield exploration. The third paper presents an approach to model the magnetic mineralized zone based on geologic data available from

drill hole cores and on petrophysical measurements taken on core samples. This is the kind of knowledge normally available on advanced exploration project phases.

The results show that the 3D modeling of measured susceptibility data seems to gives a better magnetic source definition and delineation. However, this can only be achieved through systematic, expensive and time consuming measurements and geological interpretation. This approach deals with a huge amount of petrophysical and geological data. On the other hand, the inverse magnetic modeling can be a less time consuming tool with the use of equivalent source and amplitude inversion techniques to reach a good tracking of the magnetic sources.

The proposal of this research was to deal with different approaches on the use of high-density magnetic survey and magnetic physical property measurements on deep drill holes to achieve a better understanding of the Furnas Southeast deposit and identify massive magnetite from hydrothermal alterations associated with the high-grade ore.

Key words: iron oxide - copper - gold (IOCG) deposits, mineral exploration, magnetic susceptibility, 3D magnetic amplitude inversion, 3D geophysical-geological modeling, Carajás Mineral Province - Brazil.

RESUMO

Leão-Santos, M.H., 2014, Interpretação, inversão 3D de dados magnéticos e modelagem 3D da susceptibilidade magnética medida, aplicadas à prospecção geofísica de depósitos de óxidos de ferro - cobre - ouro *(IOCG iron oxide-copper-gold)* – Província Mineral de Carajás, Brasil: Tese de Doutorado, Universidade de Brasília.

Esta Tese compreende o uso de dados magnéticos aéreos e medidas de susceptibilidade magnética para auxiliar na prospecção de mineralizações de óxidos de ferro-cobre-ouro (*iron oxide-copper-gold IOCG*) no depósito Furnas Sudeste, Província Mineral de Carajás, Brasil. O estudo da susceptibilidade permitiu a caracterização das assinaturas magnéticas da alteração hidrotermal calco-sódico-potássica-magnetítica (paragênese biotita-granada-grunerita-magnetita).

As interpretações qualitativa, semi-quantitativa e quantitativa de dados magnéticos foram utilizadas neste trabalho para a obtenção do melhor modelo tridimensional (por modelagem / inversão 3D) das fontes magnéticas responsáveis pela assinatura medida. Também foi obtido o modelo 3D referente à distribuição espacial das susceptibilidades magnéticas medidas em amostras dos testemunhos de furos de sonda. O objetivo da Tese foi definir um modelo geofísico-geológico prospectivo da mineralização de óxidos de ferro-cobre-ouro. Para isso, foram usados dois caminhos: um com a modelagem / inversão 3D dos dados magnéticos medidos no local (método indireto) e outro pela modelagem espacial das susceptibilidades magnéticas medidas (método direto). Os resultados das duas aproximações estão apresentados e encontram-se largamente discutidos.

Em ambientes com forte magnetização, às vezes é difícil interpretar com precisão suas fontes devido ao complexo papel desempenhado pelo campo induzido, magnetização remanescente e os efeitos de desmagnetização. Além disso, em baixas latitudes magnéticas o efeito de remanência é ainda mais pronunciado e o campo magnético induzido é mais fraco. Este é o caso dos depósitos tipo *IOCG* da região de Carajás.

Os resultados da pesquisa estão descritos no corpo da Tese com a introdução da informação geológica e em três artigos que tratam da: interpretação magnética (Artigo 1) para se alcançar um modelo inverso 3D (Artigo 2) e um modelo direto 3D (Artigo 3). O escopo é focar nos principais estágios da prospecção com o uso de dados magnéticos, desde o início da exploração *greenfield* até a exploração *brownfield* e projetos de avaliação de depósitos.

No que diz respeito às etapas de prospecção, a abordagem do primeiro artigo seria a interpretação de dados magnéticos em exploração *greenfield*. Na sequência, o segundo artigo descreve uma abordagem para se recuperar de forma confiável a efetiva distribuição de susceptibilidade com o uso de dados magnéticos. Este enfoque pode ser aplicado tanto na

exploração *greenfield* quanto na *brownfield*. O terceiro artigo lida com uma abordagem para modelar a zona mineralizada magnética com base em dados geológicos de testemunhos de furos de sonda disponíveis e em medidas petrofísicas realizadas em amostras de testemunhos. Este é o tipo de conhecimento normalmente disponível em fases avançadas de projetos de exploração.

Os resultados mostram que a modelagem 3D dos dados de susceptibilidade medidos permite uma melhor definição e delimitação da fonte magnética. Entretanto, isso só pode ser alcançado por meio de descrições geológicas detalhadas e medidas de susceptibilidade sistemáticas, com um grande custo e consumo de tempo. Este enfoque lida com uma grande quantidade de dados petrofísicos e geológicos. Por outro lado, a modelagem de dados magnéticos por inversão pode ser uma ferramenta que consome menos tempo, com o uso das técnicas da camada equivalente e da inversão da amplitude para atingir um bom rastreamento das fontes magnéticas.

A proposta desta pesquisa foi tratar com diferentes abordagens o uso de levantamentos magnéticos de alta densidade de dados e medidas de propriedades físicas magnéticas ao longo de testemunhos de sondagem, para conseguir um melhor entendimento do depósito Furnas Sudeste e identificar magnetita maciça de alterações hidrotermais associadas com minério de alto teor.

Palavras chave: depósitos de óxidos de ferro - cobre - ouro (*IOCG*), exploração mineral, susceptibilidade magnética, inversão 3D dados de amplitude magnética, modelagem geofísico-geológica 3D, Província Mineral de Carajás - Brasil.

SUMÁRIO

SIGLAS E ABREVIAÇÕES

2D	Duas dimensões / *Two-dimensions*
3D	Três dimensões / *Three-dimensions*
AMP	Amplitude magnética / *Magnetic amplitude*
Au	Ouro / *Gold*
BD	*Bacajá Domain*
BIF	Formação ferrífera bandada / *Banded Iron Formation*
°C	Graus Centígrados / *Degrees Celsius*
CAPES	Coordenação de Aperfeiçoamento de Pessoal de Nível Superior, Ministério da Educação do Brasil
CD	*Carajás Domain*
CGEM	*Center for Gravity, Electrical, & Magnetic Studies – Colorado School of Mines*
Cm	Centímetro / *Centimeter*
CMT	Campo Magnético Total
CPRM	Serviço Geológico do Brasil / *Brazilian Geological Service*
CSM	*Colorado School of Mines*
Cu	Cobre / *Copper*
CVRD	Companhia Vale do Rio Doce
DB	Domínio Bacajá
DC	Domínio Carajás
Demag	Desmagnetização / *Demagnetization*
DNPM	Departamento Nacional de Produção Mineral / Brazilian Department of Mineral Production
DOCEGEO	Rio Doce Geologia e Mineração S.A.
DRM	Domínio Rio Maria
DZ	Derivada Vertical / *Vertical Derivative*
E	Leste / *East*
EFC	Estrada de Ferro Carajás / *Carajás Railroad*
EGP	Elementos do Grupo da Platina
Fe	Ferro / *Iron*
FFT	Transformada Rápida de Fourier / *Fast Fourier Transform*
G	Gramas / *Grams*
Ga	Bilhões de anos / *Giga years*
GMRC	*Gravity and Magnetics Research Consortium – Colorado School of Mines*
Gr.	*Greenwich*
HQ	Diâmetro da broca do furo de sonda com 96,4 mm / *Diameter drill bits with 96.4 mm*
IAG	Instituto de Astronomia, Geofísica e Ciências Atmosféricas da Universidade de São Paulo
IAS	Inclinação do Sinal Analítico / *Tilt Derivative or Inclination of Analytic Signal*
ICP-MS	Espectrometria de massa com plasma indutivamente acoplado / *Inductively coupled plasma mass spectrometry*
IG	Instituto de Geociências da Universidade de Brasília
IGc	Instituto de Geociências da Universidade de São Paulo
IGRF	Campo Geomagnético Internacional de Referência */ International Geomagnetic Reference Field*
IOCG	Óxidos de ferro – Cobre – Ouro / *Iron oxide – Copper – Gold*
kHz	kiloHertz
KLY-4S	Susceptibilímetro de Laboratório *Kappabridge* / *Laboratory Susceptibility meter Kappabridge*
Km	Quilômetro / *Kilometer*
KT-9	Susceptibilímetro modelo KT-9 / *Susceptibility meter KT-9 model*
KT-10	Susceptibilímetro modelo KT-10 / *Susceptibility meter KT-10 model*
LGA	Laboratório de Geofísica Aplicada da Universidade de Brasília

LiDAR	Tecnologia de sensoriamento remoto / *Remote sensing technology (Light Detection And Ranging)*
M	Metro/ *Meters*
Ma	Milhões de anos / *Million years*
Mag	Magnetometria / *Magnetometry*
Mm	Milímetros / *Milimeters*
MMA	*Magnetic Magnitude Anomaly*
Mn	Manganês / *Manganese*
MPP-EM2S	Susceptibilímetro modelo MPP-EM2S / *Susceptibility meter* MPP-EM2S *model*
MS	*Magnetic susceptibility*
N	Norte / *North*
Nd	Neodímio / *Neodymium*
NE	Nordeste / *Northeast*
Ni	Níquel / *Nickel*
NQ	Diâmetro da broca do furo de sonda com 76,2 mm / *Diameter drill bits with 76.2 mm*
nT	NanoTesla
nT/m	NanoTesla por metro / *NanoTesla per meter*
NW	Noroeste / *Northwest*
O	Oxigênio / *Oxygen*
P	Grau de Anisotropia / *Anisotropy Degree*
PA	Estado do Pará / *Pará State*
Pb	Chumbo / *Lead*
PGE	*Platinoid Group Elements*
PGRV	Pseudo-gravimetria / *Pseudo-gravity*
Rad	Radiano / *Radian*
Rb	Rubídio / *Rubidium*
Rem	Remanência / *Remanence*
RMD	*Rio Maria Domain*
RTP	Redução ao Pólo / *Reducing to the Pole*
S	Segundos / *Seconds*
S	Sul / *South*
SE	Sudoeste / *Southeast*
SI	Sistema Internacional de Unidades / *International System of Units*
SIG	Sistema de Informações Geográficas / *Geographic Information System*
Sm	Samário / *Samarium*
SM	Susceptibilidade magnética
Sr	Estrôncio / *Strontium*
SW	Sudoeste / Southwest
T	Tonelada / *Tons*
TER	Terraceamento / *Terracing*
TG	Gradiente Total ou Sinal Analítico / *Total Gradient or Analytic Signal*
TG3D	Gradiente Total em 3D / *Total Gradient in 3D*
THG	Gradiente Horizontal Total / *Total Horizontal Gradient*
TMI	*Total Magnetic Intensity*
TTG	Tonalito-Trondhjemito-Granodiorito / *Tonalite-Trondhjemite-Granodiorite*
U	Urânio / *Uranium*
UFPR	Universidade Federal do Paraná
UnB	Universidade de Brasília
USP	Universidade de São Paulo
W	Oeste / *West*
%	Porcentagem / *Percentage*
B	Parâmetro de regularização / *Regularization Parameter*

LISTA DE FIGURAS

LISTA DE TABELAS

CAPÍTULO 1

INTRODUÇÃO

1.1 - CARACTERIZAÇÃO DOS PROBLEMAS

A interpretação de dados geofísicos e geológicos para a geração de alvos em ambientes computacionais tem superado muito a capacidade do cérebro humano para analisar quantitativamente grande volume de dados referenciados espacialmente. Entretanto, o cérebro humano ainda é superior para computar, com seu grande número de unidades de cálculo (neurônios) e interconexões (sinapses), que levam a um melhor desempenho do que computadores convencionais (Zaknich, 2003).

Os principais desafios encontrados neste projeto de pesquisa foram divididos em geológicos, geofísicos e prospectivos (Figura 1.1). Sistemas de forte alteração hidrotermal modificam as propriedades físicas das rochas em depósitos *IOCG*. A espessa zona de intemperismo encontrada na região amazônica dificulta o mapeamento geológico e a localização de ocorrências minerais. Além do intemperismo o terreno acidentado também deve ser levado em consideração na inversão e modelagem de dados geofísicos.

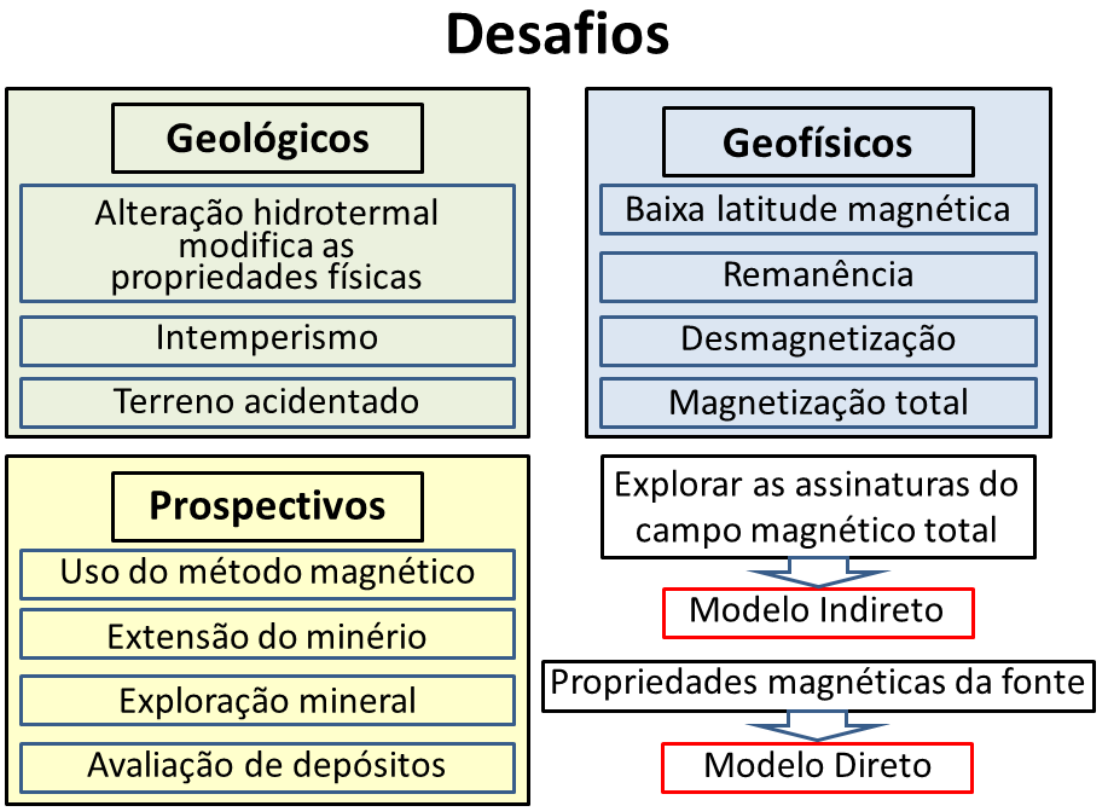

Figura 1.1. Desafios geológicos, geofísicos e prospectivos encontrados no projeto de pesquisa.

Existem diversas técnicas matemáticas e estatísticas disponíveis para processamento, inversão e modelagem de dados geofísicos magnéticos. Entretanto, fazer o uso efetivo destas técnicas é um desafio. A correta aplicação das técnicas disponíveis está correlacionada a informações apriorísticas, essencial para o sucesso em termos de objetivos exploracionistas.

A interpretação em mapas, seções e perfis utiliza diversas técnicas e produtos transformados que ajudam na localização e na estimativa das profundidades das fontes causadores das assinaturas magnéticas observáveis. Modelagens em duas dimensões ajudam a dar forma a estas fontes magnéticas. Para solucionar estes problemas, foram utilizados dados de levantamentos magnéticos aerotransportados de alta resolução para cálculo dos produtos com algoritmos especializados.

Em ambientes de campos magnéticos anômalos fortes, localizados em baixas latitudes, às vezes fica difícil fazer uma interpretação quantitativa precisa e geologicamente válida, especialmente com modelos tridimensionais em termos das assinaturas magnéticas mapeadas, devido ao complexo papel desempenhado pelo campo magnético resultante. O estudo das magnetizações atual (induzida) e pretérita (remanescente) e dos efeitos da desmagnetização ajuda a entender as mudanças na direção de magnetização do corpo e das diferentes assinaturas que aparecem relacionadas a um mesmo conjunto de fontes que formam um corpo mineralizado. Estas dificuldades estão bem retratadas em ambientes como o constituído pela mineralização em óxidos de ferro e sulfetos de cobre tipo IOCG como o encontrado no depósito Furnas.

Para solucionar este problema, foram utilizados processos de otimização, de camada equivalente e algoritmos de inversão 3D da amplitude da anomalia magnética de dados aéreos de alta resolução.

As medidas de susceptibilidade magnética, realizadas em testemunhos de furos de sonda podem ser utilizadas como informação *a priori* para diferenciar os litotipos e as zonas de alteração hidrotermal em mineralizações IOCG. O volume de dados adquiridos nesta aproximação torna esta uma atividade complexa, que se não for complementada por um entendimento das limitações dos equipamentos, dos corretos controles de qualidade, de análises estatísticas, não permite que se chegue a uma interpretação e modelagem confiável. No caso em foco os dados utilizados para contornar estes problemas foram: medidas de susceptibilidade magnética tomadas com critério e sob estrito controle de qualidade; descrição geológica e das alterações hidrotermais; medidas complementares de densidade; e resultados de análises geoquímicas para ferro, cobre e ouro nos testemunhos dos furos de sonda.

1.2 - ESTADO DA ARTE

A prospecção mineral envolve a aplicação de uma variedade de técnicas geocientíficas para a descoberta de um depósito. A integração dos resultados de métodos e técnicas da geofísica com a geologia é uma ferramenta poderosa para o sucesso de seus usos na exploração mineral. Neste trabalho, dados sobre o comportamento da intensidade do campo magnético total (CMT ou TMI) foram empregados desde a geração de temas transformados (filtragens no domínio de Fourier), até a modelagem e inversão dos dados aéreos em 2D e 3D. Além disso, foi realizada a análise de medidas de susceptibilidade e da geologia dos litotipos que formam tanto a mineralização na zona de alteração hidrotermal como em suas encaixantes. Todos estes métodos e técnicas aplicados mostram o estado da arte do conhecimento nestas áreas aqui desenvolvidas com foco na pesquisa mineral. Tudo foi apoiado em *hardware* (equipamentos de informática, equipamentos geofísicos – susceptibilímetros manuais e de laboratório); em *softwares* (algoritmos); e em dados magnéticos (levantamentos geofísicos); que são o que existe de mais moderno na tecnologia disponível no mercado atual.

1.3 - FOCO DOS RESULTADOS

O conhecimento de como as propriedades físicas e de magnetismo de rocha variavam, e de assinaturas específicas ligadas à mineralização e suas encaixantes tiveram papel fundamental para se entender o comportamento da magnetização do corpo. Os estudos feitos ajudaram inclusive na definição de modelos prospectivos para o corpo de minério no depósito Furnas Sudeste, na Província Mineral de Carajás, Pará, Brasil.

Ultimamente, o uso da modelagem de dados geofísicos assistida por técnicas de minimização controlada de erros (inversão) em duas e três dimensões constitui instrumento eficiente para ajudar o geocientista em aumentar a chance de fazer uma melhor interpretação e identificar zonas mineralizadas. O uso destas técnicas, correlacionadas com a geologia, geoquímica, geologia estrutural e outras informações geocientíficas, ampliam o êxito na pesquisa por minério.

Todas estas aproximações foram usadas na tentativa de produzir modelos bi e tridimensionais do corpo de minério. Conseguiu-se assim, obtê-lo via a interpretação e inversão dos dados magnéticos de alta resolução disponíveis, e via a modelagem espacial dos resultados das medidas de susceptibilidade magnética feitas em testemunhos de sondagens disponíveis.

Todo o conjunto de informações geológicas obtidos nos estudos de campo e das amostras de testemunhos de sondagens foi utilizado como suporte às aproximações geofísicas usadas – modelagem de dados magnéticos e modelagem de dados espacialmente distribuídos das

susceptibilidades magnéticas. Isto foi possível pela excelente cobertura de dados geocientíficos geradas sobre o lineamento Cinzento na região de Carajás em suas diversas fases de estudo.

Este trabalho enfoca justamente modos de se chegar a este modelo pelos dois caminhos mencionados, de forma a simplificar e acrescentar muito mais informações sobre o modelo gerado. Pode servir de guia em estudos sobre alvos semelhantes não só no Brasil mais em outros lugares do mundo em ambientes metalogenéticos similares.

O escopo da tese foi o de explorar as potencialidades advindas das medições da intensidade do campo magnético terrestre, com a aplicação do método com foco na prospecção da mineralização de óxidos de ferro-cobre-ouro IOCG. Os três artigos preparados e que constituem o corpo da tese em questão (submetidos para publicação) têm objetivos específicos, que se complementam para atingir o escopo descrito acima, como resultado final.

1.4 - METODOLOGIA

Foram utilizados diversos métodos e técnicas durante as várias fases do projeto de pesquisa. Estas fases podem ser divididas em quatro etapas que se complementam com o objetivo de definir uma metodologia final de pesquisa. Todas as etapas tiveram o acompanhamento e orientação do Professor Roberto Alexandre Vitória de Moraes da Universidade de Brasília. Uma grande parte da base de dados foi cedida pela Vale S.A., a outra parte dos dados foi coletada e analisada pelo trabalho de pesquisa nos testemunhos em campo e no laboratório da Universidade de São Paulo.

Na primeira etapa foi realizada a compilação bibliográfica; a caracterização e a sistematização da base de dados geofísico-geológica; e o estudo da geologia regional, da geologia do depósito e da mineralização IOCG. A base bibliográfica foi obtida na internet, de resumos expandidos de congressos, publicações em revistas, trabalhos acadêmicos, e relatórios internos do Projeto Furnas da Vale S.A..

Na segunda etapa foram utilizados diversos algoritmos computacionais com técnicas e métodos de processamento de dados magnetométricos aéreos, como o controle de qualidade dos dados; interpolações para a geração de malhas regulares; testes de eficácia deste processo; homogeneização da representação espacial destes dados com técnicas de decorrugação, de modo a conseguir a melhor imagem do campo magnético local para o depósito em estudo.

Posteriormente, foram geradas as transformações lineares com temas para ajudar na interpretação qualitativa da imagem do campo magnético obtido. Finalmente, foram realizadas interpretações semiquantitativas e quantitativas em duas dimensões para definir o melhor ajuste entre o dado e o corpo resultante com o uso de informações empíricas *a priori*. Diversos programas de Sistemas de Informações Geográficas, processamento, estimativa de profundidade e modelagem

2D de dados foi utilizada. Este trabalho contou com a orientação dos Professores Dr. Roberto Alexandre Vitória de Moraes da Universidade de Brasília e Dr. Misac Nabighian da *Colorado School of Mines*.

Na terceira etapa, foram utilizados algoritmos computacionais com capacidade de inversão do campo magnético para estruturas tridimensionais complexas do depósito Furnas Sudeste, com a seleção dos parâmetros de otimização e delimitação da profundidade de suas fontes geradoras. Como resultado, foi recuperado de forma eficaz o modelo tridimensional do corpo magnético. A interpretação do modelo magnético final foi correlacionada com os dados geológicos e estruturais em Sistemas de Informações Geográficas 2D e 3D. Os algoritmos utilizados foram desenvolvidos pelo *Center for Gravity, Electrical & Magnetic Studies, Colorado School of Mines*. Esta pesquisa foi realizada na *Colorado School of Mines*, localizada em *Golden*, Colorado, Estados Unidos, como doutorado sanduíche com período de um ano, suporte do *Gravity and Magnetics Research Consortium (GMRC)* e orientação do Professor Dr. Yaoguo Li. Esta etapa teve apoio financeiro da Vale S.A. e concessão de bolsa sanduíche da Fundação CAPES, Coordenação de Aperfeiçoamento de Pessoal de Nível Superior, Ministério da Educação do Brasil.

Na quarta etapa foi utilizada a propriedade da susceptibilidade magnética para realizar medidas sistemáticas e contínuas ao longo da maioria dos testemunhos de sondagens existentes na área. Posteriormente foi realizada a análise estatística dos dados para caracterizar a assinatura magnética dos litotipos e das alterações hidrotermais e a associação da mineralização com a magnetita. Finalmente, os dados foram integrados em um programa para a geração de *logs* dos furos de sonda, para a modelagem do corpo com alta susceptibilidade em três dimensões, e para estudar o comportamento magnético do corpo.

Os dados de susceptibilidade magnética, geologia e análises geoquímicas de ferro, cobre e ouro, foram levantados pelo Projeto Furnas da Vale S.A.. Os testes de medidas com métodos e susceptibilímetros diferentes foram realizados pela equipe deste projeto de pesquisa. Também foram realizadas análises de susceptibilidade e do grau de anisotropia no Laboratório de Anisotropias Magnéticas e de Magnetismo de Rocha, do Instituto de Geociências, da Universidade de São Paulo. As amostras e espécimes foram coletados e analisados pela equipe do projeto de pesquisa. Esta pesquisa contou com a orientação do Professor Dr. Roberto Alexandre Vitória de Moraes da Universidade de Brasília e da Professora Dra. Maria Irene Bartolomeu Raposo da Universidade de São Paulo. Este trabalho também teve a participação dos geólogos Otávio Rosendo e Arthur Cardoso na descrição e revisão do texto da geologia; e do técnico Joaquim Feijó na amostragem e análises petrofísicas, todos da empresa Vale S.A..

O uso das diversas metodologias tanto de forma isolada como complementares constituem ferramentas que podem ser utilizadas diretamente nas diferentes fases da pesquisa mineral de depósitos associados a minerais ferromagnéticos. Essas metodologias são úteis tanto para resolver questões relacionadas a depósitos de minerais magnéticos, como também outros tipos de depósitos com a mineralização de interesse associada a minerais magnéticos.

1.5 - RESULTADOS ATINGIDOS

- Consolidação do banco de dados geológico e geofísico;
- Geologia regional e do depósito;
- Geração dos Sistemas de Informações Geográficas (SIG) 2D/3D;
- Especificações, controle de qualidade, processamento e geração de imagens transformadas dos dados de levantamentos geofísicos de magnetometria aérea de alta resolução;
- Interpretação qualitativa, semiquantitativa e quantitativa do campo magnético para definir a fonte magnética, e obter o melhor ajuste entre o sinal obtido e a forma do corpo;
- Seleção dos parâmetros de otimização para a inversão dos dados;
- Inversão da amplitude magnética com o uso de camada equivalente para a geração do modelo 3D do depósito Furnas Sudeste;
- Método para levantamentos de medidas de susceptibilidade magnética;
- Seleção, descrição e preparação de amostras para análises petrofísicas;
- Medidas de susceptibilidade magnética sistemáticas nos testemunhos de furos de sonda e em laboratório, para a geração de um modelo 3D de susceptibilidade;
- Caracterização das assinaturas de susceptibilidade magnética dos litotipos e das zonas de alteração hidrotermal;
- Interpretação do modelo magnético e integração com os dados geológicos e estruturais, para definir as assinaturas prospectivas para depósitos do tipo IOCG.

1.6 - ESTRUTURA DA TESE

CAPÍTULOS

1. **INTRODUÇÃO DA TESE**
2. **GEOLOGIA REGIONAL**

3. ***MAGNETIC INTERPRETATION AND 2D MODELING AT AN IRON OXIDE–COPPER–GOLD DEPOSIT, CARAJÁS MINERAL PROVINCE, BRAZIL***
   Marcelo Leão-Santos[1,2,4]*, and Roberto Moraes[1]

4. ***APPLICATION OF 3D MAGNETIC AMPLITUDE INVERSION TO IRON OXIDE–COPPER–GOLD DEPOSITS AT LOW MAGNETIC LATITUDES: A CASE STUDY FROM CARAJÁS MINERAL PROVINCE, BRAZIL***
   Marcelo Leão-Santos[1,2,4*], Yaoguo Li[2], and Roberto Moraes[1]

5. ***MAGNETIC SUSCEPTIBILITY 3D MODEL AND SIGNATURES OF IRON OXIDE-COPPER-GOLD (IOCG) MINERALIZATION: A CASE STUDY FROM CARAJÁS MINERAL PROVINCE, BRAZIL***
   Marcelo Leão-Santos[1,2,4*], Roberto Moraes[1], Maria Irene Raposo[3], Otávio Rosendo[4], Arthur Cardoso[4], and Joaquim Feijó[4]

6. **CONCLUSÕES DA TESE**

[1] Universidade de Brasília, Instituto de Geociências, Campus Universitário Darcy Ribeiro ICC, Ala Central, Brasília, DF, 70910-900, marcelo.leao.santos@gmail.com, rmoraes@unb.br

[2] Colorado School of Mines, Center for Gravity, Electrical & Magnetic Studies, 1500 Illinois St., Golden, CO, 80401, ygli@mines.edu , mnabighi@mines.edu

[3] Universidade de São Paulo, Instituto de Geociências, Rua do Lago, 562, Cidade Universitária, São Paulo, SP, 05508-080, irene@usp.br

[4] VALE S.A., Av. Getúlio Vargas, 671, 13º andar, Funcionários, Belo Horizonte, MG, 30112-020, marcelo.leao@vale.com, otavio.rosendo@vale.com, arthur.cardoso@vale.com, joaquim.feijo@vale.com

1.7 - DIAGRAMA DOS TRABALHOS DESENVOLVIDOS NA TESE

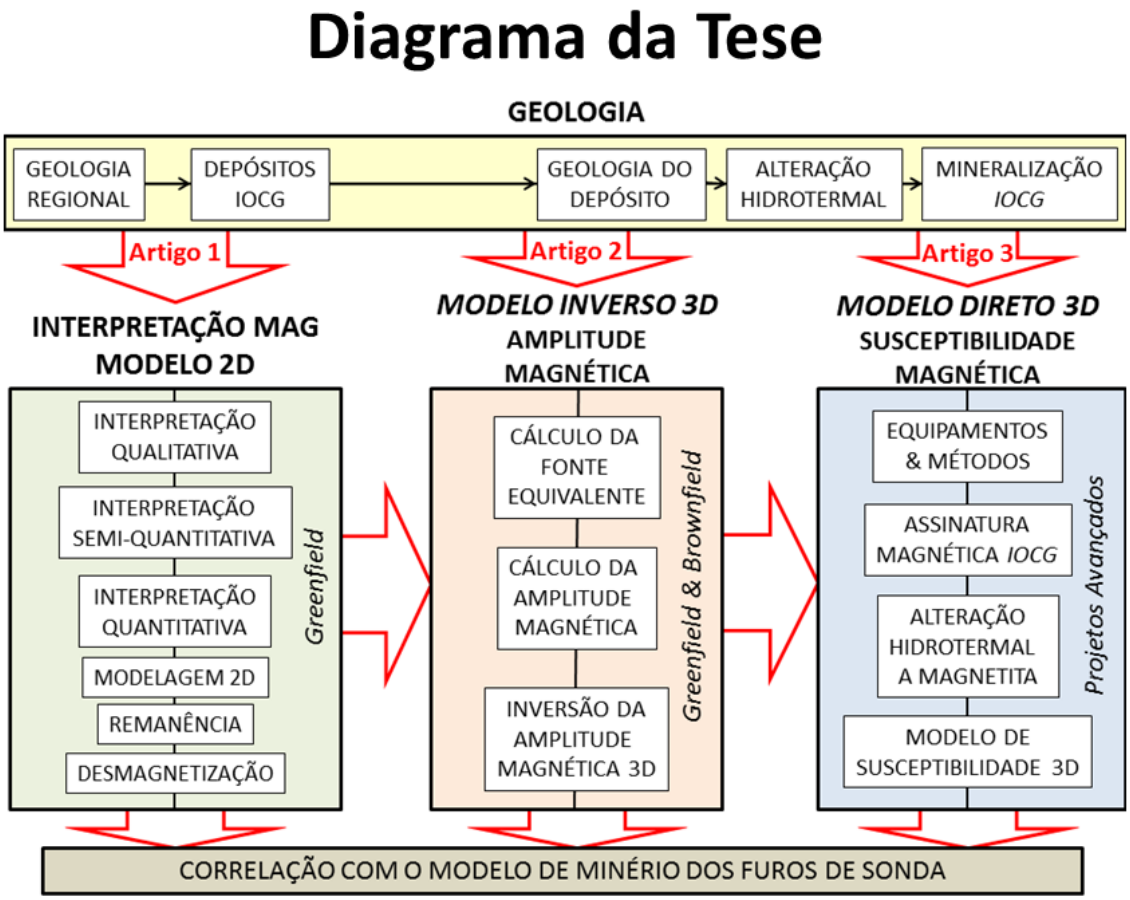

1.8 - REFERÊNCIA

A. Zaknich, 2003, Neural Networks for Intelligent Signal Processing: World Scientific, Singapore, 484.

CAPÍTULO 2

GEOLOGIA REGIONAL

Neste capítulo é abordado o arcabouço conceitual geológico referente à Província Mineral de Carajás com destaque para o Supergrupo Itacaiúnas, no qual o depósito Furnas está inserido.

Com base no contexto geotectônico, a Província de Carajás está localizada no Escudo do Brasil Central e inserida na porção sudeste da Província Amazonas Central, limitada pela Província Transamazônica (Maroni-Itacaiúnas), a norte, e pela Faixa Araguaia, a leste, conforme mostra a Figura 2.1 (Santos et al., 2000).

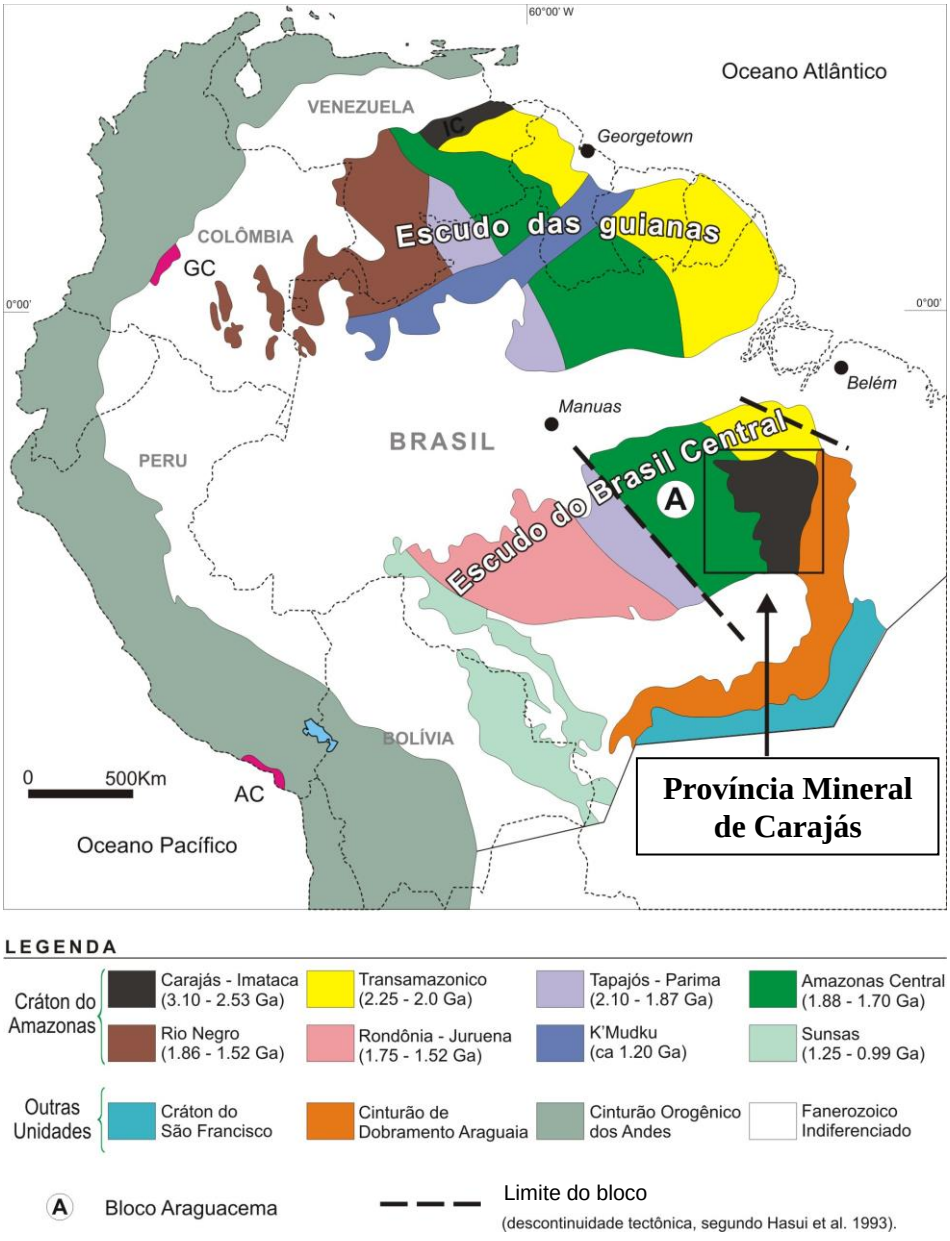

Figura 2.1. Compartimentação tectônica do Cráton Amazônico (Modificado de Santos et al., 2000).

A litoestratigrafia proposta para a Província Mineral de Carajás (Figura 2.2) é definida por diversas unidades pré-cambrianas e agrupadas por suas características em: embasamento cristalino mesoarqueano, denominados Complexos Xingu (granitóides de associação TTG - tonalito-trondhjemito-granodiorito) e Pium (rochas granulíticas); e sequências metavulcanossedimentares do tipo greenstone belt. Além dessas, foram distinguidos os granitos neoarqueanos denominados Suíte Plaquê (rochas graníticas); e as sequências metassedimentares e metavulcanossedimentares neoarqueanas, as quais constituem o Supergrupo Itacaiúnas. Outra unidade definida foram os granitóides anorogênicos, representados por plútons graníticos com idades relacionadas ao proterozoico inferior/médio. Estas intrusões cortam todas as unidades do Supergrupo Itacaiúnas, bem como as rochas da Formação Águas Claras. Finalmente, foram definidas as unidades das coberturas fanerozoicas, correlacionáveis ao Grupo Serra Grande (DOCEGEO, 1988; Araújo e Maia, 1991; Barros e Barbey, 1998; Vasquez et al., 2008).

O depósito Furnas Sudeste está inserido no contexto de rochas metavulcanossedimentares do Supergrupo Itacaiúnas (2.76 Ga; Wirth et al., 1986), rochas sedimentares da Formação Águas Claras, granito anorogênico Cigano (1,8 Ga) e coberturas fanerozoicas (Figura 2.2). Na porção noroeste do depósito Furnas, fora da área de estudo, ocorrem rochas granitóides do embasamento que foram informalmente denominadas de Granito Furnas. Este granito possui características petrológicas similares aos granitóides do fácies hornblenda-biotita monzogranito do Stock Granítico Geladinho, com idade de 2.688 ± 11 Ma (Pb-Pb por evaporação de zircão; Barbosa et al., 2001).

Do ponto de vista metalogenético, essa província mineral constitui uma das mais bem estudadas regiões do Cráton Amazônico que engloba importantes depósitos de Fe, Cu, Au, Ni, Mn e elementos do grupo da platina (EGP).

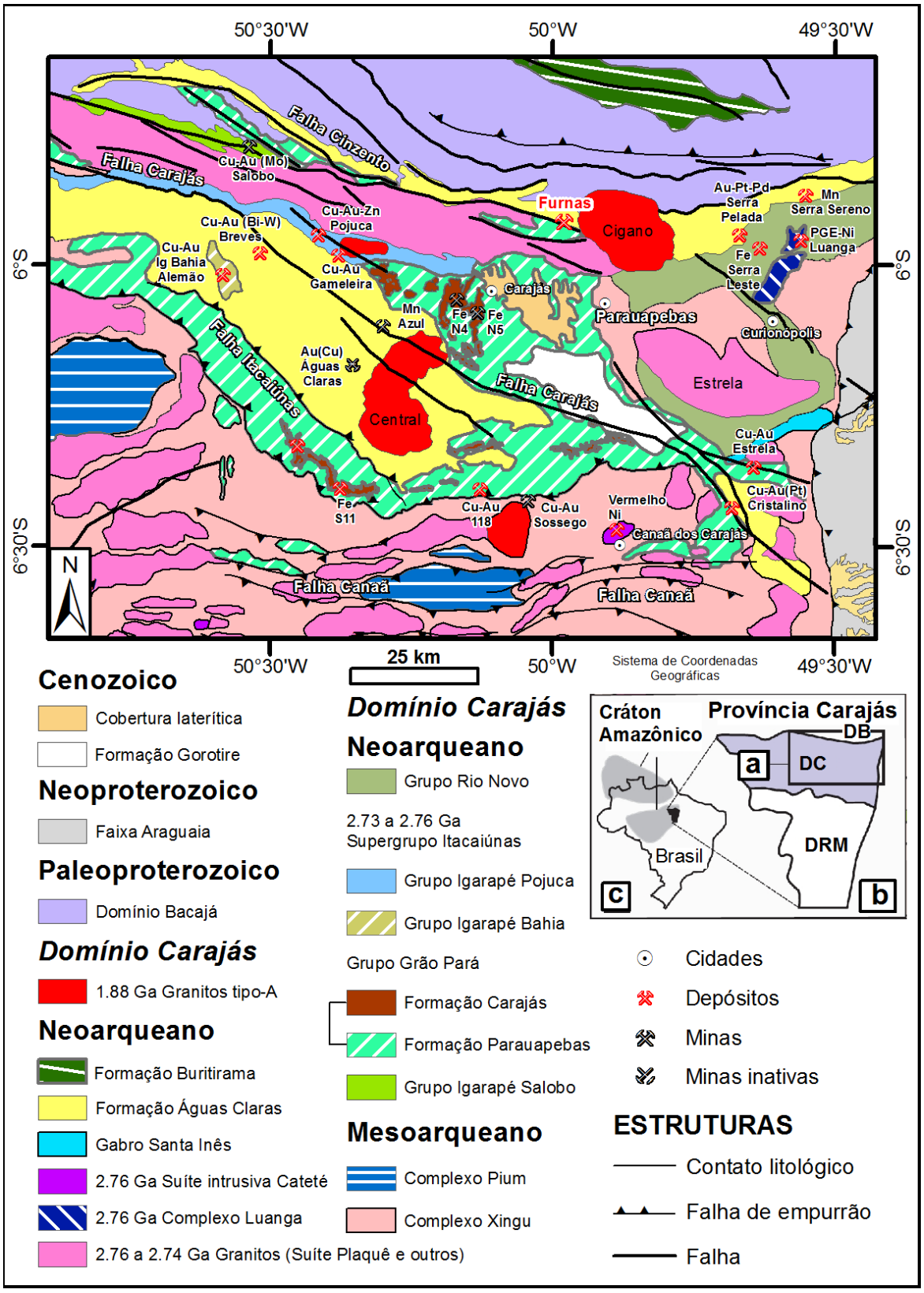

Figura 2.2. (a) Mapa geológico da Província Mineral de Carajás com a localização do depósito Furnas e dos principais depósitos de Fe, Cu-Au, Mn, Ni e elementos do grupo da Pt (EGP). (b) Mapa da Província Carajás com o Domínio Carajás (DC) e o Domínio Rio Maria (DRM). O Domínio Bacajá (DB) está localizado a norte do Domínio Carajás. (c) Mapa do Brasil com a localização da Província Carajás (em preto) e o Craton Amazônico (em cinza) (Modificado de DOCEGEO, 1988; Araújo e Maia, 1991; Barros e Barbey, 1998; Vasquez et al., 2008; e Xavier et. al., 2012).

2.1 - ESTRATIGRAFIA

A Província Mineral de Carajás é alvo de intenso debate que se reflete nas inúmeras colunas estratigráficas que foram e são propostas, à medida que novos dados são obtidos. A síntese do conhecimento regional acumulado nas décadas de 60 e 70 levou Hirata et al. (1982) a proporem uma coluna estratigráfica informal para a região.

De modo a facilitar o entendimento da evolução geológica da região e uniformizar a nomenclatura para as unidades definidas, foi proposta uma coluna litoestratigráfica pela equipe do Distrito Amazônia da DOCEGEO, elaborada a partir dos dados acumulados pela empresa desde 1974, somados aos resultados de trabalhos desenvolvidos por outras empresas e instituições de pesquisas (DOCEGEO, 1988), conforme Tabela 2.1.

Tabela 2.1. Coluna estratigráfica da Província de Carajás (Modificada de DOCEGEO, 1988; Villas e Santos, 2001).

ÉON	Idade (Ga)	Cinturão de Cisalhamento Itacaiúnas		
		Complexos, Supergrupos ou Unidades	Grupos (Gr) ou Formações (Fm)	Rochas Intrusivas
PROTEROZOICO	1,8	Granitos tipo-A		Granitos anorogênicos (Central Carajás, Cigano, Pojuca, Breves, Young Salobo, etc)
ARQUEANO	2,6		Fm. Aguas Claras/ Gr Rio Fresco	
	2,7			Sills e diques básicos, metagabros
	2,5 - 2,7	Granitos neoarqueanos		Suíte Plaquê, Old Salobo, Itacaiúnas, Estrela, Planalto, Pedra Branca, Igarapé Gelado, etc
	2,76	Supergrupo Itacaiúnas	Gr Buritirama	
			Gr Igarapé Bahia	
			Gr Grão Pará	
			Gr Ig, Pojuca	
			Gr Ig. Salobo	
	2,76	Complexo Luanga		Intrusão acamadada máfica-ultramáfica
	2,8 – 3,0	Complexo Xingu		Granitóides mesoarqueanos
	3,0	Complexo Pium (Granulitos)		

Trabalhos como os de Lindenmayer (1990), Araújo e Maia (1991), Costa et al. (1993), Barros (1997), Barros et al. (1995), e Pinheiro e Holdsworth (1995), deram atenção ao entendimento do quadro geológico regional da Serra dos Carajás.

Na década passada e trabalhos mais recentes têm dado ênfase à evolução tectonoestratigráfica, petrogênese, metalogênese e, principalmente, a geocronologia das rochas da Província Mineral de Carajás (p.e. Pinheiro e Holdsworth, 2000; Althoff et al., 2000; Pidgeon et al. 2000; Leite, 2001; Barros et al., 2001; Macambira et al., 2001; Barbosa et al., 2001; Villas e Santos, 2001; Tallarico et al., 2005; Monteiro et al., 2008; Feio, 2011; Moreto et al., 2012; Xavier et al. 2012; entre outros).

2.2 - UNIDADES LITOLÓGICAS

As principais unidades litoestratigráficas que ocorrem na região da área em estudo e arredores estão sintetizadas adiante e podem ser observadas no mapa geológico regional apresentado na Figura 2.2.

2.2.1 - Embasamento – Complexos Xingu e Pium

O termo Complexo Xingu foi sugerido originalmente por Silva et al. (1974), com referência às rochas infracrustais encontradas em praticamente todo o Cráton Amazônico. O Complexo Xingu é formado principalmente por gnaisses bandados/foliados de composição tonalítica à granodiorítica, além de anfibolitos e migmatitos. Essas rochas foram datadas em 2.856 ± 2 Ma por Machado et al. (1991), através do método U-Pb, em zircões provenientes de gnaisses. Outras datações também realizadas por Machado et al. (1991), tem idade 2.519 ± 5 Ma em anfibolito (U-Pb em titanitas), 2.859 ± 2 Ma e 2.860 ± 2 Ma em leucosomas graníticos (U-Pb em zircões) e 2.851 ± 2 Ma em gnaisses félsicos (U-Pb em zircões). Avelar et al. (1999) dataram ortognaisses granodioríticos em 2.974 ± 15 Ma (Pb-Pb em zircões). A derivação dessas rochas tem sido atribuída em parte ao retrabalho de granitóides dos terrenos granito - greenstone (vide abaixo), particularmente às rochas anfibolíticas e migmatíticas (Araújo et al., 1988; Costa et al., 1995).

Trabalhos mais recentes têm individualizado os granitóides mesoarqueanos. O granitóide Rio Verde teve sua primeira datação realizada por Sardinha et al. (2004) em leucomonzogranitos com 2.928 ± 1 Ma (Pb-Pb em zircões), posteriormente Feio (2011) datou throndjemito em 2.923 ± 15 Ma (Pb-Pb em zircões). O granito Serra Dourada foi datado por Moreto et al. (2011a) em 2.860 ± 22 Ma (U-Pb em zircões) e por Feio (2011) em 2.831 ± 6 Ma (U-Pb em zircões). O granito Canaã dos Carajás foi datado por Feio (2011) em 2.959 ± 6 Ma (U-Pb em zircões). O tonalito Bacaba foi datado por Moreto et al. (2011a) em 3.001 ± 3,6 Ma e 3.004 ± 9 Ma (U-Pb em zircões). O granito Sequeirinho foi datado por Moreto et al. (2011a) em 3.010 ± 21 Ma (U-Pb em zircões).

O Complexo Pium compreende rochas granulíticas de composições variadas: ortoderivadas, tipo charnockitos/enderbitos; e paraderivadas, tais como gnaisses kinzigíticos (Costa e Hasuí, 1996). Araújo e Maia (1991) admitem que, em geral, as rochas deste complexo estão em contato concordante com os gnaisses do Complexo Xingu, e são marcados por importantes zonas de cisalhamento dúcteis. Rodrigues et al. (1992), com base no método Pb-Pb em rocha total, obtiveram idades para essa unidade de 3.050 ± 114 Ma. Pidgeon et al. (2000) obtiveram duas idades pelo método U-Pb (SHRIMP), uma de 3.002 ± 14 Ma (cristalização do protólito ígneo do granulito), valores estes quase correspondentes àquela obtida por Rodrigues et al. (1992), e uma outra mais nova, de 2.859 ± 9 Ma, que deve corresponder ao metamorfismo de fácies granulito. Localmente,

ocorrem rochas básicas e ultrabásicas estratificadas (Hirata et al., 1982), expostas em lentes orientadas na direção E-W, principalmente na borda Sul do Sistema Transcorrente Carajás.

2.2.2 - Granitos neoarqueanos - Suíte Plaquê

A Suíte Plaquê, definida por Araújo et al. (1988), corresponde ao grupo de granitóides aflorantes em lentes com direção geral E-W, concordantes com as rochas do Complexo Xingu (Araújo et al., 1991). Esta unidade tem idade com base no método Pb-Pb em torno de 2.727 ± 29 Ma (Avelar, 1996) e 2.736 ± 24 Ma (Avelar et al., 1999). Um exemplo desse tipo de granito é o Granito Planalto (2.747 ± 2 Ma, Pb-Pb em zircão; Huhn et al., 1999) que aflora nas adjacências da Serra do Rabo. Este granito também foi datado por Feio (2011) com idade 2.733 ± 2 Ma, Pb-Pb em zircão.

Diversos trabalhos têm individualizado os granitos neooarqueanos. O granito Old Salobo, localizado nas adjacências da área do Igarapé Salobo (Lindnmayer e Fyfe, 1991; Lindenmayer et al., 1994) tem idade em torno de 2.573 ± 3 Ma (U-Pb em zircão; Machado et al., 1991). O granito Itacaiúnas com rochas dacíticas a riolíticas foi datado em 2.525 Ma ± 38 (Pb-Pb em zircão; Souza et al., 1996), 2.645 Ma ± 9 e 2.654 Ma ± 9 (SHRIMP U-Pb em zircão; Tallarico, 2003). O granito Rancho Alegre (Pinheiro, 1997) foi datado em 2.743 Ma (U-Pb zircão; Sardinha et al., 2001). O stock granítico Geladinho foi datado em 2.688 ± 11 Ma (Pb-Pb por evaporação de zircão; Barbosa et al., 2001), este granito também denominado Igarapé Gelado foi datado por Barbosa (2004) em 2.731 Ma ± 26 (Pb-Pb em zircão). O Complexo granítico Estrela (Barros, 1997) que aflora na porção leste da região de Carajás, foi datado por Rb-Sr em 2.527 ± 34 Ma (Barros et al, 1992), posteriormente foi datado em 2.763 ± 7 Ma, por Pb-Pb em zircão (Barros et al, 2004), 2.734 ± 4 Ma por Pb-Pb em zircão de biotita-hornblenda granito e 2.765 ± 39 Ma, por U-Pb em zircão de throndjemito (Sardinha et al, 2004). O diorito Cristalino foi datado por Huhn et al. (1999) em 2.738 ± 6 Ma por Pb-Pb em zircão. A Suite Pedra Branca foi datada em 2.750 ± 5 Ma por U-Pb em zircão (Feio, 2011). O granito granofírico do Sossego foi datado por Moreto et al. (2011b) em 2.740 ± 26 Ma por U-Pb em zircão.

Anteriormente, muitos desses granitos e granitóides meso a neoarqueanos estavam indiferenciados no Complexo Xingu, a partir de estudos detalhados de suas relações de contato e de suas idades, passaram a ser individualizados e ganharam nomes e posições estratigráficas próprias.

Os stocks graníticos do Geladinho subdividem-se em dez fácies petrográficas: hornblenda tonalitos, biotita-hornblenda granodioritos, hornblenda-biotita granodioritos, biotita granodioritos, hornblenda monzogranitos, biotita-hornblenda monzogranitos, hornblenda-biotita monzogranitos, biotita monzogranitos, leuco monzogranitos, leuco sienogranitos e veios pegmatóides (Barbosa,

2004). O granitóide de fácies hornblenda-biotita monzogranito se assemelha com as rochas graníticas do depósito Furnas, que foi denominado informalmente como Granito Furnas. O Granito Furnas aflora nas adjacências do depósito, compreendem rochas de composição monzogranítica, coloração cinza, granulação fina a média, constituída por quartzo, plagioclásio, microclina e biotita/clorita. Localmente, ocorrem variações para fácies pegmatóides quartzo-feldspáticas e de texturas granofíricas.

2.2.3 - Sequências vulcânicas e sedimentares - Supergrupo Itacaiúnas

O Supergrupo Itacaiúnas está em contato discordante com os gnaisses do Complexo Xingu. Este supergrupo engloba todas as sequências de rochas supracrustais da Província Mineral de Carajás, que diferem em grau metamórfico e composição das sequências de Greenstone-Belts do Supergrupo Andorinhas. Desse modo, foram agrupados, da base para o topo, os Grupos Igarapé Salobo, Igarapé Pojuca, Grão-Pará, Igarapé Bahia e Buritirama.

Grupo Igarapé Salobo

É considerado como basal por conter as rochas de mais alto grau metamórfico. Compreende uma faixa deformada, de direção WNW, composto por anfibolitos datados em 2.555 ± 3 Ma (U-Pb em zircões), anfibolitos foliados datados em 2.761 ± 3 Ma e 2.497 ± 5 Ma (U-Pb em titanitas), formações ferríferas datadas em 2.551 ± 2 Ma (U-Pb em monazitas), metagrauvacas, xistos e quartzitos (Machado et al., 1991). Veios graníticos também foram datados por Machado et al. (1991) em 2.732 Ma (Pb-Pb em zircões) e 2.581 ± 5 Ma e 2.584 ± 5 Ma (U-Pb em titanitas).

Estas rochas foram descritas inicialmente como metamórficas no depósito de Cu-Au do Salobo (Lindenmayer, 1990), posteriormente foram reinterpretadas como provenientes de processos de alteração hidrotermal em rochas supracrustais do Supergrupo Itacaiúnas que acompanharam a deposição dos sulfetos de cobre (Lindenmayer e Teixeira, 1999).

Grupo Igarapé Pojuca

O Grupo Igarapé Pojuca tem ampla distribuição nas bordas do "Sinclinório Carajás", abrange sequências de rochas metavulcanossedimentares, de fácies xisto-verde a anfibolito, orientadas segundo direção geral WNW-ESE com mergulhos que variam entre 50° NE a 60° SW. A seção tipo foi definida na área que abriga os depósitos de Cu-Zn e Cu-Au-Mo e descrita por DOCEGEO (1988) como rochas metavulcânicas básicas a intermediárias (muitas vezes com alteração hidrotermal para cordierita-antofilita, anfibólios, sílica, biotita), anfibolitos, gnaisses, cherts, formações ferríferas bandadas e xistos de composições diversas. Foi caracterizada a

Formação Corpo Quatro, que abriga depósito homônimo e caracteriza-se por dois grupamentos litológicos principais: rochas bandadas e rochas com fragmentos. As rochas bandadas correspondem a sedimentos químicos com sulfetos (pirrotita, calcopirita, esfalerita), níveis descontínuos de chert e/ou formação ferrífera bandada fácies óxido, bem como vários níveis de sulfeto maciço. As rochas com fragmentos apresentam disseminações de pirrotita, calcopirita e, eventualmente, esfalerita.

Anfibolitos do Grupo Igarapé Pojuca foram datados por Machado et al. (1991) em torno de 2.732 ± 2 Ma pelo método U-Pb em zircões. Pimentel et al (2003) dataram metaandesitos em 2.719 ± 80 Ma (Sm-Nd em rocha total).

As mineralizações de Cu-Zn são consideradas singenéticas e relacionadas à fácies sulfeto das formações ferríferas bandadas, enquanto que a mineralização de Cu-Au-Mo está provavelmente relacionada a sistemas pórfiros (Biagini, 1990).

Grupo Grão-Pará

O Grupo Grão Pará (Beisiegel et al., 1973) é profundamente importante no contexto da Província Mineral de Carajás, por incluir as jazidas de ferro de alto teor. É formado por três unidades da base para o topo: Formação Parauapebas (DOCEGEO, 1988), Formação Carajás (Beisiegel et al., 1973) e a Sequência Paleovulcânica Superior (Beisiegel et al., 1973; DOCEGEO, 1988 ou *Upper Metasedimentary Sequence*, Gibbs et al., 1986).

A Formação Parauapebas é constituída por basaltos e basaltos andesíticos datados em 2.687 ± 54 Ma (Rb-Sr em rocha total; Gibbs et al., 1986), riolitos e shoshonitos, cortados por corpos quartzo-dioríticos (Gibbs et al., 1986; Teixeira e Eggler, 1994), metamorfisados na fácies xisto-verde e pouco deformados. No topo da Formação Parauapebas dominam rochas vulcânicas félsicas datadas em 2.758 ± 39 Ma (U-Pb em zircões; Wirth et al., 1986), riolitos datados em 2.759 ± 2 Ma (U-Pb em zircões, Machado et al. 1991), metariolitos porfiríticos datados em 2.760 ± 11 Ma (SHRIMP U-Pb em zircão; Trendall et al. 1998) e traquiandesitos. Estes dados indicam sincronismo entre a Formação Parauapebas e a deposição dos Grupos Salobo e Pojuca.

A Formação Carajás abriga as formações ferríferas bandadas fácies óxido e carbonato, que representam o protominério dos depósitos de ferro supergênicos. Teixeira e Eggler (1994) observaram que existem dolomitos na base da formação em contato gradacional com as formações ferríferas. Sua idade mínima é determinada por um sill máfico datado de 2.740 ± 8 Ma. (U-Pb, zircão, Trendall et al., 1998).

A Formação Paleovulcânica Superior compreende rochas vulcânicas, metagrauvacas, siltitos tufáceos, filitos, arenitos, com derrames basálticos, tufos e arenitos tufáceos (Gibbs et al., 1986).

Grupo Igarapé Bahia

O Grupo Igarapé Bahia, de ocorrência restrita à área da mina inativa de ouro do mesmo nome, é considerado por DOCEGEO (1988), como sobreposto às rochas do Grupo Grão Pará. Compreende uma sequência de rochas metavulcanossedimentares de baixo grau metamórfico, que contém mineralização primária de Cu, associado a Au, Mo e Ag, e mineralização secundária de Au em gossans. Tem direção aproximada NNW, mergulham cerca de 70° ENE no Corpo Acampamento Sul, que afloram em uma janela estrutural. Este grupo é dominado por rochas metassedimentares (pelitos e ritmitos) e metavulcanoclásticas (félsicas a máficas), que se intercalam com metavulcânicas e intrusivas máficas (DOCEGEO, 1988). Brechas hidrotermais são bem caracterizadas nas zonas de minério, que são preferencialmente hospedadas na interface de rochas vulcânicas com rochas piroclásticas/ritmitos do pacote.

Datações geocronológicas feitas por Ferreira Filho (1985) indicam idades de 2.577 ± 72 Ma (Rb-Sr) em granófiros básicos e 2.270 ± 50 Ma (Rb-Sr) em rochas piroclásticas silicosas, admitidas como idade mínima para a sequência metavulcanossedimentar. Mougeot et al. (1996), utilizaram os métodos Rb-Sr, Sm-Nd, U-Pb e Pb-Pb para realizar análises em sulfetos (calcopirita, pirita, galena e molibdenita) em diversas zonas mineralizadas da Região de Carajás e estabeleceram para a mineralização de Cu e Au do Igarapé Bahia a idade mínima de 2.850 ± 65 Ma, o que caracteriza uma mineralização primária arqueana. Idades isotópicas (Galarza, 2002; Galarza e Macambira, 2002a) obtidas em rochas metavulcânicas máficas (2.745 ± 1 Ma, Pb-Pb em zircão) e em rochas metapiroclásticas (2.747 ± 1 Ma, Pb-Pb em zircão) mostraram definitivamente o sincronismo com as rochas do Supergrupo Itacaiúnas. Tallarico et al. (2005) também dataram rochas metavulcânicas máficas que confirmaram idades similares de 2.748 ± 34 Ma (SHRIMP U-Pb em zircão).

A intrusão máfica-ultramáfica acamadada do Luanga (2.763 ± 6 Ma., Machado et al., 1991) e o sill de gabro do depósito de Cu-Au Gameleira (2.757 ± 81 Ma., Pimentel et al., 2003) atestam também a ocorrência de magmatismo basáltico naquela época.

Grupo Buritirama

É representado por um pacote de metassedimentos clásticos e químicos de direção N55°W, que aflora na serra homônima na porção norte da Província Mineral de Carajás. Este grupo é composto, da base para o topo, por quartzitos bandados, quartzitos micáceos e xistos variados; e contém importantes reservas de manganês.

2.2.4 - Formação Águas Claras

Essa formação foi sugerida por Araújo et al., (1988) e descrita por Nogueira (1995), anteriormente correlacionada por DOCEGEO (1988) ao Grupo Rio Fresco. Compreende rochas sedimentares marinhas a fluviais cortadas por sills e diques de rochas máficas (Soares et al., 1994). Encontra-se de forma discordante sobre as rochas do Supergrupo Itacaiúnas.

Na base, é constituída, predominantemente, por siltitos e argilitos laminados de cor cinza a avermelhado. Nas faixas onde ocorre maior deformação, as rochas são transformadas em metassiltitos, metapelitos e quartzo-mica-xistos. As estruturas primárias mais comuns preservadas são laminações plano-paralelas, estratificação cruzada de baixo ângulo tipo hummocky e estruturas de fluidização e carga.

Para o topo, ocorrem metarenitos e metarcóseos de coloração branca, granulação média à grossa, com grãos sub-angulosos mal selecionados e apresentam, localmente, hematita, clorita e sericita na matriz. Intercalam-se nestes arenitos, lentes de microconglomerados. As camadas têm formato lenticularizado. Neste pacote predominam estruturas do tipo de acamamento gradacional, estratificações cruzadas tabular e acanalada de pequeno porte e marcas de ondas ligeiramente assimétricas. As rochas metassedimentares estão dispostas segundo direção NW-SE com mergulhos suaves, com média de 20^{o} para NE, as quais, nas proximidades de falhas, podem chegar a mergulhos de médio a alto ângulo.

A deformação das rochas da Formação Águas Claras possui caráter rúptil e está limitada às zonas de falhas direcionais, como a Falha Carajás. É marcante o arranjo tectônico da formação segundo horsts e grabens. O depósito de Au-Cu de Águas Claras encontra-se relacionado a esse comportamento rúptil nos arenitos do Membro Superior (Soares et al., 1994).

Trendall et al. (1998) dataram arenitos com zircão proveniente de rochas vulcânicas sindeposicionais em 2.681 ± 5 Ma (SHRIMP U-Pb em zircões); e Dias et al. (1996) dataram diques de gabro que cortam o pacote sedimentar em 2.645 ± 12 Ma (U-Pb em zircões).

2.2.5 - Diques e Sills máficos

São metagabros, metadioritos e metadiabásios abundantes na região. Sabe-se que existem várias fases de magmatismo máfico, mas a sua divisão é muito difusa. Têm idades desde arqueanas (gabros de 2,7 Ga no depósito de Águas Claras), passam a proterozoicas (dioritos do Igarapé Aquiri, com cerca 1,9 Ga, Hirata et al. 1982) a até brasilianas (diques encontrados na área do Salobo, Lindenmayer, 1990). Variam também na sua forma, desde corpos tabulares expressivos, como o gabro Santa Inês, até pequenos diques (DOCEGEO, 1988).

Mougeot et al. (1996) dataram metagabros em 2.708 ± 37 Ma (U-Pb em zircões); Galarza e Macambira (2002b) dataram rochas intrusivas máficas em 2.705 ± 2 Ma (Pb-Pb em zircões); e Pimentel et al. (2003) dataram metagabros e rochas metavulcânicas cogenéticas em 2.757 ± 81 Ma (Sm-Nd em rocha total).

2.2.6 - Granitos anorogênicos

Diversos plútons de granitos anorogênicos ocorrem na região, com idades relacionadas ao proterozoico inferior/médio. Essas intrusões cortam todas as unidades do Supergrupo Itacaiúnas, bem como as rochas da Formação Águas Claras. Datações geocronológicas, realizadas em zircões pelo método (U-Pb), estabeleceram idades em torno de 1.880 Ma. (Gibbs et al., 1986; Machado et al., 1991 e Macambira e Lafon, 1995). Possivelmente, essas intrusões estão associadas ao evento plutônico-vulcânico Uatumã, que recobre extensas porções do Cráton Amazônico com rochas extrusivas félsicas. Destacam-se, pelas proximidades geográficas com a área estudada, o Granito Central Carajás com idade de 1.820 ± 49 Ma obtida pelo método U-Pb em zircão (Wirth et al. 1986), e 1.880 ± 2 Ma obtida pelo método U-Pb em zircão; Granito Cigano com idade 1.883 ± 2 Ma em zircão U-Pb; Granito Pojuca com idade 1.874 ± 2 Ma em zircão U-Pb (Machado et al. 1988; Machado et al. 1991); Granito Breves com idade com idade 1.879 ± 6 Ma em zircão U-Pb SHRIMP (Tallarico et al. 2004) e Granito Young Salobo com idade com idade 1.880 ± 80 Ma (Rb-Sr em rocha total; Cordani, 1981); além de outros menores ainda pouco conhecidos.

2.2.7 - Coberturas fanerozoicas

Coberturas fanerozoicas são registradas como as unidades mais jovens que afloram na porção norte da região de Carajás e constituem sequências sedimentares correlacionáveis ao Grupo Serra Grande (Caputo e Lima, 1984).

2.3 - MODELO TECTONOESTRATIGRÁFICO

A região da Serra dos Carajás, inicialmente, foi compreendida como uma bacia que comportava um pacote de rochas vulcanossedimentares sob a forma de um grande sinclinório ou sinclinal (Beisiegel et al., 1973; Hirata et al., 1982; DOCEGEO 1988).

A bacia tem forma sigmoidal alongada segundo a direção geral da foliação ESE, que denota um comportamento dominantemente transcorrente-sinistral. Deslocamentos de até 30 km são registrados ao longo da Falha Carajás, que corta toda a bacia e são indicativos das falhas transcorrentes WNW-ESE. As falhas de direção NE-SW, como a falha McCandless, representam outra importante direção de estruturas, no âmbito da Província Mineral de Carajás.

O modelo proposto por Pinheiro (1997), e Holdsworth e Pinheiro (2000), sugere que a evolução tectônica de Carajás foi iniciada com o estabelecimento de uma zona de cisalhamento dúctil arqueana, de direção E-W (Zona de Cisalhamento Itacaiúnas), responsável pelo aparecimento, nas rochas do embasamento (Complexos Pium e Xingu), de uma fábrica milonítica de alta temperatura (fácies anfibolito médio a alto), gerada por transpressão sinistral.

Posteriormente, se instalou sobre o embasamento as rochas do Grupo Igarapé Pojuca, que foram deformadas por transpressão e, sobre estas, os litotipos do Grupo Grão Pará (2,7 Ga). Discordantes sobre essas rochas, foram depositados os sedimentos da Formação Águas Claras.

Seguiu-se, um evento transtensional dextral, responsável pela subsidência dessas rochas no interior da Bacia de Carajás, a Sul, e ao longo do Sistema Transcorrente Cinzento, a Norte, que gerou uma geometria sigmoidal alongada com tendência E-W, fortemente controlada pela geometria das zonas de cisalhamento pretéritas. A Falha Carajás marca o limite de subsidência e deslocamento dextral transtensivo da Estrutura de Carajás, a qual foi invadida por um enxame de diques e sills máficos por volta de 2,6 Ga. Um episódio de transpressão sinistral entre 2,6 Ga e 2,0 Ga, reativou a Falha Carajás, o que provocou a deformação das rochas situadas no interior da Estrutura Carajás e, no contexto do Sistema Transcorrente Cinzento, deu origem às estruturas *sidewall ripout* do Salobo e *duplex* do Cururu.

Um último episódio deformacional, controlado por uma extensão E-W a NE-SW, ocorrida durante o Proterozoico Inferior e o início do Mesoproterozoico, no Cráton Amazônico, deu origem a fraturas e falhas regionais de direção N-S e permitiu a intrusão de plútons graníticos (Granitos Carajás, Cigano, etc) e, possivelmente, novos diques máficos. Localmente, em virtude da reativação de falhas maiores pretéritas, ocorreu a formação de pequenas bacias, onde foram depositados os sedimentos da Formação Gorotire.

O modelo descrito acima que destaca um evento transtensional dextral relacionado ao Sistema de Cisalhamento Cinzento, representa a principal feição identificada no contexto do alvo Furnas, sobre a qual estão condicionadas as rochas do depósito.

2.4 - REFERÊNCIAS

Althoff, F.J., P. Barbey, A.M. Boullier, 2000, 2.8-3.0 Ga plutonism and deformation in the SE Amazonian craton: the Archean granitoids of Marajoara (Carajás Mineral province, Brazil): Precambrian Research, **104**, 187–206.

Araújo, O.J.B., R.G.N. Maia, X.S. Jorge João, J.B.S. Costa, 1988, A megaestruturação arqueana da Folha Serra dos Carajás: 1º Congresso Latino Americano de Geologia, Anais, 324–338.

Araújo, O.J.B., R.G.N. Maia, 1991, Projeto especial mapas de recursos minerais, de solos e de vegetação para a área do Programa Grande Carajás; Subprojeto Recursos Minerais; Folha SB.22-Z-A Serra dos Carajás - Estado do Pará: DNPM/CPRM.

Avelar, V.G., J.M. Lafon, F.C. Correia JR., E.M.B. Macambira, 1999, O magmatismo arqueano da região de Tucumã – Província Mineral de Carajás: Novos dados geocronológicos: Revista Brasileira de Geociências, **29**, no. 4, 453–460.

Avelar, V.G., 1996, Geocronologia Pb-Pb por evaporação em monocristal de zircão do magmatismo da região de Tucumã, SE do Estado do Pará, Amazônia oriental: Dissertação de Mestrado, Universidade Federal do Pará.

Barbosa, J.P.O., 2004, Geologia Estrutural, Geoquímica, Petrografia e Geocronologia de granitoides da região de Igarapé Gelado, norte da Província Mineral de Carajás: Dissertação de Mestrado, Universidade Federal do Pará.

Barbosa, J.P.O, C.E.M. Barros, M.B. Macambira, A.G. Vale, 2001, Geologia e Geocronologia do Stock Granítico Geladinho, região de Parauapebas, Província Mineral de Carajás: 7º Simpósio de Geologia da Amazônia, SBG, Resumos Expandidos.

Barros, C. E. M., 1997, Pétrologie et struture du Complexe Granitique Estrela (2.5 Ga) et de son encaissant métavolcano-sédimentaire (Province Métallifère de Carajás, Brésil): Tese de Doutorado, Université Henri Poincaré - Nancy.

Barros, C.E.M., Dall'Agnol, R., Lafon, J.M., Teixeira, N.P., Ribeiro, J.W., 1992, Geologia e geocronologia Rb-Sr do Gnaisse Estrela, Curionópolis, PA: Boletim do Museu Paraense Emilio Goeldi, Ciências da Terra, **4**, 83–102.

Barros, C.E.M., Dall'Agnol, R., Vieira, E.A.P., Magalhães, M.S., 1995. Granito Central da Serra dos Carajás: avaliação do potencial metalogenético para estanho com base em estudos da borda oeste do corpo. Boletim do Museu Paraense Emílio Goeldi. Série Ciências da Terra **7**, 93–123.

Barros, C.E.M., Barbey, P., 1998. A importância da granitogênese tardi-arqueana (2,5 Ga.) na evolução tectono-metamórfica da província mineral de Carajás – O Complexo Granítico Estrela e sua auréola de contato: Revista Brasileira de Geociências. **28**, no. 4, 513–522.

Barros, C.E.M., M.J.B. Macambira, P. Barbey, 2001, Idade de zircão do Complexo Granítico Estrela: relações entre magmatismo, deformação e metamorfismo na Província Mineral de Carajás: 7º Simpósio de Geologia da Amazônia, SBG, Resumos Expandidos.

Barros, C.E.M., Macambira, M.J.B., Barbey, P., Scheller, T., 2004, Dados isotópicos Pb-Pb em zircão (evaporação) e Sm-Nd do Complexo Granítico Estrela, Província Mineral de Carajás, Brasil: implicações petrológicas e tectônicas: Revista Brasileira de Geociências, **34**, 531−538.

Beisegel, V.R., A.L. Bernardelli, N.F. Drummond, A.W. Ruff, J.W. Tremaine, 1973, Geologia e recursos minerais da Serra dos Carajás: Revista Brasileira de Geociências, **3**, 215–242.

Biagini, D.O., 1990, Considerações sobre algumas feições metalogenéticas de Carajás: DOCEGEO, Relatório Interno.

Caputo, M.V., E.C. Lima, 1984, Estratigrafia, idade e correlação do Grupo Serra Grande - Bacia do Parnaíba: 33º Congresso Brasileiro de Geologia, SBG, Resumos Expandidos, **8**, 740–753.

Cordani, U., 1981, Comentários sobre as determinações geocronológicas da região da Serra dos Carajás: Universidade de São Paulo - Docegeo, Relatório.

Costa, J.B.S., Y. Hasuí, 1996, Evolução geológica da Amazônia, *in* M. L. Costa, R.S. Angélica, 1997, Contribuições à geologia da Amazônia, 15–90.

Costa J.B.S., O.J.B. Araújo, A. Santos, X.S. Jorge João, M.J.B. Macambira, J.M. Lafon, 1995, A Província Mineral de Carajás: aspectos tectono estruturais, estratigráficos e geocronológicos: Boletim do Museu Paraense Emílio Goeldi, Série Ciências da Terra **7**, 199–235.

Costa, J.B.S., Y. Hasuí, R.L. Bemerguy, M.S. Borges, A.R. Costa, W. Travassos, J.A. Mioto, H.L.S. Igreja, 1993, Aspectos fundamentais da neotectônica na Amazônia Brasileira: Simpósio Internacional do Quaternário da Amazônia, Resumos e Contribuições Científicas, 103–106.

Dias, G.S., Macambira, M.B., Dall'Agnol, R., Soares, A.D.V., Barros, C.E.M., 1996, Datações de zircões de sill de metagabro: comprovação de idade arqueana da Formação Águas Claras, Carajás, Pará: 5th Simpósio de Geologia da Amazônia, SBG, Resumos Expandidos, 376−378.

DOCEGEO (Rio Doce Geologia e Mineração S.A), 1988, Revisão litoestratigráfica da Província Mineral de Carajás: Congresso Brasileiro de Geologia, SBG, Resumos expandidos, **35**, 10–54.

Feio, G.R.L., 2011, Magmatismo granitóide arqueano da área de Canaã dos Carajás: implicações para a evolução crustal da Província Carajás: Tese de Doutorado, Universidade Federal do Pará.

Ferreira Filho, C.F., 1985, Geologia e mineralizações sulfetadas do Prospecto Bahia, Província Mineral de Carajás: Dissertação de Mestrado, Universidade de Brasília.

Galarza, T.M.A., 2002, Geocronologia e geoquímica isotópica dos depósitos de Cu-Au Igarapé Bahia e Gameleira, Província Mineral de Carajás (PA), Brasil: Tese de Doutorado, Universidade Federal do Pará.

Galarza, M.A., M.J.B. Macambira, 2002a, Petrologia e geocronologia das rochas encaixantes do depósito de Cu-Au Igarapé Bahia, Província Mineral de Carajás, Pará, Brasil, *in* E.L. Kein, M.L. Vasquez, L.T. Rosa-Costa: Contribuições à Geologia da Amazônia, SBG/NN **3**, 153–168.

Galarza, M.A., M.J.B. Macambira, 2002b, Geocronologia e Evolução Crustal da Área do Depósito de Cu- Au Gameleira, Província Mineral de Carajás (Pará), Brasil: Geologia USP Série Científica **2**, 143–159.

Gibbs, A.K., K.R. Wirth, W.K. Hirata, W.J. Olszewski Jr., 1986, Age and composition of the Grão Pará Group volcanics, Serra dos Carajás: Revista Brasileira de Geociências, **16**, no. 2, 201−211.

Hirata, W.K., J.C. Rigon, A.A.C. Cordeiro, E.M. Meireles, 1982, Geologia regional da Província Mineral de Carajás: 1º Simpósio de Geologia da Amazônia, SBG, Resumos Expandidos, 100–108.

Holdsworth, R., R. Pinheiro, 2000, The anatomy of shallow-crustal transpressional structures: Insights from the Archean Carajás fault zone, Amazon, Brazil: Journal of Structural Geology, **22**, 1105−1123.

Huhn S.R.B., M.J.B. Macambira, R. Dall'Agnol, 1999, Geologia e geocronologia Pb/Pb do granito alcalino Arqueano Planalto, Região da Serra do Rabo, Carajás – PA: 6º Simpósio de Geologia da Amazônia, SBG, Resumos Expandidos, 463–466.

Leite, A.A.S., 2001, Geoquímica, petrogênese e evolução estrutural dos granitóides arqueanos da região de Xinguara, SE do Cráton Amazônico: Tese de Doutorado, Universidade Federal do Pará.

Lindenmayer, Z.G., 1990, Salobo Sequence, Carajás, Brazil: geology, geochemistry and metamorphism: Ph.D. thesis, University of Western Ontario.

Lindenmayer, Z.G., W.S. Fyfe, 1991, Metamorfismo de alta temperatura e baixa pressão no depósito de cobre do Salobo: evidência do rift continental arqueano no Cráton Amazônico: 3º Simpósio de Geologia da Amazônia, SBG, Resumos Expandidos, 36–48.

Lindenmayer, Z.G., W.S. Fyfe, V.L.S. Bocalon, 1994, Nota preliminar sobre as intrusões granitóides do depósito de cobre do Salobo, Carajás: Acta Geológica Leopoldensia, **17**, no. 40, 153–184.

Lindenmayer, Z.G., J.B.G. Teixeira, 1999, Ore Genesis at the Salobo Copper Deposit, Serra dos Carajás, *in* M.G. Silva, A. Misi, eds., Base Metal Deposits of Brazil: MME/CPRM/DNPM, 33–43.

Macambira, M.J.B., J.M. Lafon, 1995, Geocronologia da Província Mineral de Carajás; Síntese dos dados e novos desafios: Boletim do Museu Paraense Emílio Goeldi, Série Ciências da Terra **7**, 263–288.

Macambira, M.J.B., L.M. Lima, R.V.L. Pinheiro, Lima, F.D., 2001, Idades de Cristais Detríticos de Zircão da Serra dos Carajás, Pará; Evidências sobre a Formação da Crosta: 7º Simpósio de Geologia da Amazônia, SBG, Resumos Expandidos, 72–75.

Machado, N., D. Lindenmayer, Z. Lindenmayer, 1988, Geocronologia U-Pb da Província Metalogenética de Carajás, Pará: resultados preliminares: 7º Congresso Latinoamericano de Geologia, SBG/DNPM, Resumos Expandidos, 339–347.

Machado, W., Z.G. Lindenmayer, T.E. Krogh, D. Lindenmayer, 1991, U-Pb geochronology of Archean magmatism and basement reactivation in the Carajás área, Amazon shield, Brazil: Precambrian Research, **49**, 329–354.

Monteiro, L.V.S., R.P. Xavier, E.R. Carvalho, M.W. Hitzman, C.A. Johnson, C.R.S. Filho, I. Torresi, 2008, Spatial and temporal zoning of hydrothermal alteration and mineralization in the Sossego iron oxide–copper–gold deposit, Carajás Mineral Province, Brazil: paragenesis and stable isotope constraints: Mineralium Deposita, **43**, 129–159.

Moreto, C.P.N., L.V.S. Monteiro, R.P. Xavier, W.S. Amaral, T.J.S. Santos, C. Juliani, C.R. Souza Filho, 2011a, Mesoarchean (3.0 and 2.86 Ga) host rocks of the iron oxide-Cu-Au Bacaba deposit, Carajás mineral province: U-Pb geochronology and metallogenetic implications: Mineralium Deposita, **46**, 789−811.

Moreto, C.P.N., L.V.S. Monteiro, R.P. Xavier, T.I.S. Kemp, C.R. Souza Filho, 2011b, In situ LA-ICPMS U-Pb zircon dating of the host rocks of the Sossego and Bacaba iron oxide-copper-gold deposits, Carajás mineral province, Brazil: 11th Biennial SGA Meeting.

Moreto, C.P.N., L.V.S. Monteiro, R.P. Xavier, T.I.S. Kemp, K. Sato, W.S. Amaral, 2012, SHRIMP and LA-ICPMS U-Pb zircon geochronology of the host rocks of the Sossego, Bacaba and Castanha IOCG deposits, Carajás mineral province, Brazil: 34th International Geology Congress.

Mougeot, R., J.P. Respaut, L. Brique, P. Lédru, J.P. Milesi, C. Lerouge, E. Maroux, S.B. Huhn, M.J.M. Macambira, 1996, Isotope geochemistry constrains for Cu, Au mineralizations and evolution of the Carajás Province (Pará, Brazil): 39th Congresso Brasileiro de Geologia, SBG, Resumos Expandidos, **7**, 321–324.

Nogueira, A.C.R., 1995, Análise faciológica e aspectos estruturais da Formação Águas Claras, Região Central da Serra dos Carajás – Pará: Dissertação de Mestrado, Universidade Federal do Pará.

Pidgeon, R.T., M.J.B. Macambira, J.M. Lafon, 2000, Th-U-Pb isotopic systems and internal structures of complex zircons from an enderbite from the Pium Complex, Carajás Province, Brazil: evidence for the ages of granulite facies metamorphism and the protolith of the enderbite: Chemical Geology, **166**, 159–171.

Pinheiro, R.V.L., 1997, Reactivation history of the Carajás and Cinzento Strike-Slip System, Amazon, Brazil: Ph.D. thesis, University of Durham.

Pinheiro, R.V.L., R.E. Holdsworth, 1995, Significado tectônico da clivagem transversa (transecting cleavage) em dobras na Mina de Serra Pelada, Pará: Boletim do Museu Paraense Emílio Goeldi, Série Ciências da Terra **7**, 259–278.

Pinheiro, R.V.L., R.E. Holdsworth, 2000, Evolução Tectonoestratigráfica dos Sistemas Transcorrentes Carajás e Cinzento, Cinturão Itacaiúnas, na borda leste do Cráton Amazônico, Pará: Revista Brasileira de Geociências, **30**, no. 4, 597–606.

Pimentel, M.M., Z.G., Lindenmayer, Laux, J.H., Armstrong, R., Araújo, J.C., 2003, Geochronology and Nd geochemistry of the Gameleira Cu-Au deposit, Serra dos Carajás, Brazil: 1.8−1.7 Ga hydrothermal alteration and mineralization: Journal of South American Earth Sciences, **15**, 803−813.

Rodrigues, E.S., J.M. Lafon, T. Scheller, 1992, Geocronologia Pb-Pb da Província Mineral de Carajás: primeiros resultados: 37º Congresso Brasileiro de Geologia, SBG, Resumos Expandidos, **2**, 183–184.

Santos, J.O.S, L.A. Hartmann, H.E. Gaudette, D.I. Groves, N.J. McNaughton, I.R. Fletcher, 2000, A new understanding of the provinces of the Amazon Craton based on integration of field mapping and U-Pb and Sm-Nd geochronology: Gondwana Research, **3**, no. 4, 453–488.

Sardinha, A.S., C.E.M. Barros, R. Krymski, M.J.B. Macambira, 2001, Petrografia e Geocronologia U-Pb em zircão do Granito Serra do Rabo, Província Mineral de Carajás, Pará: 7º Simpósio de Geologia da Amazônia, SBG, Resumos Expandidos.

Sardinha, A.S., R. Dall'Agnol, A.C.B. Gomes, M.J.B. Macambira, M.A. Galarza, 2004, Geocronologia Pb-Pb e U-Pb em zircões de granitóides arqueanos da região de Canaã dos Carajás, Província Mineral de Carajás: 42nd Congresso Brasileiro de Geologia, Resumos Expandidos.

Silva, G.G., M.J.C. Lima, A.R.F. Andrade, R.S. Issler, G. Guimarães, 1974, Geologia das folhas SB-22 Araguaia e parte SC-22 Tocantins: Projeto RADAMBRASIL, geologia, geomorfologia, solos e uso potencial da terra, Levantamento de Recursos Naturais, **4**.

Soares, A.V., A.B. Santos, E.A. Vieira, V.M. Bella, L.P.B. Martins, 1994, Área Águas Claras contexto geológico e mineralizações: 4º Simpósio de Geologia da Amazônia, SBG, Resumos Expandidos, 379–382.

Souza, S.R.B., M.J.B. Macambira, T. Sheller, 1996, Novos dados geocronológicos para os granitos deformados do Rio Itacaiúnas (Serra dos Carajás, PA); implicações estratigráficas: 5º Simpósio de Geologia da Amazônia, SBG, Resumos Expandidos, 380–383.

Tallarico, F.H.B., 2003, O cinturão cupro-aurífero de Carajás, Brasil: Tese de Doutorado, Universidade Estadual de Campinas.

Tallarico, F.H.B., N.J. McNaughton, D.I. Groves, I.R. Fletcher, B.R. Figueiredo, B.J. Carvalho, L.J. Rego, A.R. Nunes, 2004, Geological and SHRIMP II U-Pb constraints on the age and origin of the Breves Cu-Au- (W-Bi-Sn) deposit, Carajás, Brazil: Mineralium Deposita, **39**, 68−86.

Tallarico, F.H.B., B.R. Figueiredo, D.I. Groves, N. Kositcin, N.J. McNaughton, I.R. Fletcher, J.L. Rego, 2005, Geology and SHRIMP U-Pb geochronology of the Igarapé Bahia deposit, Carajás copper-gold belt, Brazil: An Archean (2.57 Ga) example of iron-oxide Cu-Au-(U-REE) mineralization: Economic Geology, **100**, 7−28.

Teixeira, J.B.G., D.H. Eggler, 1994, Petrology, Geochemistry, and Tectonic Setting of Archaean Basaltic and Dioritic Rocks from the N4 Iron Deposit, Serra dos Carajás, Pará, Brazil: Acta Geologica Leopoldensia, **17**, no. 40, 71–114.

Trendall, A.F., M.A.S. Basei, J.R. Laeter, D.R. Nelson, 1998, SHRIMP zircon U-Pb constraints on the age of the Carajás formation, Grão Pará Group, Amazon Craton: Journal of South American Earth Sciences, **11**, no. 3, 265–277.

Vasquez, M.L., C.S. Sousa, J.M.A Carvalho, 2008, Mapa Geológico e de Recursos Minerais do Estado do Pará, escala 1:1.000.000: Programa Geologia do Brasil (PGB), Companhia de Pesquisa de Recursos Minerais - Serviço Geológico do Brasil.

Villas R.N., M.D. Santos, 2001, Gold deposits of the Carajás Mineral Province: deposit types and metallogenesis: Mineralium Deposita, **36**, 300–331.

Wirth, K.R., A.K. Gibbs, W.J. Olszewski, 1986, U-Pb ages of zircons from the Grão-Pará group and Serra dos Carajás Granite, Pará, Brazil: Revista Brasileira de Geociências, **16**, no. 2, 195–200.

Xavier, R.P., L.V.S. Monteiro, C.P.N. Moreto, A.L.S. Pestilho, G.H.C. Melo, M.A.D. Silva, B. Aires, C. Ribeiro, and F.H.F. Silva, 2012, The iron oxide copper-gold systems of the Carajás Mineral Province, Brazil, *in* Geology and Genesis of Major Copper Deposits and Districts of the World: A Tribute to Richard Sillitoe, Special Publication, Society of Economic Geologists.

CAPÍTULO 3

MAGNETIC INTERPRETATION AND 2D MODELING AT AN IRON OXIDE–COPPER–GOLD DEPOSIT, CARAJÁS MINERAL PROVINCE, BRAZIL

Manuscript submitted to the Journal *Geophysics* in August 12th of 2014.

MAGNETIC INTERPRETATION AND 2D MODELING AT IRON OXIDE–COPPER–GOLD DEPOSITS, CARAJÁS MINERAL PROVINCE, BRAZIL

Journal:	*Geophysics*
Manuscript ID:	GEO-2014-0380
Manuscript Type:	Case Histories
Date Submitted by the Author:	12-Aug-2014
Complete List of Authors:	Leão-Santos, Marcelo; Vale S.A., Department of Exploration and Mineral Projects; Vale S.A., Department of Exploration and Mineral Projects Moraes, Roberto; InterGeo - Informação em Geociências, Diretoria Técnica; Home,
Keywords:	modeling, interpretation, 2D, mining, magnetics
Area of Expertise:	Magnetic Exploration Methods, Mining Geophysics

Thank you for submitting your manuscript, GEO-2014-0380, to GEOPHYSICS
e.c.slob@tudelft.nl <e.c.slob@tudelft.nl> Tue, Aug 12, 2014 at 4:37 PM
To: marcelo.leao@vale.com, marcelo.leao.santos@gmail.com
Cc: geopapers@seg.org, marcelo.leao@vale.com, marcelo.leao.santos@gmail.com, rmoraes@unb.br
12-Aug-2014
Re: GEO-2014-0380, "MAGNETIC INTERPRETATION AND 2D MODELING AT IRON OXIDE–COPPER–GOLD DEPOSITS, CARAJÁS MINERAL PROVINCE, BRAZIL",
Leão-Santos, Marcelo; Moraes, Roberto
Dear Mr. Marcelo Leão-Santos:
Thank you for submitting your manuscript listed above to GEOPHYSICS. Please refer to the manuscript number in all correspondence. Your paper is undergoing review.

MAGNETIC INTERPRETATION AND 2D MODELING AT AN IRON OXIDE–COPPER–GOLD DEPOSIT, CARAJÁS MINERAL PROVINCE, BRAZIL

Marcelo Leão-Santos[1,2,3], and Roberto Moraes[1]

[1] Universidade de Brasília, Instituto de Geociências, Brasília, Brazil.

E-mail: marcelo.leao.santos@gmail.com, rmoraes@unb.br.

[2] Colorado School of Mines, Center for Gravity, Electrical & Magnetic Studies, Golden, Colorado.

[3] VALE S.A., Department of Exploration and Mineral Projects, Belo Horizonte, Brazil.

E-mail: marcelo.leao@vale.com.

3.1 - ABSTRACT

Magnetic signatures are often used to interpret physical properties of massive magnetite from strong hydrothermal alteration in iron oxide–copper–gold deposits (IOCG). In areas with strong magnetization, the presence of remanence and self-demagnetization can yield a total magnetization orientation which differs significantly from the direction of the inducing field and which can easily lead to an erroneous interpretation. Qualitative, semi-quantitative and quantitative analysis can help to understand the behavior of the magnetic anomaly, give support to accomplish a best approach to interpretation, in obtaining a good correlation with geological data and assisting future three-dimensional (3D) modeling. Several linear transformations can be useful to a successful interpretation of the magnetic data. This can be enhanced by correct magnetic profiles interpretations to allow a better understanding of body geometry. Depth estimations provided by this approach are a powerful tool to define the body position in subsurface. Finally, the estimation of magnetic properties as priori information to two-dimensional (2D) parametric modeling can achieve good results. We demonstrate that the application of all these tools in the Furnas Southeast Fe oxide–Cu–Au deposit located at low magnetic latitude in Carajás Mineral Province, Brazil, can reliably define the structures of magnetite hydrothermal alterations associated with the high and low grade ores.

3.2 - INTRODUCTION

Airborne magnetic surveys are frequently used in the exploration for copper sulfides and gold ores in IOCG deposits because of their association with magnetite, thus providing a cost-effective systematic structural mapping and interpretation for these magnetic sources.

Magnetic data interpretation can be done both qualitatively and quantitatively using some of the techniques shown in Figure 3.1.

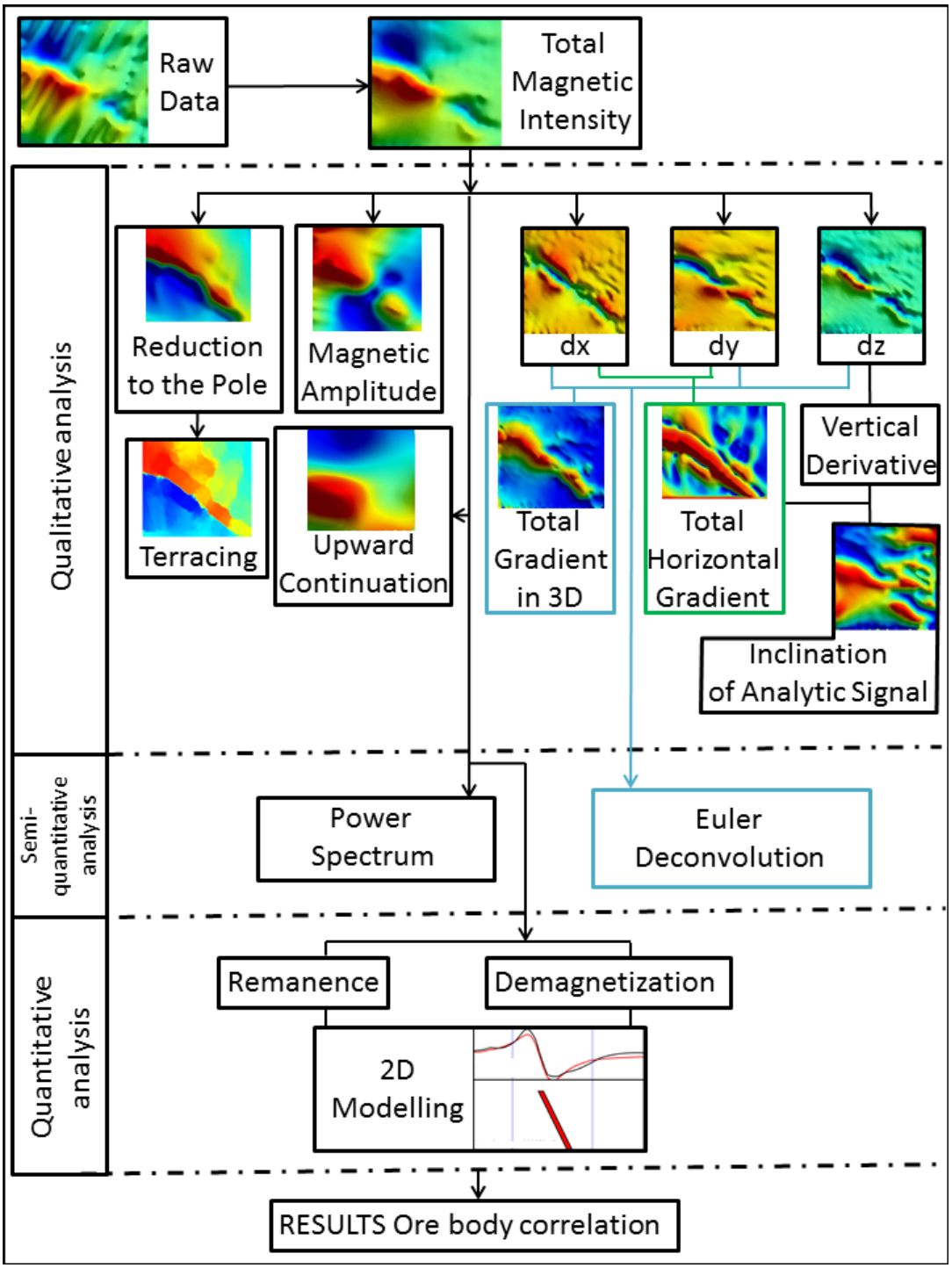

Figure 3.1. Flowchart of qualitative, semi-quantitative and quantitative methods used in interpreting magnetic data.

The qualitative interpretation can be done by visual inspection of the images and profiles in maps and cross-sections, in some of the many linear transformations available. This allows for the definition of domains and lineaments related to the local magnetic field configuration. In the present study, we focused on using the measured TMI (Total Magnetic Field Intensity) data to understand the spatial distribution of the magnetic sources and how can they be grouped spatially (magnetic fabric) which then points to the different regions where the magnetic material is distributed. Further

information can be obtained on the underlain rock volumes themselves, on the brittle, and on ductile structures imposed on them.

Several methods and techniques were used to aid the qualitative interpretation of magnetic data. One group of methods uses direct (TMI) or residual magnetic field (RMI) data to perform various filtering operations in frequency domain (e.g. reduction to the pole, pseudo-gravity, upward continuation and vertical derivatives). Another group of methods use spatial derivatives of various orders depending on the high spatial noise frequency present in the magnetic data (e.g. analytic signal, analytic signal vector inclination (tilt derivative), total and horizontal field gradients, magnetic amplitude, terracing).

These were followed by semi-quantitative methods, starting first with a technique to determine the depth to the top of magnetic sources by studying the amplitude versus wave number relation from 2D radially averaged power spectrum analysis. These results can then be complimented by using depth estimates using Euler deconvolution techniques. These methods can be applied either to the whole survey area or to selected areas with individual magnetic signatures.

The presence of remanent magnetization and self-demagnetization effects certainly pose many problems thus complicating the interpretation of magnetic sources. In addition, the fact that the inducing field intensity is much smaller at low magnetic latitudes than at higher magnetic latitudes further exacerbates the problem.

The final step attempts, using all previously gained information, is a quantitative interpretation by using two-dimensional (2D) parametric or structural modeling which can be extended to a 3D physical model representation (intrinsic magnetic susceptibility modeling).

The main objective of this paper is to apply the above mentioned magnetic data analysis procedures to study an iron oxide–copper–gold mineralization (IOCG) using a set of high-resolution airborne magnetic data at the Furnas copper-gold deposit.

Location of the study area

The Carajás Mineral Province is located in the state of Pará in northern Brazil approximately 1,100 km from Brasilia (Figure 3.2). The province is located at low latitude with magnetic inclination -7.3°. The Carajás Mineral Province is bounded to the west by the Xingu River and to the east by the Araguaia-Tocantins River. The Gradaús and Bacajá Mountain Ranges by the province to the south and north, respectively (Hirata et al., 1982).

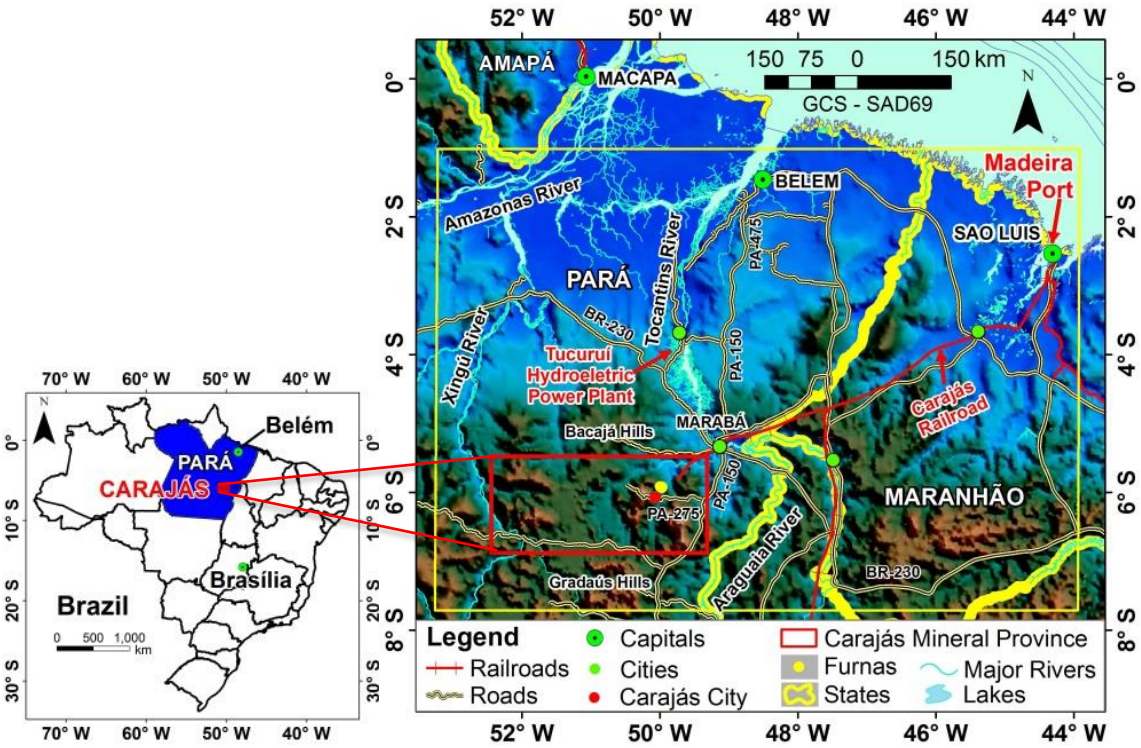

Figure 3.2. Location of Carajás Mineral Province and the infrastructure of the region: cities, main roads, hydrography, Carajás railroad and Tucuruí power plant.

The infrastructure of the region is privileged because of the easy electricity supply from the Tucuruí Hydroelectric Power Plant, which is 275 km to the north. The Carajás Railroad (*Estrada de Ferro Carajás – EFC*) with approximately 892 km in extension can be used to transportation and provides access to the Port of Madeira in São Luís – Maranhão. The study area can be accessed from the state capital, Belém, through the state highways PA-475 and PA-150 to Marabá and then through highway PA-150 to the city of Eldorado dos Carajás and PA-275 to the cities of Parauapebas and Carajás (Figure 3.2).

The Carajás Mineral Province has adequate infrastructure in place to support mineral extraction. The Furnas deposit is located approximately 35 km from the Parauapebas city, 45 km from the Carajás Airport, 60 km from the Carajás city and 10 km north of the Carajás Railroad.

Iron oxide-copper-gold (IOCG) deposits

Carajás is known as an economically important metallogenic province where numerous types of mineral deposits are found. In addition to the IOCG mineralization, there are deposits types of banded iron formations, lateritic gold, lateritic manganese, mafic-ultramafic layered intrusions hosting platinum group elements, nickel laterite and nickel sulfide deposits. In terms of geotectonics, the Carajás Province is located in the Central Brazilian Shield within the southeastern

portion of the Central Amazonian Province, which is bordered by the Transamazonian Province (Maroni-Itacaiúnas) to the north and Araguaia Belt to the east (Santos et al., 2000).

Hitzman et al. (1992) originally defined IOCG deposits as a unique type after the discovery and study of the Olympic Dam in the Gawler Craton in southern Australia (Oreskes and Einaudi 1990, 1992). IOCG deposits may contain only copper or gold, and others may be rich in iron oxides with phosphorus as an accessory (e.g., Kiruna) or with rare earth elements (e.g., Bayan Obo; Nykänen, 2008). The IOCG deposits can also be divided in three main types: magnetite group (e.g. Salobo, Sossego, Candelaria), hematite group (e.g. Olympic Dam, Prominent Hill, Manto Verde) and magnetite + hematite group (e.g. Sue Dianne, North Portia, Rakkurijärvi).

Williams et al. (2005) addresses a broad discussion on IOCG geology, space-time distribution, and possible modes of origin. From an economic perspective, the most significant IOCG deposits are those in Chile and Peru in the coastal batholithic belt (Jurassic-Cretaceous extended continental margin arc); in Australia within the Gawler craton and Cloncurry districts (late Paleoproterozoic to Mesoproterozoic debated intracratonic or distal subduction-related settings); and in Brazil in the Carajás province (Archean, Amazon craton). Williams et al. (2005), do not classify the Kiruna-type iron oxide-apatite ores and iron skarns as IOCG deposits even though they share some features with IOCG deposits. Monteiro et al. (2008) described the spatial and temporal zoning of hydrothermal alteration and mineralization in the Sossego IOCG deposit. Xavier et al. 2012 summarize the Iron Oxide Copper-Gold Systems of the Carajás Mineral Province. Groves et al. (2010) described IOCG deposits through Earth history, the implications for origin and lithospheric setting, and distinction from other epigenetic iron oxide deposits.

Although definitions vary somewhat, in this study, IOCG is used as a term to describe deposits with hydrothermal alteration and mineralization that have significant amounts of magnetite, copper and gold. The main features can be summarized as follows (Nykänen et al., 2008):

(i) proximity to cratonic areas;
(ii) controlled by structures, faults and lineament intersections;
(iii) presence of granitic intrusions, particularly those that may be enriched in either compatible and incompatible elements;
(iv) occurrence of anomalous magnetic signatures related to the concentration of magnetite in the deposit;
(v) occurrence of radiometric signatures with high values in the uranium channel;
(vi) anomalous presence of copper, gold and iron; and
(vii) association of incompatible elements with the mineralization.

Table 3.1 summarizes the predictive variables and respective geophysical methods that are used in prospecting for IOCG deposits.

Table 3.1. Evidence of IOCG deposits and geophysical methods applied to mineral exploration.

Evidence	Geophysical Method
Sequences rich in iron oxides	Magnetic
Main and secondary structures in large deep crustal faults	Magnetic
Lineament density and zones of structural opening	Magnetic
Strong hydrothermal alteration with magnetite	Magnetic
Presence of uranium	Gamma spectrometry
Potassic alteration areas	Gamma spectrometry
High density because of the presence of sulfides and magnetite	Gravimetry
High chargeability and low resistivity – disseminated ore	Induced polarization (IP)
Electromagnetic conductors – massive ore or interconnected sulfides and magnetite	Electromagnetic (EM)

3.3 - GEOLOGICAL SETTING

The Furnas Copper Deposit is located in the Carajás Mineral Province, along the regional Cinzento transcurrent shear zone striking WNW-ESE. Metavolcano-sedimentary rocks correlated to the Grão Pará Group, of the 2.76 Ga Itacaiúnas Supergroup (Wirth et al., 1986), and sedimentary rocks correlated to the Águas Claras Formation host the deposit. The shear zone defines a contact between amphibole schist to the north (hanging wall) and aluminous schist to the south (footwall) of the Itacaiúnas Supergroup (Figure 3.3), interrupted by the intrusion of the 1.8 Ga Cigano Granite to the east. The region is metamorphosed from greenschist to amphibolite facies (CVRD, 2006).

The deposit is poorly exposed with a wide laterite cover (thickness of about 60 m). The copper-gold mineralization is hosted in biotite-garnet-grunerite-magnetite hydrothermal alteration assemblages, with moderate to strong foliation. The mineralization itself is contained in massive magnetite, silicification, sodic-calcic, and potassic alteration as can be easily seen on the geological cross section through the high and low-grade orebodies (Figure 3.3). The alteration zone is associated with a late-stage chalcopyrite and bornite veinlets and breccias.

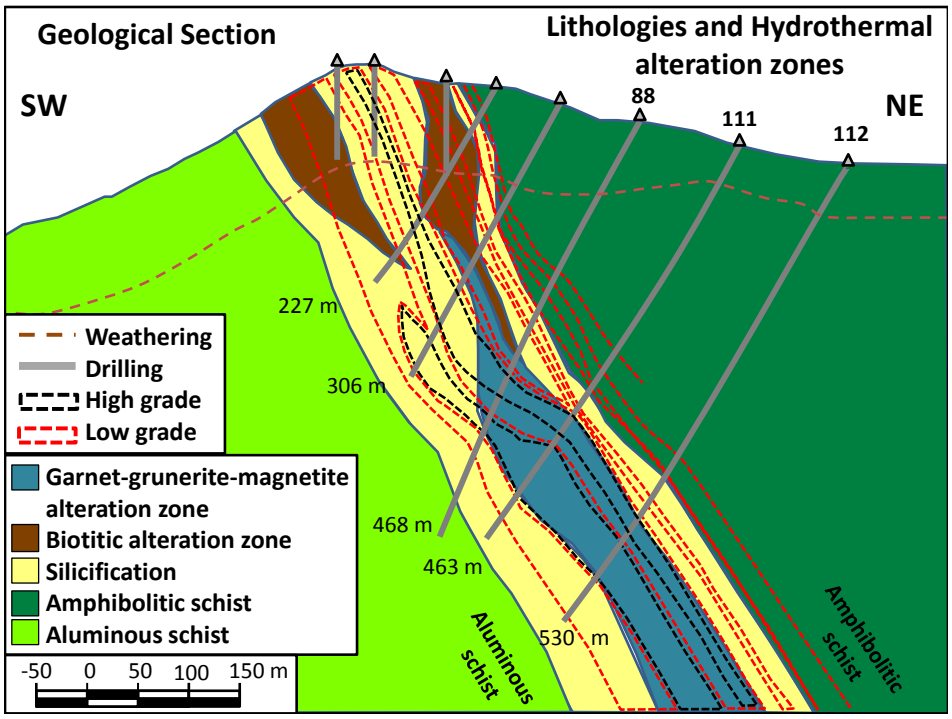

Figure 3.3. Geological section of Furnas Southeast deposit (Modified from Vale, 2012).

The Cu-Au mineralization is concentrated in right stepping, NW striking, dilational structures along the WNW striking dextral shear zone. These structures produced elongated ore shoots during episodic hydrothermal fluid flow events that caused brittle slip and brecciation.

The results of a representative drill hole log within the hydrothermal alteration zones (Figure 3.4) show:

(i) measured magnetic susceptibility on drill cores (in SI x 10^{-3}),

(ii) iron geochemistry (in percentage),

(iii) copper mineralization (in percentage),

(iv) gold mineralization (in grams per ton), and

(v) density (in grams per cubic centimeters);

which well summarizes the behavior of the mineralized hydrothermal alteration zones.

The mineralized magnetite hydrothermal alteration zone is well defined between 316 to 385 m depth by high magnetic susceptibility values (from 200 x 10^{-3} SI to 900 x 10^{-3} SI), high density values (around 3.4 g/cm^3 to 3.8 g/cm^3), high iron content (around 25 % to 40%), high copper grade (from 0.6 % to 5%), and high gold grade (from 2 g/t to 4.5 g/t).

In general, the high copper-gold grades have strong association with high magnetic susceptibility values that are correlated with high total-field magnetic anomalies. Therefore, magnetic survey is one of the most effective geophysical tools for exploration in this area. In particular, the magnetic anomalies help define the Furnas deposit's geophysical signature.

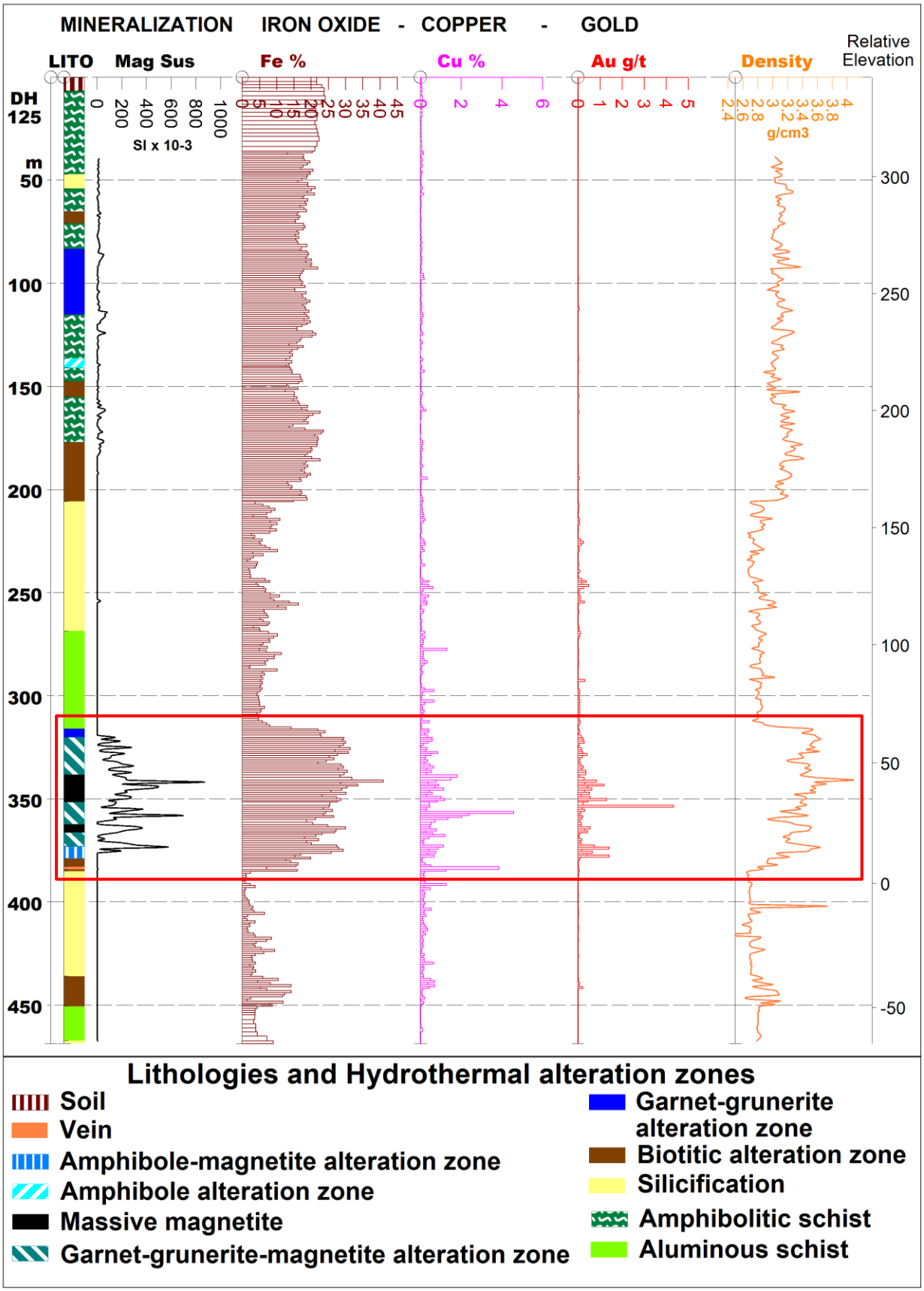

Figure 3.4. Representative drill hole 125 log with the iron oxide-copper-gold IOCG mineralization signatures: hydrothermal alterations, magnetic susceptibility in SI x 10^{-3}, iron grade geochemical assays in percentage, copper grade in percentage, gold in grams per ton and density in grams per cubic centimeter.

3.4 - MAGNETIC DATA

The magnetic data was acquired using a sensor mounted on a helicopter, and in a draped survey with a nominal terrain clearance of 80 m above ground. The survey was carried out in 2012. Survey line spacing was 200 m and the line direction was held at N30°E (Figure 3.5a). Tie line spacing was 5,000 m and the direction was N60°W. The sample rating was 0.1 s and the average sample spacing was 3 m. The ambient field has an inclination of -7.3º, a declination of -20.1º, and a field strength of 25,300 nT.

A subset of the TMI data over the southeast portion of the deposit is shown in Figure 3.5. The corrugation effect seen in raw data (Figure 3.5b) required a great amount of compensation, correction and decorrugation to obtain the final corrected total magnetic field data (Figure 3.6a).

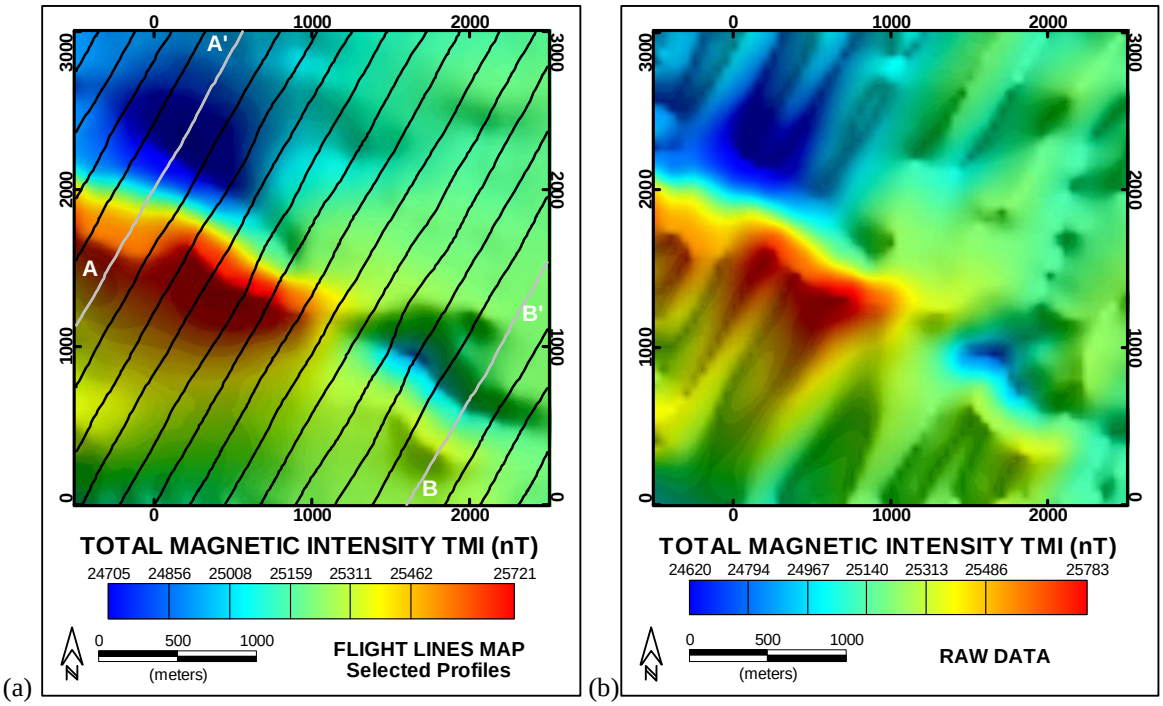

Figure 3.5. The observed total-field magnetic data of the Furnas Southeast deposit. (a) Flight lines are shown in black traces and selected profiles for interpretation are shown in gray. (b) The raw total-field magnetic data of the Furnas Southeast deposit. Units in nT.

The observed profiles over each flight line are shown in Figure 3.6b. As can be seen, the TMI data shows an anomalous target in the NW-SE direction. This anomaly exhibits an interesting feature: it changes its behavior along its length. At its NW end it resembles a typical middle northern magnetic latitude anomaly: big positive values at its southern portion and big negative values at its northern portion. In contrast, its SE end resembles the magnetic signature typical for magnetic equatorial regions, marked by negative values at its central portion and with positive

values at both the southern and northern portions (Figure 3.6b). In order to compare the different qualitative interpretation techniques two profiles were selected perpendicular over each zone (Figure 3.5a) and the two obtained profiles are shown in Figure 3.7. The profile (A – A´) corresponds to the geological section of Figure 3.3.

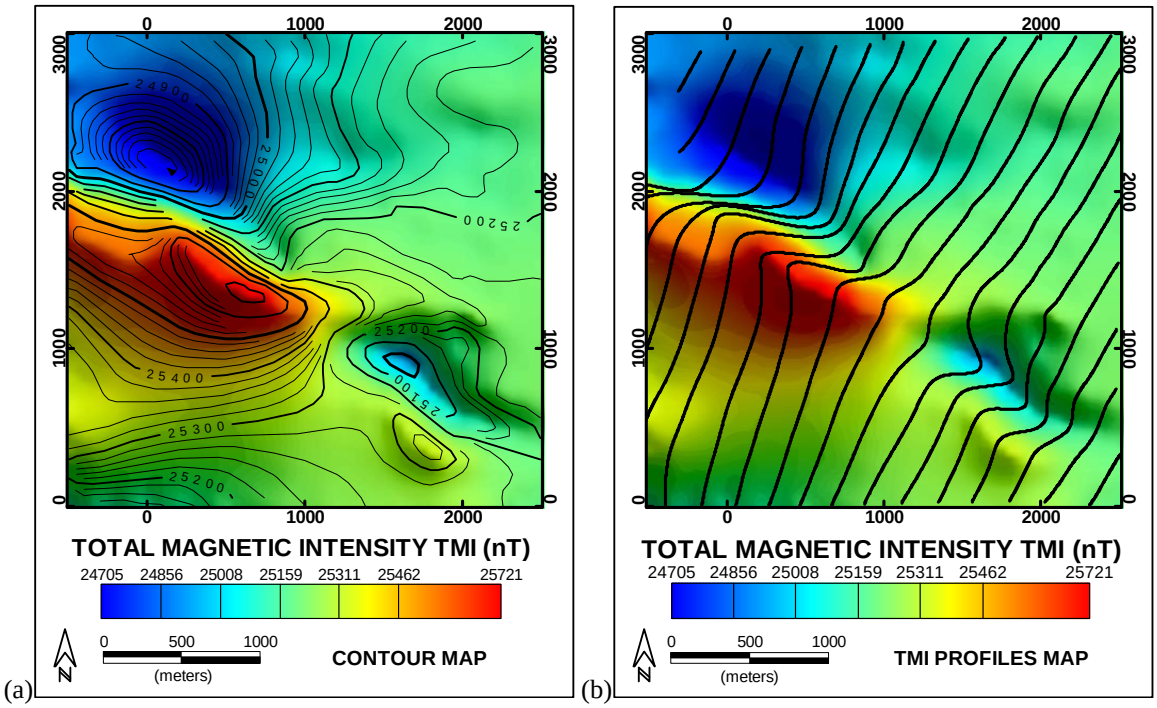

Figure 3.6. The observed total-field magnetic data of the Furnas Southeast deposit. (a) The total-field magnetic anomaly of the Furnas Southeast deposit after all corrections. (b) Total magnetic intensity profiles are shown over each flight line. Units in nT.

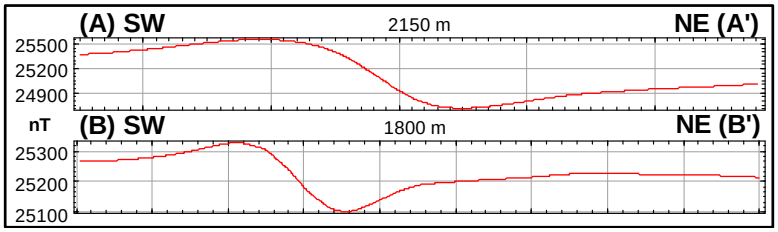

Figure 3.7. The magnetic total-field data over the two profiles shown in Figure 3.5a. Units in nT.

3.5 - METHODS

Before attempting to interpret magnetic field data, one must be aware of the main physical property, its interactions past and present with the Earth geomagnetic field and the physics behind this processes. The main magnetic property, the magnetization is a vectorial quantity related to the main inducing magnetic field as:

$$\vec{M} = \chi_m \cdot \vec{H} \qquad (1),$$

where: $\vec{M}$ is the induced magnetization (A/m); $\vec{H}$ is the inducing magnetic field (A/m); and χ_m is the magnetic susceptibility, a tensorial quantity but normally expressed by a single constant (non-dimensional). The susceptibility is the relevant physical property and is responsible for magnetic induced field anomalies in the material near the Earth surface. More important, in the case of geologic material it is usually related closely to the most common Earth magnetic rock-forming mineral, the **magnetite**. As such, magnetization is not an intrinsic rock physical property, but it is produced by magnetite concentrations that can either be dispersed in a rock volume or located in specific rock structure, such as the brittle ones (faults).

With these considerations in mind, it becomes more comfortable and reliable to extract the best possible information out of the magnetic field data (after it is properly reduced to represent the portion of the magnetic field to be analyzed).

To achieve the desired goal, which was to delineate spatially the target ore, a series of linear transformations on TMI data in the Fourier domain were performed. Following the procedure scheduled earlier for this purpose, the qualitative interpretation started with a brief analysis of the TMI data.

The observed gradient pointed out is the magnetite rich orebody, the target of this research. Since the studied area is located at low magnetic latitude the correct expected magnetic signature is the one seen on the southern portion of the area (see Figure 3.6b). The changing signature behavior on the northern part is probably a clear example of remanence.

With that, the remanent magnetization becomes more relevant in characterizing the magnetic signatures in the deposit. The resultant (induced plus remanent) magnetic anomaly resembles those that could be found on similar geological environment at middle latitudes in the northern hemisphere. This behavior was well shown on the petrophysical measurements carried out as part of these studies. It indicated that the magnetization direction may be changing within the orebody with high anisotropy.

Finally, with all information gained from the analysis, we carried out qualitative interpretation and quantitative interpretation using two-dimensional (2D) parametric and structural modeling, supposing a dipping dike-like body. It confirmed the presence of remanent magnetization and demagnetization effects observable on studying the magnetic field signatures of the TMI images.

3.6 - QUALITATIVE INTERPRETATION

The following linear and nonlinear transformations were used to qualitatively interpret the TMI data.

Reduction to the Pole (RTP)

A magnetic anomaly depends on the inclination and declination of the body's magnetization, the inclination and declination of the local earth's magnetic field, and the orientation of the body with respect to magnetic north. To simplify anomaly shape, Baranov (1957) and Baranov and Naudy (1964) proposed a mathematical approach known as reduction to the pole. This method transforms the observed magnetic anomaly into the anomaly that would have been measured if the magnetization and ambient field were both vertical — as if the measurements were made at the magnetic pole. The RTP operator however becomes unstable at lower magnetic latitudes because of a singularity that appears when the azimuth of the body and the magnetic inclination both approach zero. If not properly accounted for the obtained RTP data shows a strong striation in the direction of magnetic declination. To calculate RTP at low latitudes we used an in-house code based on modified series expansion of the RTP operator which tries to stabilize using an upward/downward continuation process (Figure 3.8). A slightly different version of this approach was developed by Mendonça and Silva, 1993.

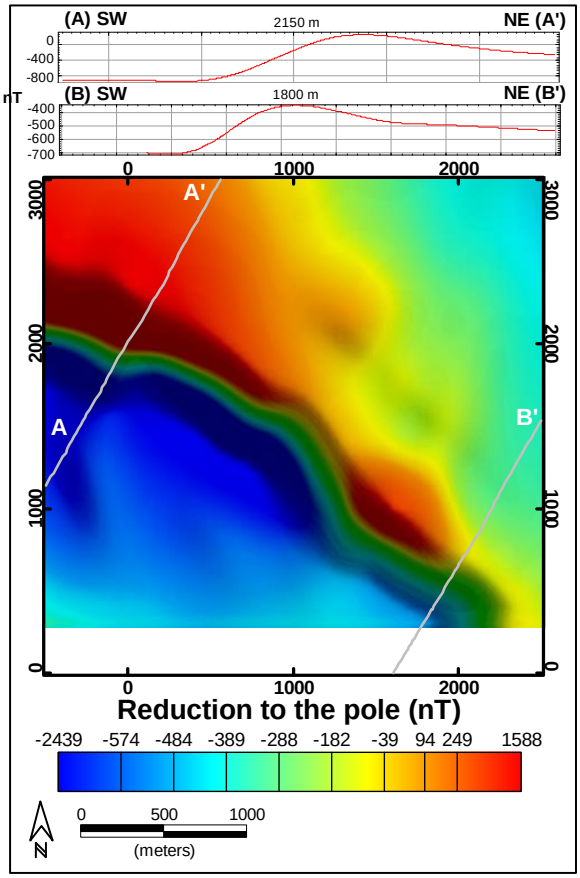

Figure 3.8. Image and profiles of reduction to the pole. Units in nT.

Terracing

Terracing operates iteratively on magnetic data to generate areas of constant field amplitude that are divided by sharp frontiers (Figure 3.9). Terracing is computed by moving a window over the data and calculating the curvature at the center of the window (Cordell and MacCafferty, 1989; Philips, 1992). The inflection points of the curvature are located approximately over the edges of the targets. The technique iteratively increases the slopes of the first horizontal derivatives around the inflection point until they become vertical. The resulting map is similar to a terraced landscape, hence the name applied to this technique. Magnetic data is generally converted to pseudo-gravity before using terracing (Baranov, 1957). We applied this transformation with an in-house code, to Furnas Southeast deposit reduction to the pole (RTP) data (Figure 3.9).

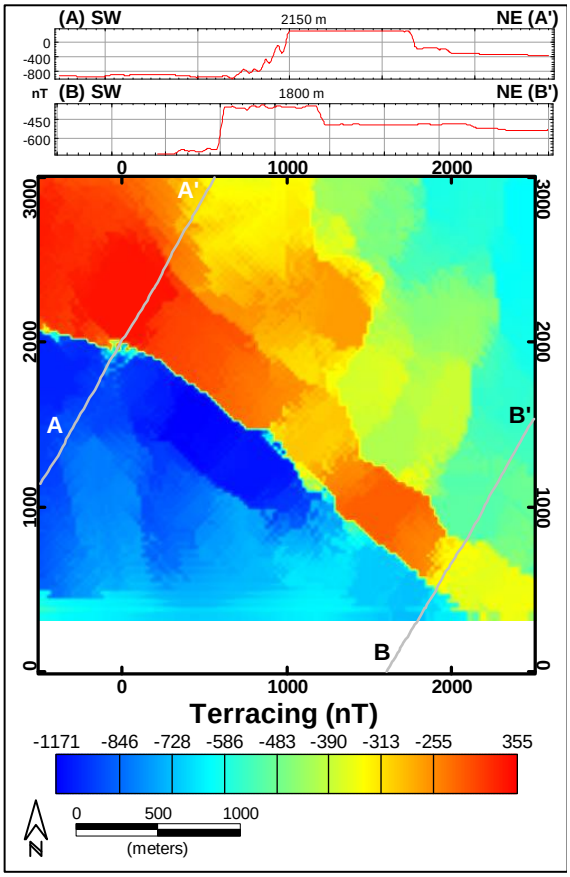

Figure 3.9. Image and profiles of terracing. Units in nT.

Magnetic Amplitude Anomaly

The best approach in processing the data was provided by the calculation of the amplitude of the anomalous magnetic field as a direct indicator of target orebody and mineralized zones. Given the influence on the magnetic data by remanent magnetization and self-demagnetization, we chose to use the magnetic amplitude calculation, which is minimally dependent on the magnetization direction (Shearer 2005; Li et al. 2010; CGEM, 2012; Leão-Santos et al, 2014). This can be considered the anomalous magnetic field intensity, also denoted Magnetic Magnitude Anomaly (MMA).

As Nabighian (1972) has shown, the amplitude of the analytic signal in 2D, which is the total gradient, is independent on the magnetization direction. This property also holds true for the amplitude of the anomalous magnetic vector in 2D. In 3D, this invariant property does not strictly hold true, but both quantities are only weakly dependent on the magnetization direction (e.g., Stavrev and Gerovska, 2000; Haney et al., 2003).

The amplitude data is defined as

$$B_a = \sqrt{B_{ax}^2 + B_{ay}^2 + B_{az}^2}, \qquad (2),$$

where B_{ax}, B_{ay}, and B_{az} are the three components of the anomalous magnetic vector in the x-, y-, and z-directions, respectively. The amplitude data conserve the low-wavenumber content and thus retain the signal due to deep magnetic bodies.

The challenge is the need to calculate the three anomalous magnetic components. In our current study, this operation is difficult to undertake because of the low survey magnetic latitude. The commonly used wavenumber-domain approach encounters the similar low-latitude instability problems as in the reduction to the pole (RTP) calculation, albeit to a lesser degree.

To overcome the difficulty of low-latitude instability, we chose to use the equivalent source technique (Dampney, 1969). Also, to accommodate the rugged observation surface, we used a 3D equivalent layer consisting of susceptibility values that can be either negative or positive. We constructed an equivalent source from the total-field anomaly (Figure 3.5b) using an algorithm similar to that in Li and Oldenburg (1996) but without any bound constraints on the susceptibility. The equivalent source layer is located immediately below the lowest topographic point and consists of cubes of 50 m size.

Once the equivalent source is obtained, we used it to calculate the three orthogonal components of the magnetic anomaly and obtain the magnetic amplitude data by equation 2 with a code developed by Shearer (2005; Figure 3.10).

The main purpose was to reduce the asymmetry in total-field magnetic anomaly due to the oblique directions of magnetization and background field, so that the magnetic anomaly is centered over the source bodies. However, RTP operation suffers from two major challenges, namely, the unknown magnetization direction and the instability at low magnetic latitudes. The amplitude data, on the other hand, achieve the same objective approximately but do not rely on the magnetization direction and suffers much less from the low latitude instability (Figure 3.10).

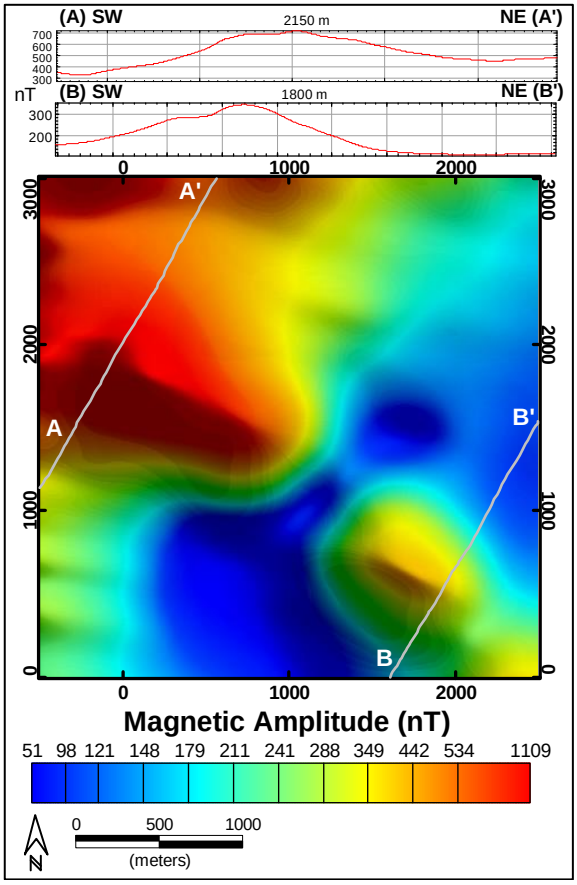

Figure 3.10. Images and profiles of magnetic amplitude calculation. Units in nT.

Upward continuation

Magnetic data measured on a given plane can be transformed to data measured at a higher or lower elevation, thus either attenuating or emphasizing shorter wavelength anomalies (Kellogg, 1953). Thus the upward continuation operator behaves as a low-pass filter as shown on the upward continuation data of 100 m, 250 m, 500 m, 750 m, 1000 m and 1500 m (Figures 3.11a to 3.11f, respectively). These results show the attenuation of high spatial frequency on the TMI data which helps the understanding of the regional magnetic background.

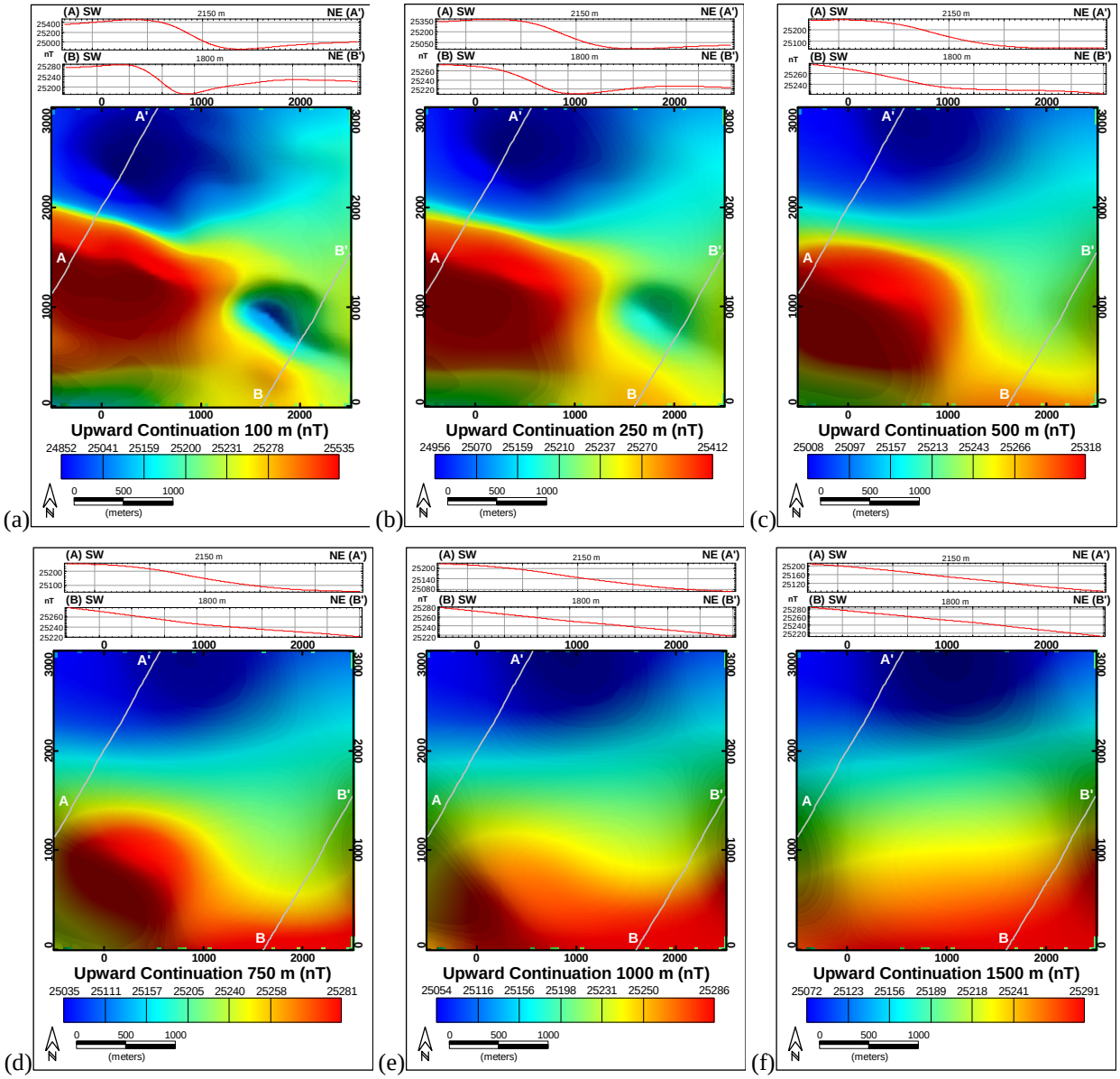

Figure 3.11. Images and profiles of Upward Continuation. (a) 100 m, (b) 250 m, (c) 500 m, (d) 750 m, (e) 1000 m and (f) 1500 m.

Derivative based filters

The first and second order partial derivatives of TMI data in X, Y and Z directions can be combined in various ways for further analysis of magnetic data. Many modern methods for edge detection and depth to source estimation rely on horizontal and vertical derivatives. Cordell and Grauch (1982, 1985) used crests of the magnitude of the horizontal gradient of the pseudo-gravity field (the total horizontal gradient) as an approximate tool for locating the edges of magnetic bodies. In practice, this approach can also be applied to the reduced-to-the-pole magnetic field (Figure 3.12a).

Similarly, vertical derivatives help to enhance the location and edges of the magnetic body in the area of the highest magnetic gradient on the NW part and low magnetic areas in the SE (Figure 3.12b).

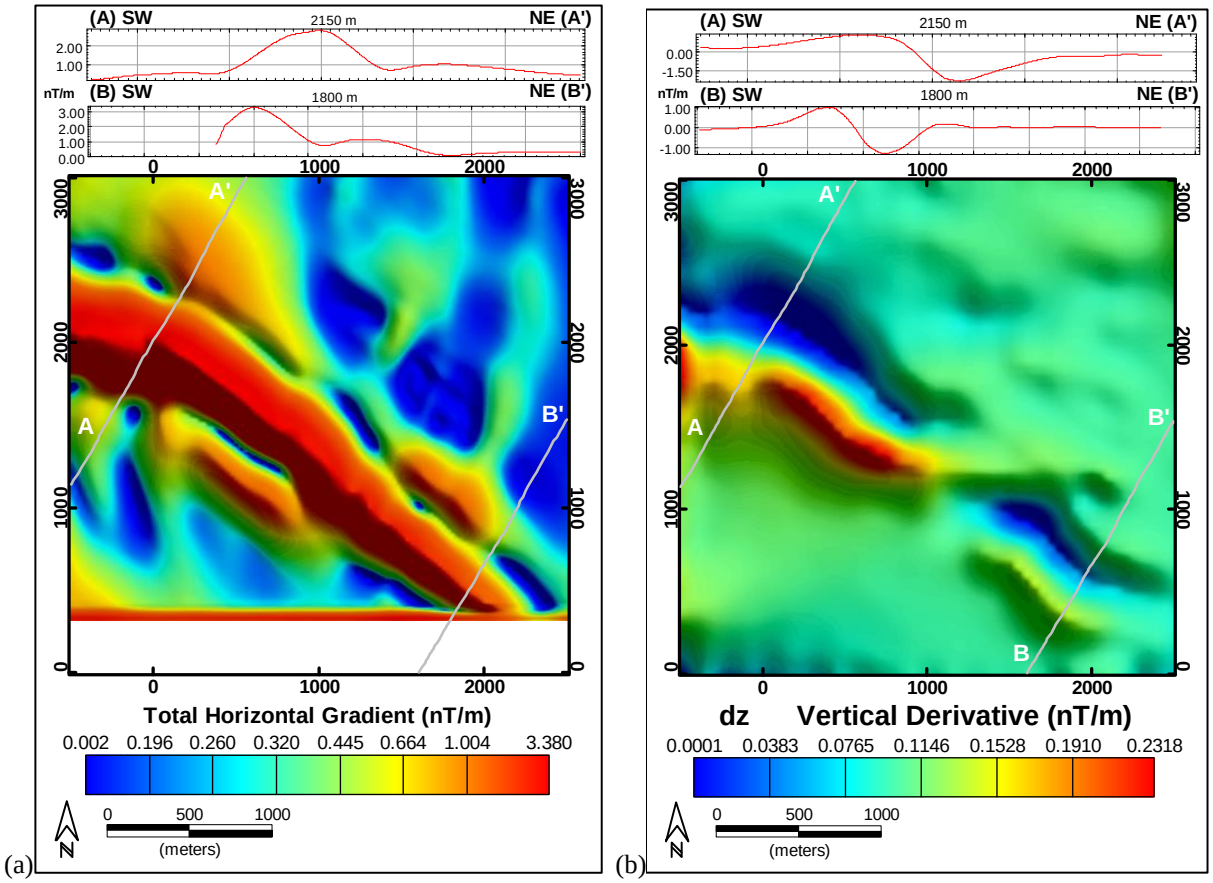

Figure 3.12. (a) Total horizontal gradient of the anomalous magnetic field; (b) vertical derivative. Units in nT/m.

Total Gradient (Analytic Signal)

The total gradient (analytic signal) is another popular method for locating the edges of magnetic bodies. For magnetic profile data, the horizontal and vertical derivatives fit naturally into the real and imaginary parts of a complex analytic signal (Nabighian, 1972, 1974, 1984; Craig, 1996). In 2D (Nabighian, 1972), the amplitude of the analytic signal is the same as the total gradient and is independent of the direction of magnetization. In 3D, Roest et al. (1992) introduced the total gradient of magnetic data as an extension to the 2D case. Unlike the 2D case, the total gradient in 3D is weakly dependent on the direction of magnetization (Haney et al., 2003). It is worth noting that what is now commonly called analytic signal should correctly be called the total gradient. The calculated amplitude of analytic signal in 2D or the total gradient (Figure 3.13) and the total gradient in 3D (also called amplitude of analytic signal in 3D; Figure 3.14) show clearly the location of magnetic sources.

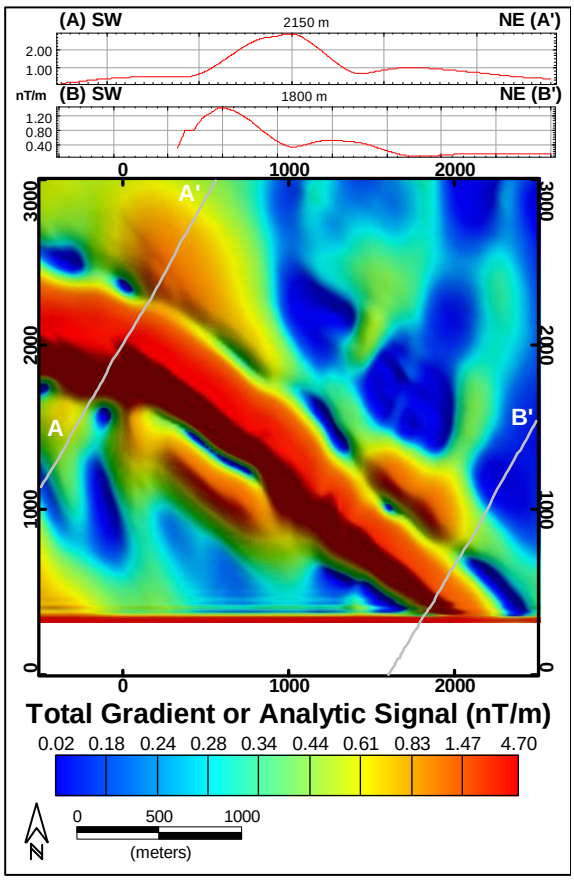

Figure 3.13. Image and profile of Total Gradient (Analytic Signal). Units in nT/m.

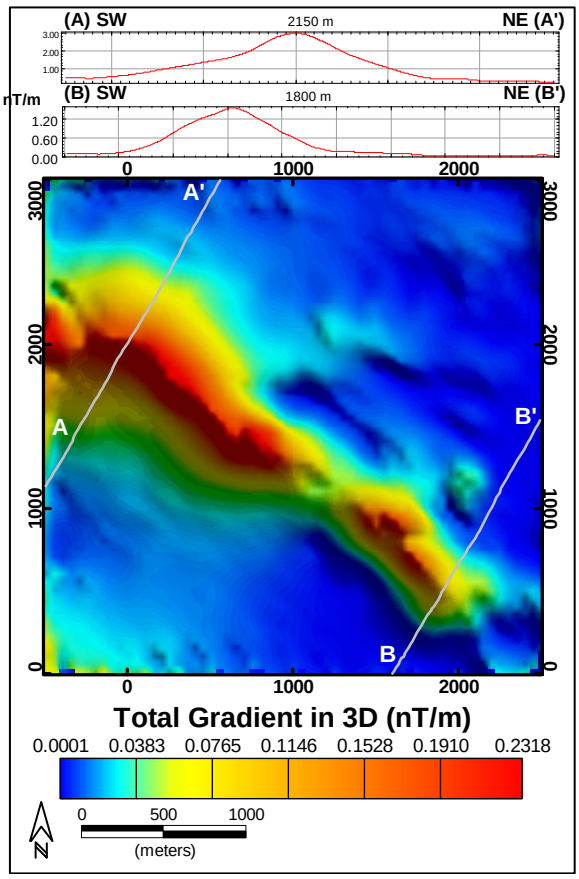

Figure 3.14. Image and profile of total gradient in 3D. Units in nT/m.

Tilt Derivative or Analytic Signal Vector Inclination

The tilt derivative, also called inclination of analytic signal, is helpful for delineating shallow and deep sources of various structures and lineaments (Figure 3.15). The tilt angle is determined by the ratio of the first vertical derivative of the potential field to the total horizontal gradient of the field (Miller and Singh, 1994).

The expected anomaly of inclination of analytic signal over a vertical dyke at equatorial magnetic latitudes is a high-low-high response whereas the shape of the anomaly at Furnas Southeast deposit resembles those at intermediate latitude (Verduzco et al., 2004).

The main purpose of this transformation is that it expresses the amplitude of the TMI vertical spatial derivative, weighted by the amplitude of the horizontal gradient (positive part) in a bandwidth of $-\pi/2$ to $+\pi/2$ thus providing an excellent tool for the magnetic fabric relief studies (magnetic structures).

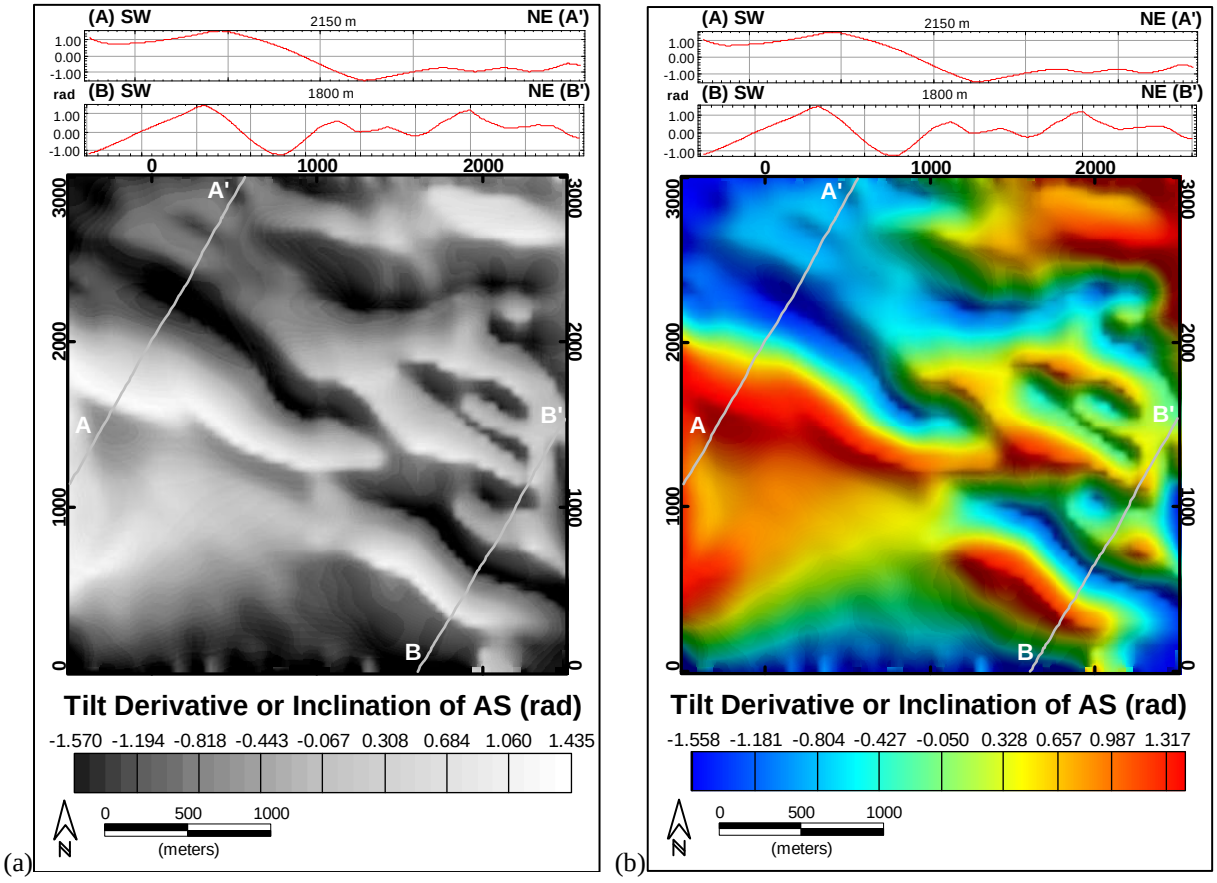

Figure 3.15. Image and profile of tilt derivative or inclination of analytic signal, (a) gray color distribution, (b) pseudocolour distribution. Units in radian.

Qualitative Interpretation

Using the data provided above the qualitative interpretation was performed by visual inspection of the images and profiles in maps and cross-sections, based on the many transformations available. The magnetic domains and lineaments related to the local magnetic field configuration were delineated by eye and by hand (Figures 3.16a and 3.16b). The magnetic relief is dominated by a high amplitude anomaly outlined by a red polygon with its axis indicated with a dashed black thick line. The main magnetic structures of the area have a NW-SE direction (Figure 3.16b).

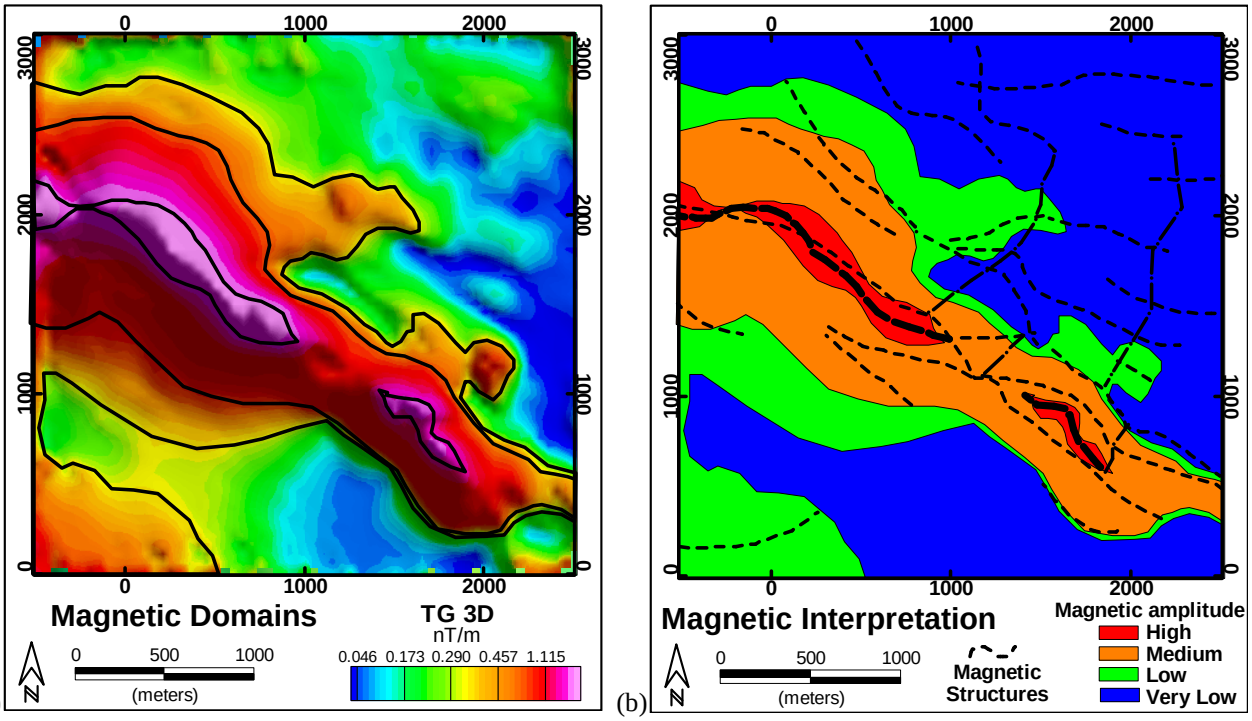

Figure 3.16. (a) Magnetic domains outline over the total gradient in 3D image. (b) Qualitative interpretation with magnetic domains and structures. Units in nT.

3.7 - SEMI-QUANTITATIVE INTERPRETATION

Power Spectrum

The radially averaged power spectrum is the average of all possible directional power spectra for a given radius. It can be summarized as the direction-autonomous average spectrum. The radially averaged power spectrum supplies an appropriate means to visualize and confront information contained in 2-D spectra in 1-D. The radially averaged power spectrum is calculated using the Fast Fourier Transform (FFT) of an input matrix and it does not account for corner values outside averaging radius (Matlab, 2014). The power spectrum was performed over the area of the maps to estimate the depth of the magnetic sources. The power spectrum of Furnas deposit shows the shallow sources from 0 m to 200 m, the intermediate sources from 200 m to 500 m, and the deep sources up to 800 m (Figure 3.17).

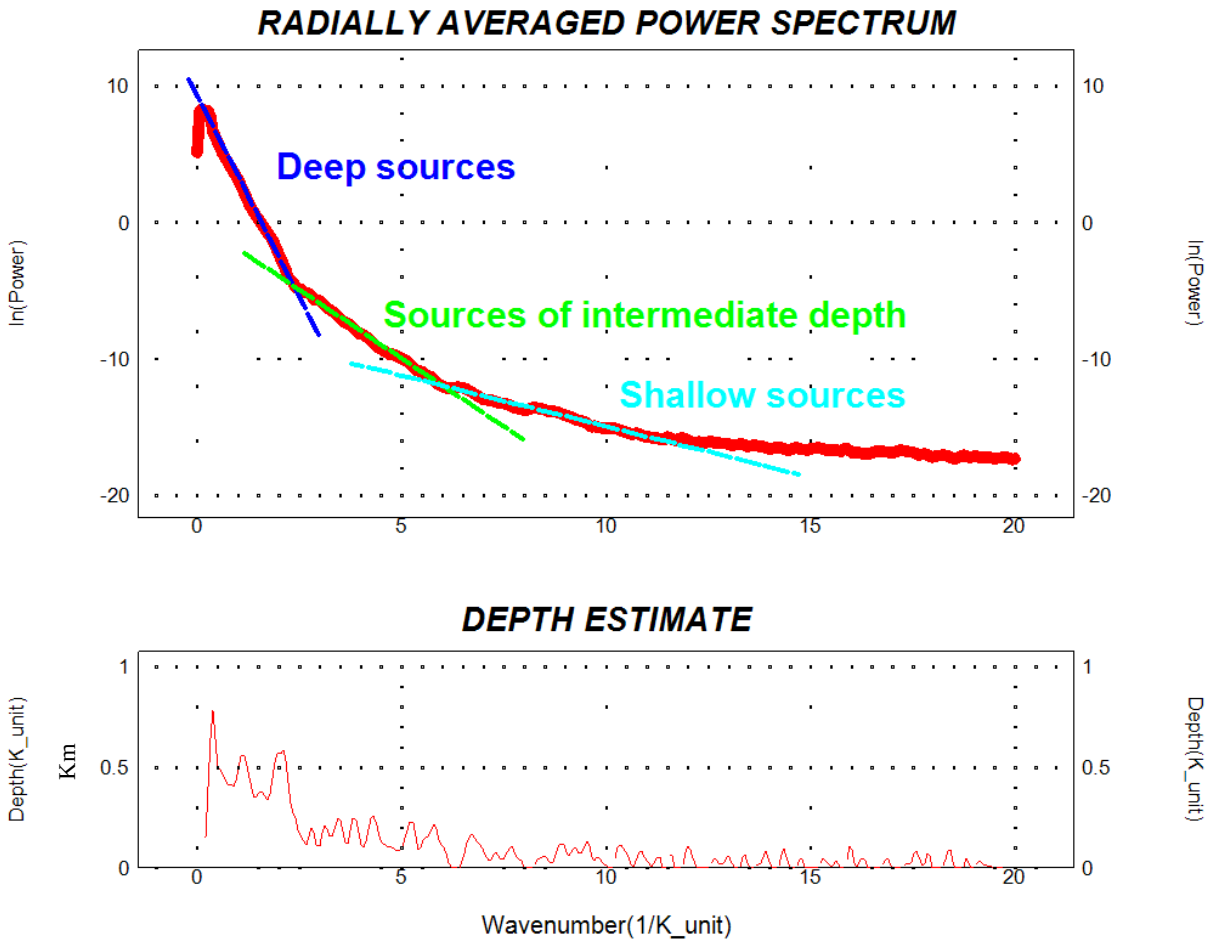

Figure 3.17. Radially averaged power spectrum with depth estimates of shallow, intermediate and deep sources.

Euler Deconvolution

The source depth can be estimated at the edge location using advanced depth determination techniques that use both the vertical and horizontal derivatives. Examples of techniques that estimate the source depths are Euler deconvolution (Thomson, 1982; Reid et al., 1990; Mushayandebvu et al., 1999; Nabighian and Hansen, 2001) and Werner deconvolution (Hartman et al, 1971; Hansen and Simmonds, 1993). For Euler deconvolution, the structural index is an exponential factor corresponding to the rate at which the field falls off with distance, for a source of a given geometry. A structural index value of 1 is appropriate for dyke geometry that is the configuration of the deposit (Figure 3.18). The complex hydrothermal alteration of Furnas deposit limits the use of the Euler deconvolution because it is based on a homogenous function and needs homogeneous targets.

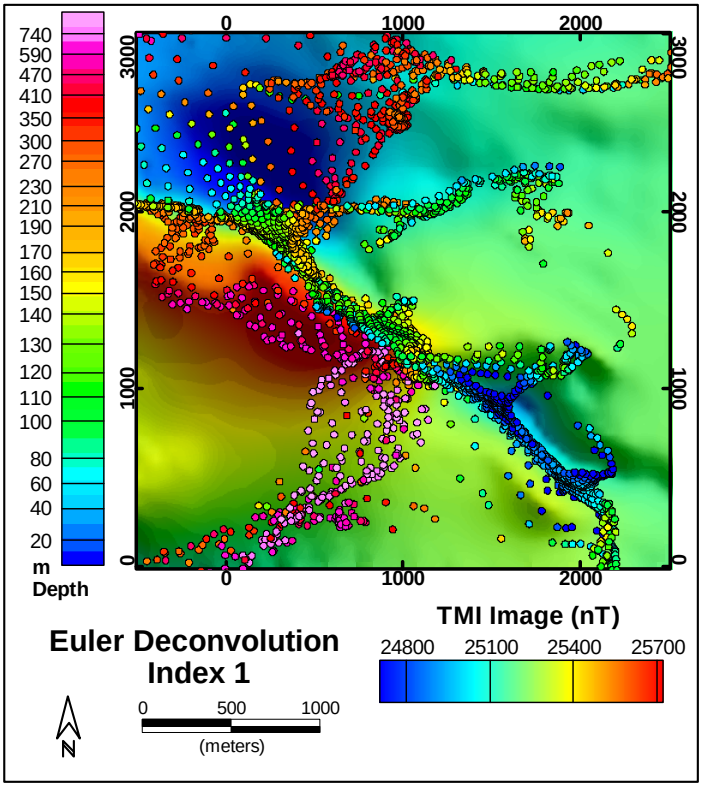

Figure 3.18. Euler deconvolution solutions of structural index value 1 to dyke geometry, with total magnetic field image background.

3.8 - QUANTITATIVE INTERPRETATION
TWO-DIMENSIONAL PARAMETRIC MODELING

Finally, with all acquired knowledge, a quantitative interpretation using two-dimensional modeling (controlled error minimization algorithm – inversion) was performed. This helped to estimate some of the magnetic feature distribution, such as apparent magnetic susceptibility and the geometry of causative bodies by using isolated elongated (2D) anomalies to understand more fully the structurally controlled hydrothermal alteration in iron oxide–copper–gold deposits (IOCG) in this region.

The 2D parametric modeling was applied to magnetic data with the empirical use of geometry, magnetic susceptibility, remanence and demagnetization to evaluate the behavior of the anomaly. Also it was used to define the presence of remanence on the total magnetization and the influence of demagnetization effects.

This problem was treated as parametric, because there are fewer parameters to describe the model than there are measurements. This is an "over-determined" problem and it`s interpretation is non unique.

First, we selected a representative section of the total magnetic field airborne dataset. The anomaly has a dipolar profile with high values on the south and low values in the north (Figure 3.19), different from the expected typical equatorial anomaly with a symmetric high-low-high structure. This shape of the anomaly could imply strong remanence and/or demagnetization. The anomaly is primarily caused by the top of the body.

Then we used a selected profile to compare with the modeled response of a dipping dike-like body with and without remanence and demagnetization. The main parameters selected were: distance around 1500 m, strike -70°, length 1000 m and density 2.67 g/cm^3. Units are assigned a relatively high susceptibility, around 2 SI, in order to fit the large measured anomalies in the magnetic data.

In the first attempt, the modeling was performed without remanence and demagnetization. The modelled response exhibits a moderate fit to anomaly shape but the dips are too shallow (Figure 3.19).

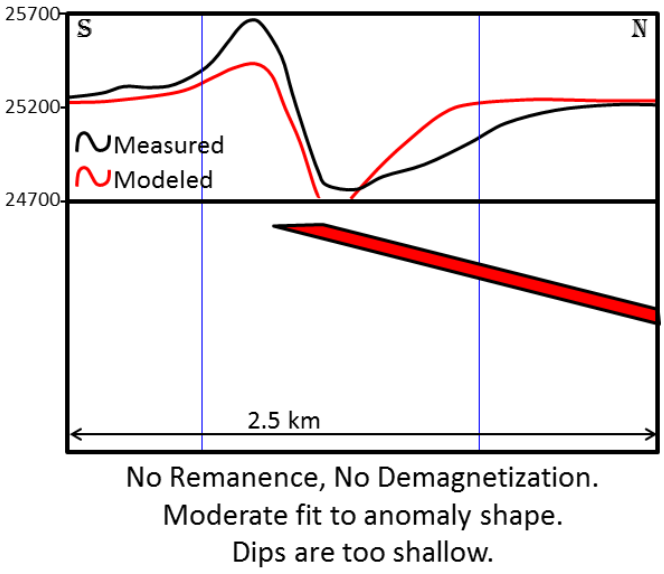

Property	Value	Vary
Body Type	Thick Sheet	
Distance	1561 m	Yes
Top	-201 m	Yes
Strike	-70° Az	No
Dip	16°	Yes
Width	88 m	Yes
Length	1000 m	No
Offset	200 m	No
Density	2.67 g/cm³	Yes
Susceptibility	2.14 SI	Yes
Remanence J	0	No
Rem Inclination	0	No
Rem Declination	0	No
Demag.	No	

Figure 3.19. Parametric modeling of magnetic profile without remanence and demagnetization.

In the second attempt, the modeling was performed without remanence and with demagnetization included. The modelled response exhibits a moderate fit to anomaly shape and the dips are still too shallow (Figure 3.20).

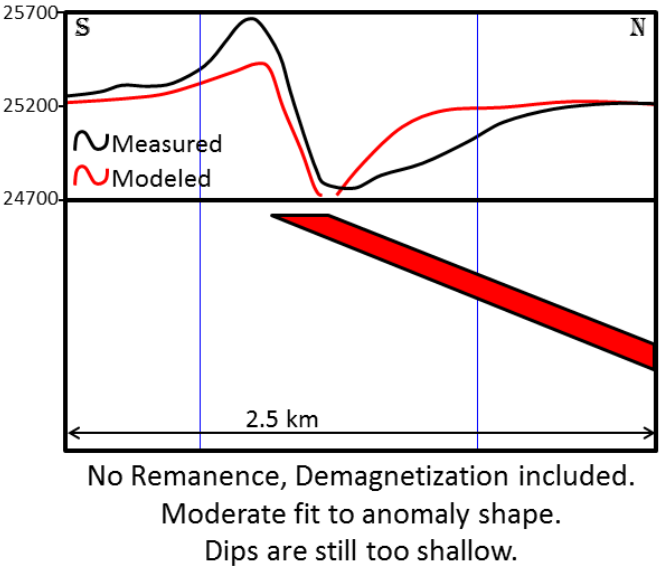

Property	Value	Vary
Body Type	Thick Sheet	
Distance	1536 m	Yes
Top	-150 m	Yes
Strike	-70° Az	No
Dip	25°	Yes
Width	140 m	Yes
Length	1000 m	No
Offset	200 m	No
Density	2.67 g/cm³	Yes
Susceptibility	2.00 SI	Yes
Remanence J	0	No
Rem Inclination	0	No
Rem Declination	0	No
Demag.	Yes	

Figure 3.20. Parametric modeling of magnetic profile without remanence and with demagnetization included.

In the third attempt, the modeling was performed with a steep dip constraint, remanence included but without demagnetization. The remanence (K_n=1.5) is assigned roughly along the dip direction (Inclination = -65° and Declination = 0°). The modelled response exhibits a poor fit to anomaly shape but the anomaly has a symmetric equatorial style (Figure 3.21).

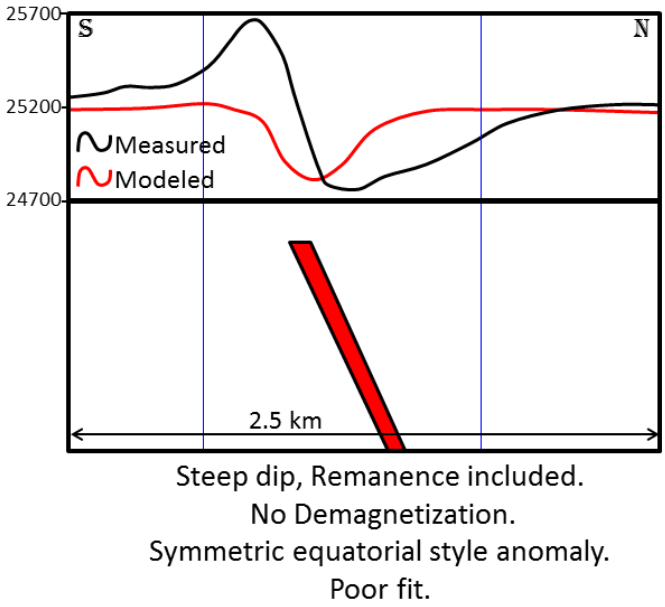

Property	Value	Vary
Body Type	Thick Sheet	
Distance	1672 m	Yes
Top	-325 m	Yes
Strike	-70° Az	No
Dip	69°	No
Width	100 m	Yes
Length	1000 m	No
Offset	200 m	No
Density	2.67 g/cm³	Yes
Susceptibility	2.03 SI	Yes
Remanence J	1.5 A/m	Yes
Rem Inclination	-65°	No
Rem Declination	0°	No
Demag.	No	

Figure 3.21. Parametric modeling of magnetic profile with steep dip and remanence included, and without demagnetization.

In the fourth attempt, the modeling was performed with steep dip constraint, remanence and demagnetization included. The modelled response now fits well the anomaly shape (Figure 3.22).

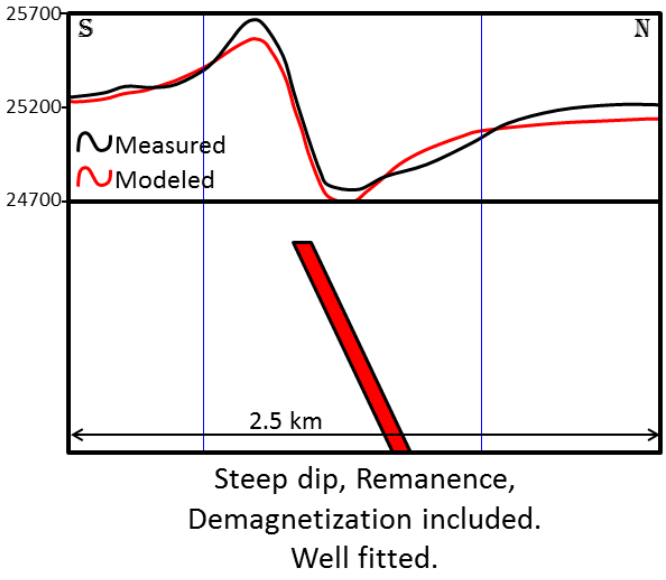

Property	Value	Vary
Body Type	Thick Sheet	
Distance	1672 m	Yes
Top	-325 m	Yes
Strike	-70° Az	No
Dip	69°	No
Width	100 m	Yes
Length	1000 m	No
Offset	200 m	No
Density	2.67 g/cm³	Yes
Susceptibility	2.03 SI	Yes
Remanence J	1.5 A/m	Yes
Rem Inclination	-65°	No
Rem Declination	0°	No
Demag.	Yes	

Figure 3.22. Parametric modeling of magnetic profile with steep dip, remanence and demagnetization included.

In summary, the body is strongly magnetized, exhibits strong demagnetization effects, is thin and with a down-dip extent to emphasize anomaly from top surface. Also, it has remanent magnetization and magnetic anisotropy.

3.9 - RESULTS

The success of the quantitative and qualitative interpretation is evaluated not only by the level of correlation with the orebody, but more importantly, by the correspondence between the estimated magnetic properties of 2D model structure and the known source, which is the massive magnetite orebody in this case.

The flight lines A – A' and B – B', highlighted in the maps, were selected to evaluate and compare the shape of the signals. The profile (A – A´) corresponds to the geological section of Figure 3.3. The results show the good correlation of the projection of the orebody at surface, and the transformations profiles: total magnetic intensity field (TMI), reduction to the pole (RTP), pseudo-gravity (PGRV), magnetic amplitude (AMP), terracing (TER), total horizontal gradient (THG), vertical derivative (DZ), total gradient or analytic signal (TG), total gradient in 3D (TG3D) and tilt derivative or inclination of analytic signal (IAS), from top to base (Figures 3.23 and 3.24).

Total magnetic intensity correlated with the high and low grade ore shows that the northern body has an anomaly that resembles those at middle latitude probably due to remanence. Part of the southern anomaly pattern is consistent with the anomalies at low magnetic latitude (Figure 3.25a).

Reduction to the pole transformed the observed magnetic anomaly into the anomaly as if the measurements were made at the magnetic pole. The results peaks have a good correlation with the orebody and have positive values indicating dip to NE (Figure 3.25b).

The magnetic amplitude was one of the main interpretation tools. This set of computed amplitude data is much simpler in pattern and its peak coincides with the location of the orebody. The excellent correspondence with known geology indicate that the equivalent source technique has worked well (Figure 3.25c).

Terracing applied to the Furnas' Southeast deposit TMI data delineated the low grade SW limit along the deposit. It also created a sharp step that defined a terrace over the orebody that continues to NE indicating the dip direction (Figure 3.25d).

Horizontal derivatives enhanced the horizontal gradient and consequently helped to find the lateral limits of the anomaly sources (Figure 3.25e). Vertical derivative enhanced the location of the magnetic source in the highest magnetic gradient on the NW ore body and within low magnetic value at SE ore body (Figure 3.25f).

The interpretation of the calculated amplitude of analytic signal in 2D or total gradient of Furnas Southeast deposit show a good correlation between the low and high grade orebodies due to the strong association of copper sulfides and magnetite (Figure 3.25g). The total gradient in 3D and the orebodies also showed a good correlation (Figure 3.25h). Comparing the two transformations it can be seen that the 3D total gradient (Figure 3.25h) gives a smoother and cleaner response

compared to the total gradient (analytic signal) that gives effective boundary delineation (Figure 3.25g).

The inclination of analytic signal delineates the orebody between the low in the north and the high in the south. The main magnetic lineaments indicate the predominant NW-SE structures directions (Figure 3.25i).

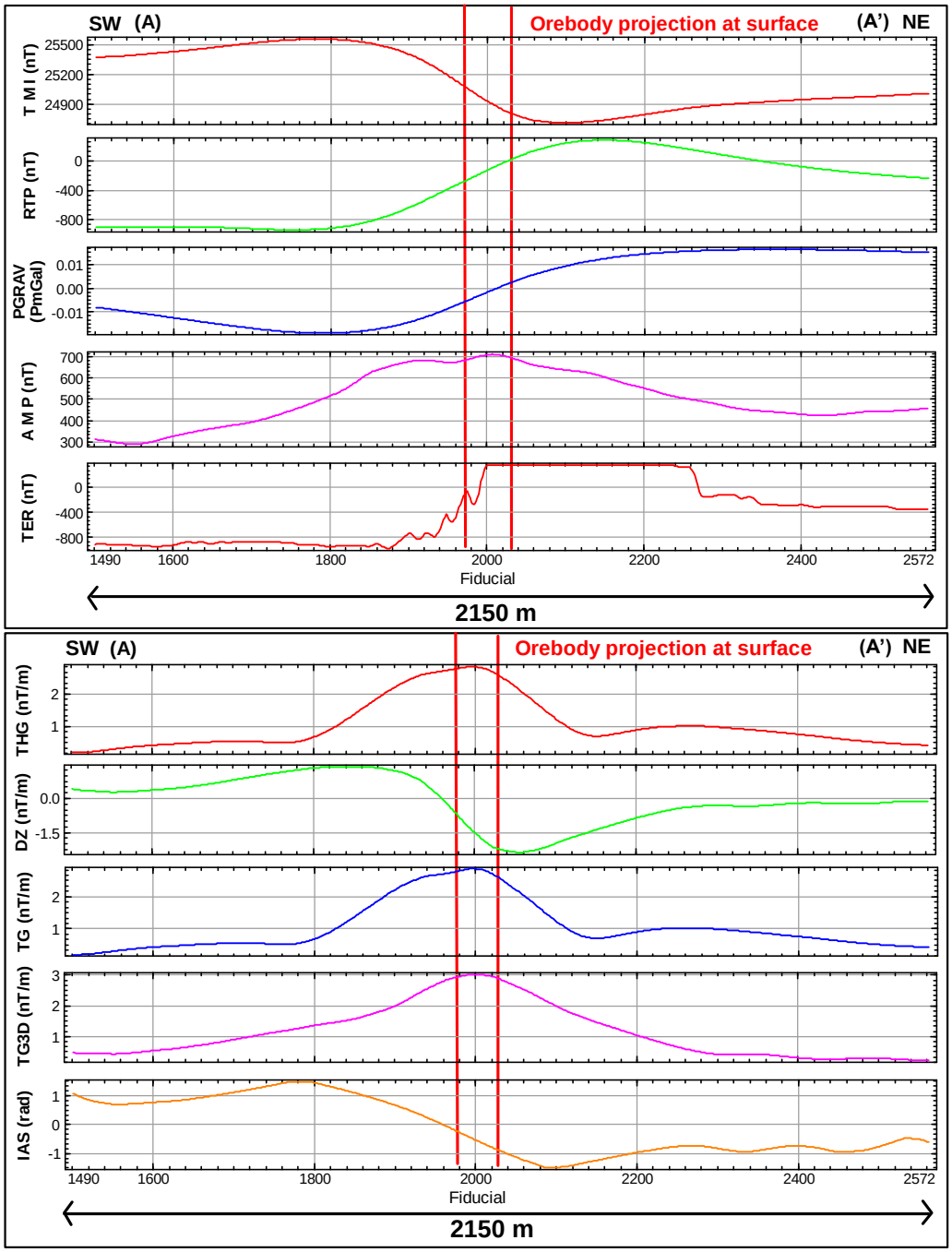

Figure 3.23. Correlation of magnetic profiles with orebody projection at surface of flight line A – A'. TMI = total magnetic intensity field, RTP = reduction to the pole, PGRV = pseudo-gravity, AMP = magnetic amplitude, TER = terracing, THG = total horizontal gradient, DZ = vertical derivative, TG = total gradient or analytic signal, TG3D = total gradient in 3D and IAS = tilt derivative or inclination of analytic signal.

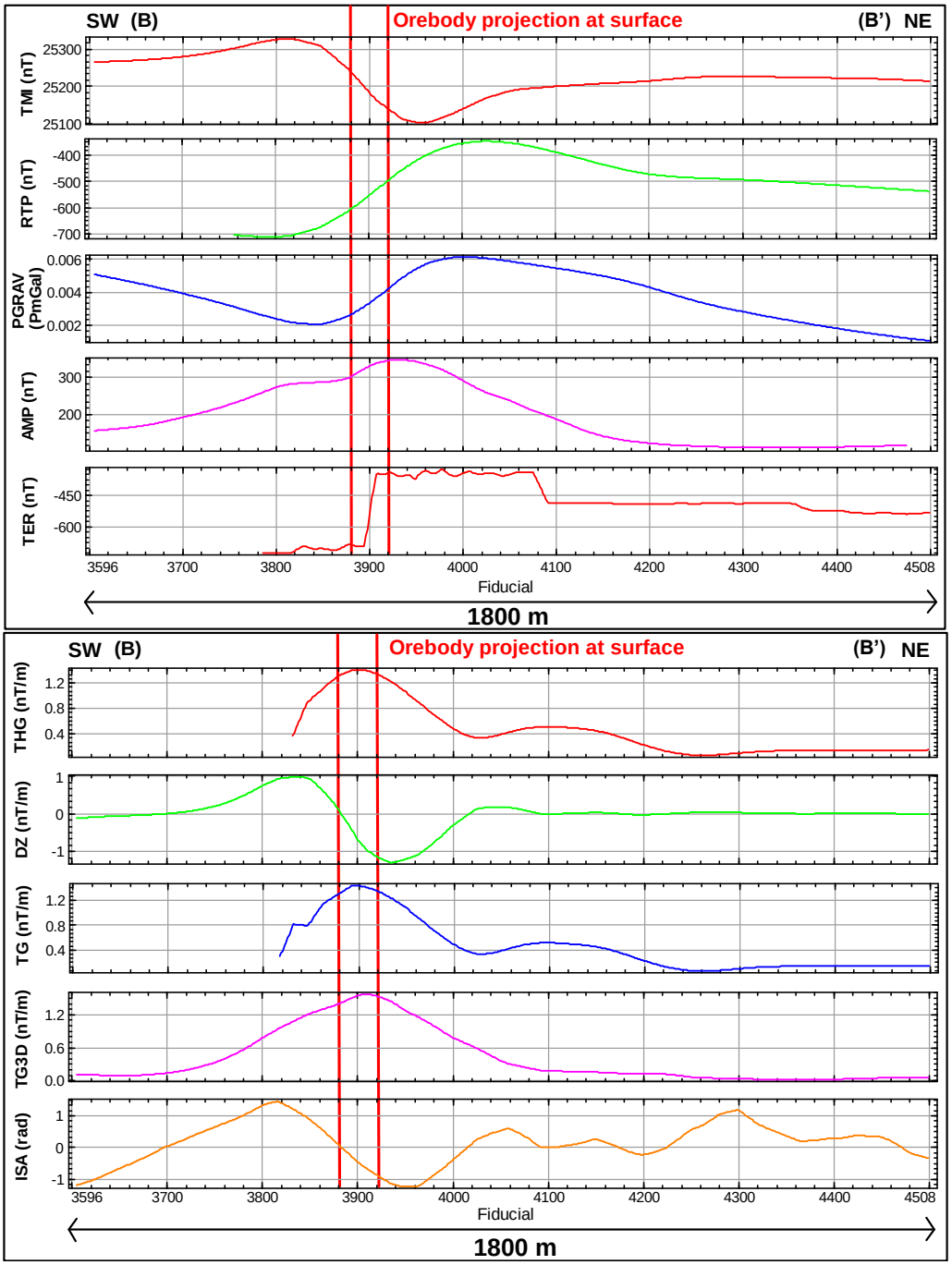

Figure 3.24. Correlation of magnetic profiles with orebody projection at surface of flight line B – B'. TMI = total magnetic intensity field, RTP = reduction to the pole, PGRV = pseudo-gravity, AMP = magnetic amplitude, TER = terracing, THG = total horizontal gradient, DZ = vertical derivative, TG = total gradient or analytic signal, TG3D = total gradient in 3D and IAS = tilt derivative or inclination of analytic signal.

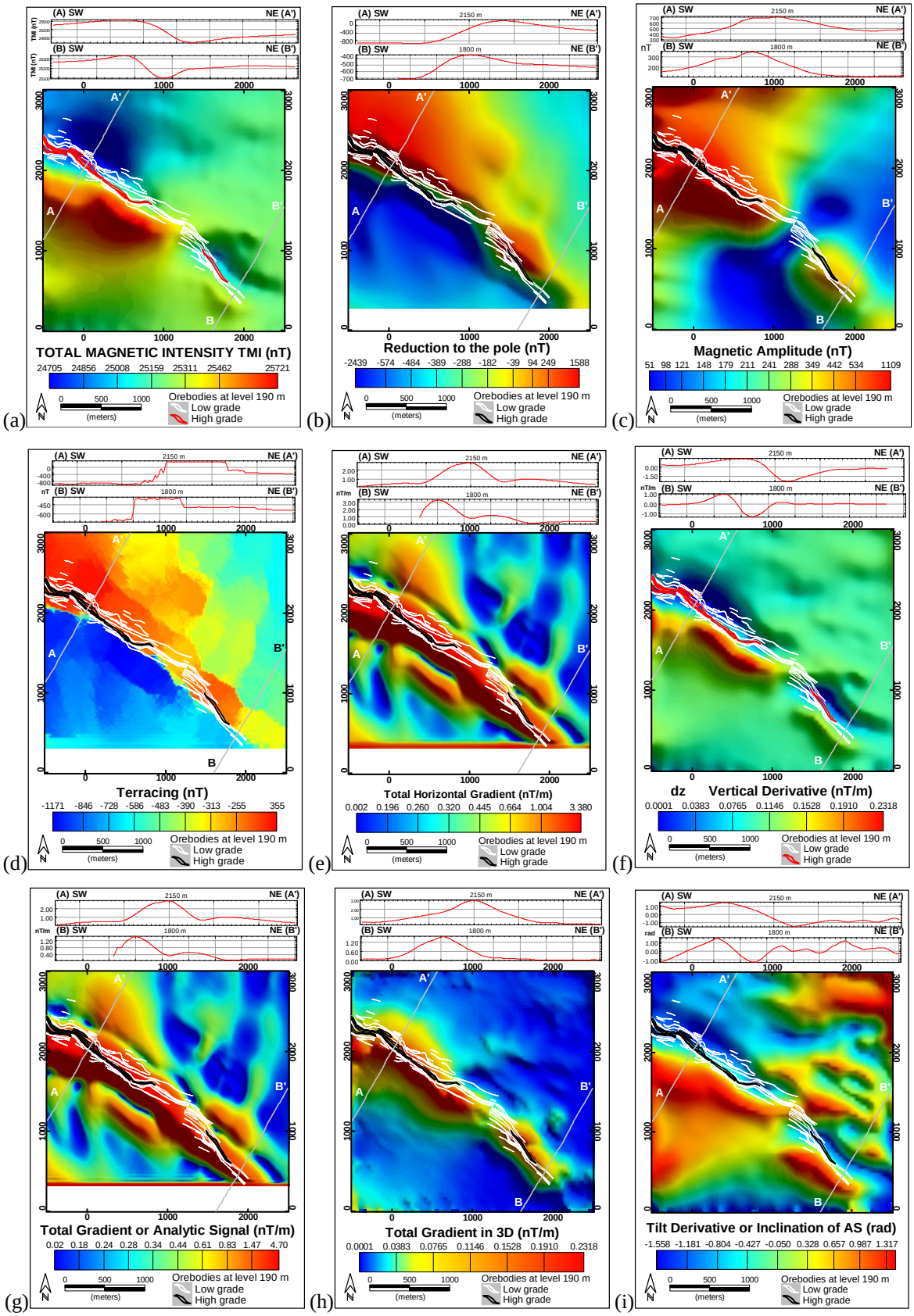

Figure 3.25. Correlation of high and low grade orebodies with images and profiles of: (a) total magnetic intensity, (b) reduction to the pole, (c) magnetic amplitude, (d) terracing, (e) total horizontal gradient (f) vertical derivative, (g) total gradient or amplitude of analytic signal in 2D, (h) total gradient in 3D, and (i) tilt derivative or inclination of analytic signal.

The Euler solutions delineated the main structures and lineaments in the area. The Euler deconvolution results, with structural index 1 representing dyke geometry, indicated the main NW-SE direction of the orebodies (Figure 3.26). Also, the depth estimations show the dip direction of the NW magnetic body from cold colors, indicating shallow estimations, to hot colors, indicating deep estimations. The depth estimations to the SE magnetic body indicated shallow responses.

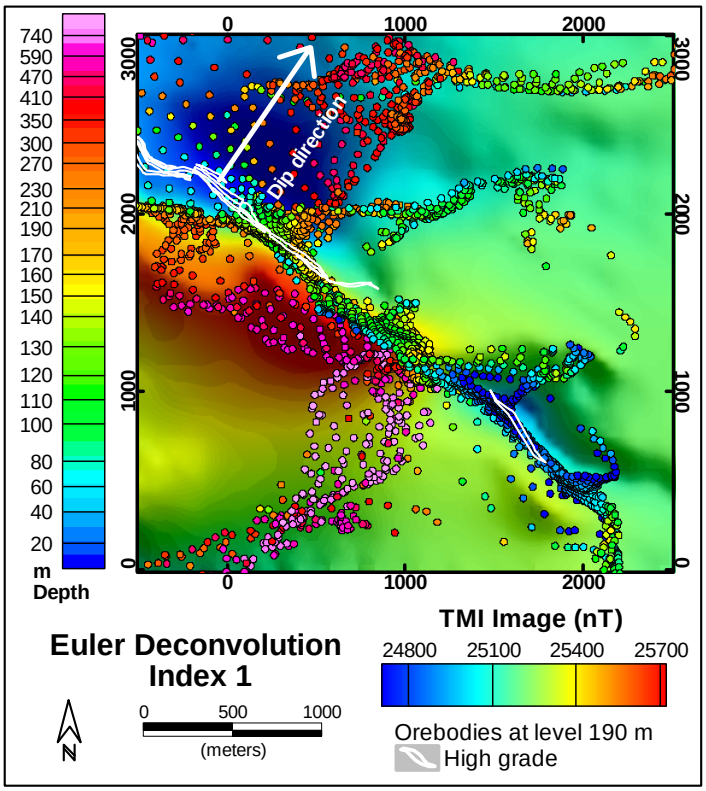

Figure 3.26. Euler deconvolution correlation with high grade orebody and dip direction of NW orebody. Structural index value 1 to dyke geometry.

The joint qualitative interpretation of those several linear transformations delineated the location of the orebody. The images and profiles of terracing indicated that the orebody direction dips to northeast. The analytic signal or total horizontal gradient determined the peak anomaly above the causative magnetic body. The power spectrum semi-quantitative analysis, estimated shallow, intermediate and deep sources associated with the dipping-dike orebody, from 0 m to 800 m depth. The semi-quantitative Euler deconvolution estimated the source depth from 0 m to 700 m. The use of parametric 2D modeling quantitative analysis indicated the presence of remanence, self-demagnetization and recovered the geometry of the orebody. The deeper extension of the 2D parametric modeling indicates that the actual orebody might extend much deeper than that intersected by the existing drill holes.

3.10 - CONCLUSIONS

The qualitative and quantitative magnetic interpretation techniques in the presence of strong remanent magnetization, self-demagnetization and at equatorial latitudes is applied to a dataset acquired at Furnas Southeast deposit as a case study in the exploration for iron oxide-copper-gold deposits (IOCG) in Carajás Mineral Province, Brazil.

In this work, we have first calculated several magnetic transformations for qualitative interpretation. Then we carried out some depth estimations to semi-quantitative interpretation. Finally, we performed two-dimensional parametric modeling for quantitative interpretation. The results successfully delineated the massive magnetite associated with the high-grade copper-gold ore. The good correspondence between the transformations, the depth estimations and the 2D modeling results using a priori information constraints, with the known geology and the orebody demonstrate the value of this approach.

The qualitative and quantitative analysis performed allow us to conclude that to obtain a dipolar anomaly for steeply dipping east-west magnetic dike like bodies at equatorial latitudes we must follow the above procedures. The body must be strongly magnetized. The body must be affected by demagnetization, *i.e.* thin with a considerable down dip extent to emphasize anomaly from top surface. And the body must have remanent magnetization or a magnetic anisotropy that creates additional magnetization down dip.

This case study shows that this approach is effective in this complex scenario to aid interpretation and recover the geometry of the orebody. The methodology has good potential in the exploration for IOCG-type deposits and magnetite related deposits.

3.11 - ACKNOWLEDGMENTS

The authors would like to thank Vale – Department of Exploration and Mineral Projects – for supporting and permission to publish this work and for providing magnetic data. Vale – Furnas Project for providing the geological data used in this study and for many discussions. We also would like to thank Dr. Misac Nabighian who advised us in some aspects of data processing. We also thank CAPES–Capes Foundation, Ministry of Education of Brazil for the scholarship. This work was supported in part by the Gravity and Magnetics Research Consortium (GMRC) and we express our appreciation to Dr. Yaoguo Li for his help. The current sponsoring companies are Anadarko, Bell Geospace, BG Group, BGP, BP, CGG, ConocoPhillips, ExxonMobil, Gedex, Lockheed Martin, Marathon Oil, Micro-g LaCoste, Shell, Petra Energia, Petrobras, Tullow Oil and Vale.

3.12 - REFERENCES

Baranov, V., 1957, A new method for the interpretation of aeromagnetic maps: pseudogravimetric anomalies: Geophysics, **22**, 359–383.

Baranov, V., and Naudy, H., 1964, Numerical calculation of the formula of reduction to the magnetic pole: Geophysics, **29**, 67–79.

Blakely, R.J., 1996, Potential Theory in Gravity & Magnetic Applications: Cambridge University Press.

CGEM Software, 2012, AMP3D Software package for magnetic amplitude inversion: Colorado School of Mines, http://geophysics.mines.edu/cgem/software.html, accessed 21 October 2013.

Cordell, L., and V.J.S. Grauch, 1982, Mapping basement magnetization zones from aeromagnetic data in the San Juan Basin, New Mexico: 52nd Annual International Meeting, SEG, Expanded Abstracts, 246–247.

Cordell, L., and V.J.S. Grauch, 1985, Mapping basement magnetization zones from aeromagnetic data in the San Juan Basin, New Mexico, *in* W. J. Hinze, eds., The utility of regional gravity and magnetic anomalies maps: SEG, 181–197.

Cordell, L., and A.E. McCafferty, 1989, A terracing operator for physical property mapping with potential field data: Geophysics, **54**, 621–634.

Craig, M., 1996, Analytic Signals for Multivariate Data: Mathematical Geology, **28**, 315.

CVRD (Companhia Vale do Rio Doce), 2006, Relatório de etapa, Alvo Furnas, Volume 1: Internal report: Technical report.

Dampney, C. N. G., 1969, The equivalent source technique: Geophysics, **34**, 39–53.

Gerkens, J.C.d'A., 1989, Foundation of Exploration Geophysics: Methods in Geochemistry and Geophysics: Elsevier.

Groves, D.I., F.P. Bierlein, L.D. Meinert, and M.W. Hitzman, 2010, Iron oxide copper-gold (IOCG) deposits through Earth history: Implications for origin, lithospheric setting, and distinction from other epigenetic iron oxide deposits: Economic Geology, **105**, no. 3, 641–654.

Haney, M., C. Johnston, Y. Li, and M. Nabighian, 2003, Envelopes of 2d and 3d magnetic data and their relationship to the analytic signal: Preliminary results: 73rd Annual International Meeting, SEG, Expanded Abstracts, 596–599.

Hansen, R.O., and M. Simmonds, 1993, Multiple source Werner deconvolution: Geophysics, **58**, no. 12, 1792–1800.

Hartman, R.R., Teskey, D.J., and Friedberg, J.L., 1971, A system for rapid digital aeromagnetic interpretation: Geophysics, **36**, no.5, 891–918.

Hirata, W.K., J.C. Rigon, A.A.C. Cordeiro, and E. M. Meireles, 1982, Geologia Regional da Província Mineral de Carajás: 1o Simpósio de Geologia da Amazônia, SBG, 100–108.

Hitzman, M.W., N. Oreskes, and M.T. Einaudi, 1992, Geological characteristics and tectonic setting of Proterozoic iron oxide (Cu–U–Au–REE) deposits: Precambrian Research, **58**, 241–287.

Kellogg, O. D., 1953, Foundations of potential theory: Dover publications Inc.

Leão-Santos, M.H., Y. Li, and R.A.V. Moraes, 2014, Application of 3D magnetic amplitude inversion to Fe oxide–Cu–Au deposits at low magnetic latitudes: A case study from Carajás Mineral Province, Brazil: Geophysics, In Press.

Li, Y., and D. W. Oldenburg, 1996, 3-D inversion of magnetic data: Geophysics, **61**, 394–408.

Li, Y., S. E. Shearer, M. M. Haney, and N. Dannemiller, 2010, Comprehensive approaches to 3d inversion of magnetic data affected by remanent magnetization: Geophysics, **75**, L1–L11.

Matlab, 2014, Matlab webpage, Mathworks, http://www.mathworks.com/matlabcentral, accessed 31 March 2014.

Mendonça, C.A., and J.B.C. Silva, 1993, A stable truncated series approximation of the reduction-to-the-pole operator: Geophysics, **58**, no. 8, 1084–1090.

Miller, H.G., and V.J. Singh, 1994, Potential Field tilt - A new concept for location of potential field sources: Applied Geophysics, **32**, 213–217.

Monteiro, L.V.S., R.P. Xavier, E.R. Carvalho, M.W. Hitzman, C.A. Johnson, C.R.S. Filho and I. Torresi, 2008, Spatial and temporal zoning of hydrothermal alteration and mineralization in the Sossego iron oxide–copper–gold deposit, Carajás Mineral Province, Brazil: paragenesis and stable isotope constraints: Mineralium Deposita, **43**, 129–159.

Mushayandebvu, M.F., P. Van Driel, A.B. Reid, and J.D. Fairhead, 1999, Magnetic source parameters of two dimensional structures using extended Euler deconvolution: Geophysics, **66**, 814–823.

Nabighian, M., 1972, The analytic signal of two-dimensional magnetic bodies with polygonal cross-section: its properties and use for automated anomaly interpretation: Geophysics, **37**, 507–517.

Nabighian, M., 1974, Additional comments on the analytic signal of two-dimensional magnetic bodies with polygonal cross-section: Geophysics, **39**, 507–517.

Nabighian, M., 1984, Toward a three-dimensional automatic interpretation of potential field data via generalized Hilbert transforms – Fundamental relations: Geophysics, **49**, 780–786.

Nabighian, M., and R.O. Hansen, 2001, Unification of Euler and Werner deconvolution in three dimensions via the generalized Hilbert transform: Geophysics, **66**, no. 6, 1805–1810.

Nykänen, V.M., 2008, Spatial data analysis as a tool for mineral prospectivity mapping: Academic dissertation, University of Oulu.

Nykänen, V., D.I. Groves, V.J. Ojala, P. Eilu, and S.J. Gardoll, 2008, Reconnaissance-scale conceptual fuzzy-logic prospectivity modeling for iron oxide copper – gold deposits in the northern Fennoscandian Shield, Finland: Australian Journal of Earth Sciences, **55**, no. 1, 25–38.

Oreskes, N., and M.T. Einaudi, 1990, Origin of rare earth element enriched hematite breccias at the Olympic Dam Cu-U-Au-Ag deposit, Roxby Downs, South Australia: Economic Geology, **85**, no. 1, 1–28.

Oreskes, N., and M.T. Einaudi, 1992, Origin of hydrothermal fluids at Olympic Dam: preliminary results from fluid inclusion and stable isotopes: Economic Geology, **87**, no. 1, 64–90.

Philips J.D., 1992, TERRACE: A terracing procedure for gridded data, with Fortran programs, and VAX Command Procedure, Unix C-Shell, and DOS batch file implementations: Department of the interior, US geological survey open file report, 5–92.

Reid, A.B., J.M. Allsop, H. Granser, A.J. Millett, and I.W. Somerton, 1990, Magnetic interpretation in the three dimension using Euler deconvolution: Geophysics, **55**, 80–91.

Roest, W.R., J. Verhoef, and M. Pilkington, 1992, Magnetic interpretation using the 3-D analytic signal: Geophysics, **57**, 116–125.

Santos, J.O.S, L.A. Hartmann, H.E. Gaudette, D.I. Groves, N.J. McNaughton, I.R. Fletcher, 2000, A new understanding of the provinces of the Amazon Craton based on integration of field mapping and U-Pb and Sm-Nd geochronology: Gondwana Research, **3**, no. 4, 453–488.

Shearer, S., 2005, Three-dimensional inversion of magnetic data in the presence of remanent magnetization: M.S. thesis, Colorado School of Mines.

Stavrev, P., and D. Gerovska, 2000, Magnetic field transforms with low sensitivity to the direction of source magnetization and high centricity: Geophysical Prospecting, **48**, 317–340.

Thomson, D.T., 1982, EULDEPH: a new technique for making computer-assisted depth estimates from magnetic data: Geophysics, **47**, 31–37.

Vale S.A., 2012, Projeto Furnas, Relatório Final de Geologia: Internal report: Technical report.

Verduzco, B., J.D. Fairhead, C.M. Green, and C. Mackenzie, 2004, New insights into magnetic derivatives for structural mapping: The Leading Edge, **23**, 116–119.

Williams, P.J., M.D. Barton, D.A. Johnson, L. Fontboté, A. Haller, G. Mark, N.H.S. Oliver, R. Marschik, 2005, Iron Oxide Copper-Gold Deposits: Geology, Space-Time Distribution, and Possible Modes of Origin: Economic Geology, 100th Anniversary Volume, 371–405.

Wirth, K.R., A.K. Gibbs, and W.J. Olszewski, 1986, U-Pb ages of zircons from the Grão-Pará group and Serra dos Carajás Granite, Pará, Brazil: Revista Brasileira de Geociências, **16**, no. 2, 195–200.

Xavier, R.P., L.V.S. Monteiro, C.P.N. Moreto, A.L.S. Pestilho, G.H.C. Melo, M.A.D. Silva, B. Aires, C. Ribeiro, and F.H.F. Silva, 2012, The iron oxide copper-gold systems of the Carajás Mineral Province, Brazil, in Geology and Genesis of Major Copper Deposits and Districts of the World: A Tribute to Richard Sillitoe, Special Publication, Society of Economic Geologists.

CAPÍTULO 4

APPLICATION OF 3D MAGNETIC AMPLITUDE INVERSION TO IRON OXIDE-COPPER-GOLD DEPOSITS AT LOW MAGNETIC LATITUDES: A CASE STUDY FROM CARAJÁS MINERAL PROVINCE, BRAZIL

Manuscript submitted to the Journal *Geophysics* in February 18th of 2014, currently the minor revision needed requested by the reviewers was performed and submitted in August 6th of 2014.

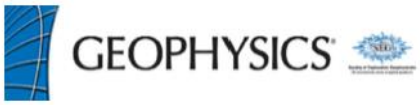

Journal:	*Geophysics*
Manuscript ID:	GEO-2014-0082
Manuscript Type:	Case Histories
Date Submitted by the Author:	18-Feb-2014
Complete List of Authors:	Santos, Marcelo; Vale S.A., Li, Yaoguo; Colorado School of Mines, Dept. of Geophysics Moraes, Roberto; InterGeo - Informação em Geociências, Diretoria Técnica; Universidade de Brasília, Instituto de Geociências
Keywords:	magnetics, amplitude, magnetization, inversion, mining
Area of Expertise:	Case Histories, Magnetic Exploration Methods

GEO-2014-0082 - Minor revision needed
jshragge@gmail.com <jshragge@gmail.com> Wed, Jul 9, 2014 at 12:15 AM
To: ygli@mines.edu Cc: sdanker@seg.org, marcelo.leao@vale.com, marcelo.leao.santos@gmail.com, ygli@mines.edu, rmoraes@unb.br, jshragge@gmail.com
08-Jul-2014
Re: GEO-2014-0082, Application of 3D magnetic amplitude inversion to iron oxide-copper-gold deposits at low magnetic latitudes: A case study from Caraj\'{a}s Mineral Province, Brazil

Reviewer 1: Open comments to editors and authors:
This manuscript deals with the issues of inverting magnetic data that contains the response of bodies that exhibit remanent magnetization and self-demagnetization. Further issues related to low magnetic latitude are also considered. The authors invert a challenging set of magnetic data for an interesting geological scenario and achieve impressive results. They perform some interesting and intelligent analyses. The manuscript is well written with very helpful illustrations. This is excellent work. I think more can be done to improve the paper (see comments) but this manuscript is certainly good enough to be published as-is.

Thank you for submitting your manuscript, GEO-2014-0082.R1 , to GEOPHYSICS
e.c.slob@tudelft.nl <e.c.slob@tudelft.nl> Wed, Aug 6, 2014 at 12:43 AM
To: ygli@mines.edu
Cc: marcelo.leao@vale.com, marcelo.leao.santos@gmail.com, ygli@mines.edu, rmoraes@unb.br
05-Aug-2014
Re: GEO-2014-0082.R1, "Application of 3D magnetic amplitude inversion to iron oxide-copper-gold deposits at low magnetic latitudes: A case study from Caraj\'{a}s Mineral Province, Brazil"

Thank you for submitting your revised manuscript listed above to GEOPHYSICS. Please refer to the manuscript number in all correspondence. Your paper is being processed.

APPLICATION OF 3D MAGNETIC AMPLITUDE INVERSION TO IRON OXIDE-COPPER-GOLD DEPOSITS AT LOW MAGNETIC LATITUDES: A CASE STUDY FROM CARAJÁS MINERAL PROVINCE, BRAZIL

Marcelo Leão-Santos[1,2,3], Yaoguo Li[2], and Roberto Moraes[1]

[1] Universidade de Brasília, Instituto de Geociências, Brasília, Brazil.

E-mail: marcelo.leao.santos@gmail.com, rmoraes@unb.br.

[2] Colorado School of Mines, Center for Gravity, Electrical & Magnetic Studies, Golden, Colorado.

E-mail: ygli@mines.edu.

[3] VALE S.A., Department of Exploration and Mineral Projects, Belo Horizonte, Brazil.

E-mail: marcelo.leao@vale.com.

4.1 - ABSTRACT

Strong hydrothermal alteration modifies rock physical properties in iron oxide-copper-gold deposits (IOCG) and may result in characteristic signatures detectable in geophysical surveys. Magnetic data are commonly used in characterizing orebodies and 3D inversions are often employed to assist in interpretations. In areas with strong remanence and self-demagnetization, the total magnetization can have directions different from the inducing field direction. This deviation precludes the use of traditional inversion methods. Magnetic amplitude inversion offers one solution to this challenge since the amplitude data are weakly dependent on the magnetization direction. In addition, low magnetic latitude also imposes difficulty to amplitude data calculation due to the instability in the component conversion in the wavenumber domain. To formulate a practical approach, we present a case study on applying the magnetic amplitude inversion to the Furnas Southeast iron oxide-copper-gold deposit at low magnetic latitude in Carajás Mineral Province, Brazil, and demonstrate that the approach can reliably recover an interpretable distribution of effective magnetic susceptibility and identify massive magnetite from hydrothermal alterations associated with the high-grade ore.

4.2 - INTRODUCTION

The exploration for copper sulfides and gold ore in iron oxide-copper-gold deposits (IOCG) frequently uses the magnetic method because of the strong association between mineralization and high magnetic susceptibility due to the presence of abundant magnetite. However, in strongly magnetic geological environments, it is sometimes difficult to reliably interpret for magnetic

sources due to the complex role played by remanent magnetization and the self-demagnetization effect.

In low magnetic latitude and equatorial regions, the effect of remanent magnetization is even more pronounced. Near the equatorial region such as in Brazil, the inducing magnetic field is approximately three times weaker compared with that in regions of high magnetic latitudes, and so is the corresponding induced magnetization given the same magnetic susceptibility. Consequently, the effect of remanent magnetization is more important in these regions.

The Furnas deposit is such a case in point. It is located in the magnetic equatorial zone, but has a total-field magnetic anomaly resembling those at middle latitudes in the northern hemisphere. It is clear that the magnetization at Furnas deposit is significantly different from the current inducing field direction at this site.

The Furnas copper-gold disseminated mineralization was produced by biotite-garnet-grunerite-magnetite hydrothermal alteration with the chalcopyrite and bornite high-grade ores associated with the presence of magnetite. The drill core sample measurements indicate that the average and median susceptibility of the massive magnetite hydrothermal zone is 2.7 and 0.989 SI, respectively. The laboratory measurements have shown strong anisotropy in magnetic susceptibility, with a ratio of major over minor axis of the anisotropy ellipsoid (anisotropy degree) of 1.5 in the host rocks. The anisotropy degree can be as high as 2.5 to 3 in the magnetic hydrothermal alteration zones. The major axis of the anisotropy ellipsoid is aligned with the dip of the orebodies. Thus, it is certain that both self-demagnetization effect and the susceptibility anisotropy contribute to deviating magnetization direction. Laboratory work also indicates that the Curie temperature in the orebody is higher than in the host rocks and the pure magnetite. Therefore, a stronger remanent magnetization is expected in the orebodies.

Laboratory measurements of oriented samples have also shown strong remanent magnetization. Furthermore, petrophysical measurements show that the remanent magnetization direction not only deviates significantly from the current inducing field direction but is also changing within the orebody. The hydrothermal alteration emplacing the orebodies is structurally controlled and resulting deposit consists of a number of bodies of sigmoidal shape. The injection of magnetite pulses from hydrothermal fluids form multiple magnetic source bodies that acquired remanent magnetization at different times and have different magnetization directions.

The significant remanence and self-demagnetization present in the Furnas deposit and the resultant deviating magnetization direction severely limit the use of magnetic inversion methods that recover the susceptibility distribution by assuming a magnetization in the same direction as the current inducing field. Alternative approaches are required. Paine et al. (2001) transformed the

total-field anomaly into quantities that are weakly dependent on the magnetization direction by vertically integrating the total gradient of total-field anomaly or by calculating the total gradient of the vertical integration of the magnetic anomaly. They then treated these quantities as if they were RTP data and applied the magnetic susceptibility inversion by Li and Oldenburg (1996). Despite the severe inconsistency between these quantities and the algorithm used to invert them, the approach produced interpretable results and became an inspiration for other development. Li et al. (2010) presented a two-pronged approach to tackling the problem of remanent magnetization. For simple isolated anomalies, one can estimate the magnetization direction by using methods such as Helbig's moment method (Lourenco and Morrison, 1973; Phillips, 2005) or the cross-correlation methods (Dannemiller and Li, 2006; Gerovska et al., 2009), and then supply the direction to invert for the magnitude of the magnetization. An alternative method is to invert the amplitude of anomalous magnetic vector for the magnitude of the total magnetization. This method is more effective when the magnetization direction is variable (Shearer, 2005). Lelièvre and Oldenburg (2009) formulated a direct approach by inverting for the 3D distribution of magnetization vectors. Later on, Ellis et al. (2012) also presented this method, and Liu et al. (2013) applied it to multi-component borehole data. This approach is generally applicable, but requires site-specific constraints to be effective (Lelièvre and Oldenburg, 2009). A similar approach based on parametric inversion is to invert for the magnetization vectors within causative bodies together with their geometric shapes. Mueller et al. (1997) used this approach to interpret borehole magnetic data in the presence of strong remanent magnetization. Foss and McKenzie (2011) apply this approach to multiple sources in order to model complex anomalies.

In this paper, we focus on the application of 3D magnetic amplitude inversion to a set of high-resolution aeromagnetic data at Furnas Southeast deposit to recover the distribution of the magnitude of the total magnetization. The reasons are twofold. First, the total magnetization direction is variable and a single estimated direction is not expected to perform well. Secondly, it is desirable to develop a strategy in this exploration region to invert magnetic data without detailed constraints so that it can have the maximum applicability. We also use this data set as a case study to examine the required processing steps that ensure the general applicability and success of the magnetic amplitude inversion technique in exploration problems at low-latitude and equatorial regions.

In the following, we first describe the site geology, mineral deposit model, and the magnetic properties of different geological units. We then examine the total-field anomaly data and the use of the equivalent source technique to stably calculate the magnetic amplitude data for use in the subsequent inversion. We next carry out the amplitude inversion and investigate the use of the L-

curve criterions to select the optimal regularization parameter in such inversions. We conclude the study by carrying out the geological interpretation of the 3D inversion, and demonstrate the strong correlation between amplitude inversion results with the known geology and mineralized zones from drilling.

4.3 - GEOLOGICAL SETTING AND GEOPHYSICAL DATA

Geology and Petrophysics

The Furnas deposit is located in the Carajás Mineral Province, in the Northern region of Brazil. The deposit is situated along the regional Cinzento transcurrent shear zone striking WNW-ESE. The Cinzento lineament can be observed in the total horizontal gradient in Figure 4.1. Metavolcano-sedimentary rocks correlated to the Grão Pará Group, of the 2.76 Ga Itacaiúnas Supergroup (Wirth et al., 1986), and sedimentary rocks correlated to the Águas Claras Formation host this portion of the deposit. The shear zone defines a contact between amphibole schist to the north (hanging wall) and aluminous schist to the south (footwall) of the Itacaiúnas Supergroup, interrupted by the intrusion of the 1.8 Ga Cigano Granite to the east (Wirth et al., 1986; Figure 4.2). Regionally, the Itacaiúnas Supergroup is surrounded by tonalitic to trondhjemitic gneisses of the Xingu Complex (2.8 Ga U-Pb in zircon; Machado et al. 1991). The region is metamorphosed to greenschist to amphibolite facies (CVRD, 2006).

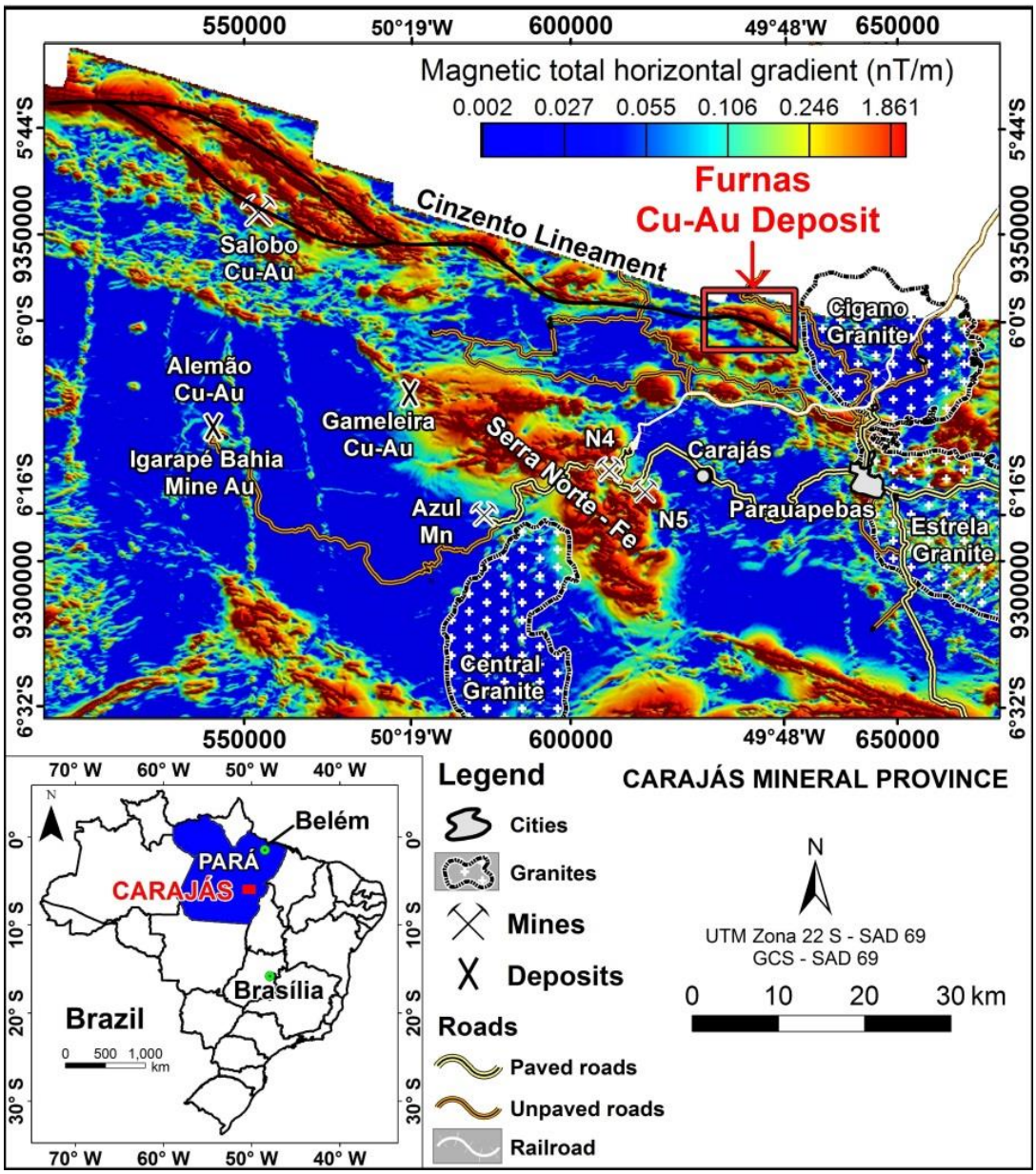

Figure 4.1. Location of the study area and the distribution of main granites. The study area is in the northeastern Carajás. Furnas Cu-Au deposit occurs along the Cinzento lineament with a strike in NWW direction, which is visible in the total horizontal gradient map of magnetic data.

The southeast segment of the Furnas copper-gold disseminated mineralization has a biotite-garnet-grunerite-magnetite hydrothermal alteration assemblage. The mineralization is hosted by massive magnetite, silicification, sodic-calcic, and potassic alteration. Figure 4.2 shows the detailed local geology in the selected study area of 3 km by 3 km. Figure 4.3 displays the geology in a cross section through the high-grade orebody. The location of the section is indicated in Figure 4.2. The alteration zone is associated with a late-stage chalcopyrite and bornite veinlets and breccia. The deposit is poorly exposed with a wide laterite profile of about 60 m.

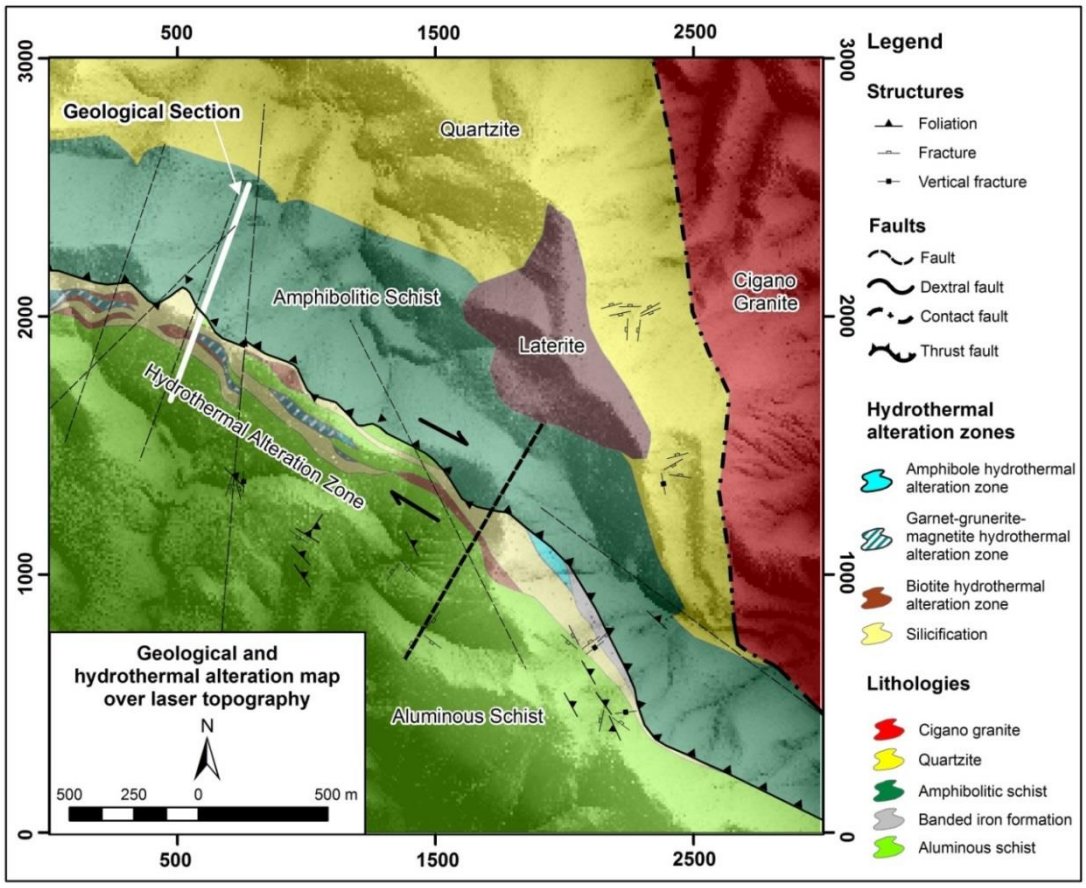

Figure 4.2. Alteration map superimposed on the LiDAR topography in the study area. The mineralization zone is located along the thrust fault striking NW-SE. The NE-striking fault (thick dashed line) in the south central portion of the map demarcates the two major sections of high-grade orebodies (Modified from Vale, 2012).

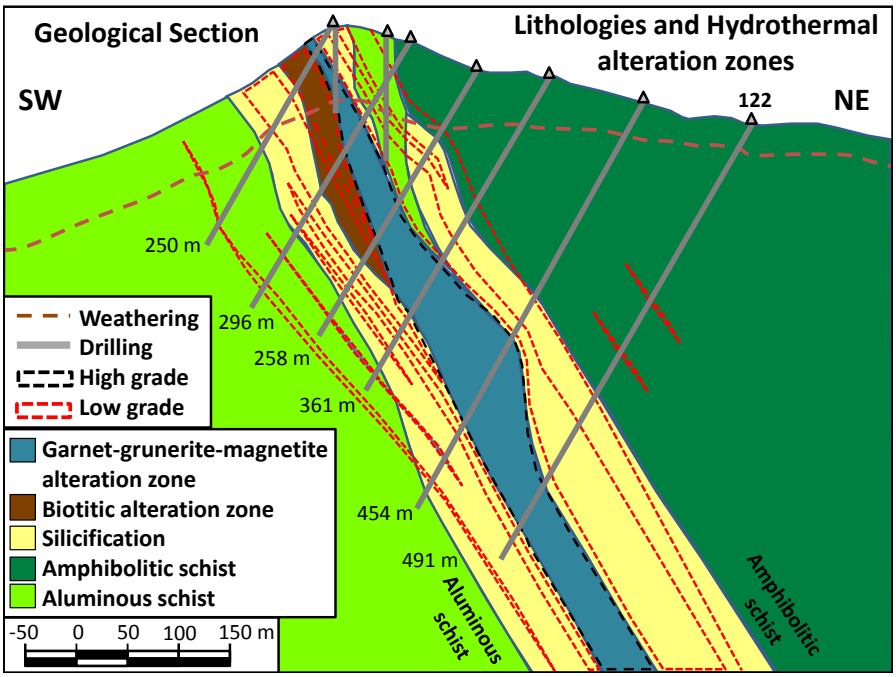

Figure 4.3. A geological section of Furnas Southeast deposit at the location shown in Figure 4.2 (Modified from Vale, 2012).

The alteration zone is associated with moderate to strong foliation. The Cu-Au mineralization is concentrated in right stepping, NW striking, dilational structures along the WNW-striking dextral shear zone. These structures produced elongated ore shoots during episodic hydrothermal fluid flow events that caused brittle slip and brecciation.

The Furnas project carried out 17,789 measurements of magnetic susceptibility continuously along 17,739 m of drill core from 69 drill holes (Vale, 2012). The hydrothermal magnetite alteration is divided in three zones with strong magnetic susceptibility signatures (Table 4.1).

Table 4.1. The hydrothermal magnetite alteration zones susceptibilities.

Hydrothermal alteration zone	Mean (SI x 10^{-3})	Median (SI x 10^{-3})
Massive magnetite	2,777	989
Amphibole and magnetite	1,550	308
Garnet, grunerite and magnetite	1,383	409

Figure 4.4 shows a representative drill hole log with the lithologies, hydrothermal alteration zones, magnetic susceptibility measured on drill cores (in SI x 10^{-3}), iron geochemistry (in percentage), copper mineralization (in percentage) and gold mineralization (in grams per ton). This figure summarizes the magnetic susceptibility behavior of the mineralized hydrothermal alteration zones. We can observe that the mineralized magnetite hydrothermal alteration zone is well defined between 275 to 350 m depth by high magnetic susceptibility values. Inside this interval we can observe, around 310 and 340 m depth, two narrow mineralized silicification zones without magnetite and consequently without magnetic susceptibility response. The same response can be observed from 225 to 275 m depth on a mineralized silicification and chloritization zone. Around 180 and 215 m, we can see peaks of high magnetic susceptibility values associated with two narrow magnetic hydrothermal alteration pulses. In general, the high copper-gold grades have strong association with high magnetic susceptibility values that are correlated with high total-field magnetic anomalies. Therefore, magnetic survey is one of the most effective geophysical tools for exploration in this area. In particular, the magnetic anomalies help define the Furnas Southeast deposit's geophysical signature.

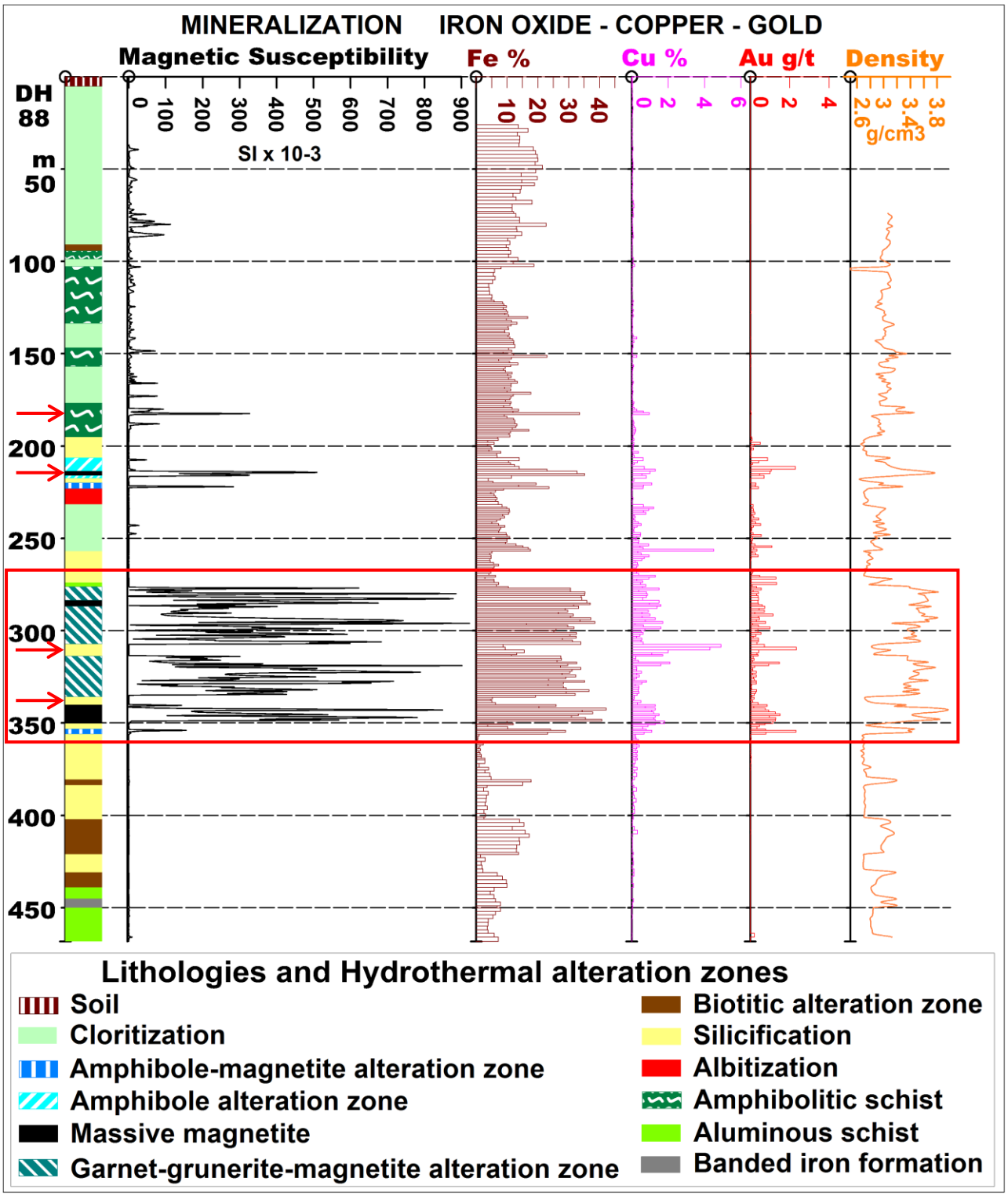

Figure 4.4. Representative drill hole 88 log with the lithologies, hydrothermal alteration zones, magnetic susceptibility, iron geochemistry, copper mineralization, and gold mineralization.

Magnetic data

The magnetic data were acquired in 2010 in a draped survey using a fixed wing aircraft and a nominal terrain clearance of 100 m. The line direction was held at 78° NW and the line spacing was 100 m. We use a subset of the data in the southeast portion of the deposit in this study in Figure 4.5a. The ambient field has an inclination of -5.7°, a declination of -19.8°, and a field strength of 25,400 nT. The corresponding local geology in the same area is shown in Figure 4.2.

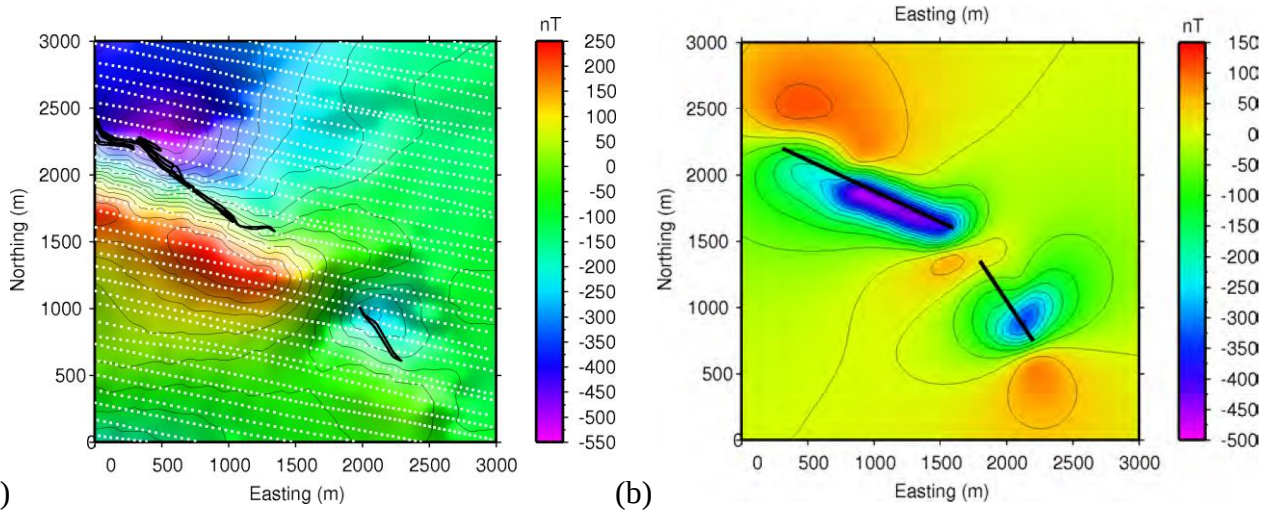

Figure 4.5. (a) The observed total-field magnetic anomaly over the southeast portion of the Furnas deposit. The data area is the same as the local geology in Figure 4.2. The white dots show the location of the decimated data. The location of the high-grade orebodies at 190-m level is shown in by thick black lines. The inducing field direction is I = -5.7° and D = -19.8°. Each anomaly is characterized by a peak shifted to the south and an accompanying strong trough to the north. This pattern is highly inconsistent with the total-field anomaly due to induced magnetization at the equatorial region. (b) Theoretical total-field anomaly produced by induced magnetization at the same location. The horizontal location of the source body is again shown by the black lines.

We decimated the total-field data from approximately 0.6 m sample spacing of the original dataset to approximately 50-m spacing along the flight lines. We removed the IGRF field (25,400 nT) and performed no additional regional-residual separation. There are two main anomalies in Figure 4.5a. A weak one is located in the southeast part of the area and a stronger anomaly in the central-northwest part of the data area. The two anomalies are separated by a northeast-southwest fault that has been previously mapped (Figure 4.2). The topography data were acquired in 2010 with a LiDAR system. We incorporate the elevation data fully in the processing and inversion, but choose not to reproduce them here for brevity.

Superimposed on the total-field magnetic anomaly is also high-grade orebody at the elevation of 190-m, which has a strike direction of NWW and dips to NE (see Figure 4.3). The two

anomalies follow the direction of the orebody, but the peak of the anomalies are shifted to the southwest, and there is a pronounced negative peak towards the north accompanying each anomaly. It is clear that these anomalies are not of the pattern that would be produced by induced magnetization at this low magnetic latitude. For comparison, Figure 4.5b shows the total-field anomaly produced by two source bodies with induced magnetization only. Instead, the anomalies appear more similar to anomalies at middle latitudes in north hemisphere. Given this observation and the petrophysical information discussed in the preceding section, it is clear that remanent magnetization and self-demagnetization are playing an important role here.

4.4 - AMPLITUDE INVERSION

Calculation of Amplitude Data

The main objective of this study is to recover a three-dimensional representation of the magnitude of the total magnetization as a direct indicator of target orebody and mineralized zones. Given the influence on the magnetic data by remanent magnetization and self-demagnetization, we choose to use the magnetic amplitude inversion (e.g., Shearer, 2005; Li et al., 2010), which does not rely critically on the knowledge of the magnetization direction.

As Nabighian (1972) has shown, the amplitude of the analytic signal in 2D, which is the total gradient, is independent on the magnetization direction. This property also holds true for the amplitude of the anomalous magnetic vector in 2D. In 3D, this invariant property does not strictly hold true, but both quantities are only weakly dependent on the magnetization direction (e.g., Stavrev and Gerovska, 2000; Haney et al., 2003).

In particular, the amplitude data is defined as

$$B_a = \sqrt{B_{ax}^2 + B_{ay}^2 + B_{az}^2}, \qquad (1),$$

where B_{ax}, B_{ay}, and B_{az} are the three components of the anomalous magnetic vector in the *x*-, *y*-, and *z*-directions, respectively. Given the weak dependence of B_a on the magnetization direction, we can treat this quantity as our data and invert directly for the magnitude of magnetization vector with an assumed magnetization direction. The amplitude data conserve the low-wavenumber content and retain the signal due to deep magnetic bodies. The benefit of the amplitude inversion is that we can invert multiple anomalies with different magnetization directions in complicated areas.

Although there is a small number of systems that can acquire three-component magnetic data (e.g., Dransfield et al., 2003) and the data can be used directly in amplitude data calculation, the majority of current surveys measure total-field and the majority of existing data from on-going

exploration projects world wide are total-field data. The challenge, therefore, is the need to calculate the three components from total-field magnetic data. In our current study, this operation is difficult because of the low magnetic latitude (-5.7°). The commonly used wavenumber-domain approach encounters the similar low-latitude instability as in the reduction-to-the-pole (RTP) calculation, albeit to a lesser degree.

To illustrate the low-latitude instability, we calculate the three orthogonal components of the magnetic anomaly in the Fourier domain, and then obtain the magnetic amplitude data using equation 1. The result is displayed in Figure 4.6. The result has strong striation in the direction of declination, as well the separation of two peaks along the same direction. There is little correspondence between the computed amplitude anomaly and the known geology. The amplitude inversion using this set of computed amplitude data is nonsensical and uninterpretable. For brevity, we have not reproduced it. Thus, the Fourier domain conversion has failed as expected at this low magnetic latitude.

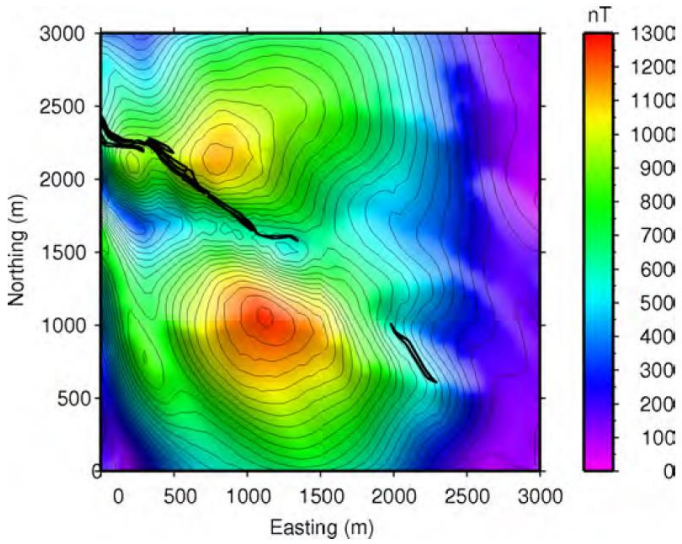

Figure 4.6. Illustration of the difficulties in calculating magnetic amplitude data at low magnetic latitudes in Fourier domain. The result has strong striation in the direction of declination (D = -19.8°), as well the separation of two peaks along the same direction. There is no correspondence between the computed amplitude anomaly and the known geology.

To overcome the difficulty of low-latitude instability, we choose to use the equivalent source technique Dampney (1969). Many authors have used equivalent source technique in magnetic data processing (e.g., Hansen and Miyazaki, 1984; Blakely, 1996; Silva, 1986; Li and Oldenburg, 2010). More recently, Li and Li (2014) used this technique to calculate amplitude data in order to accommodate an rugged observation surface. We use the similar approach here to deal with low

magnetic latitude and an uneven surface at the same time. We use a 3D equivalent source consisting of susceptibility values that can be either negative or positive. We construct an equivalent source consisting of 50-m cubic cells from the total-field anomaly data shown in Figure 4.5a by placing it immediately below the lowest topographic point. The optimal misfit level to the observed total-field anomaly is determined by using the L-curve criterion during.

To verify the validity of the equivalent source calculation, we display the predicted total-field magnetic anomaly and the difference map in Figure 4.7. We note that the predicted data reproduces the observed total-field anomaly in Figure 4.5a well. The difference is small and distributed symmetrically about zero. There is no long-wavelength residual either.

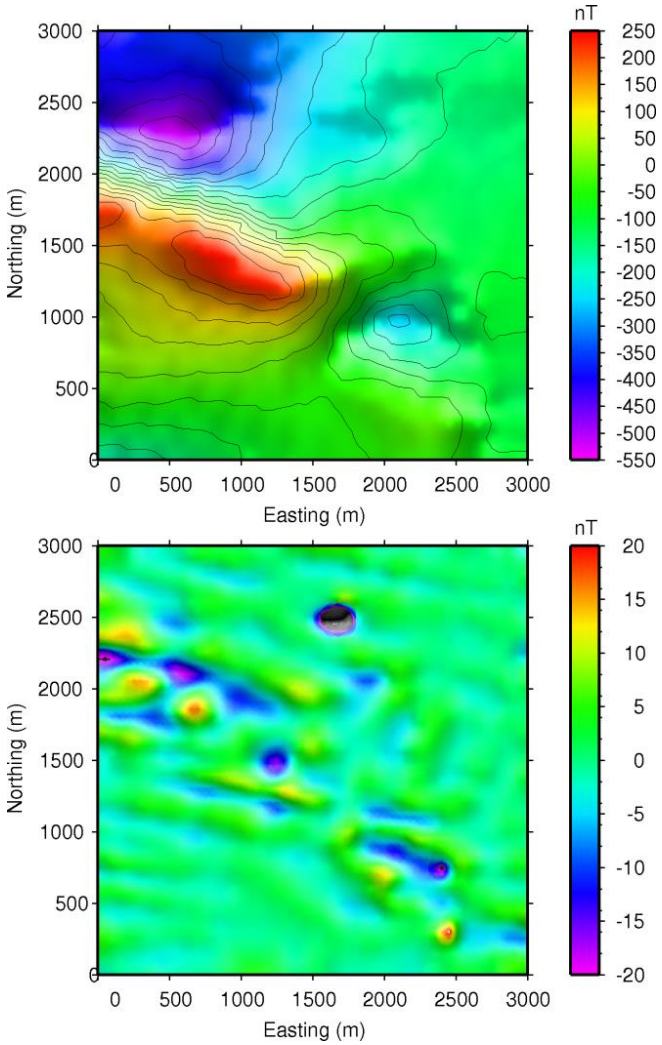

Figure 4.7. Top panel shows the predicted total-field anomaly from the equivalent source processing. The bottom panel shows the difference between the observed total-field anomaly and the predicted data.

Once the equivalent source is obtained, we use it to calculate the three orthogonal components of the magnetic anomaly and obtain the magnetic amplitude data by equation 1. The

result is shown in Figure 4.8. This set of computed amplitude data is much simpler in pattern and its peak coincides with the location of the orebody. The excellent correspondence with known geology indicates that the equivalent source technique has worked well.

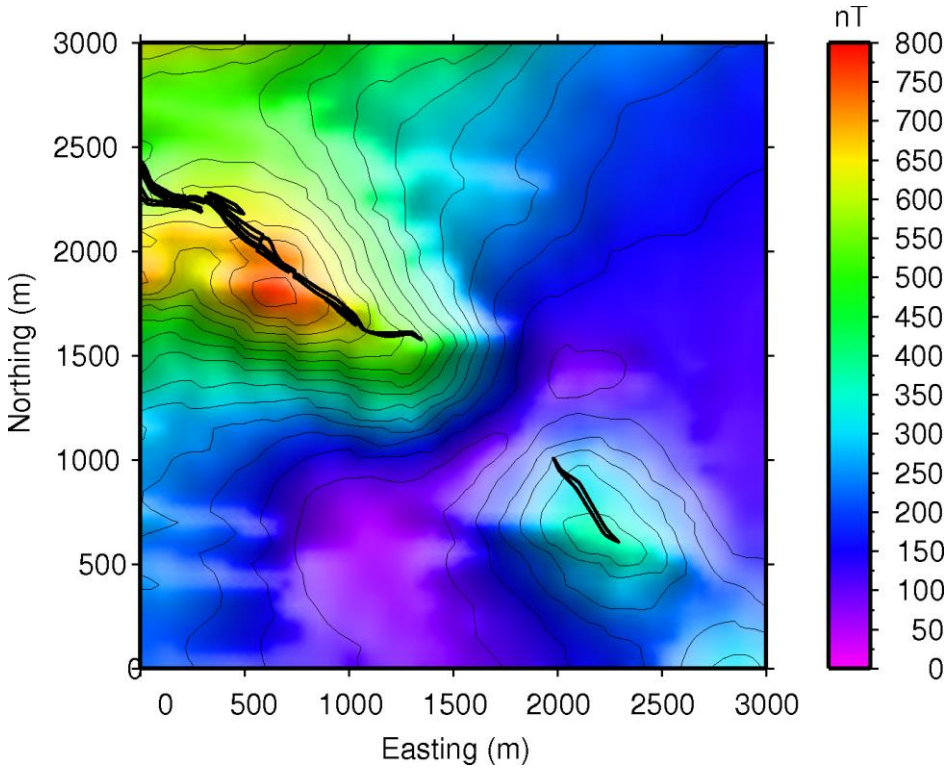

Figure 4.8. Magnetic amplitude using equivalent source calculation. The location of the orebodies at 190-m level is shown in by thick black lines. The peaks of the amplitude data correlate well with the location of the high-grade massive magnetite orebodies (thick black lines). The gap between the two amplitude anomalies coincides with the location of NE fault shown in Figure 4.2 where the alteration is dominated by silicification and biotite-garnet-grunerite assemblage without magnetite.

Although it is not central to our study, we remark that this example is also a good demonstration of the power of amplitude data as a mapping tool in place of the traditional reduction-to-pole (RTP) data. RTP operations are routinely applied to magnetic data in exploration problems on a wide range of scales. The main purpose is to reduce the asymmetry in total-field magnetic anomaly due to the oblique directions of magnetization and background field, so that the magnetic anomaly is centered over the source bodies. However, RTP operation suffers from two major challenges, namely, the unknown magnetization direction and the instability at low magnetic latitudes. The amplitude data, on the other hand, achieve the same objective approximately but do not rely on the magnetization direction and suffers much less from the low latitude instability. This is clearly shown in Figure 4.8.

3D Amplitude Inversion

We now proceed to the inversion of the amplitude data in Figure 4.8. We use the algorithm presented by Shearer (2005) and Li et al. (2010). The method recovers a 3D distribution of the magnitude of magnetization. For convenience, we normalized the magnetization by the inducing field strength to define an effective susceptibility. The algorithm uses a Tikhonov regularization formalism and relies on the nonlinear relationship between the amplitude data and the 3D effective susceptibility model. Similar to 3D inversion of total-field anomaly, a depth weighting function is applied and bound constraints are imposed to ensure the effective susceptibility is positive. The inverse solution is obtained by solving the following constrained minimization problem,

$$\begin{aligned} &\text{minimize} && \emptyset = \emptyset_d + \beta\emptyset_m, \\ &\text{subject to} && 0 \leq \kappa \leq b_u \end{aligned} \qquad (2),$$

where $\emptyset_d$ is the data misfit function, $\emptyset_m$ the model objective function, β the regularization parameter, and b_u an upper bound on the effective susceptibility κ.

To perform the inversion, we first used a coarse mesh whose cells have width of 50 m in x-, and y-directions and thickness ranging from 25 m near the surface to 50 m in the vertical direction down to a depth of 1.2 km. Padding cells were added to extend the mesh beyond the data area in all directions to account for any regional component that may be in the data. Once we determine the optimal parameters using this coarse mesh, we complete the final inversion with a finer mesh whose cell width is 12.5 m in the core. We have used a depth weighting function consistent with the inverse distance-cubed decay of magnetic kernel function, a model objective function consisting a smallest term and flatness terms in all three-directions, and zero reference model. The zero reference model is chosen to test the performance of the amplitude inversion in the absence of site specific geological constraints so as to understand its utility in greenfield explorations.

The primary concern is the regularization parameter. Figure 4.9 display the change of data misfit and model objective function with the regularization parameter. Both are well-behaved monotonic functions. Since we do not have a prior estimation of the error standard deviation, we rely on the L-curve criterion (Hansen, 1992) to determine the optimal level of regularization. This is illustrated in Figure 4.10a, by using the similar graphical representation as in Krahenbuhl and Li (2011). The Tikhonov curve (plot of model objective function versus the data misfit on a log-log scale) has a well defined corner near the regularization parameter value of 10. We also visually inspect the recovered models with all regularization parameters using similar cutoff values (Figure 4.10b) to see the effect of data misfit level on the recovered model. It is clear that the models are

overly smooth when the regularization parameter is much greater than 10, and information from the signal is not extracted. On the other hand, the models are affected by the noise in the amplitude data and show excessive structures when the regularization parameter is much smaller than 10.

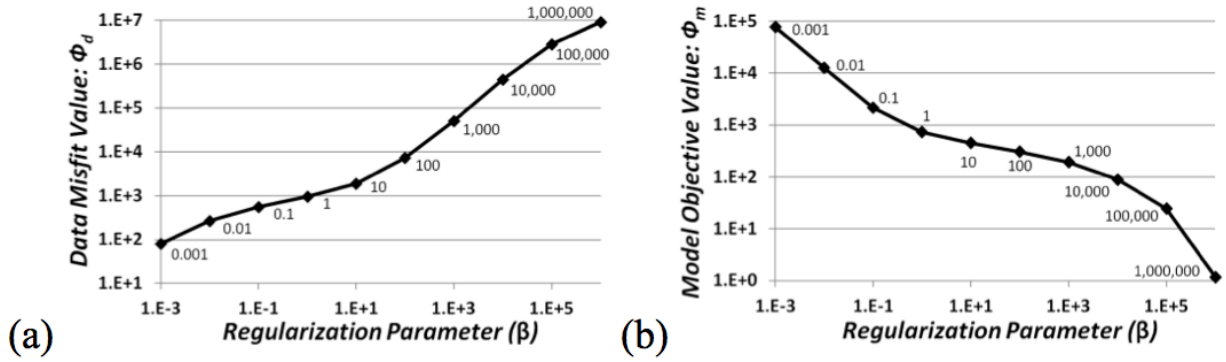

Figure 4.9. The variation of data misfit (a) and model objective function (b) with the regularization parameter in the inversion of the amplitude data in Figure 4.8. Both are monotonic curves and have characteristic behaviors as expected in such inversions.

The fact that the Tikhonov curve exhibits a characteristic corner indicates there is clearly identifiable noise level in the calculated amplitude data. Therefore, we can use the L-curve criterion to select the optimal regularization parameter. This criterion states that the corner point of the Tikhonov curve is the optimal trade off between fitting the data and having a structurally simple model. The estimated optimal value for the regularization parameter is 10. Visual inspections of the resulting model and the residual data map also indicate that this particular choice of regularization parameter is appropriate. Thus the L-curve criterion has worked well in this case for estimating the optimal regularization parameter and, equivalently, the corresponding errors in the amplitude data.

This in itself is an interesting result. For many amplitude inversions performed, the L-curve criterion has not worked well. Part of the reason is that the amplitude data on a wide range of wavelengths can be reproduced with relative ease during the inversion at a low data misfit level. As a result, it is sometimes difficult to distinguish noise from signal in the amplitude data. Thus, the current result is rather encouraging in this respect.

We then use the misfit level in the final inversion using the finer mesh. Figure 4.11 shows the curves of data misfit and model norm values for the inversion of data with the selected regularization parameter of 10. The convergence curve of the data misfit indicates that the fit between observed and predicted data improved as the inversion advanced, the misfit decreases and consequently structure of the model increases (Figure 4.11a). The model objective function increases quickly during the first 9 iterations then decreases to a plateau, indicating that the major

structures were constructed during the first iterations (Figure 4.11b). The solution converges in 28 iterations when the intended misfit is achieved and there is no more large reduction in the model objective function.

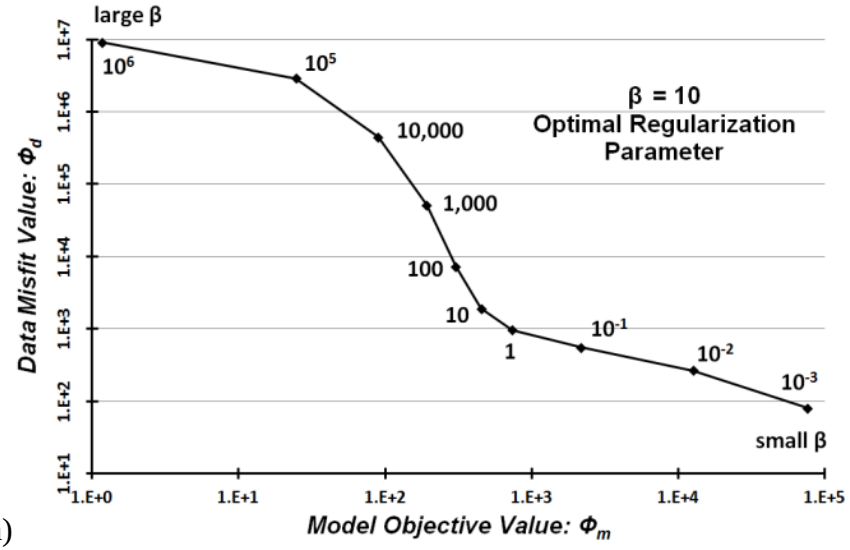

(a)

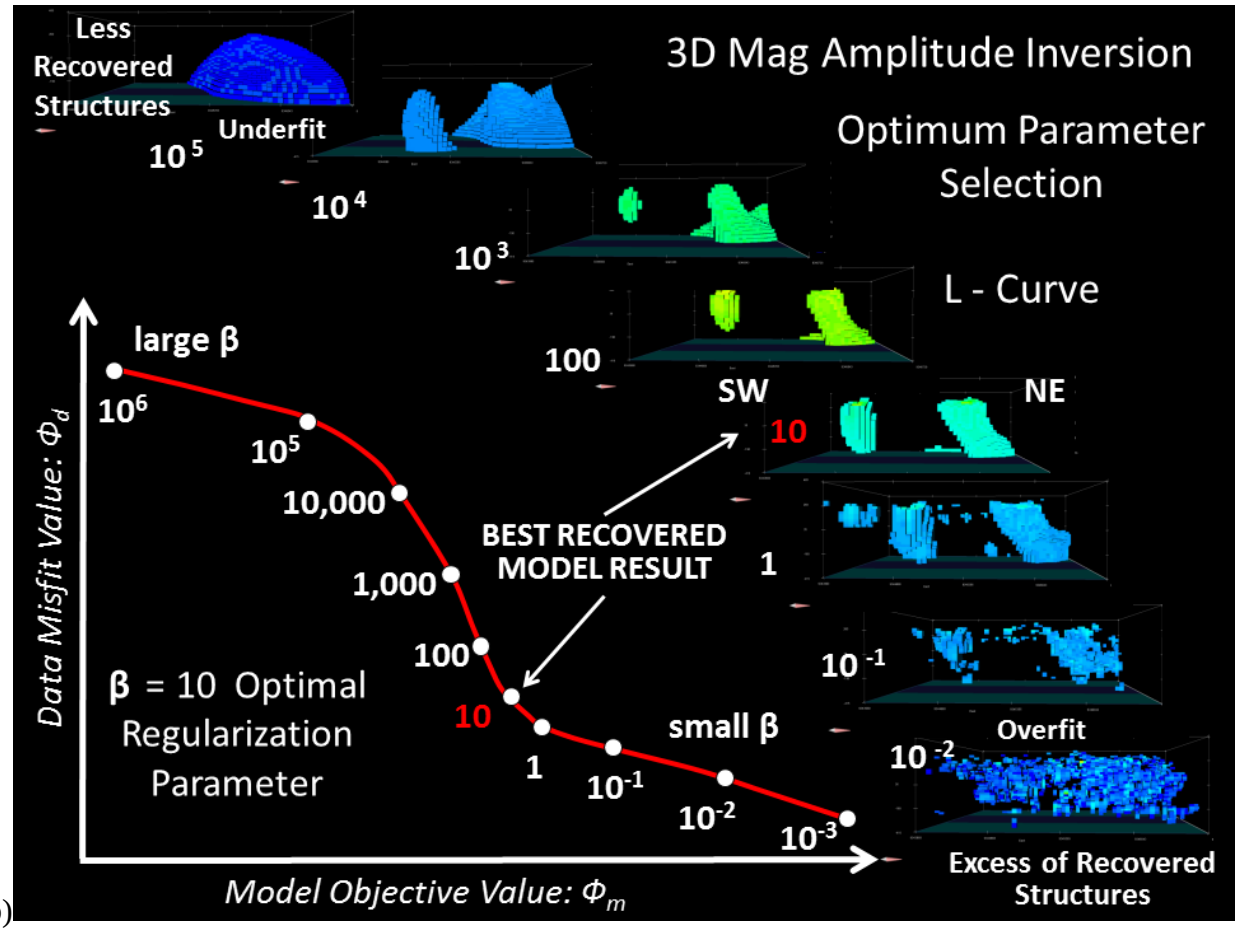

(b)

Figure 4.10. L-curve estimation of optimal regularization parameter. (a) is the Tikhonov curve, which has a well-defined corner at $\beta = 10$. (b) shows the variation of the complexity of recovered 3D effective susceptibility models with the regularization parameter. All models are displayed as volume-rendered images with a cutoff value of 0.15 SI.

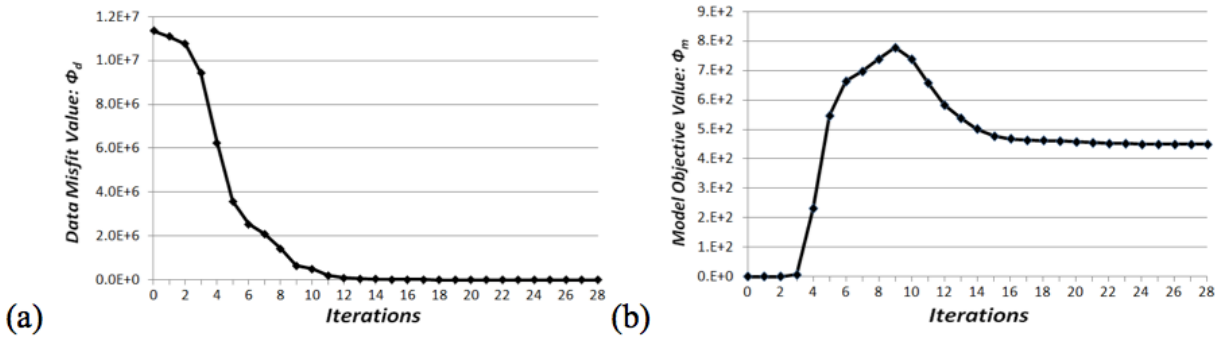

Figure 4.11. Convergence curves for the final inversion of the amplitude data using the selected optimal regularization parameter of 10.

The final inverted effective susceptibility model is shown in Figure 4.12 without padding cells. Two strongly magnetic units are present as shown by the volume rendered image with a cutoff value of 0.15 SI. The variation of the recovered effective susceptibility is also shown as color contours in two cross-sections that intersect the two inverted magnetic bodies. Superimposed in the image is also the position of the low-grade orebodies at level 190 m altitude and the drill hole traces. We observe that the recovered magnetic bodies are aligned in the NW direction and dip to the NE. To the first order, the amplitude inversion has produced a model that is consistent with the general geology at the deposit.

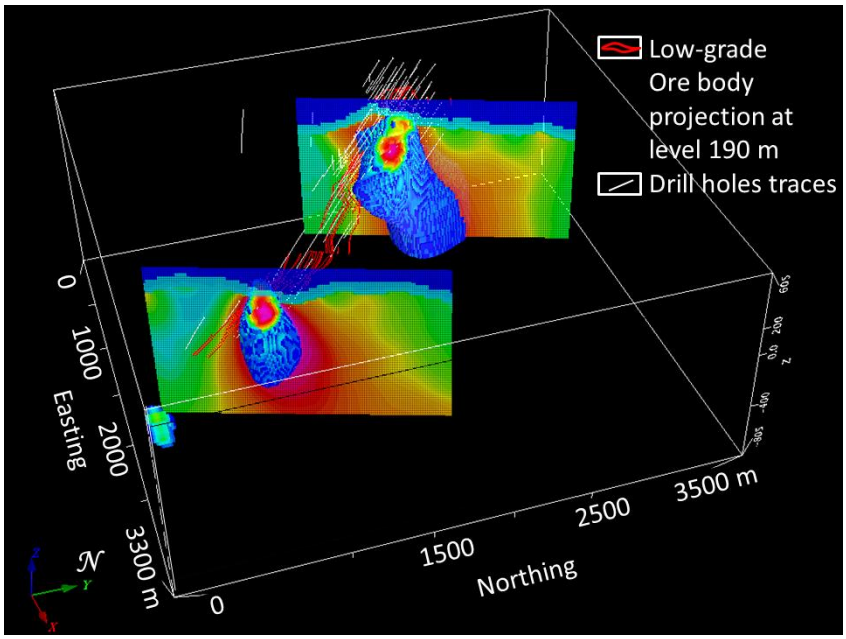

Figure 4.12. Recovered 3D model of the magnetic susceptibility. The two 3D objects are the volume rendered effective susceptibility from the amplitude inversion shown with a cutoff value of 0.15 SI, viewed from southeast. Superimposed are two cross-sections with color contours of the effective susceptibility. The section located towards the NW of the image coincides with the geological section in Figure 4.3.

4.5 - CORRELATION OF INVERSION RESULT WITH KNOWN GEOLOGY

The success of the amplitude inversion is evaluated not only by the level of data misfit and the structural simplicity of the recovered model, but more importantly, by the correspondence between the recovered 3D model of the effective susceptibility and the known source, which is the massive magnetite orebody in this case. We now proceed to the detailed interpretation by correlating with the specifics of the orebodies.

The structurally controlled hydrothermal alteration has large variations along the strike. The deposit exhibits dilational structures, brecciations, and it consists of a number of bodies of sigmoidal shape. These separate bodies open and close the ore shoots. The injection of magnetite pulses from hydrothermal fluids form multiple magnetic source bodies that acquired remanent magnetization at different times and have different magnetization directions. Despite the complexity of the hydrothermal alteration system, the magnetic amplitude calculation and the inversion result have a good correlation with the strike and the dip of the orebodies. In the following, we examine the inversion result in plan- and cross-sections, and in 3D representations.

First, we note again that the magnetic amplitude calculated using equivalent source technique is highly consistent with the horizontal location of the orebody as shown in Figure 4.8. Also this image shows the gap between the two anomalies, which is consistent with a mapped fault and the mineralization associated to silicification zone without the presence of magnetite. This correlation has also translated to the inversion result as shown in Figure 4.12.

As shown in Figure 4.4, there is a strong association of copper-gold grades with magnetic susceptibility. Thus, it follows that any subsurface region with high recovered effective susceptibility can be interpreted as the high-grade orebodies.

The amplitude inversion has recovered two distinct magnetic bodies. The 3D correlation between their strike direction and dip with the strike and dip of the known orebodies is excellent (Figure 4.12).

Vale's Furnas Project has delineated the 3D deposit model of the high-grade copper orebodies that represents the mineralized magnetite hydrothermal alteration zones using 69 drill holes and has accurate information about their 3D configurations. Thus, we can compare the interpreted orebodies from the amplitude inversion with the true orebodies. This is shown in 3D volume rendered images viewed end-on (Figure 4.13a) and top-down (Figure 4.13b) from the southeast. We observed that the elongated broad source (purple color) towards the NW resembles the main massive magnetite body with high-grade ores (green). The smaller source resembles the injection of mineralized magnetite pulses from hydrothermal fluid. There is an excellent spatial correlation between the orebodies imaged by the amplitude inversion and orebodies delineated from

drill holes. The region between the two orebodies has mineralization from hydrothermal alteration, but it is dominated by silicification and biotite-garnet-grunerite assemblage without magnetite. The amplitude inversion therefore did not recover significant magnetic source and, as expected, could not image the presence of mineralization there. Thus, the strong correlation both with magnetic orebodies and non-magnetic mineralized zone demonstrates that the amplitude inversion has performed well in this case. We further remark that this inversion has produced a good result without using specific geological constraints. This is particularly important in greenfield mineral exploration. Therefore, the methodology used in this test case is transferrable to other areas in this region.

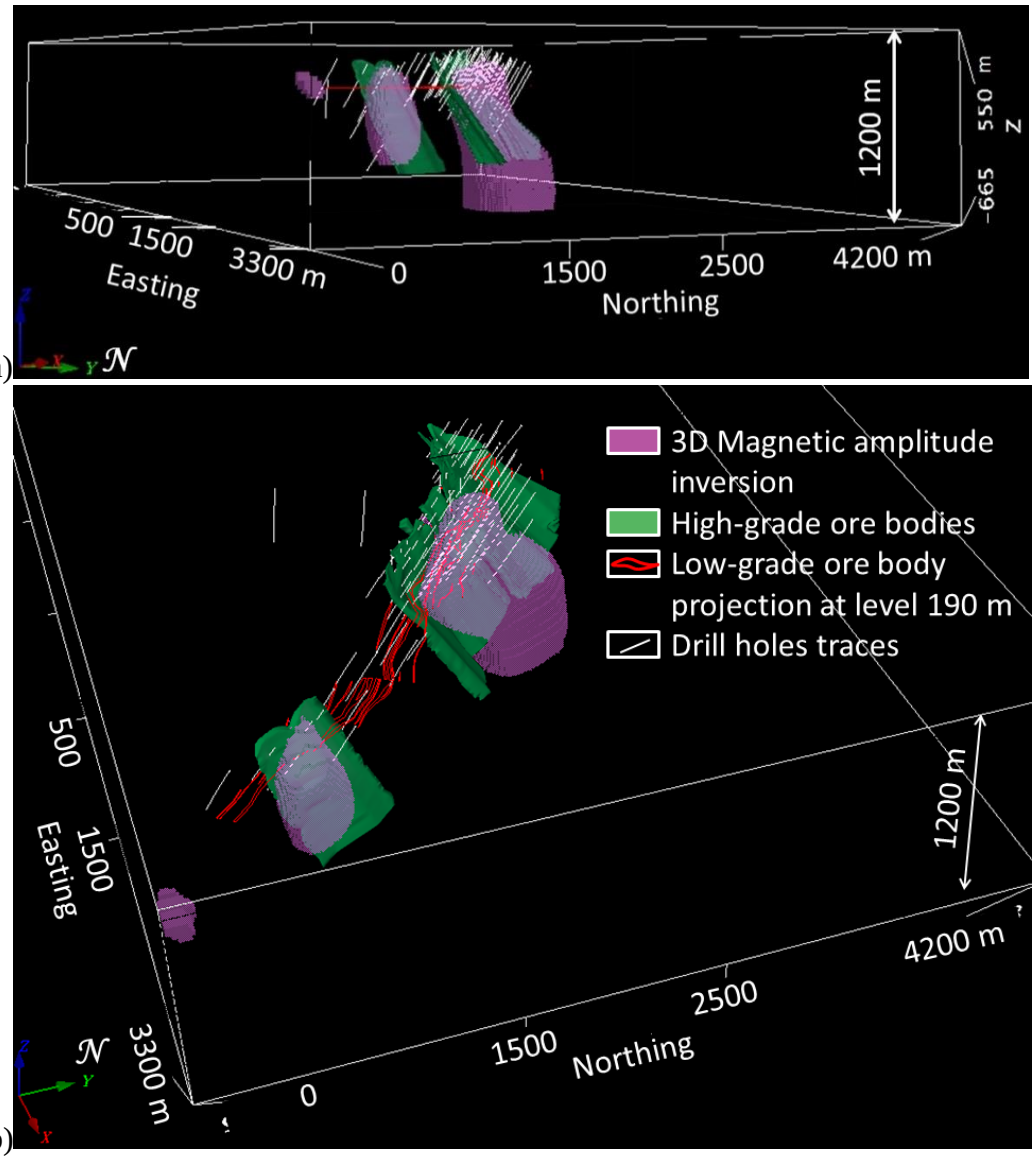

Figure 4.13. 3D correlation of the recovered susceptibility model (purple) with the known orebodies (green) in the 3D geological model of the high-grade mineralization zones constructed from extensive drilling in the Vale-Furnas Project.

As a summary comparison, Figure 4.14 shows the geologic interpretation of the amplitude inversion result in the representative section of the deposit displayed in Figure 4.3. There is a good correlation between the recovered magnetic zone and the massive magnetite, the measured susceptibility from drill cores, and the copper-gold mineralization zone. Over all, the recovered susceptibility model has characterized the massive magnetite (outlined in light blue), and the known mineralized zone (dark blue). The deeper extension of the recovered susceptibility indicates that the actual orebody might extend much deeper than that intersected by the existing drill holes.

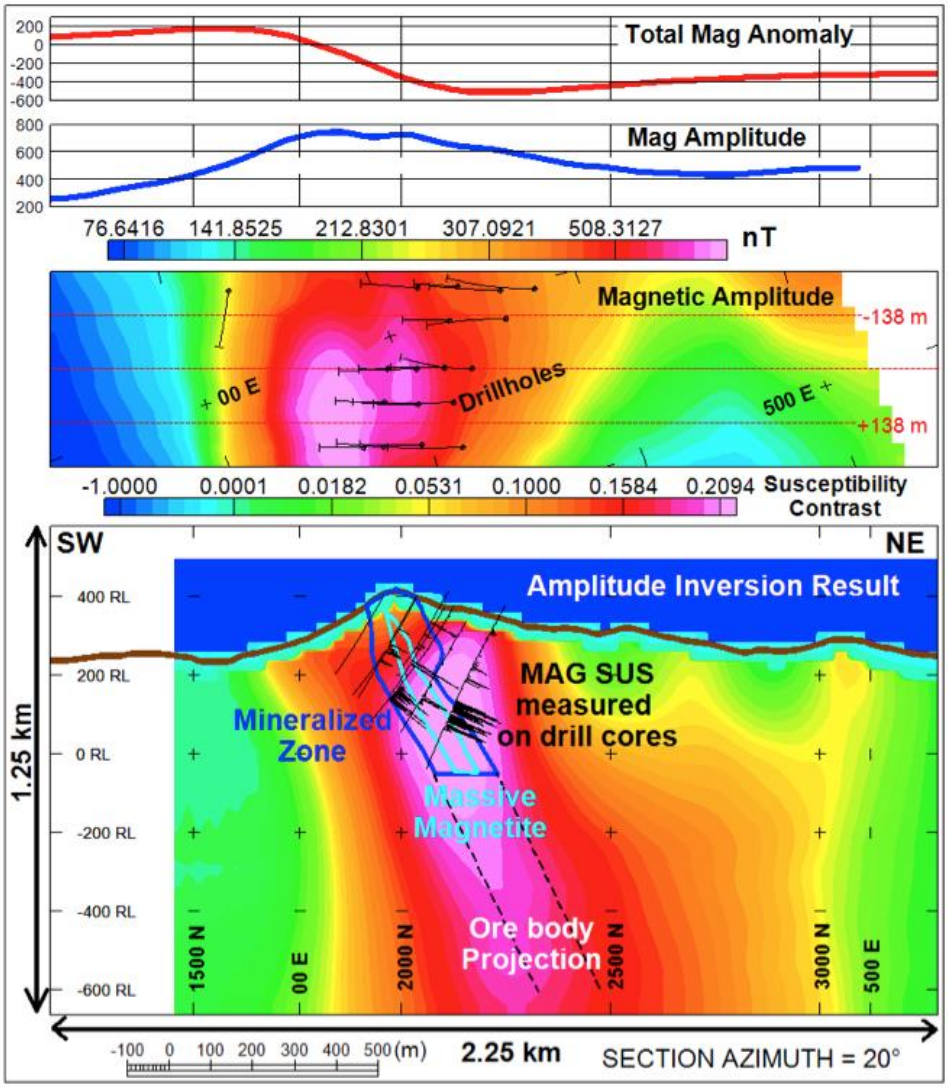

Figure 4.14. Summary of the geologic interpretation of the amplitude inversion result in the cross-section coinciding with that in Figure 4.3. The top panel shows the comparison between the total-field anomaly and calculated amplitude data. The middle panel shows the calculated amplitude data in a narrow strip surrounding the section. The bottom panel shows the comparison between the inversion result and the geology. The recovered effective susceptibility model (color contour) has characterized the massive magnetite (outlined in light blue), and the known mineralized zone in dark blue. Measured magnetic susceptibilities are also shown along several drill holes. The east most drill hole in this cross-section is the same as that shown in Figure 4.4.

4.6 - CONCLUSIONS

The magnetic amplitude inversion in the presence of strong remanent magnetization is applied to a dataset acquired at Furnas Southeast deposit as a case study in the exploration for iron oxide-copper-gold deposits (IOCG) in Carajás Mineral Province, Brazil. The Furnas deposit is magnetically anisotropic, remanently magnetized, and has self-demagnetization effect. Further compounding the difficulty is the location at an extremely low magnetic latitude, which poses challenges in data processing.

In this work, we have first calculated the magnetic amplitude data using the equivalent source technique. Then we carry out the amplitude inversion using an optimal regularization parameter obtained using the L-curve criterion. The inverted effective susceptibility successfully delineates the massive magnetite associated with the high-grade copper-gold ore. The strong correspondence between the amplitude inversion without using structural or drill hole constraints and the known geology and deposit model demonstrate the value of this approach.

This study also highlights the utility of amplitude data as a means for qualitative interpretation and mapping tool in place of the traditional reduction-to-pole (RTP) data. Similar to RTP data, amplitude data also reduce the asymmetry in total-field magnetic anomaly with respect to the horizontal locations of source bodies. Amplitude may be more advantageous since their calculation do not require the knowledge of magnetization direction. However, they are not entirely independent of the magnetization direction, and it is important to be aware of this limitation in interpretation based on such data directly or via inversions. Detailed numerical studies may be required to further understand this aspect.

Overall, the case study shows that the approach of amplitude inversion is effective in this complex scenario with multiple factors such as remanent magnetization and self-demagnetization that affect the total magnetization direction, as well as the complications due to the extremely low magnetic latitude. The methodology has high potential in the exploration for IOCG-type deposits in the Carajás Mineral Province and other similar areas.

4.7 - ACKNOWLEDGMENTS

The authors would like to thank Vale – Department of Exploration and Mineral Projects – for permission to publish this work, Vale – Department of Planning and Development of Ferrous – for providing the magnetic data, and Vale – Furnas Project – for providing the geophysical and geological data used in this study and for many discussions. The first author wishes to thank CAPES-Capes Foundation, Ministry of Education of Brazil for the scholarship. We thank Maria Irene Raposo for advice on the laboratory petrophysical measurements and Misac Nabighian for

helpful discussions. The comments by Reviewer Peter Lelièvre and an anonymous Reviewer have helped improve the manuscript. This work is supported in part by the Gravity and Magnetics Research Consortium (GMRC) and Vale. The current sponsoring companies are Anadarko, Bell Geospace, BG Group, BGP, BP, CGG, ConocoPhillips, ExxonMobil, Gedex, Lockheed Martin, Marathon Oil, Micro-g LaCoste, Shell, Petra Energia, Petrobras, Tullow Oil and Vale.

4.8 - REFERENCES

Blakely, R., 1996, Potential theory in gravity and magnetic applications: Cambridge University Press.

CVRD (Companhia Vale do Rio Doce), 2006, Relatório de etapa, Alvo Furnas, Volume 1: Internal report: Technical report.

Dampney, C.N.G., 1969, The equivalent source technique: Geophysics, **34**, 39–53.

Dannemiller, N., and Y. Li, 2006, A new method for estimation of magnetization direction: Geophysics, **71**, L69–L73.

Dransfield, M., A. Christensen, and G. Liu, 2003, Airborne vector magnetic mapping of remanently magnetized banded iron formations at Rocklea, Western Australia: Exploration Geophysics, **34**, 93–96.

Ellis, R., B. de Wet, and I.M. Macleod, 2012, Inversion of magnetic data from remanent and induced sources: Presented at the 22nd ASEG International Geophysical Conference.

Foss, C., and B. McKenzie, 2011, Inversion of anomalies due to remanent magnetisation: an example from the Black Hill Norite of South Australia: Australian Journal of Earth Sciences, **58**, 391–405.

Gerovska, D., M.J. Aráuzo-Bravo, and P. Stavrev, 2009, Estimating the magnetization direction of sources from southeast Bulgaria through correlation between reduced-to-the-pole and total magnitude anomalies: Geophysical Prospecting, **57**, 491–505.

Haney, M., C. Johnston, Y. Li, and M. Nabighian, 2003, Envelopes of 2d and 3d magnetic data and their relationship to the analytic signal: Preliminary results: 73rd Annual International Meeting, SEG, Expanded Abstract, 596–599.

Hansen, P.C., 1992, Analysis of discrete ill-posed problems by means of the L-curve: SIAM Review, **34**, 561–580.

Hansen, R.O., and Y. Miyazaki, 1984, Continuation of potential fields between arbitrary surfaces: Geophysics, **49**, 787–795.

Krahenbuhl, R., and Y. Li, 2011, Regularization, model weighting and solution appraisal in binary inversion for time-lapse gravity monitoring: Presented at the GEM Beijing 2011: International Workshop on Gravity, Electrical and Magnetic Methods and their Applications, SEG.

Lelièvre, P.G., and D.W. Oldenburg, 2009, A 3d total magnetization inversion applicable when significant, complicated remanence is present: Geophysics, **74**, L21–L30.

Li, S., and Y. Li, 2014, Inversion of magnetic anomaly on rugged observation surface in the presence of strong remanent magnetization: Geophysics, **79**, J11–J19.

Li, Y., and D.W. Oldenburg, 1996, 3-D inversion of magnetic data: Geophysics, **61**, 394–408.

Li, Y., and D.W. Oldenburg, 2010, Rapid construction of equivalent sources using wavelets: Geophysics, **75**, L51–L59.

Li, Y., S.E. Shearer, M.M. Haney, and N. Dannemiller, 2010, Comprehensive approaches to 3d inversion of magnetic data affected by remanent magnetization: Geophysics, **75**, L1–L11.

Liu, S., X. Hu, T. Liu, J. Feng, W. Gao, and L. Qiu, 2013, Magnetization vector imaging for borehole magnetic data based on magnitude magnetic anomaly: Geophysics, **78**, D429–D444.

Lourenco, J. S., and H.F. Morrison, 1973, Vector magnetic anomalies derived from measurements of a single component of the field: Geophysics, **38**, 359–368.

Machado, W., Z. Lindenmayer, T.E. Krogh and D. Lindenmayer, 1991, U-Pb geochronology of Archean magmatism and basement reactivation in the Carajás area, Amazon shield, Brazil: Precambrian Research, **49**, 29–354.

Mueller, E.L., W.A. Morris, P.G. Killeen, and S. Balch, 1997, Combined 3-d interpretation of airborne, surface, and borehole vector magnetics at the McConnell nickel deposit: Presented at the 67th Annual International Meeting, SEG.

Nabighian, M., 1972, The analytic signal of two-dimensional magnetic bodies with polygonal cross-section: Geophysics, **37**, 507–517.

Paine, J., M. Haederle, and M. Flis, 2001, Using transformed TMI data to invert for remanently magnetised bodies: Exploration Geophysics, **32**, 238–242.

Phillips, J. D., 2005, Can we estimate total magnetization directions from aeromagnetic data using Helbig's formulas: Earth, Planets, and Space, **57**, 681–689.

Shearer, S., 2005, Three-dimensional inversion of magnetic data in the presence of remanent magnetization: M.S. thesis, Colorado School of Mines.

Silva, J.B.C., 1986, Reduction-to-the-pole as an inverse problem and its application to low-latitude anomalies: Geophysics, **51**, 369–382.

Stavrev, P., and D. Gerovska, 2000, Magnetic field transforms with low sensitivity to the direction of source magnetization and high centricity: Geophysical Prospecting, **48**, 317–340.

Vale S.A., 2012, Projeto Furnas, Relatório Final de Geologia: Internal report: Technical report.

Wirth, K.R., A.K. Gibbs, and W.J. Olszewski, 1986, U-Pb ages of zircons from the Grão-Pará Group and Serra dos Carajás Granite, Pará, Brazil: Revista Brasileira de Geociências, **16**, no. 2, 195–200.

CAPÍTULO 5

MAGNETIC SUSCEPTIBILITY 3D MODEL AND SIGNATURES OF IRON OXIDE-COPPER-GOLD (IOCG) MINERALIZATION: A CASE STUDY FROM CARAJÁS MINERAL PROVINCE, BRAZIL

Manuscript submitted to the Journal *Economic Geology* in August 13th of 2014.

Economic Geology

MAGNETIC SUSCEPTIBILITY 3D MODEL AND SIGNATURES OF IRON OXIDE-COPPER-GOLD (IOCG) MINERALIZATION: A CASE STUDY FROM CARAJÁS MINERAL PROVINCE, BRAZIL

--Manuscript Draft--

Manuscript Number:	
Full Title:	MAGNETIC SUSCEPTIBILITY 3D MODEL AND SIGNATURES OF IRON OXIDE-COPPER-GOLD (IOCG) MINERALIZATION: A CASE STUDY FROM CARAJÁS MINERAL PROVINCE, BRAZIL
Article Type:	Regular Paper
Corresponding Author:	Marcelo Henrique Leão-Santos, M.D. Vale S.A. Belo Horizonte, Minas Gerais BRAZIL

Submission Confirmation for MAGNETIC SUSCEPTIBILITY 3D MODEL AND SIGNATURES OF IRON OXIDE - COPPER - GOLD (IOCG) MINERALIZATION: A CASE STUDY FROM CARAJÁS MINERAL PROVINCE, BRAZIL
Economic Geology <em@editorialmanager.com> Wed, Aug 13, 2014 at 10:27 AM

A manuscript number has been assigned to MAGNETIC SUSCEPTIBILITY 3D MODEL AND SIGNATURES OF IRON OXIDE-COPPER-GOLD (IOCG) MINERALIZATION: A CASE STUDY FROM CARAJÁS MINERAL PROVINCE, BRAZIL
Economic Geology <em@editorialmanager.com> Wed, Aug 13, 2014 at 11:18 AM
Reply-To: Economic Geology <econgeol@segweb.org>
To: Marcelo Henrique Leão-Santos <marcelo.leao.santos@gmail.com>
Dear Dr. Leão-Santos,
Your submission entitled "MAGNETIC SUSCEPTIBILITY 3D MODEL AND SIGNATURES OF IRON OXIDE-COPPER-GOLD (IOCG) MINERALIZATION: A CASE STUDY FROM CARAJÁS MINERAL PROVINCE, BRAZIL" has been been assigned the following manuscript number: SEG-D-14-00111.
You will be able to check on the progress of your paper by logging on to Editorial Manager as an author.
The URL is http://seg.edmgr.com/.
Thank you for submitting your work to Economic Geology.
Kind regards,
Larry Meinert
Editor
Economic Geology

MAGNETIC SUSCEPTIBILITY 3D MODEL AND SIGNATURES OF IRON OXIDE-COPPER-GOLD (IOCG) MINERALIZATION: A CASE STUDY FROM CARAJÁS MINERAL PROVINCE, BRAZIL

Marcelo Leão-Santos[1,2], Roberto Moraes[1], Maria Irene Raposo[3], Otávio Rosendo[2], Arthur Cardoso[2], and Joaquim Feijó[2]

[1] Universidade de Brasília, Instituto de Geociências, Brasília, Brazil.

E-mail: marcelo.leao.santos@gmail.com, rmoraes@unb.br.

[2] VALE S.A., Department of Exploration and Mineral Projects, Belo Horizonte, Brazil.

E-mail: marcelo.leao@vale.com, otavio.rosendo@vale.com, arthur.cardoso@vale.com, joaquim.feijo@vale.com.

[3] Universidade de São Paulo, Instituto de Geociências, São Paulo, Brazil.

E-mail: irene@usp.br.

5.1 - ABSTRACT

Petrophysical measurements were performed along drill cores from the Furnas Southeast deposit, which is located in the Carajás Mineral Province, Brazil. Magnetic susceptibilities were incorporated into a three dimensional (3D) model and used to define the magnetic signatures of the various hydrothermal alteration types associated with the iron oxide-copper-gold (IOCG) mineralization. The disseminated copper and gold mineralization is associated with a calcic-sodic-potassic hydrothermal alteration (dominated by biotite-garnet-amphibole-magnetite alteration minerals) and followed by intense iron metasomatism with massive magnetite. The copper (chalcopyrite and bornite) and gold mineralization are usually associated with magnetite. Magnetic characterization related to the different hydrothermal alteration types and their host rocks show an association of high-grade mineralization with magnetite.

High measured magnetic susceptibility values (mean = 2,277 x 10^{-3} SI and median = 989 x 10^{-3} SI) on hydrothermally altered rocks that contain massive magnetite indicate an abundance of ferromagnetic minerals.

Measurements made using different equipment and measurement protocols were assessed to determine the appropriate methodology needed to efficiently, and effectively, characterize the magnetic signature of the host rocks and ore deposit.

The hydrothermal alteration is controlled by breccias, dilational structures, and several bodies with sigmoidal shape that open and close the ore zones. The alteration types have large variations along the deposit.

The geological knowledge included here followed qualitative criteria that can be subjective in the definition of lithotypes because of the great complexity in hydrothermal alteration types. This study shows how the detailed characterization of physical properties in the IOCG system and three-dimensional modeling can be used to define magnetic susceptibility signatures and describe hydrothermal alteration zones with quantitative criteria to improve mineral exploration and the evaluation of deposits.

Keywords: magnetic susceptibility, magnetite hydrothermal alterations, magnetic susceptibility signatures, iron oxide-copper-gold (IOCG) deposit, Carajás Mineral Province.

5.2 - INTRODUCTION

In recent decades, geophysical surveys have been used for prospecting iron oxide-copper-gold (IOCG) deposits. Although the main characteristics of this type of mineralization are known, a more detailed characterization is still required of how their physical properties define and characterize their geophysical signatures, especially their magnetic signature.

The importance of iron oxide-copper-gold (IOCG) deposits has increased as one of the most important classes of mineral deposits because of a number of major discoveries, such as the Olympic Dam, Salobo, Prominent Hill, etc. The complexity and variability of this type of deposit do not permit the definition of a single geological exploration model. Thus, detailed physical property measurements on drill cores of the host rocks and hydrothermal alteration zones can help characterize these deposits and assist with defining an exploration model.

The geological and magnetic characteristics of IOCG deposits have been discussed in the literature. Worldwide, IOCG deposits were defined by Hitzman et al. (1992) and further described by Porter (2000). In Brazil, Hitzman et al. (1992) include the Sossego and Salobo deposits from the Carajás Mineral Province within the IOCG type. Some work applied magnetic petrophysics and magnetic petrology to geological interpretation of magnetic surveys (Clark et al., 1992; Clark, 1997, 1999). Smith (2002) provided a generic description of the geophysical features of an IOCG deposit. Afterwards, Sandrin and Elming (2007), and Sandrin et al. (2009) offered a more detailed description of the physical properties, petrology and geophysics of this type of deposit. Recently, numerous petrophysical studies have been conducted to solve the various problems and difficulties encountered in the modeling of magnetic data, such as remanence, demagnetization and low latitudes. Studies such as the one by Austin et al. (2013) used constrained modeling of petrophysical data for IOCG deposits in Australia. The magnetic effects of hydrothermal alteration in porphyry copper and iron-oxide copper–gold systems were reviewed by Clark (2014).

In magnetite-rich hydrothermal environments, it is sometimes difficult to interpret physical property measurements because of the strong magnetization and the variation of magnetic properties as a result of different types of hydrothermal alteration events. The deposit has undergone multiple alteration events that have imparted variations in the magnetic properties of the rocks within and surrounding the deposit. Such an environment is represented by the IOCG type mineralization found in the Furnas Southeast deposit. The mineralization consists of copper sulfides (chalcopyrite and bornite) and gold ore that are spatially and genetically associated with iron oxide.

There are no previous studies that use petrophysical measurements to develop a magnetic susceptibility model of an IOCG deposit in the Carajás region. This study presents physical property measurements that were made on drill cores from the Furnas Southeast deposit. Particular attention was given to a section of the deposit with high grade mineralization associated with the presence of massive magnetite. In this section, multiple methods were used to measure the magnetic susceptibility. The results are compared and an efficient methodology is established.

The purpose of this study was threefold: 1) to investigate the relationship between the high grade mineralization and magnetite, 2) to distinguish the different magnetic susceptibility signatures of the hydrothermal alteration zones, and 3) to conduct a 3D modeling based on appropriate magnetic susceptibility measurements. The measurements were made on drill core samples from the deposit using handheld magnetic susceptibility meters and laboratory techniques.

The final goal of this study was to characterize the magnetic susceptibility signature of the copper-gold prospect, define a susceptibility model for the IOCG mineralization and hydrothermal alterations of the same type. The results can be used when generating an IOCG exploration model.

5.3 - DEPOSIT GEOLOGICAL SETTINGS

The lithostratigraphy in the Carajás Mineral Province is complex and mostly consists of Precambrian rocks that are overlain by younger sediments (Figure 5.1; Hirata et al., 1982; DOCEGEO, 1988). The lithostratigraphy consists of several Precambrian units (Xingu, Pium and Luanga Complexes; Plaquê and Cateté Suites), Neoarchean metasedimentary and metavolcanosedimentary sequences (Itacaiúnas Supergroup), Proterozoic anorogenic granitoids (granitic plutons with Lower/Middle Proterozoic ages) and Phanerozoic cover units (Hirata et al., 1982; DOCEGEO, 1988).

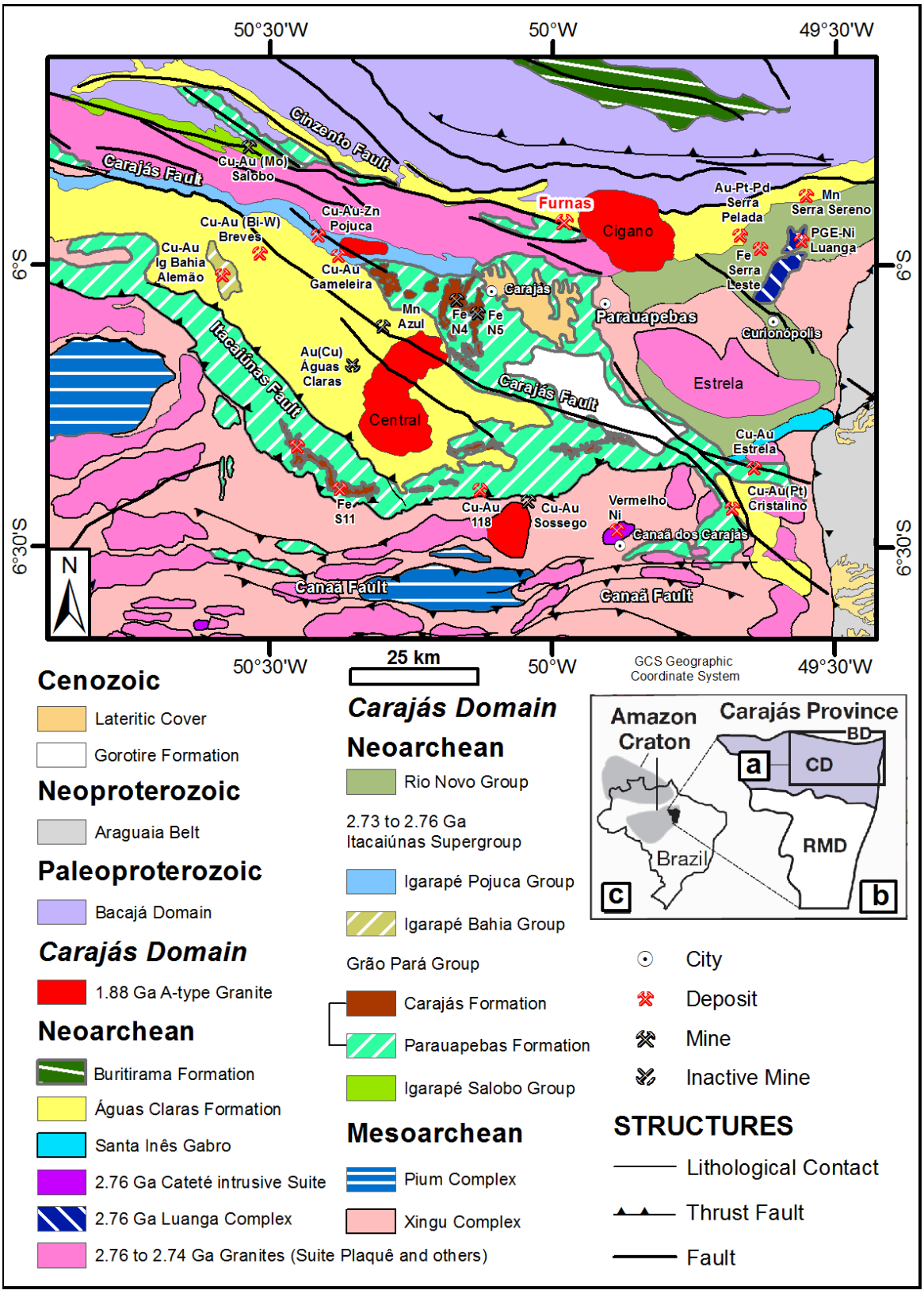

Figure 5.1. (a) Geological map of the Carajás Mineral Province with the location of the Furnas deposit and the main Cu, Au, Fe, Mn, Ni and Pt group element (PGE) deposits. (b) Carajás Province map with the Carajás domain (CD) and Rio Maria domain (RMD). The Bacajá domain (BD) is located north of the Carajás domain. (c) Map of Brazil with the location of Carajás Province (in black) and the Amazon Craton (in gray) (Modified from DOCEGEO, 1988; Araújo and Maia, 1991; Barros and Barbey, 1998; Vasquez et al., 2008; and Xavier et. al., 2012).

The Furnas Southeast deposit is located along the WNW-trending Cinzento Transcurrent System that is approximately 200 km long (Figure 5.2). The deposit is hosted in rocks correlated with the metamorphosed volcano-sedimentary rocks of the Grão Pará Group, which belongs to the Itacaiúnas Supergroup (2.76 Ga) and Águas Claras Formation (Wirth et al., 1986; Figure 5.2). In the Furnas Southeast deposit, a shear zone defines a contact between an amphibole schist on the north (hanging wall) and aluminous schist on the south (footwall; Figures 5.3 and 5.4). These host rocks were also, altered by hydrothermal processes. The Cinzento shear zone was intruded by the anorogenic Cigano Granite (1.8 Ga) to the east and continues northwestward towards the Salobo deposit (Wirth et al., 1986; Figure 5.2). The region is metamorphosed in the greenschist to amphibolite facies and is covered by a thick lateritic cover.

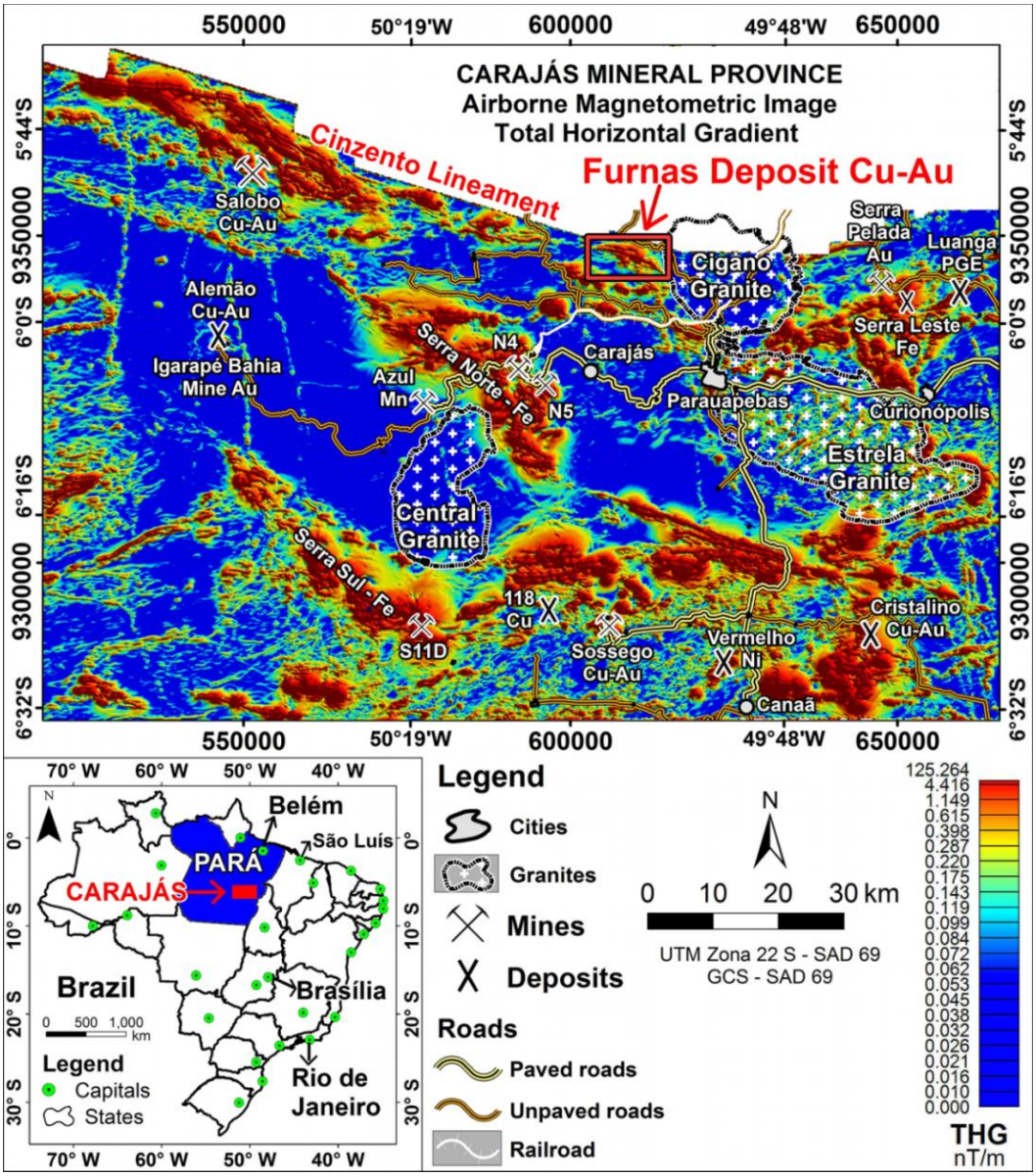

Figure 5.2. Magnetic total horizontal gradient with the location of the Furnas deposit along the Cinzento lineament.

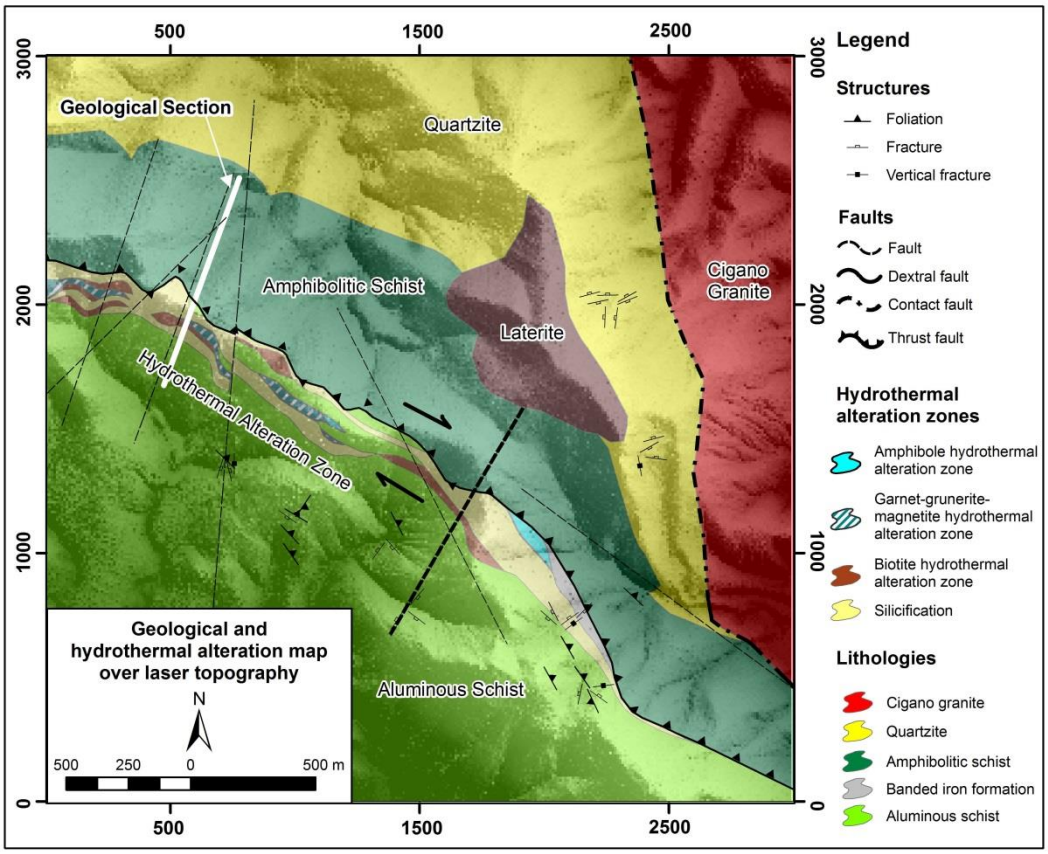

Figure 5.3. Geological and hydrothermal alteration zone map of the Furnas Southeast deposit over laser-LiDAR topography; the geological section location of Figure 5.4 is included (Modified from Vale S.A., 2012).

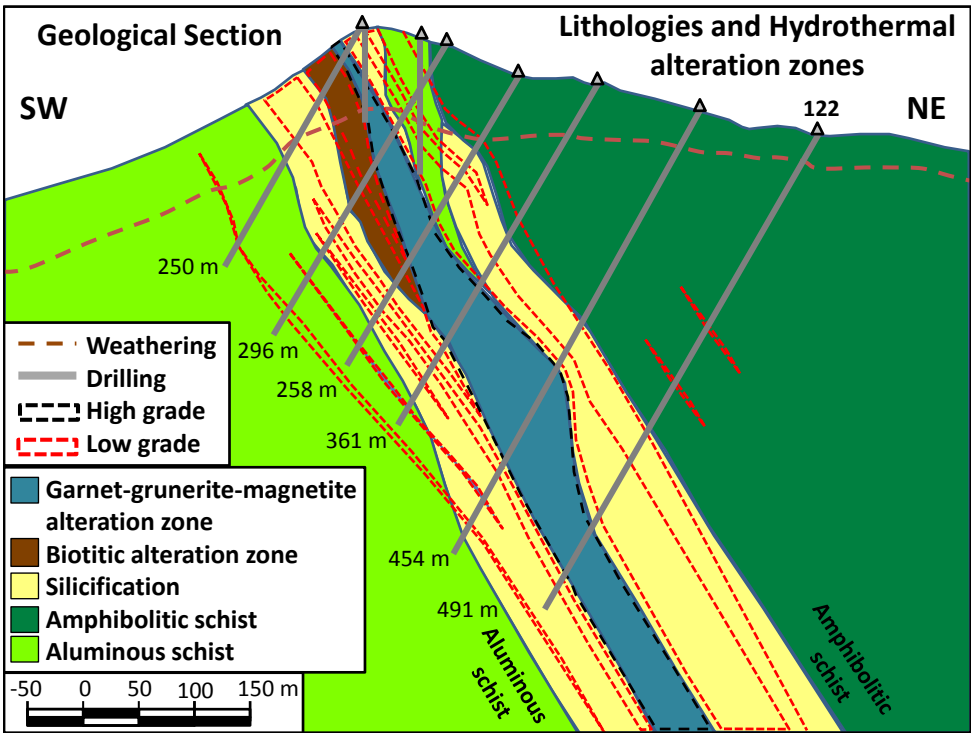

Figure 5.4. Geological section with the host rocks, hydrothermal alteration zones and mineralized zones (Modified from Vale S.A., 2012).

The rocks of the Furnas Southeast deposit can be correlated with supracrustal rocks of the Igarape Salobo Group observed at the nearby Salobo Cu-Au deposit (Lindenmayer, 1990; Lindenmayer and Teixeira, 1999). The rocks are difficult to interpret because of the intense alteration. In general, an alteration that progresses from high- to low-temperatures is observed. The high-temperature alteration is characterized by a biotite-garnet-amphibole-magnetite hydrothermal assemblage, whereas the subsequent low-temperature alteration shows a biotite-chlorite-tourmaline-carbonate-quartz-epidote-albite-hematite-magnetite assemblage. The mineralization itself is associated with chalcopyrite- and bornite-rich late stage veins and breccias (Figure 5.5). The hydrothermal alteration zones have a lenticular shape and thicknesses of 20 to 600 m, and extending approximately 9 kilometers along the entire deposit. The study area of this paper is located at two kilometers in the extreme southeast of the deposit being dominated by high-temperature alterations (biotite-garnet-amphibole-magnetite hydrothermal assemblage).

(a)

(b)

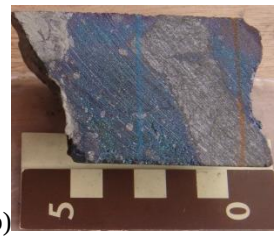

Figure 5.5. Photographs of ore samples. (a) Chalcopyrite. (b) Bornite.

In the Furnas Northwest deposit, which is outside of the study area, a basement monzogranitic rock with local pegmatites and granophyres is found. This unit is informally referred to as Furnas granitoid and has penetrative foliation from heterogeneous ductile deformation events. They are similar to the hornblende-biotite monzogranite facies from the Geladinho Granite Stock, aged 2.688 ± 11 Ma (Pb-Pb by zircon evaporation; Barbosa et al., 2001).

Quartzites and schists occur to the north and south of the deposit, respectively (Figure 5.3). The quartzites may be correlated with the Águas Claras Formation. The schists contain andalusite-kyanite-sillimanite-staurolite and have been described as resulting from the deformation and metamorphism of aluminous pelitic sediments that are most likely correlated with the Águas Claras Formation. In the northern portion, schists contain amphiboles (Figure 5.3). They are interpreted to

result from deformation and metamorphism of volcanic rocks with the mostly likely protoliths being the Grão-Pará Group. The presence of both, the aluminous and the amphibole alteration could be considered pre-mineralization distal halos. There are banded iron formations in the Grão-Pará Group.

In the eastern portion, the anorogenic Cigano Granite, aged 1.8 Ga (Wirth et al., 1986), is described as an isotropic monzogranitic rock with portions of moderate primary foliation (Figure 5.3). Cigano Granite rocks are leucocratic with gray-pinkish colour, coarse to medium grained, monzogranitic composition, with amphibole and biotite. Those rocks have a discordant contact with the quartzites correlated with Águas Claras Formation.

The observed tectonic features of Furnas Southeast deposit are related to heterogeneous deformation of different grades. In general, the deposit rocks have mylonitic fabrics (transposition foliation) with a brittle-ductile behavior at spaced zones. They present at least two brittle to brittle-ductile overlapping fabrics (concordant or not). The brittle to brittle-ductile fabrics are characterized by bands of cataclastic flows. They also bear regions of hydraulic fracturing marked by a predominance of breccias (cataclastic, hydraulic, hydrothermal), faults and veins/veinlets consisting of quartz + albite + hematite + specularite + chlorite + amphibole ± biotite ± epidote ± tourmaline ± carbonate, and with sulfides overlapping these fabrics. The directions range from WNW-ESE to NNW-SSE (plunging from 30° NE to 88° NE). These are the most common and important fabrics in the tectonic-hydrothermal context of the area and they conditioned the mineralizing input of the deposit. The fabrics are related to the mechanism of shear deformation under high amounts of hydrothermal fluids. Furthermore, the fabrics are typical for hydrothermal conduits controlled by cataclastic flow with fragmentation of crystals and grains, and dragging along the conduits.

5.4 - HYDROTHERMAL ALTERATION AND MINERALIZATION

The Furnas Southeast deposit copper-gold disseminated mineralization has a biotite-garnet-amphibole-magnetite hydrothermal alteration assemblage. Although the hydrothermal alteration and mineralization type and intensity vary throughout the orebodies, a consistent alteration and mineralization paragenetic sequence could be distinguished (Table 5.1). The hydrothermal alteration characterizations were based on the macroscopic observations supported by petrographic studies.

Table 5.1. Lithotypes, hydrothermal alteration zones and mineralogy.

	DESCRIPTION	ALTERATION TYPE	MINERALOGY
Hydrothermal alteration zones	Chlorite alteration	Chloritization	Chlorite
	Amphibole-Magnetite hydrothermal alteration	Calcic-Sodic-Magnetite	Amphibole (Actinolite), Magnetite ± Garnet ± Quartz ± Biotite ± Chlorite
	Amphibole hydrothermal alteration	Calcic-Sodic	Amphibole (Actinolite) ± Quartz ± Biotite ± Chlorite
	Massive Magnetite hydrothermal alteration	Magnetite	Magnetite ± Amphibole (Grunerite, Actinolite, Hornblende = Hastingsite) ± Quartz
	Garnet-Grunerite-Magnetite hydrothermal alteration	Calcic-Magnetite	Garnet (Almandine), Amphibole (Grunerite), Magnetite ± Biotite ± Chlorite
	Garnet-Grunerite hydrothermal alteration	Calcic	Garnet (Almandine), Amphibole (Grunerite) ± Quartz ± Chlorite ± Biotite
	Biotite hydrothermal alteration	Potassic	Biotite, Quartz, Plagioclase, Phengite ± Garnet
	Silicification	Silicic	Silica, Sericite
	Albitization	Sodic	Albite
Host rocks	Monzogranite		Quartz, Plagioclase, Microcline, Biotite, Chlorite (±pegmatites, granophyres)
	Quartzite		Quartz ± Sericite
	Amphibolitic schist		Amphibole (Grunerite), Quartz ± Hornblende = Hastingsite
	Banded iron formation		Magnetite, Silica
	Aluminous schist		Quartz, Biotite, Sericite, Andalusite, Staurolite, Silimanite ± Garnet ± Chlorite

The presence of magnetite was first tested using a handheld magnet. Magnetic susceptibility measurements were subsequently used to show magnetic properties of the various lithologies and alteration zones.

Sodic alteration is the earliest alteration type observed. The sodic alteration is mainly associated with albite veins in the Furnas Southeast deposit. However, the alteration is best observed in the Furnas Northwest deposit, outside the study area, where host rocks consist of the Furnas Granite.

A silicic alteration type is widely distributed over the deposit that can completely transform the host rock. The silica-rich alteration forms zones that are lenticular. Narrow bands of sericite and quartz characterize the silicic alteration type. The silicic alteration may also contain chalcopyrite and rarely bornite. Importantly, magnetite is absent.

Potassic alteration type is common near the brittle-ductile to brittle deformed rocks. Mineralized bodies are commonly associated with potassic zones that are essentially composed of biotite with a schistose texture and locally within tectonic-hydrothermal breccias cemented with

biotite. In addition, the potassic zone has a significant association with garnet, magnetite and silica alteration minerals.

The calcic alteration type is concurrent with or subsequent to potassic alteration. Calcic alteration exhibits coarse-grained garnet proximal to mineralized zones with fine-grained garnets found more distal. This alteration is associated with aluminous schists and biotite, grunerite and magnetite alteration minerals.

The calcic alteration type typically overprints potassic alteration. The mineral assemblage includes garnet-grunerite. The alteration occurs in association with bands of silicic alteration. The garnet-grunerite calcic alteration has variations from isotropic to anisotropic textures, and from ductile to brittle-ductile deformations. This alteration also occurs in association with a garnet-grunerite-magnetite mineral assemblage.

Magnetite is directly associated with high-grade copper and gold mineralization. This stage of high iron metasomatism forms massive magnetite. The magnetite-bearing fluid flow was structurally controlled. The magnetite alteration type overprints the calcic-sodic alteration type and forms bands with the garnet-grunerite-magnetite assemblage. There is also a strong association with the brecciated silicification.

The calcic-sodic atleration type is dominated by amphiboles (predominance of actinolite) and has variable amounts of quartz, tourmaline and plagioclase. Chalcopyrite and bornite are locally found. This alteration type often occurs after the magnetite, potassic and silicic alteration types. However, magnetite infiltrations also appear in the calcic-sodic alteration that is dominated by the amphiboles. In general, sulfidation occurs in association with these amphibole-magnetite assemblages.

Subsequently, some final weak alteration types occur and were not included in Table 2. The first is a new potassic alteration process with biotitization that occurs followed by a strong chloritic process, which partially or completely alters the rocks of the area, with local areas of hydrothermal breccias with mineralized chlorite-hematite-magnetite. The other late alterations are related to carbonation and silicification. Calcite occurs in association with quartz-hematite-magnetite-pyrite-chalcopyrite-epidote-albite-biotite-tourmaline veinlets.

5.5 - METHODS

Rock magnetism

Magnetic susceptibility (χ_m) measures the magnetization capacity of a material when subjected to a magnetic field. The proportionality coefficient (χ_m) defines the magnetic susceptibility of the environment or material considered.

$$\vec{M} = \chi_m \cdot \vec{H}, \quad (1),$$

where $\vec{M}$ is the induced magnetization in ampere per meter (A/m); $\vec{H}$ is the inducing magnetic field in ampere per meter (A/m); and χ_m is the magnetic susceptibility of the material (non-dimensional).

The magnetic behavior of a rock under the action of a magnetic field depends on its mineralogical composition. All the diamagnetic, paramagnetic and ferromagnetic minerals present in a rock contribute to its magnetic susceptibility. Most existing minerals have low susceptibility, and a small portion of the magnetic minerals that compose the rocks is usually responsible for the higher susceptibility values.

In diamagnetic minerals, susceptibility is weak, negative and reversible; the mineral is magnetized in the direction opposite to the applied magnetic field, and the magnetization drops to zero when the magnetic field is removed. Diamagnetic minerals have susceptibility values of approximately -10^{-6} SI, with quartz and calcite as examples.

In paramagnetic minerals, susceptibility is small, positive, reversible and varies inversely with temperature; the mineral is magnetized in the same direction as the applied magnetic field, and the magnetization drops to zero when the magnetic field is removed. In paramagnetic minerals, the susceptibility values vary between 10^{-5} and 10^{-4} SI, and examples of minerals with this property are amphibole, biotite, feldspar and plagioclase.

Ferromagnetic minerals exhibit strong spontaneous magnetization and high magnetic susceptibility values. Ferromagnetic is a general term that encompasses both ferrimagnetic minerals, such as magnetite, and antiferromagnetic minerals, such as hematite[1]. The iron-titanium-oxygen series has a solid solution of magnetic minerals that ranges from magnetite (Fe_2O_4) to ulvospinel (Fe_2TiO_4). The most abundant ferromagnetic mineral is magnetite, whose *Curie* temperature is 580° C. The magnetic characteristic of the rock is affected by the fabric, distribution,

[1] Hematite (Fe_2O_3) is a commom iron oxide classified as an antiferromagnetic material. The occurrence of a parasite antiferromagnetism can generate magnetic anomalies in hematites. In the iron-sulfur series, pyrrhotite can be either ferromagnetic or antiferromagnetic depending on its composition with iron-poor end-members being ferromagnetic and iron-rich end-members being antiferromagnetic.

shape and size of the magnetic grains. A common method of classifying the magnetic character of the rock is to evaluate the amount of magnetite (Kearey et al. 2002).

Magnetic anomalies can be associated with the alteration of magnetic minerals in rocks that host mineral deposits related to hydrothermal systems (Hanna, 1969; Criss and Champion, 1984; Clark, 2014) and delineate "fossil" hydrothermal activity zones. Porphyry systems commonly make/destroy magnetite in host rocks (Hoschke, 2008). However, direct detection of ore body is limited to iron resources that occur in magnetite-rich banded iron formations. The magnetic method is a key tool for inferring the subsurface structures and for mapping anomalous concentrations of magnetite, which is the main magnetic material in the crust. It can similarly be used on magnetite concentration mapping occurring on many economic mineral deposits where this mineral is associated (Hoover et al. 1992; Clark, 2014).

Magnetic susceptibility measurements

The susceptibility meters KT-9 and KT-10 (Figure 5.6a) and the susceptibility (and conductivity) meter MPP – EM2S (Figure 5.6b) were used. Their manufacturers and basic technical specifications are listed below (Table 5.2).

It was seen that the magnetic susceptibility value:

(i) increases with the amount of magnetite in the sample (expected),

(ii) decreases as the distance between the sensor and the sample increases,

(iii) depends on the shape of the sample and

(iv) tends to increase with an increase of the contact surface for an equivalent content magnetic ore (Figure 5.6c).

All the measurements were conducted on split drill cores that were at least 40-mm-thick to ensure a good contact area with the sensor (Figures 5.6d and 5.6e). Measured conductivity values were recorded and positive results were not obtained, which are possibly related to the disseminated character of the mineralization (not massive).

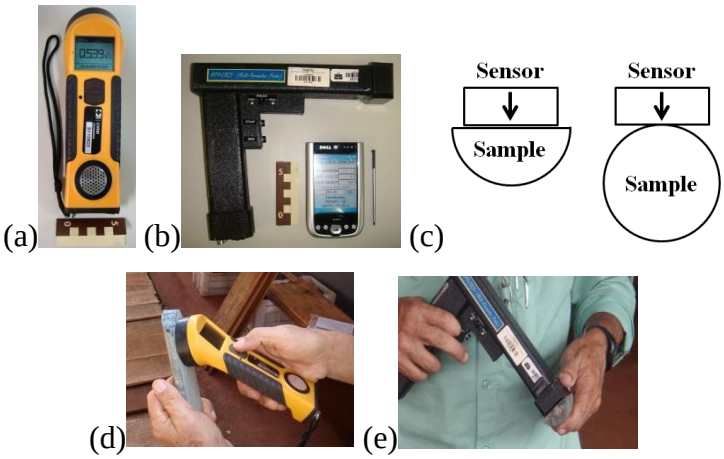

Figure 5.6. (a) Susceptibility meter KT-10. (b) Susceptibility/conductivity meter MPP - EM2S. (c) Sketch of the sample - sensor contact surface. (d) Measurement procedure with the susceptibility meter KT-10. (e) Measurement procedure with susceptibility meter/conductivity meter MPP - EM2S.

Table 5.2. Main specifications of susceptibility meters KT-9 and KT-10 and susceptibility meter/conductivity meter MPP-EM2S.

Susceptibility meter	**KT-9**	**KT-10 – Plus**	**MPP – EM2S**
Manufacturer	*Georadis*		*Instrumentation GDD*
Susceptibility sensitivity	1 x 10^{-5} SI	1 x 10^{-6} SI	1 x 10^{-3} SI
Susceptibility range	9.9 x 10^{-3} SI to 999.9 x 10^{-3} SI	-0.999 x 10^{-3} to 9,999 x 10^{-3} SI	10^{-3} to 9,000 x 10^{-3} SI
Operating frequency	10 kHz	10 kHz	10 kHz
Operating temperature	-10 to 55°C	-20 to 60°C	0 to 50°C
Dimensions	18.7 x 6.5 cm	20 x 5.7 x 3 cm	31 x 25 x 18 cm
Coil diameter	6.5 cm	6.5 cm	2.54 cm

Sampling methods of the magnetic susceptibility measurements

Magnetic susceptibility measurements were made on drill cores from the Furnas Southeast deposit. These measurements were used to characterize the magnetic signature of the lithotypes and hydrothermal alteration zones associated with the deposit. A total of 17,789 measurements were made along 17,739 meters of drill cores from 69 drill holes. The drill cores were HQ diameter (96.40 mm) through the weathered material and NQ diameter (76.20 mm) in fresh rock. The systematic magnetic susceptibility measurements along the deposit were taken with two different sensitivities described below (Figure 5.7).

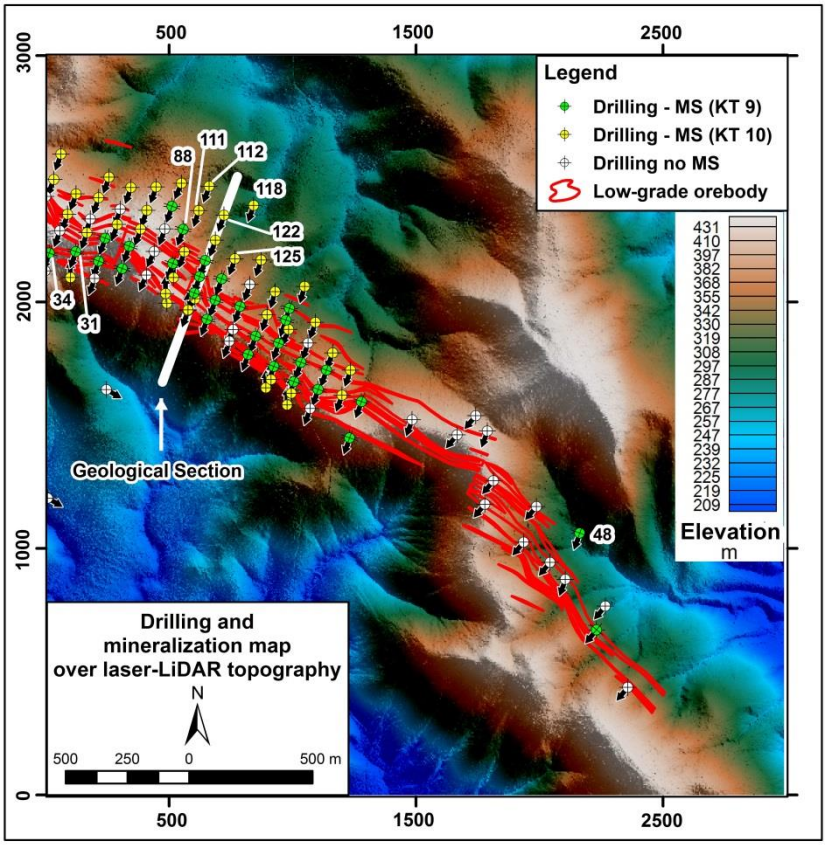

Figure 5.7. Drill hole location map. Measurement schematics: lower sensitivity magnetic susceptibility (MS) measurements (KT-9) in green; higher sensitivity MS measurements (KT-10) in yellow; drill holes without MS measurements in white; and low grade orebody projections at an elevation of 190-m in red. The geological section location (see Figure 5.4) is indicated in the map, and the numbers of the drill holes used in this work are highlighted.

Four rounds of magnetic susceptibility measurements were made:

1 - The first round of data collection used the KT-9 susceptibility meter (having lower sensitivity of 1 x 10^{-5} SI units), with 8,514 measurements acquired along 6,862.35 m of 30 drill holes. Measurements were taken every 1 m (CVRD, 2006).

2 - The second round used the KT-10 meter (with a sensitivity of 1 x 10^{-6} SI units). A total of 9,275 measurements were acquired along 10,877.13 m of 39 drill holes. Measurements were taken every 1 m (Vale S.A., 2012).

3 - In the third round, different equipment and measuring configurations were conducted on the drill hole number 88. The purpose was to establish an optimal sampling and measurement procedure. Sample intervals of 0.2 m and 0.5 m along the drill cores were tested. Also, measurements were made on sample aliquots collected every meter along the drill core that were analyzed for chemistry. These aliquots were prepared by homogenizing the drill cores along each

meter to perform geochemical assays. Besides the KT-9 and KT-10 susceptibility meters the MPP equipment was also used.

4 - In the fourth and final round, the susceptibility and anisotropy degree measurements were carried out at the laboratory (*Laboratório de Anisotropias Magnéticas e de Magnetismo de Rochas, Instituto de Geociências – IGc, Universidade de São Paulo – USP*). In this round, laboratory measurements were used to validate measurements taken with handheld susceptibility meters and to evaluate the anisotropy degree of the mineralization. Measurements were made on 487 specimens from 136 samples that were collected from 6 drill holes (88, 111, 112, 114, 118 and 125). In general, each sample had four specimens with a cylinder having size of 25.4 mm in diameter and 22 mm in length. The equipment used was a Kappabridge KLY-4S (Figure 5.8), which is a modular system designed to measure the magnetic susceptibility and its anisotropy in variable fields (anisotropy of magnetic susceptibility - AMS; AGICO, 2004).

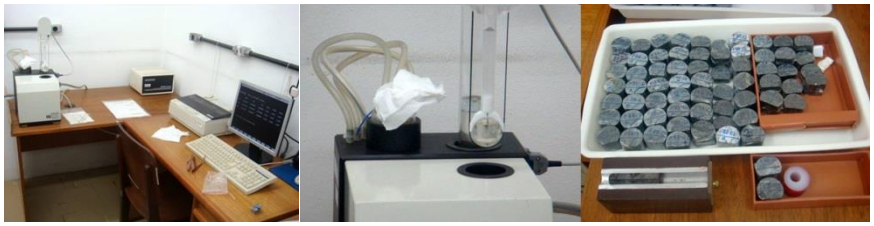

Figure 5.8. Equipment used for laboratory determinations, *Kappabridge* model *KLY-4S* (*Laboratório de Anisotropias Magnéticas e de Magnetismo de Rocha - Instituto de Geociências - Universidade de São Paulo*).

A quality control procedure was established for all magnetic susceptibility measurements. Because of the large variation between the sensitivities and the detection limits of the two susceptibility meters used in the first two rounds, their specific databases were analyzed and interpreted separately. This was because joined databases showed means and histograms that do not represent the lithotypes and hydrothermal alteration zones.

Statistical analysis consisted of frequency diagrams of magnetic susceptibility values in uniform classes and, as such, characterizing the susceptibility signatures for each lithotype and each hydrothermal alteration zone. They indicated the data distribution and its populations, symmetries and dispersions.

The mean, median, mode, and standard deviation values were assessed. Here, the mean indicates where the data are most concentrated and represents the frequencies equilibrium point in the histograms. When the distribution was too dispersed or the standard deviation was too high, the median was used. The median is a central tendency value that separates the lower half of the population from the upper half. The mode is the value that has the greatest number of observations

and occurs most frequently in the data set. Thus, in situations where the mean and the median were not well defined, the mode was used. The standard deviation is the common measure of statistical dispersion showing the variation around the mean.

The geochemical assays of iron, copper and gold from the drill cores were performed in the samples collected along every 1 meter. The analytical methods included Fire Assay for gold (in g/t) and multi-acid/ICP-MS for iron and copper (in percentage) (CVRD, 2006; Vale S.A., 2012).

5.6 - COMPARISON BETWEEN DIFFERENT SUSCEPTIBILITY METERS AND SAMPLING METHODS

Profiles sampled with different intervals and equipment in the third round of measurements from drill hole 88 were plotted for comparison. As expected, the readings with a spacing of 0.5 m from KT-9 meter (black profile) have much lower resolution compared to that from KT-10 meter (blue profile; Figure 5.9). Differences in sensitivity and detection limits of the equipment are the reasons of this contrast (Table 3). These results indicate that the KT-10 meter may provide more reliable measurements.

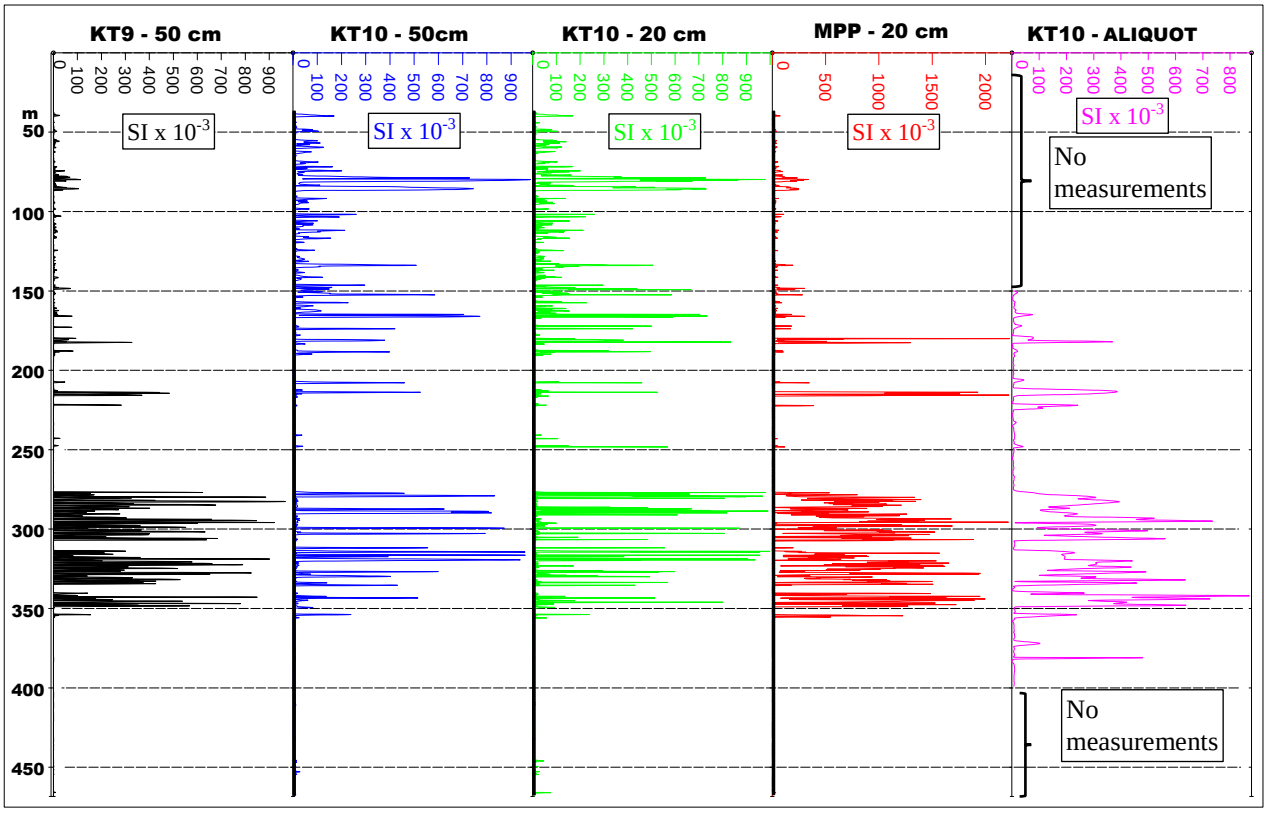

Figure 5.9. Magnetic susceptibility measurements of the drill cores and geochemical sample aliquots. Measurements with KT-9 and 0.5 m spacing (black profile), KT-10 and 0.5 m spacing (blue profile), KT-10 and 0.2 m spacing (green profile), MPP and 0.2 m spacing (red profile), and KT-10 in geochemical sample aliquots (magenta profile).

The KT-10 meter data, with an increase in sampling density readings at 0.2 m intervals (green profile), provided a better definition for the magnetic levels when compared to the 0.5 m spaced data (blue profile; Figure 5.9). Another interesting observation is that the KT-10 meter data (green profile) proved more effective in delineating lower susceptibility values than the MPP (red profile; for example depth interval 0-150 m in Figure 5.9). This may be due to its lower detection limit compared to the MPP meter (Table 3).

For measurements taken at depths interval from 150 to 400 m on the samples prepared for the geochemical assays (magenta profile), the results showed better stability when compared to the measurements on the drill cores. Also, the aliquot measurements are, in general, lower than the measurements made on the drill core (Figure 5.9). Possibly, this is because of the greater homogenization of the contents of these samples in the representation of the same intervals.

5.7 - LABORATORY MEASUREMENTS

The high sensitivity magnetic susceptibility laboratory measurements performed in the fourth round with the Kappabridge (KLY-4S) meter were used to check and to validate the handheld acquired data. Comparison of measurements from the different meters shows that there is agreement between data from KT-10, MPP, and KLY-4S (Figure 5.10). Thus there is high confidence in the KT-10 measurements made on drill cores.

Magnetic susceptibility measurements have been plotted along with corresponding alteration types (Figure 5.11). The magnetic susceptibility measurements depict three main signatures (Figures 5.11a, 5.11c, 5.11e and 5.11g):

(i) intermediate values (averaging 1 x 10^{-3} SI) correlated with the aluminous schists host rocks and hydrothermal alteration zones without magnetite (garnet-grunerite and amphibole hydrothermal alteration zones),

(ii) low values (less than 0.5 x 10^{-3} SI) occur in the silicic zone, and

(iii) (very) high values (over 100 x 10^{-3} SI to >9999 x 10^{-3} SI) in the hydrothermal alteration zones that contains magnetite (massive magnetite, garnet-grunerite-magnetite and amphibole-magnetite hydrothermal alteration zones).

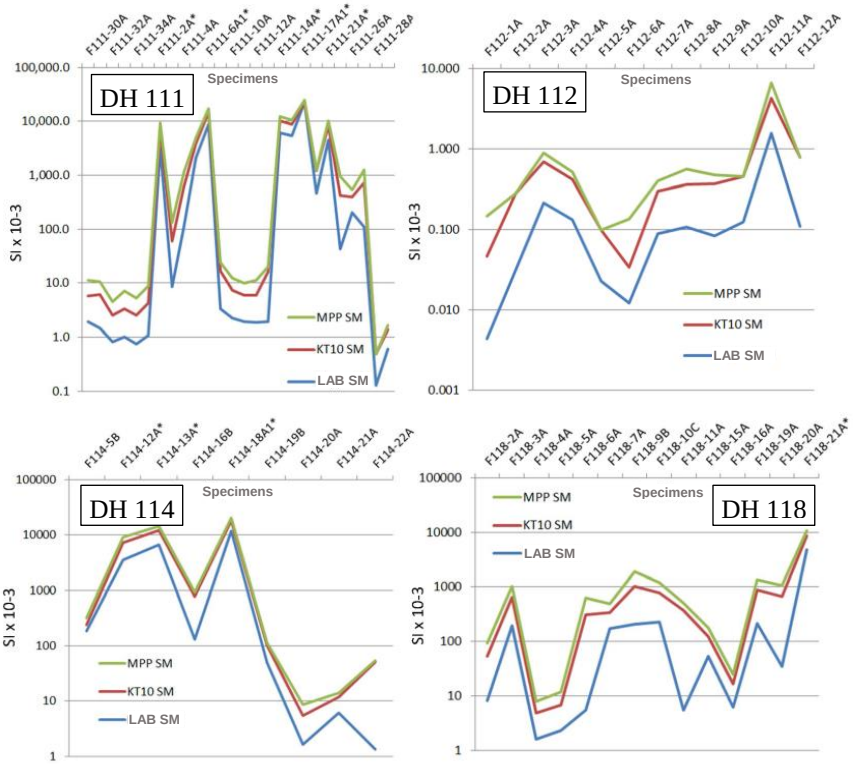

Figure 5.10. Magnetic susceptibility measurements with laboratory (LAB SM), KT-10 meter and MPP meter compared along the relative depths of drill holes 111, 112, 114 and 118.

The laboratory magnetic susceptibility measurements show strong anisotropic characteristics (Figure 5.11) where magnetic susceptibility is preferentially oriented. The degree of anisotropy is a measure of the ratio of the major and minor axis measurements and range between 2 to 5 in the magnetite-rich alteration zones. The anisotropy degree is very low in the host rocks and hydrothermal alteration zones without magnetite (Figures 5.11b, 5.11d, 5.11f and 5.11h). The major axis of the anisotropy ellipsoid is aligned with the dip of the orebodies. Thus, it is certain that both self-demagnetization effect and the susceptibility anisotropy contribute to deviating magnetization direction.

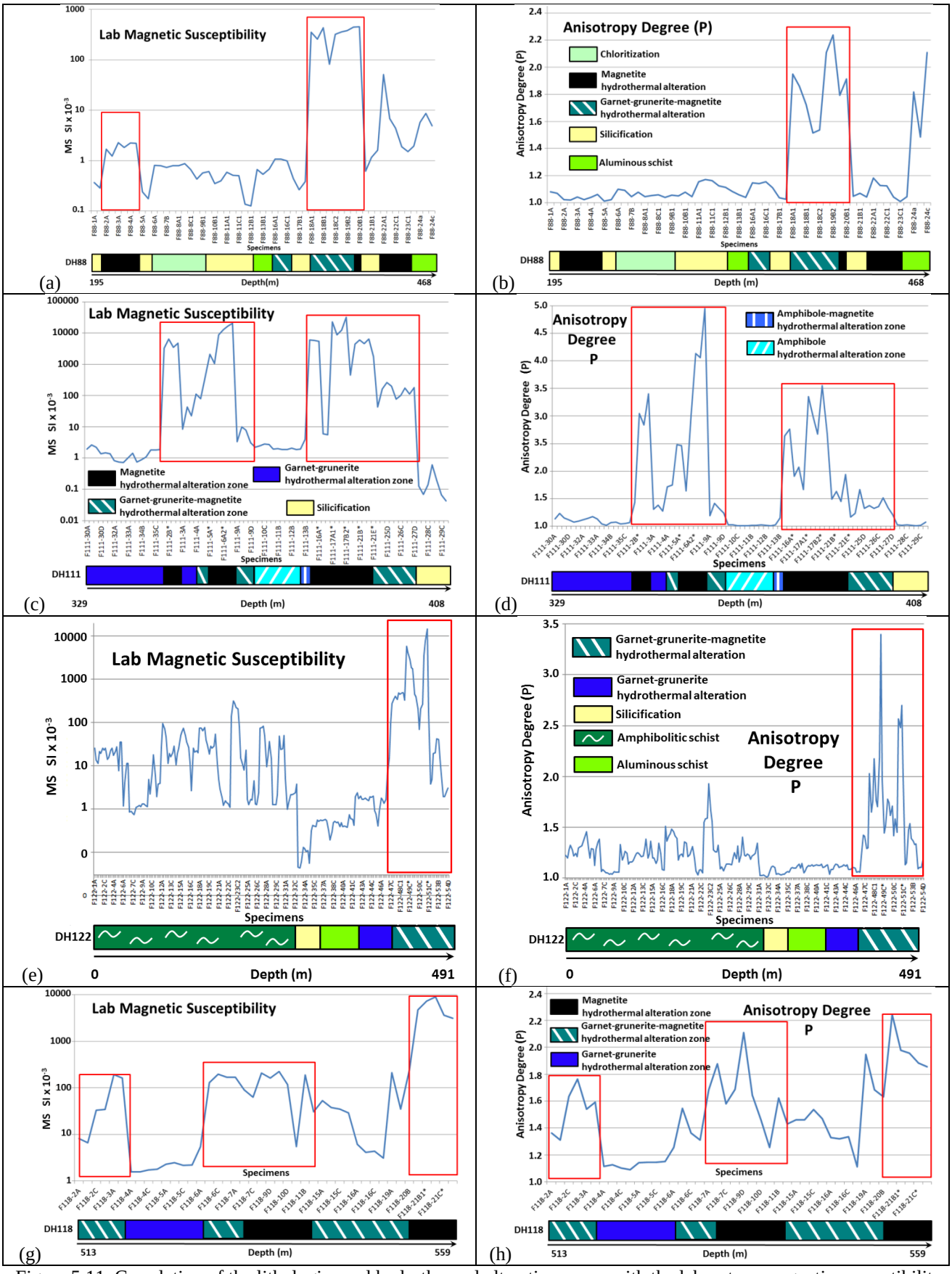

Figure 5.11. Correlation of the lithologies and hydrothermal alteration zones with the laboratory magnetic susceptibility (graphs to the left) and anisotropy degree measurements (graphs to the right). Drill holes 88, 111, 122 and 118.

5.8 - MAGNETIC SUSCEPTIBILITY SIGNATURES OF THE IRON OXIDE-COPPER-GOLD (IOCG) MINERALIZATION

Magnetic susceptibility measurements are used to characterize the magnetic signature of the Furnas Southeast IOCG deposit. Statistical analyses on measured data are related to drill core observations. A synthesis shows the magnetic susceptibility behavior of the various rocks and alteration types (Figure 5.12).

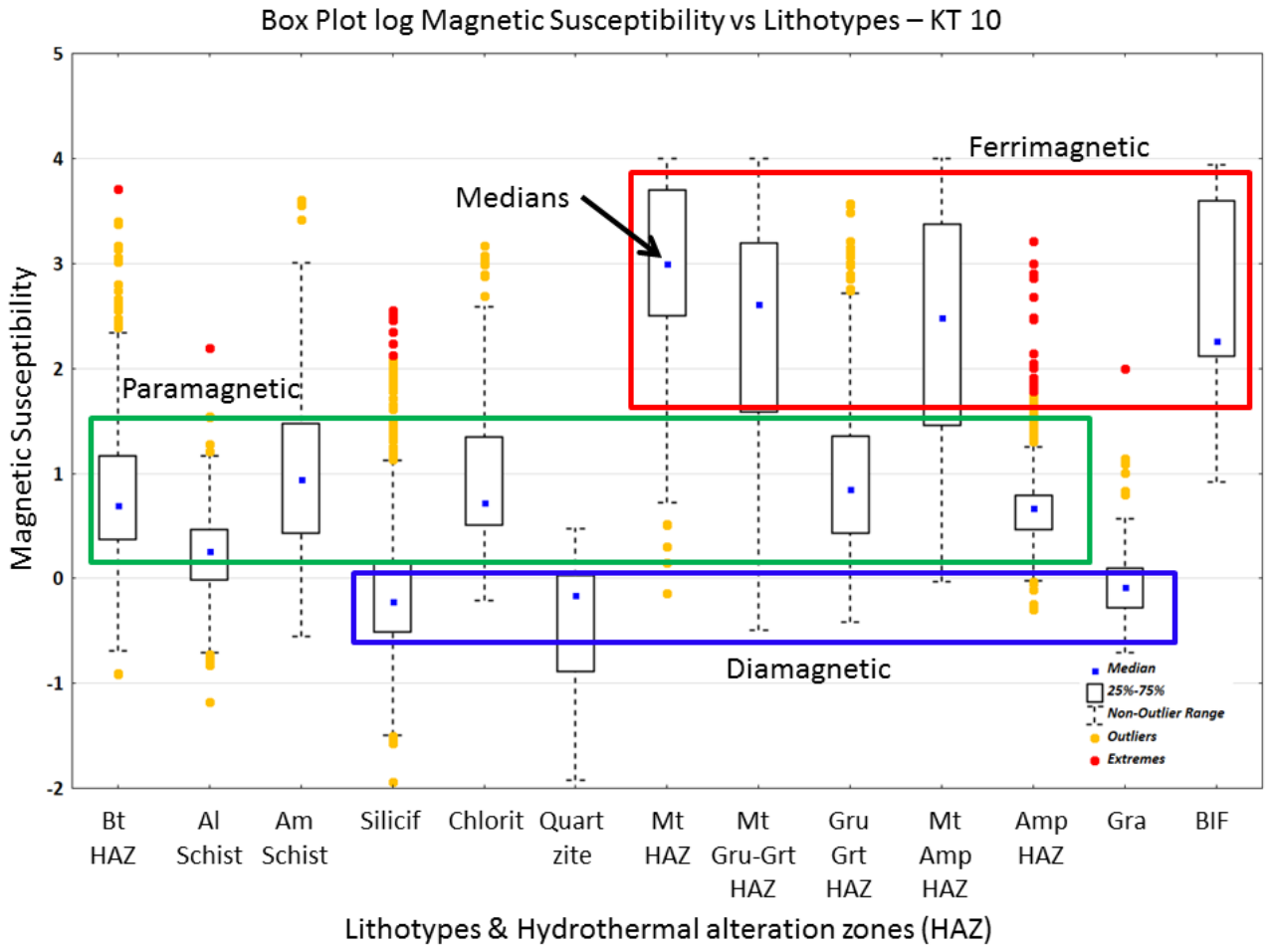

Figure 5.12. Box plot log of magnetic susceptibility versus lithotypes with values from the higher sensitivity susceptibility meter (KT-10). The predominance of ferrimagnetic, paramagnetic and diamagnetic minerals is represented in red, green and blue rectangles respectively. HAZ = hydrothermal alteration zone, Bt = biotite, Al = aluminous, Am = amphibolitic, Silicif = silicification, Chlorit = chloritization, Mt = magnetite, Gru = grunerite, Grt = garnet, Amp = amphibole, Gra = granite, BIF = banded iron formation.

High median values were tied to lithotypes bearing ferromagnetic minerals: magnetite, in this case. The highest values are associated with massive magnetite in the hydrothermal alteration zone. Additional high values are observed in the garnet-grunerite-magnetite and amphibole-magnetite altered rocks, as well as unaltered rocks in the banded iron formations. The intermediate median values are representative of the biotite, garnet-grunerite, amphibole and chlorite hydrothermal alteration zones, which is likely due to the presence of more paramagnetic minerals, opposed to ferromagnetic magnetite. In addition, the amphibolitic and aluminous schist lithotypes also have intermediate values. The lowest median values are correlated with granite and quartzite lithotypes, as well as the silicic alteration type. This is interpreted to be due to an abundance of paramagnetic and diamagnetic minerals.

Five drill holes, numbers 88, 48, 34, 31 and 125, were selected to show characteristic magnetic susceptibility signatures because they best represent the lithotypes and the mineralization. Their individual core logs (Figures 5.13 to 5.17) were used to describe the lithotypes and hydrothermal alteration zones synthetized above (Figure 5.12).

Drill hole 88 shows strong correlation between lithotypes, alteration, and magnetic susceptibility (Figure 5.13). A magnetic zone with high grade mineralization is well defined between 275 m and 350 m depths by their high magnetic susceptibility values. Inside this magnetite zone, there are two narrow zones with no response at 310 m and 340 m depths, which correspond to silicic altered rocks with higher Cu and Au grades. The same response can be observed in the depth range of 257 to 275 m, in another mineralized silicification zone. Two narrow zones with high grade mineralization are located in secondary faults at depths of 180 m and 215 m. These zones have high magnetic susceptibility values that are related to magnetite-rich hydrothermal alteration (Figure 5.13). Similar behavior can also be found on data for drill holes 48 (Figure 5.14), 34 (Figure 5.15), 31 (Figure 5.16) and 125 (Figure 5.17).

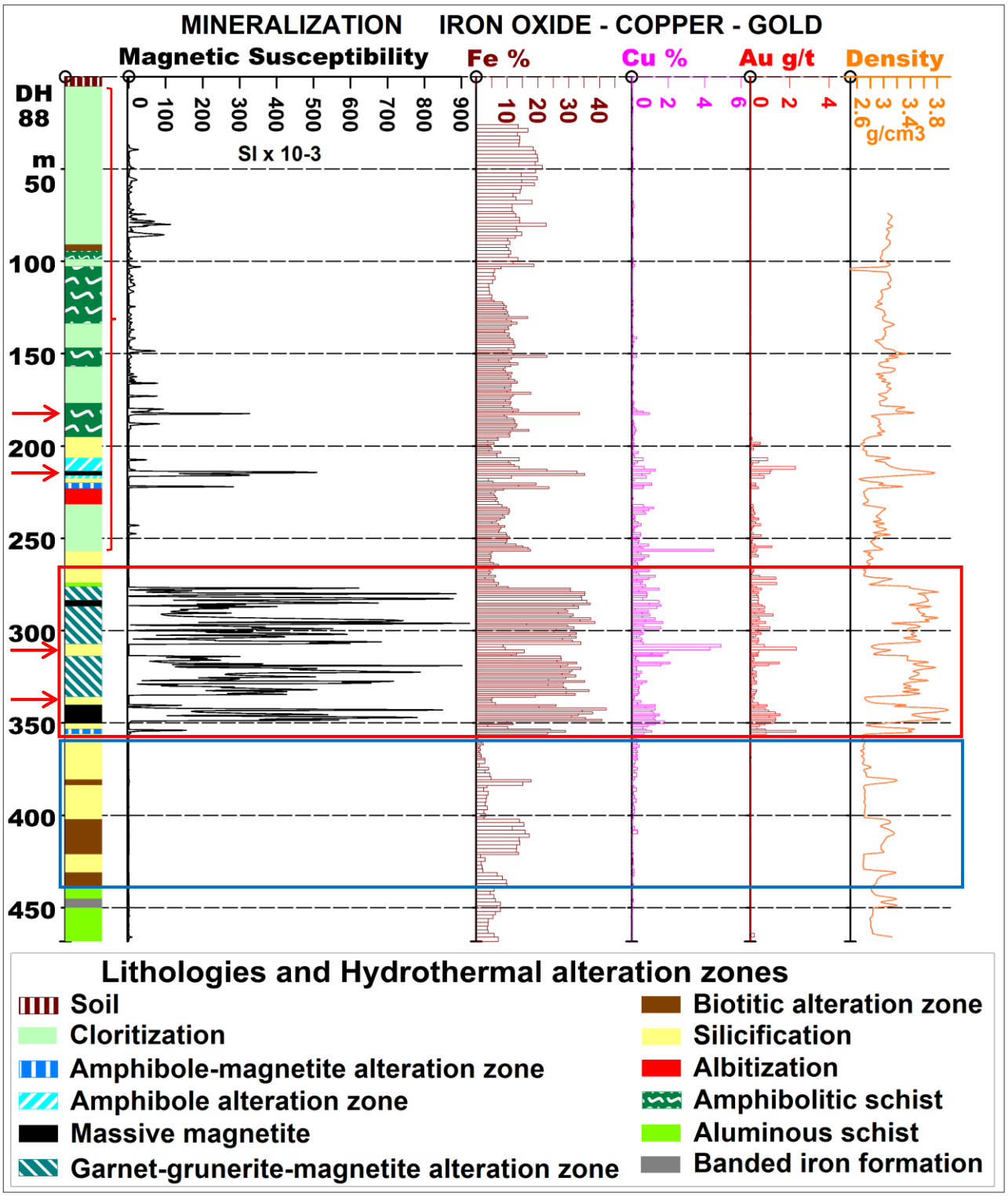

Figure 5.13. Drill hole 88 log with strong iron oxide-copper-gold IOCG mineralization between 275 m and 350 m depths. Chloritization can be observed at the top and potassification and silicification at the log base. The drill hole location can be found in Figure 5.7.

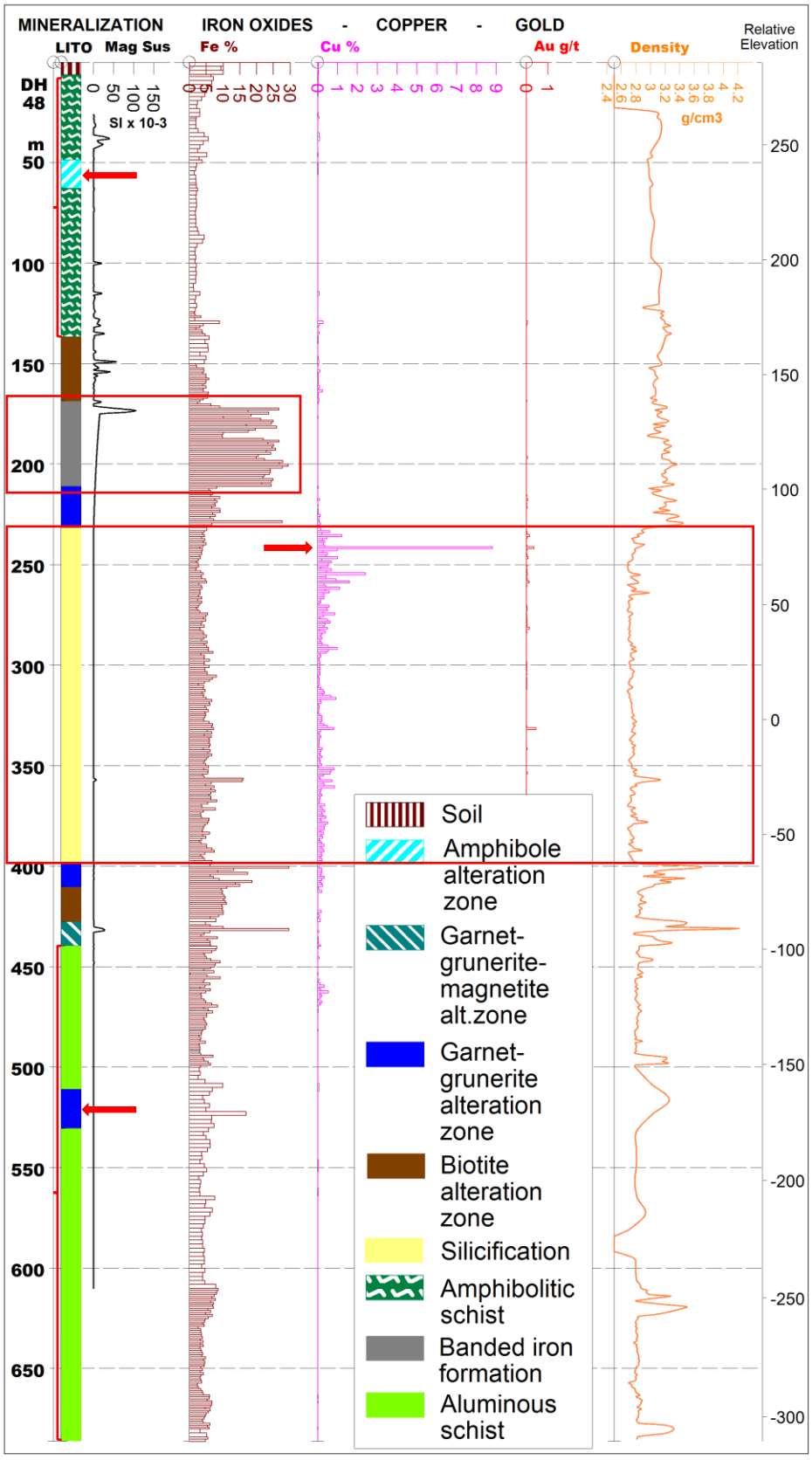

Figure 5.14. Drill hole 48 log with the amphibolitic schist on top and aluminous schist on the base hosting the mineralized zone. From depths of 169 to 211 m, the low magnetic susceptibility and high iron grade signatures of the banded iron formation are shown. From depths of 230 to 400 m, the mineralized zone is dominated by silicification. The drill hole location can be found in Figure 5.7. No positive gold assay values were obtained below the legend.

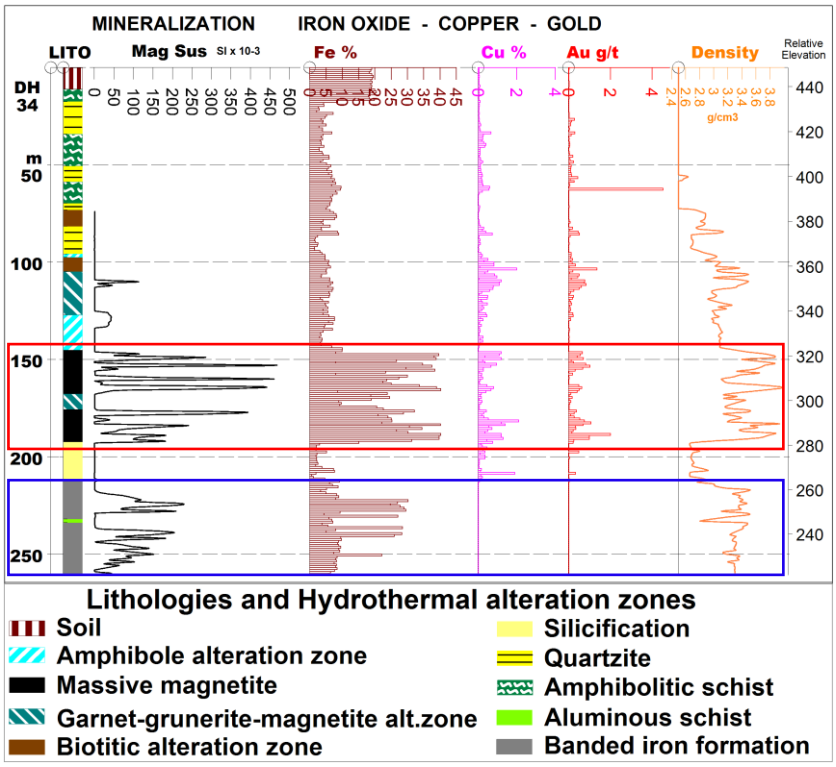

Figure 5.15. Drill hole 34 log with the banded iron formation, magnetite and silica bands well defined in the magnetic susceptibility, iron grade and density properties (212 to 260 m depths). From depths of 145 to 192 m, the strong iron oxide-copper-gold IOCG mineralization can be observed. The drill hole location can be found in Figure 5.7.

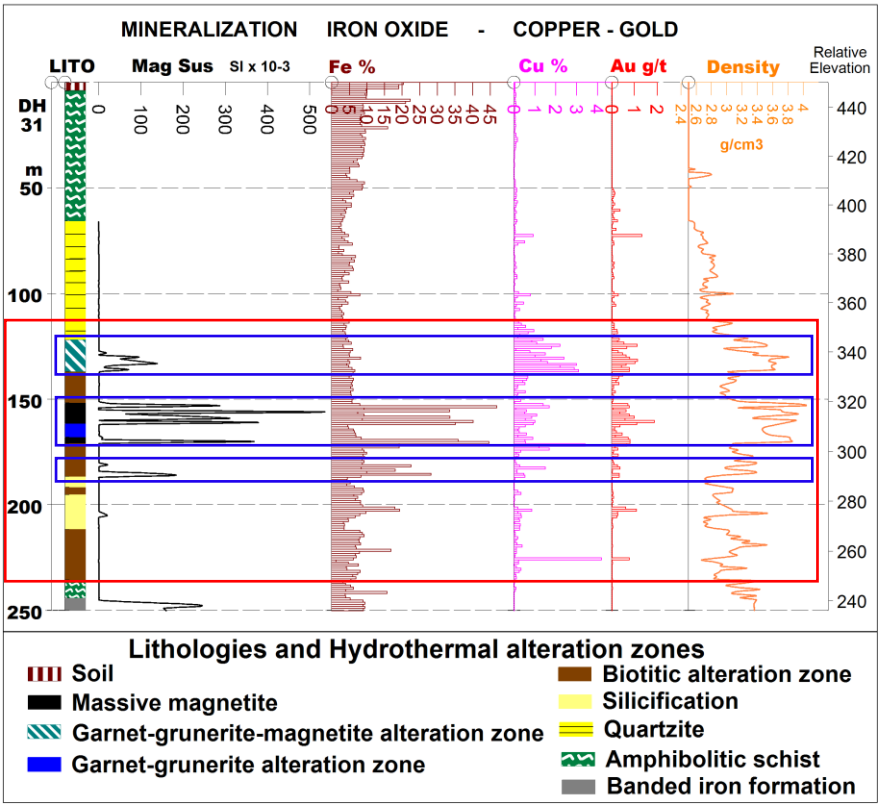

Figure 5.16. Drill hole 31 log with the quartzite low susceptibility, low iron grade and low density signature (65 to 122 m depths). From depths of 152 to 171 m, the strong iron oxide-copper-gold IOCG mineralization can be observed. The drill hole location can be found in Figure 5.7.

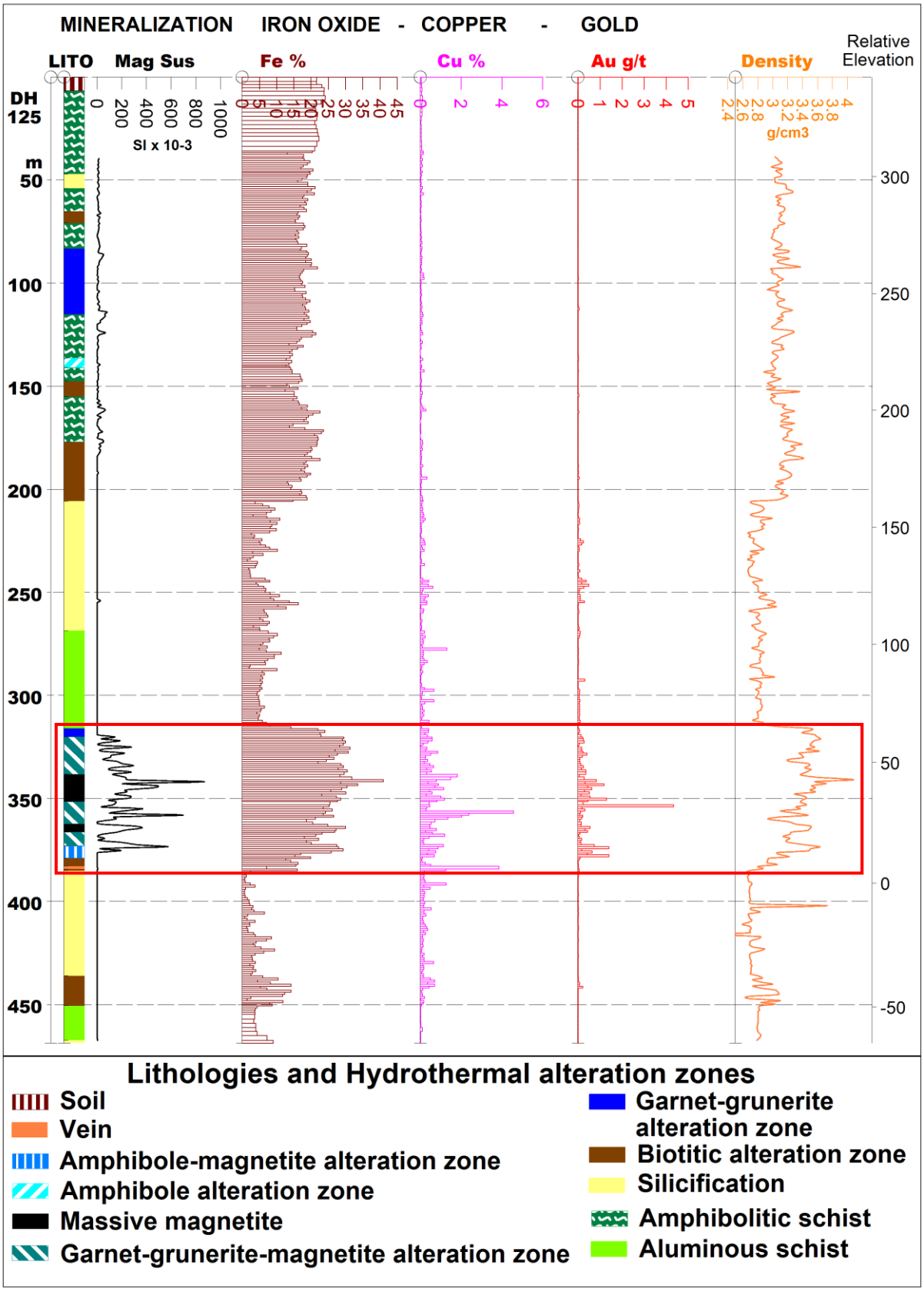

Figure 5.17. Drill hole 125 log with the iron oxide-copper-gold IOCG mineralization signatures: hydrothermal alterations, magnetic susceptibility in SI x 10^{-3}, iron grade geochemical assays in percentage, copper grade in percentage, gold in grams per ton and density in grams per cubic centimeter. The drill hole location can be found in Figure 5.7.

Lithotypes

The magnetic responses of the lithotypes are characterized using measurements taken with the higher sensitivity equipment (KT-10). The exception was on the banded iron formations that were analyzed with both the higher sensitivity data (KT-10) to evaluate the absolute values and the lower sensitivity equipment (KT-9) to generate the histogram because of the larger number of samples measured.

The schist host rocks have susceptibilities grouped in histograms that show normal distribution (Figures 5.18a and 5.18b). Typical magnetic susceptibility values for schists are around 1.5 x 10^{-3} SI (Telford et al., 1990) which agrees well with the observed median and mean values, 1.8 and 2.44 x 10^{-3} SI respectively, for the **aluminous schists**. The **amphibolitic schist** has higher susceptibility values. It has a median value of 8 x 10^{-3} SI, a mean value of 36 x 10^{-3} SI and mode of 4 x 10^{-3} SI. The large number of samples for these rocks (3,119) reflects the large extension drilled to intercept the mineralized area, especially in the amphibolitic schist, which is the upper host rock (2,085 samples).

Drill hole 48 shows the amphibolitic schist at the top and aluminous schist at the base hosting the mineralized zone. At depths of 49 m and 511 m, the input of non-mineralized hydrothermal alteration fluids is observed along with amphibole and garnet-grunerite (Figure 5.14).

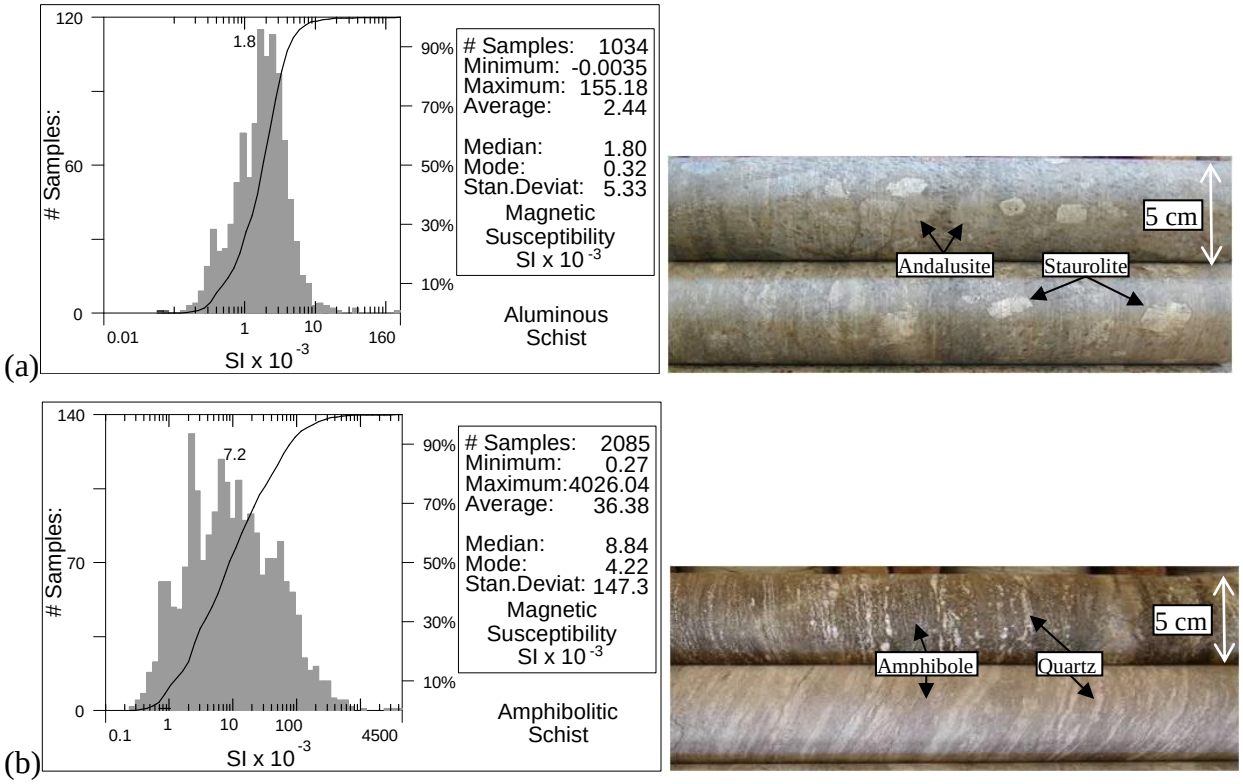

Figure 5.18. Statistics and histograms of the magnetic susceptibility measurements. (a) Aluminous schist. (b) Amphibolitic schist.

The **banded iron formations** occur mainly on the southeast portion of the studied area. Statistical analysis of the magnetic susceptibility measurements using the higher sensitivity data (KT-10) for these rocks show that they have median value of 182 x 10^{-3} SI, a mean value of 1,758 x 10^{-3} SI and the maximum value of 8,665 x 10^{-3} SI. The lower sensitivity equipment (KT-9) was used to generate the histogram because of the larger number of samples measured (Figure 5.19). The histogram shows bimodal distribution with high values reflecting the ferrimagnetic behavior of the bands with magnetite, which peak at 104.8 x 10^{-3} SI, whereas the lower values reflects the diamagnetic behavior of the silica bands, which peak at 0.72 x 10^{-3} SI (Figure 5.19).

In drill hole 48, the banded iron formation signature can be observed between depths of 169 and 211 m (in gray); there is an absence of magnetic susceptibility response because of the presence of hematite in this interval, which was observed in the iron geochemistry. The susceptibility response associated with the punctual presence of magnetite can be observed at the beginning of this interval (Figure 5.14).

For drill hole 34, a similarity of magnetic susceptibility signatures, iron grade and density is found between depths of 212 and 260 m for the magnetite and silica bands in the iron formations. No copper and gold mineralization is present on the banded iron formations (Figure 5.15).

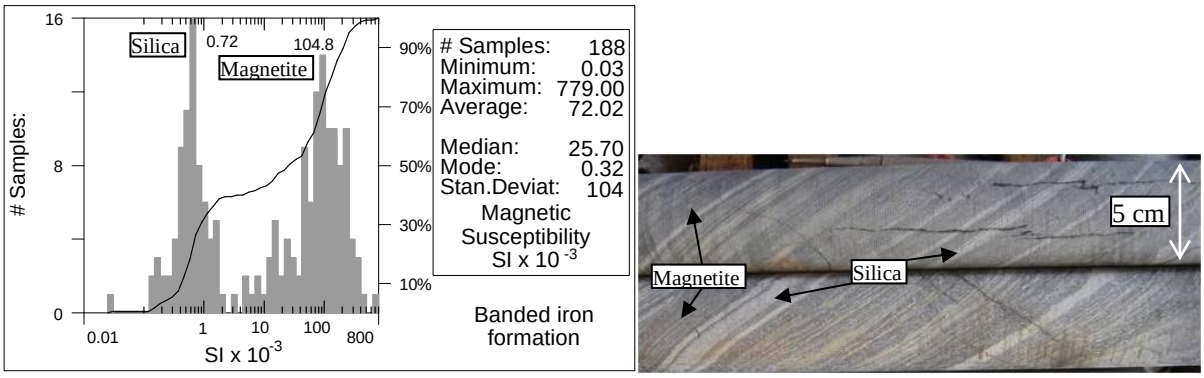

Figure 5.19. Statistics and histogram of the banded iron formation magnetic susceptibility measurements.

The **monzogranite rocks** have been affected by **albite hydrothermal** alteration. These rocks have low magnetic susceptibility values which likely reflect the predominance of paramagnetic minerals in the rock, such as feldspar, plagioclase and biotite, and diamagnetic minerals, such as quartz. The median value is 0.8 x 10^{-3} SI, the mode is 0.2 x 10^{-3} SI and the mean is 3.5 x 10^{-3} SI, (Figure 5.20a). The low number of samples (61) is a result of the low occurrence of these rocks in the Furnas Southeast deposit.

The **quartzite** show relatively low magnetic susceptibility values (Figure 5.20b). For quartzite, the minimum value of -0.03 x 10^{-3} SI (Figure 5.20b), is due to the diamagnetic characteristics of the quartz, which include weak susceptibility and negative values in its purest form. Statistical analysis of quartzite samples show low mode value of 0.04 x 10^{-3} SI, median of 0.66 x 10^{-3} SI and mean of 0.66 x 10^{-3} SI (Figure 5.20b). These values are high for pure quartzite. However, negative values probably do not occur in abundance because of the elevated presence of paramagnetic minerals such as sericite and equipment limitations.

Drill hole 31 shows low values for both magnetic susceptibility and density for the quartzite (65 to 122 m depths; Figure 5.16). Mineralization in host rocks such as quartzite shows that mineralizing fluids can penetrate any rock type. Quartzite is more mineralized when in contact with the magnetite-garnet-grunerite high grade zone. The strong signature of the mineralization of iron oxide, copper and gold (IOCG) is observed from 110 to 171 m depths (Figure 5.16).

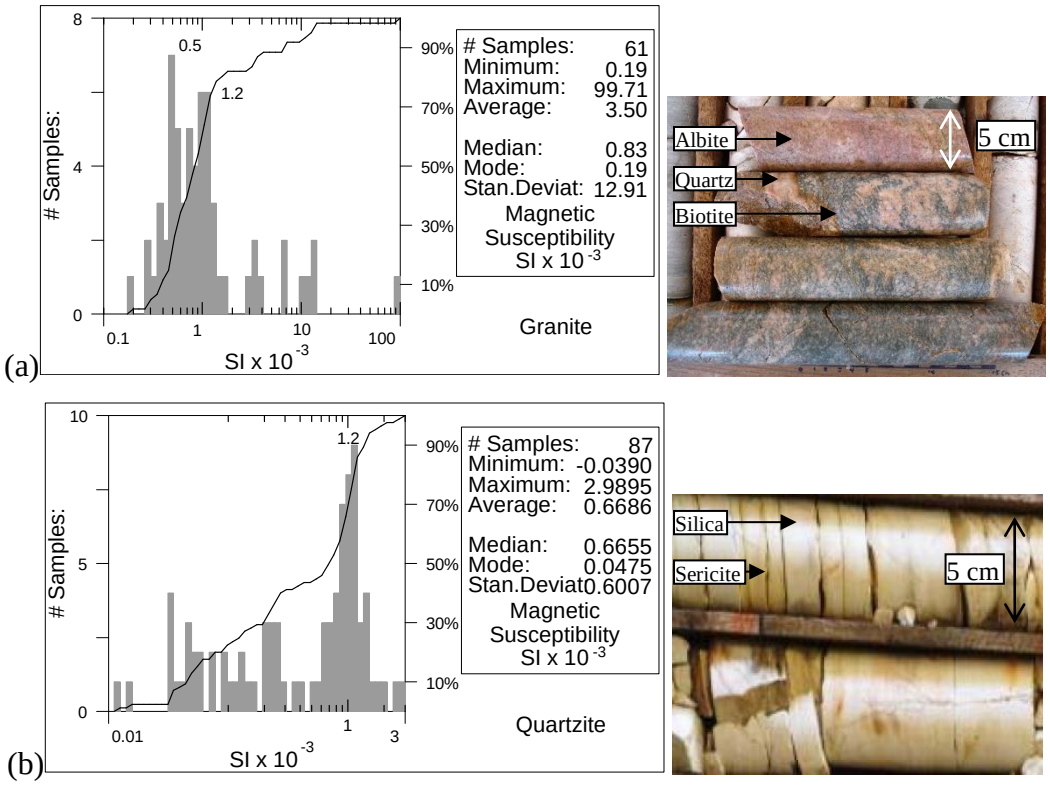

Figure 5.20. Statistics and histograms of magnetic susceptibility measurements. (a) Granite. (b) Quartzite.

Hydrothermal alteration zones

Within the hydrothermal alteration zones, a trend of higher susceptibility values compared to the host rocks can be observed, especially in the **potassic zone** and **garnet-grunerite zone**. In these zones, the maximum values reach 5,113 x 10^{-3} SI and 3,717 x 10^{-3} SI, respectively, and likely reflects magnetite precipitated during the hydrothermal event (Figures 5.21a and 5.21b). The only exception is the silicic alteration.

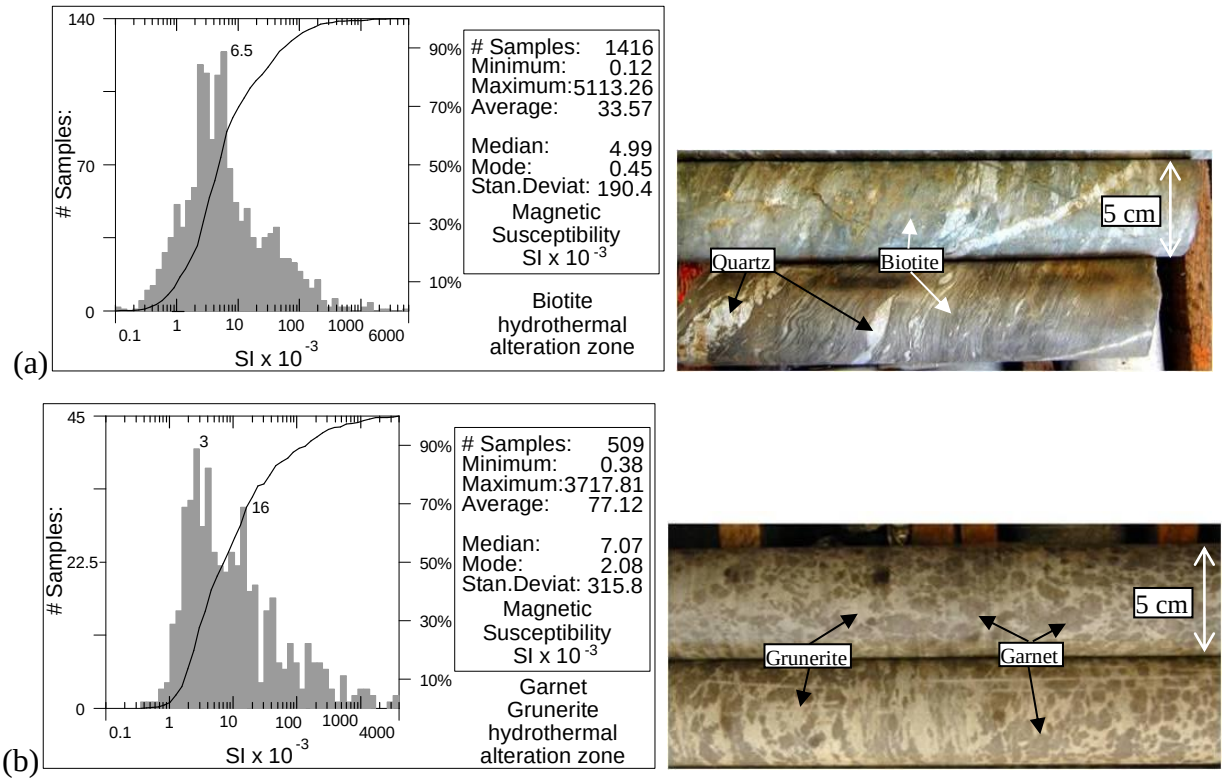

Figure 5.21. Statistics and histograms of the magnetic susceptibility measurements. (a) Potassic hydrothermal alteration zone. (b) Garnet-grunerite hydrothermal alteration zone.

Amphibole, garnet, biotite, and chlorite are the main silicate alteration phases. These minerals have paramagnetic behavior because of the presence of Fe^{2+}, Fe^{3+} or Mn^{3+}. However, some silicates can appear ferromagnetic because of impurities such as magnetite. In complex hydrothermal environments the impurities becomes common. These minerals start to show remanence and exhibit hysteresis. In general, the predominance of paramagnetic minerals such as biotite (Figure 5.21a), garnet-amphibole (Figure 5.21b), **amphibole** (Figure 5.22a) and **chlorite** (Figure 5.22b) in the hydrothermal alteration zones keeps the median susceptibility values between 4 x 10^{-3} SI and 7 x 10^{-3} SI, the mean between 23 x 10^{-3} SI and 77 x 10^{-3} SI and modes between 0.4 x 10^{-3} SI and 4 x 10^{-3} SI.

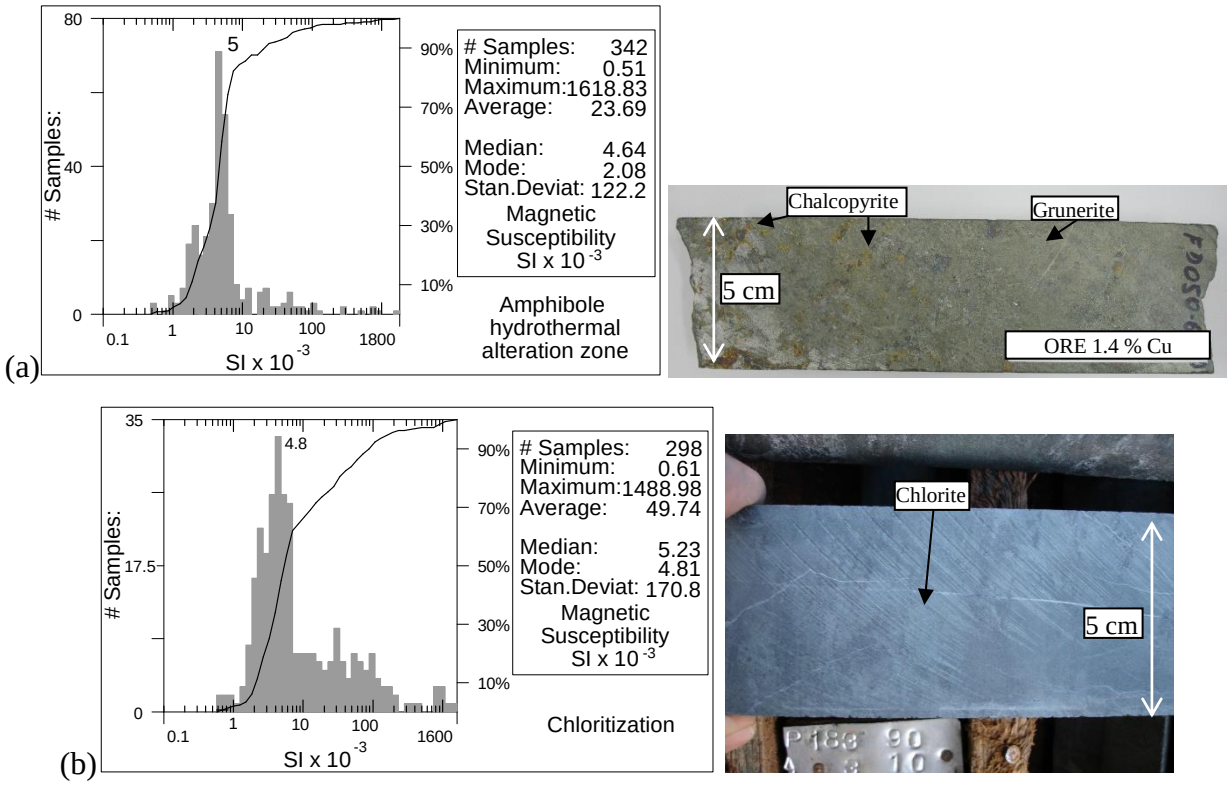

Figure 5.22. Statistics and histograms of the magnetic susceptibility measurements. (a) Amphibole hydrothermal alteration zone. (b) Chloritization.

The only exception is the **silicification alteration zone**. Since quartz is diamagnetic it's expected negative values, as observed, has a minimum of -0.04 x 10^{-3} SI. The histogram for the silicic alteration type shows a typical normal distribution with a median value of 0.6 x 10^{-3} SI, a mean value of 2.51 x 10^{-3} SI and a maximum value of 357 x 10^{-3} SI (Figure 5.23). The presence of paramagnetic minerals and instrumental limitations to measure negative values justify the low positive susceptibility values. In almost all the drill cores, an abundance of silicification is closely related to the low grade mineralization (Figures 5.14, 5.16 and 5.17). However, in many places, it can also be associated with high grade mineralization (such as in Figure 5.13 at a 310 m depth and in Figure 5.14 near the contact zone at 241 m depth).

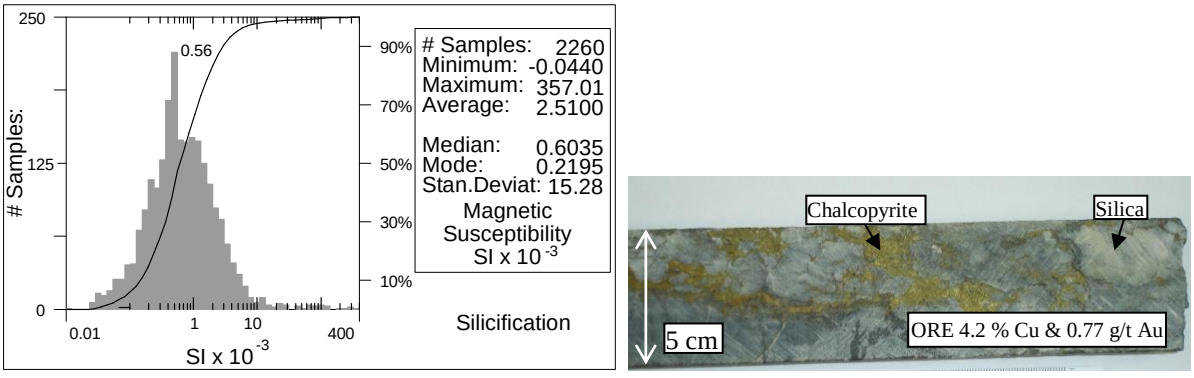

Figure 5.23. Statistics and histogram of the silicification zone magnetic susceptibility measurements.

The potassic alteration type fingerprint is the **biotite hydrothermal alteration zone** that may or may not be associated with mineralization. Biotite can be both paramagnetic and ferromagnetic. In addition, magnetite commonly precipitates between the biotite sheets planar voids, as well as in fractures associated with this type of alteration. Together, these phenomena likely account for the higher observed susceptibilities within the potassic altered rocks (Figure 5.21a).

In drill hole 88 between the depths of 380 and 438 m, alternating zones of biotite hydrothermal alteration and silicic alteration with low copper grade are observed. The signatures are well defined by the contrast in iron geochemical signatures and density (Figure 5.13). For drill hole 31, the biotite hydrothermal alteration zone is interspersed with the magnetite hydrothermal alteration zones and with silicification, and they are all mineralized (137 to 236 m depths; Figure 5.16).

The **garnet-grunerite and amphibole hydrothermal alteration zones** have a close relationship with the low to medium grade mineralized zones. As can be seen in drill hole 125, between the depths of 83 and 115 m, the magnetic signature of the garnet-grunerite hydrothermal alteration zone shows low susceptibility values (Figure 5.17).

Along drill hole 34, between the depths of 127 and 140 m, the amphibole hydrothermal alteration zone has a low copper-gold grade and a low density relative to the magnetite hydrothermal alteration zone. At the top of this interval, the contact between the amphibole and garnet-grunerite hydrothermal alteration zones have values that reach 50 x 10^{-3} SI because of the infill of magnetite (Figure 5.15).

Drill hole 88 also shows at the top a strong **chlorite hydrothermal alteration zone** that may or may not be associated with mineralization (Figure 5.13). This process has low susceptibility values with a median of 5 x 10^{-3} SI (Figure 5.22b). The variation from low and intermediate values is interpreted to be the result of magnetite precipitation along fractures or between sheets of biotite. The hydrothermal process of chloritization is strong. It alters partially or completely the rocks of the area.

Magnetite, garnet-grunerite-magnetite and amphibole-magnetite hydrothermal alteration zones

Magnetite is the most abundant ferromagnetic mineral in the hydrothermal alteration and, as said, is responsible for the high susceptibility values. The median magnetic susceptibility values decrease from the **massive magnetite alteration zone** with 989 x 10^{-3} SI (Figure 5.24a) to the **garnet-grunerite-magnetite alteration zone** with 409 x 10^{-3} SI (Figure 5.24b) and **amphibole-**

magnetite alteration zone with 308 x 10^{-3} SI (Figure 5.24c). Among the magnetite-rich alteration zones, the mean susceptibility values are 2,777 x 10^{-3} for the massive magnetite zone (Figure 5.24a), 1,550 x 10^{-3} for the amphibole-magnetite zone (Figure 5.24c), and 1,383 x 10^{-3} for the garnet-grunerite-magnetite zone (Figure 5.24b). Both the median and mean are consistent with what is observed in the drill core samples, which shows that the magnetite hydrothermal alteration zone has higher magnetite content than the garnet-grunerite-magnetite and amphibole-magnetite zones (Figures 5.16 and 5.17).

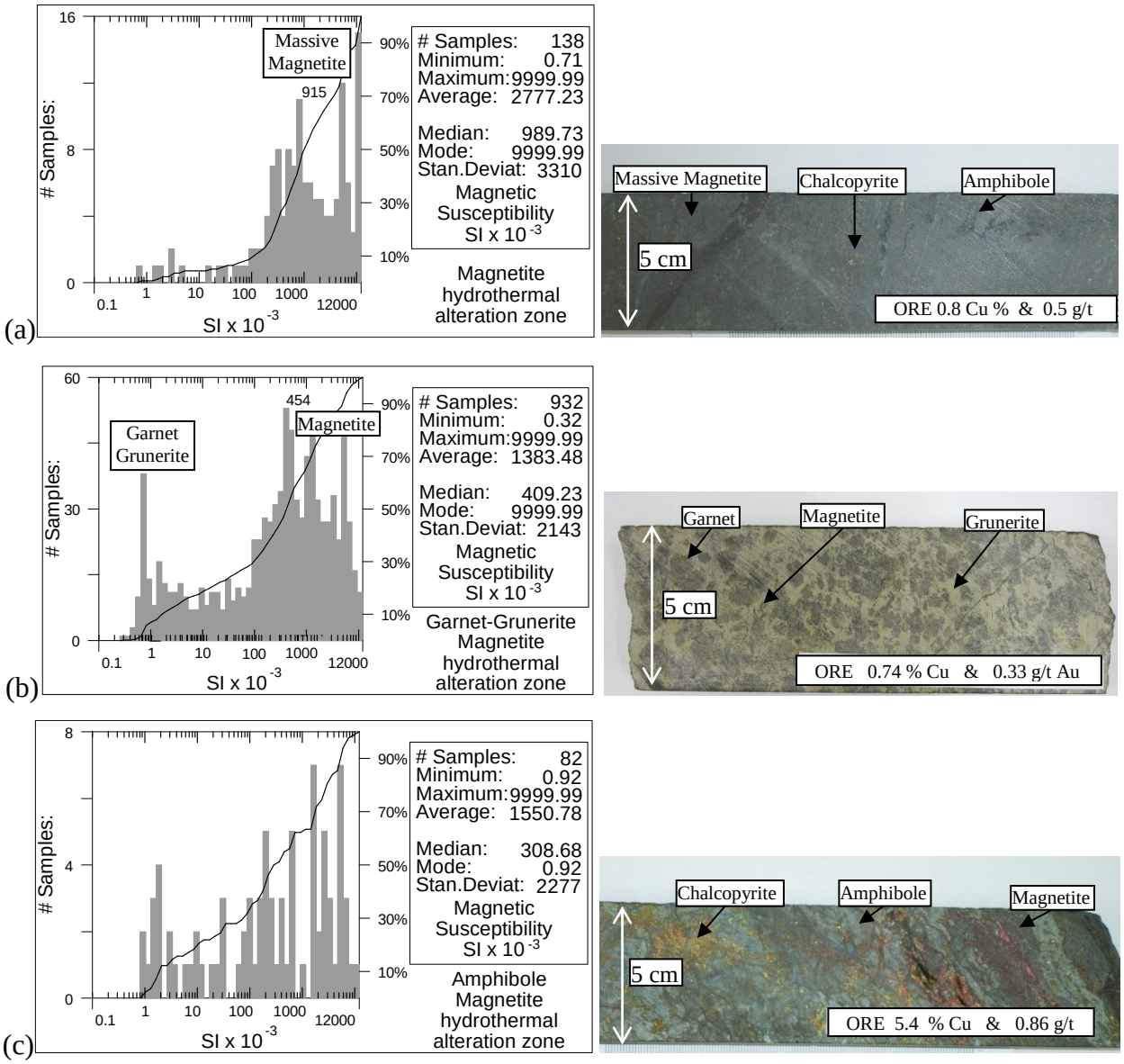

Figure 5.24. Statistics and histograms of magnetic susceptibility measurements for magnetite rich-alteration types. (a) Massive magnetite hydrothermal alteration zone. (b) Garnet-grunerite-magnetite hydrothermal alteration zone. (c) Amphibole-magnetite hydrothermal alteration zone.

In the **magnetite alteration zone**, there is a susceptibility population centered at high values around 915 x 10^{-3} SI, which is near the median of 989 x 10^{-3} SI and represents the presence of massive magnetite (Figure 5.24a).

In the **garnet-grunerite-magnetite alteration zone** the distribution becomes more complex. It shows two populations of high susceptibility values. The highest valued population is centered near 454 x 10^{-3} SI and represents massive magnetite. The other population has values lower than 10 x 10^{-3} SI. This population has a significant concentration of paramagnetic minerals such as grunerite and garnet (Figure 5.24b).

A third population observed in the **amphibole-magnetite alteration zone**, indicates that the values in histogram are much widely distributed, which is most likely a result of the greater presence of amphiboles (Figure 5.24c).

This variation from high to intermediate to low values is observed in the drill cores, wherein the garnet-grunerite and amphibole alteration zones are constantly altered by the input of magnetite, which produces a great fluctuation in the susceptibility measurements (Figures 5.13, 5,15, 5.16 and 5.17).

The garnet-grunerite-magnetite alteration occurs in greater abundance relative to the amphibole-magnetite alteration zone (Figure 5.17). In addition, the garnet-grunerite-magnetite alteration has higher correlation with the massive magnetite zone. This observation is corroborated by analyzing the mode, which is >9,999 x 10^{-3} SI and 0.92 x 10^{-3} SI in the garnet-grunerite-magnetite and amphibole-magnetite alteration zones, respectively (Figures 5.24b and 5.24c).

When magnetite and silicic banding is present, descriptively differentiating the banded iron formation from the magnetite hydrothermal alteration zone becomes more difficult. However, when comparing the susceptibility values, this difference is easily noticeable. Between the depths of 145 m and 192 m in drill hole 34, the magnetite hydrothermal alteration zone is marked by a high increase on the values of magnetic susceptibility, iron, copper, gold and density, when compared to the banded iron formation between the depths of 212 and 260 m (Figure 5.15). The banded iron formations are not mineralized, and normally show low values for susceptibility, iron content and density, when compared to the magnetite hydrothermal alteration zone. This difference can be observed when looking at the median values, which is 182 x 10^{-3} SI for the banded iron formation (Figure 5.19) and 989 x 10^{-3} SI for the magnetite hydrothermal alteration zone (Figure 5.24a). The median value of the banded iron formation is low, even when compared to the medians of the garnet-grunerite-magnetite (400 x 10^{-3} SI; Figure 5.24b) and amphibole-magnetite (300 x 10^{-3} SI; Figure 5.24c) hydrothermal alteration zones.

5.9 - MAGNETIC SUSCEPTIBILITY 3D MODELING

A 3D magnetic susceptibility model was derived from the measurements made on drill core. The measurements were geolocated in 3D space and contoured using a 3D kriging algorithm (Geosoft, 2014). Drill hole spacing was approximately 100 m with down hole measurements every 1 m, with the resultant susceptibility model having 5 m cubic cells. The weight of the direction with a 300° azimuth was used to improve the effect of sampling in this direction, which is the deposit strike direction with less sampling relative to perpendicular direction of greatest sampling.

The physical models show data with values greater than 500 x 10^{-3} SI for the measurements made with the high sensitivity equipment (KT-10) and values greater than 60 x 10^{-3} SI for those made with the low sensitivity equipment (KT-9). These values were selected based on the statistical analyses of the susceptibility data, as previously analyzed. The two envelope surfaces results of the susceptibilities higher than the threshold values in both cases, complement each other because of the different distributions of the drill holes used in the measurements (see Figure 5.7). It is important to emphasize that the susceptibility model reflects only the northwestern portion of the study area, which is where the studied drill holes are located (Figure 5.7).

The 3D magnetic susceptibility model shows similarities to ore-grade models. Comparison of the obtained susceptibility model (Figure 5.25a) with the copper high grade ore model from 69 drill holes (Figure 5.25b; Vale S.A., 2012), shows excellent correlation.

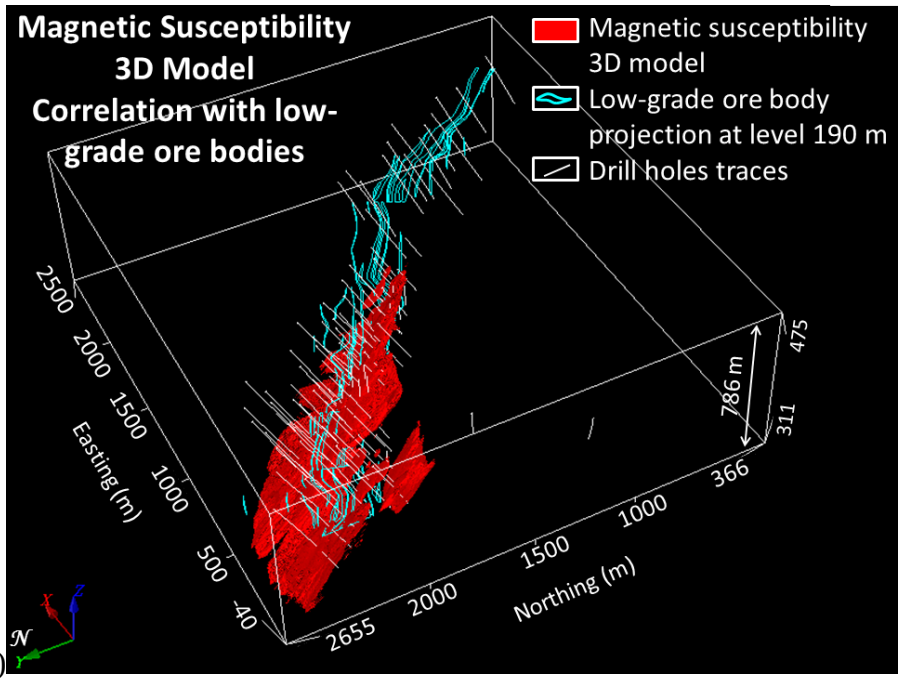

(a)

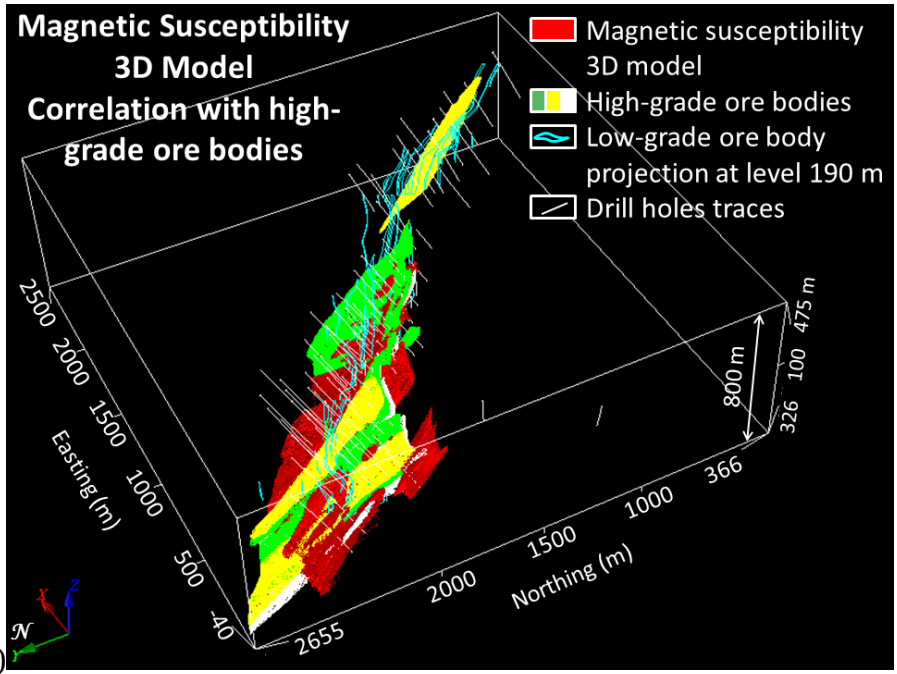

(b)

Figure 5.25. (a) Three dimensional magnetic susceptibility model correlation with the copper low grade orebodies projection at level 190 m. (b) Three dimensional magnetic susceptibility model correlation with the copper high grade orebodies.

This susceptibility model versus ore concentration when seen in detail, shows the direct correlation between the magnetite hydrothermal alteration zones, represented by high magnetic susceptibility values (envelope of the values greater than 500 x 10^{-3} SI), and high grade orebodies with values higher than 0.6 % copper (Figure 5.26).

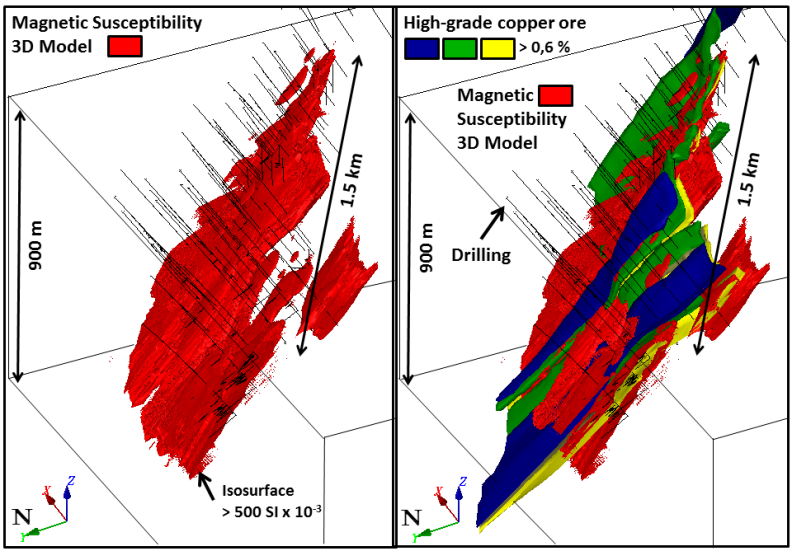

Figure 5.26. Detail of the magnetic susceptibility 3D model with isosurface of values higher than 500 x 10^{-3} SI (in red), and correlation with the copper high-grade orebodies (in blue, green and yellow). Drill holes in black traces.

5.10 - CONCLUSIONS

Magnetic susceptibility measurements on drill core were used to define a physical property model that can help target exploration for IOCG deposits. The results showed strong correlation between magnetite-rich, hydrothermally altered rocks and iron, copper, and gold enrichment

The values obtained in the magnetic susceptibility measurements also enabled the interpolation of a 3D model with their distribution, which traces fairly well the known boundaries of the studied mineralization.

Magnetic susceptibility measurements were carried out using different instrumentation and related drill core logs that described lithology and alteration types. In all cases, increased magnetite content seemed to correlate with alteration types.

The magnetic susceptibility measurements carried out on the geochemical samples showed an excellent correlation with those performed on the drill cores, and they also represent a better approximation of the mineralization model because of the sample material homogenization. This methodology could easily be implemented rather than measuring along drill core samples and provides a high return on investment as the equipment and time needed for measurements is minimal.

It is interesting to note that an efficient quality control of measured data discussed herein is crucial for the correct analysis of measured magnetic susceptibilities and interpolation of a reliable 3D model.

The methods and geological-geophysical interpretations presented in this study can be useful for:

(i) characterizing ore zones and hydrothermal alteration zones;

(ii) assisting in the correlation and geological interpretation of mineralized lithotypes;

(iii) supporting sections interpretation for the generation of geological and ore models;

(iv) improving and validating the use of magnetic surveys as well as mineral prospecting techniques and geophysical equipment; and

(v) providing an excellent support for using magnetic data for constrained inversion.

In the case here presented, in general, the hydrothermal alteration zones with magnetite are proximal to the mineralized zone. Outward from the magnetite-rich zones are silicic, garnet-grunerite, amphibole, potassic and chloritic type alteration zones. Geological macroscopic observations supported by petrographic studies, and the knowledge of magnetic susceptibility signatures were used to establish the paragenetic sequence of the deposit. The use of physical properties to define the magnetic behavior in a quantitative manner showed the importance of the approach exercised for a better characterization of the magnetic susceptibility signatures. This helped to improve the paragenetic sequence in the studied area.

The correlation between the increase in magnetic susceptibility values and mineralization is shown by iron, copper and gold high grades. The direct relationship between high densities and mineralized hydrothermal alteration bodies is also evident because of the presence of dense minerals (magnetite and sulfides).

It is known that in the studied deposit, the magnetite, garnet-grunerite-magnetite and amphibole-magnetite hydrothermal alteration zones are the most important zones because of their direct relationship with chalcopyrite and bornite sulfides. The best susceptibility signatures were outlined for these magnetite-rich zones, and the 3D interpolation showed an excellent correlation between the generated susceptibility model and the orebody that was modeled based on the drill holes. Thus, it is believed that the approach described herein can be of great value in a mineral program.

5.11 - ACKNOWLEDGMENTS

The authors would like to thank Vale S.A. – Department of Mineral Exploration and Projects – for the financial support, permission to publish this study, and permission to use the geophysical and geological data in this research project. We also would like to thank the Vale S.A. Geophysical Team for all their support, the Vale S.A. Furnas Project for the data and numerous geological arguments used in this study, and geologists Gabriel Paulo and Sálvio Ribeiro for their assistance with the ore models and graphs. We express our appreciation to Dr. Misac Nabighian and geophysicist Daniel Brake for their help in English review.

5.12 - REFERENCES

AGICO Advanced Geoscience Instruments Co., 2004, KLY- 4 / KLY- 4S / CS- 3 / CS- L User's Guide, Modular system for measuring magnetic susceptibility, anisotropy of magnetic susceptibility, and temperature variation of magnetic susceptibility, Version 1.2, http://www.agico.com/, accessed 15 October 2004.

Araújo, O.J.B., and R.G.N. Maia, 1991, Projeto especial mapas de recursos minerais, de solos e de vegetação para a área do Programa Grande Carajás; Subprojeto Recursos Minerais; Folha SB.22-Z-A Serra dos Carajás - Estado do Pará: DNPM/CPRM, Brasília.

Austin, J.R., P.W. Schmidt, and C.A. Foss, 2013, Magnetic modeling of iron oxide copper-gold mineralization constrained by 3D multiscale integration of petrophysical and geochemical data: Cloncurry District, Australia: Interpretation, **1**, no.1, T63–T84.

Barbosa, J.P.O, C.E.M. Barros, M.B. Macambira, and A.G. Vale, 2001, Geologia e Geocronologia do Stock Granítico Geladinho, região de Parauapebas, Província Mineral de Carajás: 7th Simpósio de Geologia da Amazônia, SBG, Expanded Abstract.

Barros, C.E.M., and P. Barbey, 1998, A importância da granitogênese tardi-arqueana (2.5 Ga.) na evolução tectono-metamórfica da província mineral de Carajás – O Complexo Granítico Estrela e sua auréola de contato: Revista Brasileira de Geociências, **28**, no. 4, 513–522.

Clark, D.A., 1997, Magnetic petrophysics and magnetic petrology: aids to geological interpretation of magnetic surveys: Journal of Australian Geology and Geophysics, **17**, 83–103.

Clark, D.A., 1999, Magnetic petrology of igneous intrusions: implications for exploration and magnetic interpretation: Exploration Geophysics, **30**, 5–26.

Clark, D.A., 2014, Magnetic effects of hydrothermal alteration in porphyry copper and iron-oxide copper–gold systems: A review: Tectonophysics, **624**, 46–65.

Clark, D.A., D.H. French, M.A. Lackie, and P.W. Schmidt, 1992, Magnetic petrology: Application of integrated rock magnetic and petrological techniques to geological interpretation of magnetic surveys: Exploration Geophysics, **23**, 65–68.

Criss, R.E., and D.E. Champion, 1984, Magnetic properties of granitic rocks from the southern half of the Idaho Batholith - influences of hydrothermal alteration and implications for aeromagnetic interpretation: Journal of Geophysical Research, **89**, no. B8, 7061–7076.

CVRD (Companhia Vale do Rio Doce), 2006, Relatório de etapa, Alvo Furnas, Volume 1: Internal report: Technical report.

DOCEGEO (Rio Doce Geologia e Mineração S.A), 1988, Revisão Litoestratigráfica da Província Mineral de Carajás: 35th Congresso Brasileiro de Geologia, SBG, Expanded Abstract, 11-56.

Geosoft Inc., 2014, Target Software, 3D Kriging GX, http://www.geosoft.com, accessed 15 April 2014.

Hanna, W.F., 1969, Negative aeromagnetic anomalies over mineralized areas of the Boulder batholith, Montana: U.S. Geological Survey Professional Paper, **650,** D, 159–167.

Hirata, W.K., J.C. Rigon, A.A.C. Cordeiro, and E.M. Meireles, 1982, Geologia Regional da Província Mineral de Carajás: 1o Simpósio de Geologia da Amazônia, SBG, 100–108.

Hitzman, M.W., N. Oreskes, and M.T. Einaudi, 1992, Geological characteristics and tectonic setting of Proterozoic iron oxide (Cu–U–Au–REE) deposits: Precambrian Research, **58**, 241–287.

Hoover, D.B., W.D. Heran, P.L. Hill, 1992, The Geophysical Expression of Selected Mineral Deposit Models: Editors, USGS Open File Report, 92–557.

Hoschke, T., 2008, Geophysical signatures of copper-gold porphyry and epithermal gold deposits: Arizona Geological Society Digest, **22**, 85–100.

Kearey, P., M. Brooks, and I. Hill, 2002, An introduction to geophysical exploration: Blackwell Science.

Lindenmayer, Z.G., 1990, Salobo Sequence, Carajás, Brazil: geology, geochemistry and metamorphism: Ph.D. thesis, University of Western Ontario.

Lindenmayer, Z.G., and J.B.G. Teixeira, 1999, Ore Genesis at the Salobo Copper Deposit, Serra dos Carajás, *in* M.G. Silva, and A. Misi, eds., Base Metal Deposits of Brazil: MME/CPRM/DNPM, 33–43.

Porter, T.M., 2000, Hydrothermal Iron Oxide–Copper–Gold and Related Deposits: A Global Perspective: Eds., PGC Publishing.

Sandrin, A, and S. Elming, 2007, Physical properties of rocks from borehole TJ71305 and geophysical outline of the Tjårrojåkka Cu-prospect, northern Sweden: Ore Geology Reviews, **30**, 56–73.

Sandrin, A, Å. Edfelt, T.E. Waight, R. Berggren, and S. Elming, 2009, Physical properties and petrologic description of rock samples from an IOCG mineralized area in the northern Fennoscandian Shield, Sweden: Journal of Geochemical Exploration, **103**, 80–96.

Smith, R.J., 2002, Geophysics of iron oxide-copper-gold deposits, *in* T.M. Porter, ed., Hydrothermal Iron Oxide–Copper–Gold and Related Deposits: A Global Perspective vol. 2: PGC Publishing, 357–367.

Telford, W.M., L.P. Geldart, and R.E. Sheriff, 1990, Applied geophysics 2 ed.: Cambridge University Press.

Vale S.A., 2012, Projeto Furnas, Relatório Final de Geologia: Internal report: Technical report.

Vasquez, M.L., C.S. Sousa, and J.M.A Carvalho, 2008, Mapa Geológico e de Recursos Minerais do Estado do Pará, escala 1:1.000.000: Programa Geologia do Brasil (PGB), Companhia de Pesquisa de Recursos Minerais - Serviço Geológico do Brasil.

Wirth, K.R., A.K. Gibbs, and W.J. Olszewski, 1986, U-Pb ages of zircons from the Grão-Pará group and Serra dos Carajás Granite, Pará, Brazil: Revista Brasileira de Geociências, **16**, no. 2, 195–200.

Xavier, R.P., L.V.S. Monteiro, C.P.N. Moreto, A.L.S. Pestilho, G.H.C. Melo, M.A.D. Silva, B. Aires, C. Ribeiro, and F.H.F. Silva, 2012, The iron oxide copper-gold systems of the Carajás Mineral Province, Brazil, *in* Geology and Genesis of Major Copper Deposits and Districts of the World: A Tribute to Richard Sillitoe, Special Publication, Society of Economic Geologists.

CAPÍTULO 6

CONCLUSÕES DA TESE

Neste projeto de pesquisa foram realizadas determinações das propriedades físicas, assim como uma ampla interpretação, com o uso de diversas técnicas e métodos magnéticos correlacionados ao contexto geológico, que teve como resultado um modelo prospectivo da mineralização de óxidos de ferro-cobre-ouro (*IOCG*). Isto foi possível devido à mineralização disseminada de calcopirita ± bornita estar relacionada à alteração hidrotermal cálcio-sódico-potássica (bornita-granada-anfibólio-magnetita) com os altos teores de cobre-ouro associados à presença de magnetita.

O trabalho foi implementado em três artigos que se complementam para atingir as várias etapas da exploração mineral. O primeiro artigo teve como resultado as interpretações qualitativas e semi-quantitativas de dados de magnetometria, que mapearam a configuração estrutural do depósito. Este artigo também teve como resultado uma interpretação quantitativa com a modelagem paramétrica 2D que forneceu uma primeira visão em profundidade da geometria do corpo e o entendimento de fatores complicadores como a presença de remanência e desmagnetização.

O segundo artigo, também com base apenas nos dados magnéticos da área, focou nas transformações destes dados com o uso do princípio da camada equivalente para a obtenção do que seria a intensidade do campo magnético anômalo (*MMA, Magnetic Magnitude Anomaly*), seguida da modelagem (inversão) 3D para estruturas complexas, assistida por técnicas de otimização, numa recuperação mais eficaz e detalhada da distribuição da susceptibilidade magnética intrínseca. O principal desafio encontrado para se atingir resultados positivos foi a presença de remanência agravado pelo fato do depósito estar situado numa região de baixas latitudes magnéticas que podem resultar em direções da magnetização total bem diferentes daquela induzida.

O terceiro artigo teve como base o conjunto de dados geológicos e das susceptibilidades magnéticas medidas em testemunhos de furos de sonda. O trabalho desenvolvido possibilitou a caracterização das assinaturas de susceptibilidade para os diversos litotipos encaixantes e para as zonas de alterações hidrotermais. Mais do que isso, possibilitou-se obter o modelo 3D referente à distribuição espacial das susceptibilidades magnéticas medidas.

Com isso, os principais resultados obtidos com este trabalho foi a definição de dois modelos para a mineralização no local estudado: (i) o geofísico, conseguido pela modelagem / inversão 3D dos dados magnéticos (método indireto) e (ii) o geológico obtido pela modelagem espacial das susceptibilidades magnéticas medidas (método direto).

Para uma validação dos resultados, estes modelos foram comparados entre si e com as informações provenientes da extensiva campanha de sondagem exploratória realizada. As conclusões mostram que a modelagem 3D dos dados de susceptibilidade medidos permite uma melhor definição e delimitação da fonte magnética. Entretanto, o trabalho mostrou que isso só pode ser alcançado por meio de medidas sistemáticas bastante trabalhosas e de uma interpretação complexa e exaustiva, com um grande custo e consumo de tempo. Este enfoque lida com uma grande quantidade de dados petrofísicos (susceptibilidade magnéticas medidas) e geológicos (estudos pormenorizados dos testemunhos de sondagens). Por outro lado, a modelagem de dados magnéticos por inversão de sua transformação em amplitude da anomalia magnética (através da camada equivalente), consome menos tempo, e fornece, mesmo assim, uma excelente aproximação ao mapeamento espacial das fontes magnéticas complexas.

Ambas as aproximações delimitaram a zona de magnetita maciça associada aos altos teores de minério. As metodologias abordadas neste estudo tem alto potencial para as diversas etapas de exploração (*greenfield*, *brownfield* e avaliação de recursos) de depósitos tipo *IOCG* e para depósitos associados à magnetita.

Magnetic interpretation and 2D modeling at iron oxide-copper-gold deposits, Carajás Mineral Province

Este trabalho aborda os diversos passos seguidos na interpretação dos dados magnéticos disponibilizados para o estudo. Descreve os resultados das diversas transformações lineares usadas para alicerçar a interpretação qualitativa com a caracterização em mapa das diversas fontes que compõem o relevo magnético local. Sua evolução, possibilitou estimar as profundidades destas fontes numa interpretação semi-quantitativa. Finalmente, este conjunto de informações serviu de base a uma modelagem paramétrica 2D para a interpretação quantitativa. A boa correspondência entre os resultados da modelagem 2D, e a geologia conhecida a o corpo de minério demonstram o sucesso desta abordagem.

Este trabalho mostrou caminhos para que se possa lidar com um corpo magnético complexo que constitui o ambiente da mineralização, como é o caso da remanência acentuada que varia ao longo do mesmo. O ensaio com a modelagem 2D possibilitou a verificação de que o corpo é fortemente magnético, que se tem que lidar com o fenômeno da desmagnetização, e de uma magnetização remanente associada a uma anisotropia magnética.

Este estudo de caso mostra que esta seria uma abordagem eficaz em cenários com esta complexidade, permitindo-se ter uma ideia da geometria do corpo de minério.

Application of 3D magnetic amplitude inversion to iron oxide-copper-gold deposits at low magnetic latitudes: a case study from Carajás Mineral Province

Este trabalho sequencia o anterior e inicia-se pelo cálculo da amplitude da anomalia magnética com o uso do conceito de camada equivalente para lidar com o terreno acidentado da área. Sobre esta transformação, e com informações do primeiro ensaio interpretativo, foi realizada a modelagem assistida por técnicas de minimização de erros (inversão) com o uso do parâmetro ótimo de regularização obtido com o critério da curva L. A susceptibilidade invertida recuperada delineou com sucesso a magnetita maciça associada ao minério de cobre e ouro de alto teor. Este processo de inversão mostrou-se bastante robusto no sentido de prescindir aprioristicamente, do controle estrutural, da geologia e do modelo de minério de dados dos testemunhos de furos de sonda do depósito, usados depois para comprovar o êxito desta abordagem.

Este estudo também reforça a utilidade da transformação empregada da amplitude da anomalia magnética, também como substituta da tradicional redução ao polo (RTP). Similarmente à RTP, dados de amplitude também representam uma versão corrigida dos efeitos de fase do sinal magnético e reduzem a polarização magnética para inclinações diferentes de 90º. A amplitude da anomalia magnética pode ser mais vantajosa do que a RTP devido não ser necessário o conhecimento da direção da magnetização para seu cálculo.

Este estudo de caso mostra que a inversão da amplitude é eficiente neste complexo ambiente com múltiplos fatores como magnetização remanente e desmagnetização que afetam a direção da magnetização total. Assim como as complicações devidas a localização em latitudes magnéticas extremamente baixas.

Magnetic susceptibility 3D model and signatures of iron oxide-copper-gold (IOCG) mineralization: A case study from Carajás Mineral Province, Brazil

As assinaturas da susceptibilidade magnética medidas em testemunhos de furos de sonda se provaram um método eficiente para caracterizar as zonas onde houve o enriquecimento em ferro, cobre e ouro. Além disso, o comportamento magnético dos minerais permitiram a descrição das assinaturas magnéticas associadas com os litotipos e zonas de alteração hidrotermal. Os valores obtidos nas medidas de susceptibilidade também permitiram uma interpolação 3D que possibilitou verificar sua distribuição espacial. Este resultado delimitou muito bem a mineralização conhecida.

Medidas de susceptibilidade realizadas igualmente, mas agora com o uso de amostras que representam alíquotas empregadas nas dosagens geoquímicas, mostraram excelente correlação

àquelas realizadas em testemunhos de furos de sondas mecânicas. Elas representaram uma melhor aproximação ao modelo de mineralização devido à homogeneização realizada no material previamente preparado para dosagens geoquímicas.

Os resultados obtidos ao longo dos testemunhos com susceptibilímetros portáteis foram aferidos por medidas laboratoriais. Em ambos os casos, mostraram a presença de valores elevados para a susceptibilidade magnética, e para os resultados em laboratório um alto grau de anisotropia.

No caso aqui estudado, de forma geral, as zonas de alteração hidrotermal com magnetita são proximais a zona mineralizada, seguidas da silicificação, zona de granada-grunerita, zona de anfibólio, potassificação e cloritização. O conhecimento geológico e o comportamento magnético qualitativo foram utilizados para estabelecer a sequência paragenética do depósito.

O uso da susceptibilidade para definir o comportamento magnético de uma forma quantitativa mostrou a importância desta abordagem para a caracterização das assinaturas magnéticas. Isto pode ajudar a melhorar a sequência paragenética de uma área estudada.

Aqui é conhecido que as zonas de alteração hidrotermal a magnetita, granada-grunerita-magnetita e anfibólio-magnetita são as zonas mais importantes por causa de sua relação direta com os sulfetos de calcopirita e bornita. As melhores assinaturas de susceptibilidade foram delineadas para estas zonas ricas em magnetita.

Por fim, a interpolação volumétrica destas medidas projetadas ao longo de seus respectivos segmentos nos furos de sondas mostrou uma excelente correlação entre o modelo de susceptibilidade 3D assim gerado com o modelo conseguido com as interpretações e modelagens magnéticas conduzidas e destas com os dados dos testemunhos usados.